UNIVERSITY OF SOUTHAMPTON

The Nordic Seas Circulation and Exchanges

ELIZABETH HAWKER

A thesis submitted for the degree of Doctor of Philosophy

School of Ocean and Earth Science

March 2005

UNIVERSITY OF SOUTHAMPTON

ABSTRACT

FACULTY OF ENGINEERING, SCIENCE & MATHEMATICS
SCHOOL OF OCEAN & EARTH SCIENCES

Doctor of Philosophy

THE NORDIC SEAS CIRCULATION AND EXCHANGES

Elizabeth Hawker

The Nordic Seas provide the main oceanic connection between the Arctic and the deep global oceans via dense overflows between Greenland and Scotland, into the North Atlantic. An understanding of the circulation and exchanges of this region is vital for any consideration of the implications of high latitude climate change to variability in the Atlantic thermohaline circulation and consequences for regional (European) climate.

This thesis makes use of a unique data set of near synoptic hydrographic and LADCP (lowered acoustic Doppler current profiler) measurements across the entire region during summer 1999. The box inverse method is applied to this hydrographic data, using computed geostrophic velocities referenced to detided LADCP measurements. The full summer Nordic Sea flux field (volume, heat and freshwater) is quantified, studying both the exchanges across the openings to the Nordic Seas, and the interior circulation. The total volume transports imply an inflow of 1.3±0.5Sv to the Nordic Seas from the Arctic Ocean, and a net export of 1.2±0.5Sv across the Greenland–Scotland Ridge into the North Atlantic. Within the Nordic Seas 4.0±1.3Sv of the warm saline inflow (σ_0<27.8) are converted to more dense waters, with the majority of the transformation (and ocean–atmosphere heat loss) occurring over the southern part of the Nordic Seas. The total heat convergence within the Nordic Seas is 137±44TW, giving an average flux of 51±16Wm^{-2}, and the net input of freshwater to the Nordic Seas is 0.059±0.019Sv.

The sensitivity of the summer circulation and fluxes is investigated; considering the formal error estimates from the inverse model, together with the errors implied from inverse and oceanographic sensitivity tests. Supplementary winter data is used to construct a winter circulation providing an indication of significant seasonal variability. This infers that an estimate of the annual mean fluxes based on summer data alone cannot be justified.

Table of Contents

List of Figures

List of Tables

Graduate School of the
Southampton Oceanography Centre

This PhD dissertation by

Elizabeth Hawker

has been produced under the supervision of the following persons

Supervisor/s	Dr Sheldon Bacon and Professor Harry Bryden
Chair of Advisory Panel	Professor John Murray (to July 2003) Professor Peter Killworth (from July 2003)
Member/s of Advisory Panel	Professor Bill Jenkins (to December 2001)

DECLARATION OF AUTHORSHIP

I, ……..,

declare that the thesis entitled

……..……

and the work presented in it are my own. I confirm that:

- this work was done wholly or mainly while in candidature for a research degree at this University;
- where any part of this thesis has previously been submitted for a degree or any other qualification at this University or any other institution, this has been clearly stated;
- where I have consulted the published work of others, this is always clearly attributed;
- where I have quoted from the work of others, the source is always given. With the exception of such quotations, this thesis is entirely my own work;
- I have acknowledged all main sources of help;
- where the thesis is based on work done by myself jointly with others, I have made clear exactly what was done by others and what I have contributed myself;
- none of this work has been published before submission

Signed: ……..

Date:…….

Acknowledgements

I would like to formally thank NERC for the use of ARCICE data from JR44 and JM3/2000; Sheldon Bacon and Margaret Yelland as the PSO's on JR44; Peter Wadhams, Jan Backhaus and Else Nøst Hegseth as the PSO's on JM3; and Stuart Cunningham (Southampton Oceanography Centre) for D242 data, Ursula Schauer (Alfred-Wegener-Institut) for ARKTIS XV/3 data and Johann Blindheim for data from the Svinøy section. My thanks also to the officers, crews and all cruise participants, without whose efforts this thesis would not exist.

My sincere thanks to my supervisors Sheldon Bacon and Harry Bryden, and to my advisory panel; but particularly to Sheldon for his insight and encouragement, and for giving me a long rein.

Thanks to the crew and officers of the RRS *James Clark Ross* who were there the first time I went to sea, and to all shipmates on that and subsequent cruises - for reminding me what this is for. Thanks also to all in the hydrography team of the James Rennell Division; to Alberto Garabato and Cecilie Mauritzen for helpful discussion; to Rebecca Woodgate and Peter Rhines for guidance during my exchange to the University of Washington, Seattle, and afterwards; and to Deb Shoosmith for her continued encouragement.

I am indebted to Sheldon and Margaret Yelland who quite literally gave me a home in Southampton, and whose company and friendship gave my time here purpose. Thanks to my housemates; Anna who understood about the PhD, and Chess who understood the urge to escape Southampton and who was with me during the darkest hours. Thanks to SV *Tenacious* and all who sail on her, for showing me there are other ways to '*go to sea*'. Similarly, of course, thanks to all those who have kept me company on a hilltop or mountainside, for showing me '*there are other mountains*' than those down south. Finally, my thanks to Mark Brandon, for his support, for being there the first time I went south, and for understanding.

And it goes without saying, I am forever grateful for the love and support of my parents, even when it is difficult to understand!

for Mark Brandon,

who shared his South with me

One does not discover new lands without consenting to lose sight of the shore for a very long time.

Andre Gide

Chapter One

Introduction

'Begin at the beginning,' the King said, gravely, 'and go on till you come to the end: then stop.'

Lewis Carroll
Alice's Adventures in Wonderland

The primary motivation for studying ocean circulation is to understand its importance to the climate system, particularly with respect to modern concern over climate change. The Earth's surface receives an uneven distribution of energy from the sun, with a greater influx of solar radiation at low latitudes (Figure 1.1). The global oceanic and atmospheric circulations balance this meridional bias by a transport of heat from low to high latitudes (Figure 1.2; Bryden and Imawaki, 2001).

The meridional overturning circulation (MOC) of the North Atlantic releases considerable amounts of heat to the atmosphere as warm subtropical waters are transported to high latitudes where they are transformed to cold (and so more dense) waters. This results in a southward flow of deep cold water and a northward ocean heat transport at all latitudes in the Atlantic Ocean (Bryden and Imawaki, 2001). This northward heat transport (even south of the equator) is peculiar to the Atlantic Ocean, and emphasises the influence that the high latitudes of the Nordic Seas and Arctic Mediterranean have on the global ocean circulation.

The North Atlantic Current (NAtlC) carries warm Atlantic waters from the subtropics to higher latitudes within the North Atlantic. It is cooled and freshened as it splits to follow one pathway through the subpolar gyre and another through the Nordic and Polar Seas (Figure 1.3) to the north (Mauritzen, 1996a). The principal transformations of the Atlantic waters occur in the seas of the Arctic Mediterranean, where they lose heat and become more dense. The intermediate waters which then overflow the Greenland-Iceland-Scotland ridge contribute to the source waters of North Atlantic Deep Water (NADW). The importance of understanding the variability and formation mechanisms of these overflows has been emphasised by studies of the North Atlantic which have shown how both the strength and structure of the meridional overturning are affected by the downstream development of the overflows (Saunders, 2001; Wood et al., 1999).

The data which provided the framework and motivation for this PhD were collected under the auspices of ARCICE (Arctic Sea Ice and Environmental Variability), a thematic programme of the UK Natural Environment Research Council (NERC). The core cruise from the ARCICE programme, JR44 (CATS-MIAOW), was the most extensive modern major synoptic survey to be made within the Nordic Seas, and the data provide a unique set of near synoptic hydrographic and LADCP (lowered acoustic Doppler current profiler) measurements across the entire region during summer 1999. The box inverse method is applied here, to this data together with supplementary hydrographic data, using geostrophic velocities referenced to detided LADCP measurements where possible. A further ARCICE cruise (JM3) also collected winter data over a reduced region of the Nordic Seas. This data set is used to characterise the winter circulation and to contrast it to the summer circulation.

The Nordic Seas provide a substantial part of the headwaters of the Atlantic thermohaline circulation. The water mass transformations within them provide a direct link between the atmosphere and ocean and are of consequence for the stability of the global thermohaline circulation. Historical knowledge of the Nordic Seas extends back to the voyages of the 19th century

sealers and whalers, and earlier (e.g. Koch, 1945), and there have been oceanographic studies since the era of Knudsen (1899) and Nansen (1902). However, while many of the key processes involved in the ventilation, pathways and overflows of the Nordic Seas are quantified and understood, there remain many outstanding questions, and an overall understanding of the components of the Nordic Seas system is yet to be established. To this end, this thesis quantifies the full Nordic Sea flux field (volume, heat and freshwater), thus determining the exchanges between the Nordic Seas and the Arctic Ocean to the north, the Barents Sea to the east, and North Atlantic to the south, via the North Atlantic Current inflow and the Denmark Strait and Iceland-Scotland overflows. This is the first study to be able to make use of synoptic hydrographic data across the entire region with concurrent direct velocity measurements on most sections; and can therefore provide a new estimate of the long-term mean summer fluxes and exchanges. The winter data also allow a winter circulation to be constructed, suggesting how the summer mean field might be extrapolated to provide an estimate of the 'true' annual mean flux field.

The structure of this thesis is as follows: Chapter 2 gives a general overview to set the work in context and outlines the aims in view of the outstanding questions concerning the circulation of the Nordic Seas. Chapters 3 and 4 give detailed descriptions of the data and methods used for this study. The main results are presented in Chapter 5, which describes the summer circulation and fluxes of the Nordic Seas. A study of the sensitivity of the inverse model and a discussion of errors are the subject of Chapter 6. A discussion of the variability of the circulation and fluxes of the Nordic Seas is made in Chapter 7, with reference to winter hydrographic data and the general ocean climate. Chapter 8 summarises the conclusions of this thesis and briefly considers the future of hydrography within the Nordic Seas.

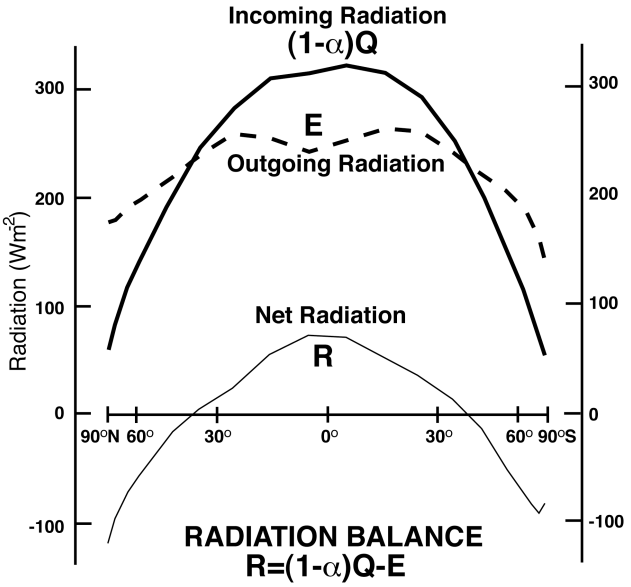

Figure 1.1: Latitudinal profiles of net incoming short-wave radiation, outgoing long-wave radiation, and the net radiative heating of the earth (Bryden and Imawaki, 2001). The latitudinal scale is stretched so that it is proportional to the radius of the earth. Q is the incoming short wave solar radiation, α is the albedo of the Earth, E is the outgoing long wave black body radiation, and R is the net radiation balance.

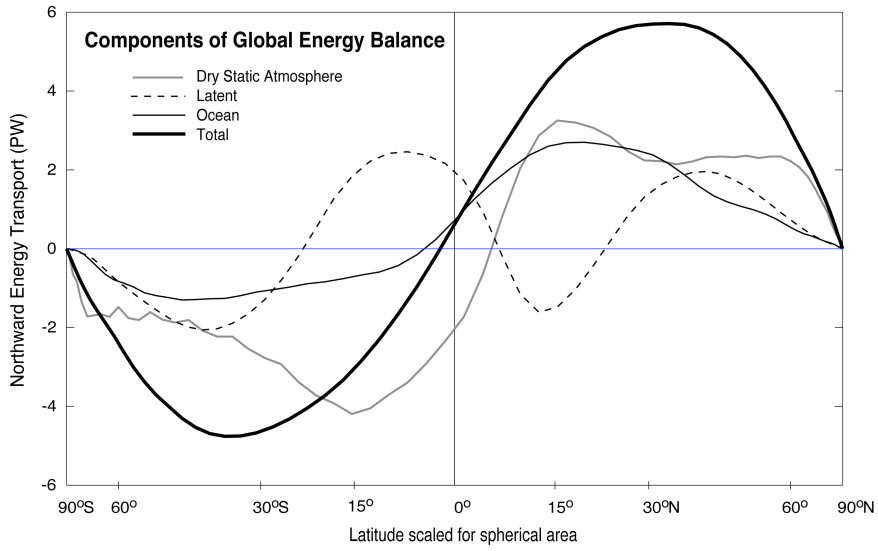

Figure 1.2: Components of the atmosphere and ocean energy transports required to balance the net radiative heating of the earth following Figure 1.1 (Bryden and Imawaki, 2001). The total energy transport is that required to balance the net radiative heating/cooling of the earth following Figure 1.1. The standard atmospheric energy transport is here divided into the dry static atmospheric energy transport and the latent heat transport, because the latent heat transport is fundamentally a joint atmosphere-ocean process as the atmospheric water vapour transport is balanced by an opposing oceanic freshwater transport. The ocean heat transport is determined by integrating over the oceans the spatial distribution of atmosphere-surface heat exchange calculated by subtracting the atmospheric energy transport divergence from the radiative heating at the top of the atmosphere.

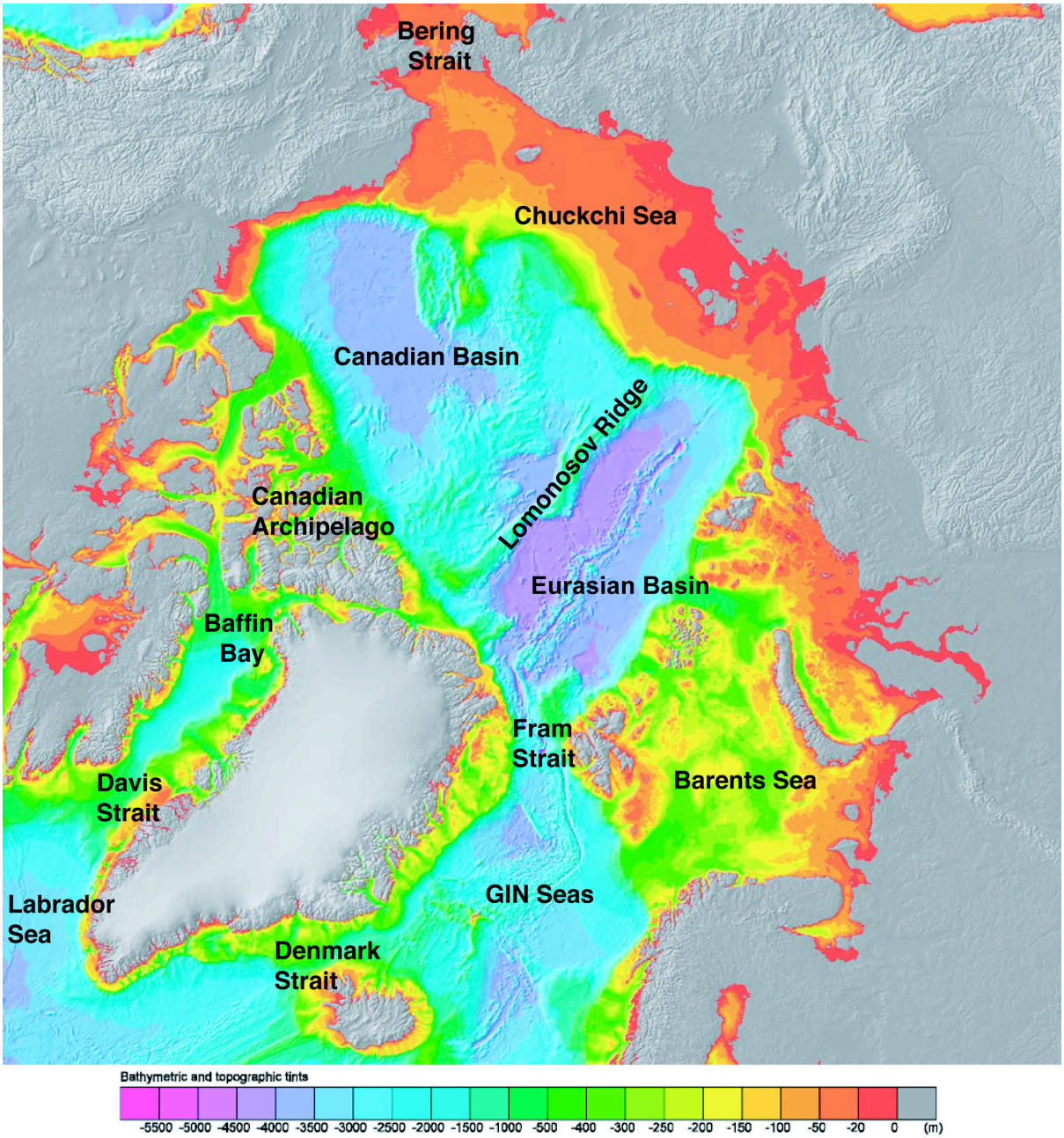

Figure 1.3: Map of the Arctic Region using the International Bathymetric Chart of the Arctic Ocean (IBCAO) (Jakobsson et al., 2000) from http://www.ngde.noaa.gov/mgg/bathymetry/arctic/arctic.html.

Chapter Two

Overview

2.1 Introduction

The Nordic Seas provide the main oceanic connection between the Arctic and the deep global oceans via the exchanges with the North Atlantic across the Greenland-Scotland Ridge. The inflow of warm, salty Atlantic waters and the outflow of ice and cold, fresh Arctic waters form two major components of the Nordic Sea circulation, and influence the long-term variability of the overflows into the North Atlantic. An understanding of the circulation and exchanges of the Nordic Seas is vital for any consideration of the implications of high latitude climate change to variability in the Atlantic thermohaline circulation and consequences for regional (European) climate.

This chapter gives a general overview to set the work of this thesis in context. The outstanding questions concerning the circulation of the Nordic Seas reveal the impetus for this thesis, the aims of which are outlined at the end of this chapter.

2.2 Topography

Oceanic topography influences the circulation, both by restricting exchanges and steering flow. The study of the Nordic Seas (Figure 2.1) has, since before the time of Nansen, been confused by the use of different terminology to describe geographical features and define water masses. For Helland-Hansen and Nansen (1909) discussion of the Norwegian Sea included the waters of the Greenland, Iceland and Norwegian Seas. These have also been aptly referred to as the 'GIN Seas' (Aagaard and Carmack, 1989). Today they are known collectively as the Nordic Seas (Hurdle 1986), and together with the Arctic Ocean, form the Arctic Mediterranean. Even today, however, their status is contentious; whether to be regarded as the northern marginal seas of the Atlantic, or the southward 'Atlantic sector' extension of the Arctic?

The Greenland-Scotland Ridge itself (Figure 2.2) was discovered by various expeditions in the late 1800s (for overview, see Bacon, 2000). In particular, Denmark Strait, the part of the ridge between Greenland and Iceland, was identified by soundings made by the Royal Danish Navy from 1877 to 1879. The presence of a ridge had been inferred by contemporary oceanographic expeditions which identified subsurface 'warm' and 'cold' areas to the south and north of Iceland respectively. It effectively acts as a dam to the deep waters of the Arctic, but allows exchanges of surface and intermediate waters through various gaps. Denmark Strait and the Faroe Bank Channel (the southward extension of the Faroe-Shetland Channel between the Faroe Islands and Scotland), provide the deepest connections with sill depths of 600□m and 850□m respectively, while the Iceland-Faroes ridge is cut by four 'notches' with sill depths of less than 450□m (Meincke, 1983).

The Greenland-Scotland Ridge constitutes a physical barrier between the Nordic Seas and Arctic Ocean to the north, and the Atlantic Ocean to the south. As such, it restricts the exchanges of surface and intermediate waters to the extent that the different character of the subsurface waters to

the north and the south of the ridge were noted as far back at the late 1800s. It may therefore be more reasonable to consider the Nordic Seas as the southerly extension of the Arctic rather than within the northern margins of the Atlantic.

The individual sub-basins of the Nordic Seas are defined by the submarine topography (Figure 2.1). The Iceland Sea (~1800□m in depth), between Greenland, Iceland and the island of Jan Mayen, is bounded by the Greenland-Iceland ridge to the south, and the Jan Mayen Fracture Zone to the north. The Norwegian Sea is separated into the Norwegian (~3600□m in depth) and Lofoten (~3200□m in depth) Basins and further north, extends east of the Knipovich Ridge towards Fram Strait. The Greenland Sea is separated from the Norwegian and Iceland Seas by the Mohns Ridge and the Jan Mayen Fracture Zone, respectively. The Mohns Ridge has numerous traverse gaps, some of which are very important in the exchange of waters between and within basins, such as the broad saddle (~2400□m depth) at ~75°30'N. The western depression of the Iceland Sea and the southern depression of the Greenland Basin are connected (at a depth of ~1600□m) between the Greenland continental slope and the westernmost portion of the Mohns Ridge by the Greenland□□Jan Mayen Gap. A shallow shelf leads east from the Nordic Seas into the Barents Sea, between Norway, Bear Island and Svalbard. To the south of Bear Island lies Bjørnøyrenna, a channel with a maximum depth of ~500□m. Storfjordrenna lies to the north of Bear Island, a channel with depth of ~300□m, which shoals to the east, and is blocked by Svalbard to the north.

Fram Strait, between Greenland and Svalbard, provides the deep connection (sill depth of 2600□m) between the Nordic Seas and the Arctic Ocean. The Arctic Ocean itself is a semi-enclosed ocean (Figure 1.3). Its connections to the global oceans, apart from Fram Strait, are restricted to exchanges with the North Atlantic through the Barents Sea (~250□m depth) via the Nordic Seas, and the Canadian Archipelago (~200□m depth); and exchanges with the Pacific through the Bering Strait (50□m depth). The Arctic Ocean is most simply considered to comprise of the Arctic Shelf Seas and two deep basins; the Canadian basin (maximum depth of ~3800□m) and the Eurasian basin (maximum depth of 4200□m) divided by the Lomonosov Ridge (sill depth of ~1400□m). The shallow continental shelf regions make up as much as ~53□% of the entire area of the Arctic Ocean (Jakobsson, 2002), compared to a range of 9.1 to 17.7□% for the remainder of the global oceans, implying that its circulation may be particularly sensitive to sea level changes. The physical restrictions of Bering Strait and the Canadian Archipelago mean the principal exchanges between the Arctic and the global oceans occur across the Greenland-Scotland ridge system.

The Nordic Seas are also connected to the North Atlantic via the North Sea and English Channel (Figure 2.2). The North Sea is a shallow (~100□m) marginal shelf sea bounded by the landmasses of the United Kingdom and continental Europe. The only deep connection between the Nordic Seas and the North Sea is a continental shelf depression called the Norwegian Trench. The deeper parts of this follow the Norwegian coast into the Skagerrak (maximum depth of 710□m) and onwards into the Baltic Sea (Gustafsson, 1997).

Within the North Atlantic, to the south of the Greenland-Scotland Ridge, the Irminger Basin off the east coast of Greenland is separated from the Iceland basin by the Reykjanes Ridge, and further to the east the Rockall-Hatton Plateau separates these basins from the Rockall Trough. Exchanges between the Irminger and Iceland basins (between the western and eastern North Atlantic) are limited, with the deepest passage being through the Charlie-Gibbs Fracture Zone.

2.3 Climate

The oceanic and atmospheric circulations of the Nordic Seas, together with the cryosphere, form major components in the high-latitude climate system.

2.3.1 Ocean Circulation

A schematic of the oceanic circulation of the Nordic Seas is illustrated in Figure 2.3. Although the broad features (inflows, overflows, boundary currents, basin-scale gyre circulations) are relatively well understood, the specific details of the interior circulation, in particular, are not yet well determined. The general oceanic circulation of the Nordic Seas is characterised by a surface inflow of Atlantic Water towards the Arctic (via Barents Sea and Fram Strait) and a surface outflow of cold, fresh water from the Arctic to the North Atlantic, separated by cyclonic gyres in the Greenland and Norwegian Seas (Hopkins, 1991).

(i) General Circulation

The Nordic Seas can be considered as an oceanic system with the East Greenland Current (EGC) as its Western Boundary Current. The term 'Sea' is used here to identify parts of the ocean with distinguishing characteristics. However, the region can also be considered as a 'marginal sea' in as much as communication with the Atlantic Ocean is restricted by the Greenland-Scotland Ridge, and is limited to exchanges through the deeper channels. Topography plays an important role in steering the general flow.

A continuation of the NAtlC carries an inflow of warm, saline North Atlantic surface waters (6□□10°C; 35.1□□35.3) over the Greenland-Scotland Ridge into the Nordic Seas. It has been suggested that Mediterranean Sea outflow may form a contribution to this inflow (Reid, 1979). Although the distinct silicate signature of Mediterranean Water indicates its influence within the Norwegian Sea, it is now thought this is via an indirect route, supplying the interior Atlantic with high salinity water (McCarney and Mauritzen, 2001; New et al., 2001; Slater, 2003), rather than via a direct undercurrent along the eastern boundary.

Within the Nordic Seas, the Norwegian Atlantic Current (NAC) transports inflowing Atlantic Water (AW) northwards along the coast of Norway, dominating the surface waters of the Norwegian Sea (Orvik and Niiler, 2002). This intrusion of warmer waters keeps these regions relatively ice-free

and provides Norway with its relatively mild climate despite its northern latitude. Some Atlantic waters also enter the Nordic Seas through Denmark Strait via the Irminger Current which follows the northwest coast of Iceland (Stefansson, 1962). These join the western branch of the NAC which is topographically guided from the Iceland-Faroe Front through the Nordic Seas towards Fram Strait. The eastern branch of the NAC carries AW inflow through the Faroe-Shetland Channel northward along the Norwegian shelf edge, reaching current speeds of above 30 $cm\,s^{-1}$. Some of the waters in this eastern branch continue towards the Arctic Ocean via the Barents Sea, while the remainder join the western branch and flow towards Fram Strait.

The exchanges between the Nordic Seas and the North and Baltic Seas are limited, but are of particular consequence with respect to the freshwater fluxes. Waters within the Baltic are typically very fresh, with an average salinity of 8 (Rodhe and Winsor, 2003), since river runoff and precipitation strongly exceed evaporation. The relatively high sea level within the North and Baltic Seas (compared to the Nordic Seas), attributed to this low-salinity water, impedes the entrance of NAW and prevents any significant portion from exiting via the English Channel (Hopkins, 1991). Any of the Atlantic Water within the NAC that does enter the North Sea either recirculates, or is mixed into the North Sea. The North Sea outflow includes fresh Norwegian Shelf Water, originating in the Baltic Sea, which is carried northwards along the Norwegian coast in the Norwegian Coastal Current (NCC). Hopkins (1991) suggested that the Baltic outflow to typically be ~0.02 Sv, with the remainder of the North Sea runoff contributing 0.01 Sv; such that a typical outflow of 1 Sv would be balanced by a recirculating inflow of about 0.97 Sv.

The complicated topographic structure of Fram Strait leads to a splitting of the West Spitsbergen Current carrying Atlantic Water northward into at least three parts. One part follows the shelf edge and enters the Arctic Ocean north of Svalbard. This part has to cross the Yermak Plateau, which presents a sill for the flow with a depth of about 700 m. A second branch flows northward along the northwestern slope of the Yermak Plateau and the third part recirculates immediately in Fram Strait at about 79ºN and exits in the EGC. The size and strength of the different branches largely determine the input of oceanic heat to the inner Arctic Ocean.

To the west of the Nordic Seas, the EGC provides the most direct connection from the Arctic to the North Atlantic. It flows south-westwards along the eastern coast of Greenland carrying cold, fresh polar water and ice out of the high Arctic through Fram Strait, and on towards Cape Farewell at the southern tip of Greenland via Denmark Strait. Return Atlantic Water from the Fram Strait region is carried the length of the East Greenland coast into the northern North Atlantic. North of Denmark Strait, the EGC also carries waters recirculating within the Greenland Sea gyre, and deep and intermediate waters from the Arctic and Nordic Seas, some of which contribute to the overflow waters. The content and characteristics of the current change from north to south, and transformations within the current may contribute to the formation of Denmark Strait Overflow Water (Strass et al., 1993). The strength of the EGC varies as it flows downstream along the

Greenland coast (Rudels et al., 1999), increasing from ~10 Sv in Fram Strait to a maximum transport of ~30 Sv in the Greenland Sea gyre in winter, and decreasing to a strength of ~3 Sv as it leaves the Nordic Seas via Denmark Strait. Woodgate et al. (1999) found that current speeds within the EGC can reach up to about 50 cms^{-1} and estimated the mean annual transport at 75°N to be 21±3 Sv (with a maximum winter transport of 37 Sv), using 9°W as the eastern boundary of the current.

The cyclonic Greenland Sea gyre comprises a northward warm water branch and a southward cold water branch. The former is the northward flowing warm, saline AW in the NAC. Some of this AW flows westward into the interior of the gyre before forming the Spitzbergen Current through Fram Strait into the Arctic Ocean. The latter is the southward flow of cold, fresh water in the EGC out of the Arctic Ocean, some of which flows eastward into the interior of the gyre as the Jan Mayen Current (JMC) along the Jan Mayen Ridge, and as the East Icelandic Current further south. The JMC is an eastward flow emanating from the EGC, flowing to the north of Jan Mayen Island, closing the southern limb of the Greenland Sea gyre (Bourke et al., 1992). The surface waters of the JMC are cold and fresh (due to their origin in the EGC) relative to surface waters elsewhere in the gyre, and so have a significant role in carrying freshwater into the gyre. During winter, the current can sometimes be associated with the formation of the Odden ice tongue (section 2.4.3). Within the central region of the gyre, results from a tracer-release experiment suggest that, under present conditions vertical mixing may be dominated by rapid year-round turbulent mixing, rather than convection (Watson et al., 1999).

The Jan Mayen Fracture Zone provides a deep connection (~2200m) through the Mohns Ridge separating the deep basins of the Greenland and Norwegian Seas (Seolen, 1986). Current meter measurements from the early 1980s show a steady flow from the Greenland Sea to the Norwegian Sea with an average speed of about 7-8 cms^{-1} (Swift and Koltermann, 1988). However, with the virtual cease of GSDW production (section 2.5) Osterhus and Gammelsrod (1999) suggest that the transport through the Jan Mayen Channel may have reduced or even reversed, cutting off the deep Norwegian Sea from the influence of the GSDW and its changes. From current meter measurements during 1992 and 1993, they indeed found a very weak flow into the Greenland Sea. It remains open to question whether this reversal of the deep-basin exchanges within the Nordic Seas is a permanent or intermittent feature.

It has been known that dense water overspills the Greenland-Scotland Ridge into the North Atlantic for more than a century (Knudsen, 1899). It was not, however, appreciated that these overflows were implicated in the formation of North Atlantic Deep Water (NADW) and the ventilation of the deep oceans. Initially it was suggested that most NADW was formed to the southeast of Greenland, and the overflows were assumed not to make a substantial contribution (Nansen, 1912). Sverdrup et al. (1942) in a major review of physical oceanography also overlooked their importance. Cooper

(1955) was the first to realise the significance of the dense northern overflows across the Greenland-Scotland Ridge.

The deepest parts of the Denmark Strait overflow have temperatures below 0ºC and salinities between 34.92 and 34.93 (characteristic of Norwegian Sea Deep Water found in the Iceland Sea). At intermediate depths, waters typically have temperatures between 0ºC and 1ºC and salinities between 34.5 and 34.94. At shallow depths, the cold, fresh waters of the East Greenland Current have temperatures below 0ºC and salinities below 34.5. The mean (time-averaged) flux of water colder than 2ºC has been found to be in the region of 2.9 Sv (Ross, 1984).

The principal overflow of the Iceland-Scotland section of the ridge occurs through the Faroe Bank Channel (sill depth 850 m), although episodic overflows do occur west of the Faroe Islands (Meincke, 1983; Saunders 2001). Estimates of the volume transport of overflow through the Faroe Bank Channel give a flux of about 1.9 Sv (< 3°C) (Østerhus and Gammelsrod, 1999; Saunders, 1990a), while the Iceland-Faroe overflow is thought to be ~1 Sv (Hansen and Østerhus, 2000; Meincke, 1983).

Within the North Atlantic, the paths of the overflows are determined by the topography of the Iceland and Irminger basins. The downstream properties of the cold, fresh, dense overflow waters change as the ambient Atlantic waters are entrained. The Iceland-Scotland component flows anticlockwise round the Iceland Basin, and through the Charlie-Gibbs Fracture Zone into the Irminger Basin. Here, it is incorporated with the Denmark Strait overflow descending to form the Deep Northern Boundary Current (DNBC) of the North Atlantic (McCartney, 1992). These dense northern overflows contribute to the formation of North Atlantic Deep Water (NADW) (Dickson and Brown, 1994). North Atlantic Deep Water (NADW) forms the deep component of the overturning circulation and can be traced into the Southern, Indian and Pacific Oceans (Schmitz and McCartney, 1993).

(ii) Deep water formation

The formation of dense water and the associated water mass transformations underpin the thermohaline circulation and set the properties of the deep ocean. Within the Arctic Mediterranean, deep water formation has occurred through both open-ocean deep convection in the Greenland Sea and convection mechanisms due to the formation of ice within the Arctic shelf seas.

The deep ocean is insulated from the direct influence of the atmosphere by the strong vertical density gradients of the oceanic thermocline (Marshall and Schott, 1999). The surface layers of the ocean undergo a regular cycle of homogenisation and restratification in response to the annual cycle of buoyancy fluxes at the sea surface. Over the majority of the ocean the mixed layers extend to depths of several hundred metres at most. In a few regions, however, deep convection mixes most of the water column. These regions are characterised by weak stratification below the mixed layer and strong atmospheric forcing (intense buoyancy loss to the atmosphere in winter).

The intermittent process of deep convection involves three phases (Marshall and Schott, 1999); large-scale preconditioning (occurring over 100's kms), localised deep convection (on scales of the order 1 km), and lateral exchange between the convection site and the ambient ocean (advective processes on the scale of 10's kms). Large heat and freshwater fluxes are induced over the Greenland Sea by cold, dry winds blowing over the water from land or ice surfaces. Within the Greenland Sea, the weakly stratified waters of the interior are close to the surface where they are subject to intense surface forcing during winter. In particular, the depth of the $\sigma_0 = 27.9$ isopycnal rises from greater than 200 m at the periphery to less than 50 m in the central Greenland Sea (Marshall and Schott, 1999). In the interior of the gyre a thin layer of Arctic surface water originating from the East Greenland Current overlies a layer of intermediate water. Weakly stratified Greenland Sea Deep Water, formed during previous convection events, lies below these water masses. In early winter, as ice is formed eastward across the Greenland Sea, brine rejection increases the density of the surface layer, while the mixed layer under the ice cools and deepens to about 150 m. During some years, later in the winter season, the Odden ice feature forms (section 2.4.3). This was a regular feature, well known to whalers and sealers as the 'Isodden' or 'Odden' (Promontory) (Koch, 1945; Wadhams, 1981). It extends to the northeast enclosing an ice-free bay the 'Nordbukta'. This ice-free bay is thought to be largely a result of southward ice export due to strong northerly winds (Visbeck et al., 1995). The eventual occurrence of deep convection depends on the seasonal development of the surface buoyancy flux with respect to the initial stratification at the beginning of the winter period. If the near surface stratification is eroded by the winter buoyancy loss and meterological conditions are favourable then deep convection may occur. The vertical heat transfer of deep convection then progresses to an advective horizontal transfer associated with eddies.

In addition to open ocean deep convection, dense waters are also formed by convection mechanisms due to the formation of ice. During periods of ice growth the salinity of the underlying water is increased as brine is rejected. The high density of this cold, saline surface water causes it to sink, entraining the ambient water. When this occurs in the shelf seas these cold, saline waters accumulate and spread from the interior shelves towards the shelf edge. As they sink to depth in the central ocean basins they modify and contribute to the deep waters (Schauer, 1995).

Dense waters formed in the Arctic shelf seas through the process of brine rejection act to ventilate the deep waters of the Arctic Ocean (Rudels, 1995; Rudels and Quadfasel, 1991). Within the Barents Sea, the formation of dense shelf waters occurs mainly in the coastal polynas (areas of open water within ice covered regions) off Svalbard, Novaya Zemlya, and Franz Josef Land. Storfjorden is a shallow fjord south of Svalbard with a wide southern opening towards the Barents Sea. Under certain conditions a polyna will form as cold polar air is advected by easterly winds and drives ice off the coast. New ice rapidly forms in this area of open water, rejecting salt into the underlying surface waters through the process of brine rejection. These surface waters become more dense as

their salinity is increased, until eventually they sink. There has been direct observational evidence for the sinking of this dense shelf water into a deep ocean basin (Quadfasel et al., 1988). Storfjorden is bounded to the south by a shallow sill over which the dense shelf water eventually spills. This plume of bottom water flows around the southern tip of Svalbard, along the western continental slope and into Fram Strait where it sinks to depths of more than 2000□m. Along its descent path it entrains warm Atlantic water from the West Spitsbergen Current, and Norwegian Sea Deep Water.

(iii) Variability

Seasonality in the flow over the domain of the Nordic Seas generally takes the form of a winter intensification of the circulation. Moored current meters in the EGC at 75°N showed the current to vary from 11□Sv in summer to 37□Sv in winter (Woodgate et al., 1999). Since no significant seasonal signal has been observed in either Fram Strait or Denmark Strait, this suggests that the seasonal flow is confined within the Greenland Sea and that the winter intensification of the gyre circulation is of the order 100%. Jakobsen et al. (2003) found the winter intensification to correspond to about 20□% of the mean flow over the remainder of the Nordic Seas, although stronger for the eastern boundary currents and jets associated with topographic features. This seasonal variability was also observed using long-term measurements with moored instruments in the NAC near 63°N (Orvik et al., 2001).

Open-ocean deep water formation is not a steady state process, illustrated by the great variability in the intensity of convection in the Greenland Sea on interannual and interdecadal timescales (Dickson et al., 1996). In particular, conditions for deep convection in the Greenland Sea are influenced by the effect of freshwater export (ice transport) on the oceanic density stratification. Direct evidence of the extent of the convection regime is sparse since over the past two decades deep convective activity in the Greenland Sea has weakened. Indirect evidence from tracer concentrations indicates that there was ventilation of the deep waters below 2000□m during the active convective period in the 1970's (Smethie et al., 1986), and has allowed estimates of renewal times to be made (Schlosser et al., 1991). More recent observational data suggest that convection has latterly reached only to depths of about 1500□m (Rudels, 1989), although deep convection was triggered in the Nordbukta region in 1989 with individual deep mixed profiles observed by shipboard hydrographic profiling (Rhein, 1991). Based on oceanographic cruises to the central Greenland Sea between 1991 and 2000, using temperature and salinity data, Budeus et al. (1998) conclude that winter convection was extremely weak after 1993, not even ventilating the intermediate waters, despite increasing salinities in the upper layers. Tracer inventories from the same cruises, however, do show that some ventilation of the deeper waters did occur, with the strongest ventilation between 1994 to 1995 and 1999 to 2000 (Bonisch et al., 1997; Karstensen et al., 2002). With the absence of deep convection the temperatures of the deep waters within the Greenland Gyre were observed to increase by 0.03°C between 1993 and 1996 (Budeus et al., 1998).

Variability in the temperature and salinity of the North Atlantic inflow has been observed on seasonal to decadal timescales (Loeng et al., 1992). Mork and Blindheim (2000) used hydrographic observations on the Svinøy section, which runs northwest from about 62°N on the Norwegian coast to 64°40'N 0°E, to investigate variations in the Atlantic inflow to the Nordic Seas using data from the winter 1955 to 1973 and from the summer 1978 to 1996. They concluded that interannual variations in the Svinøy section are controlled mostly by a large-scale pressure system that influences the transport of Atlantic water over the Scotland-Iceland Ridge. They suggested that variations in the North Atlantic Oscillation (NAO; see section 2.3.2) may influence the strength of the transports over the Ridge. For example, an increase of westerly winds would move more Atlantic water closer to Norway, bringing colder and fresher water from the Norwegian and Iceland Seas further east. A recent survey of the Atlantic inflow to the Nordic Seas using moored current meters, VM-ADCP and CTD observations has, to date, not found inter-annual or longer-term trends in the Atlantic inflow (Orvik et al., 2001).

Several time series in the western Norwegian Sea indicate a long-term trend of cooling and freshening of the upper layers in the western Norwegian Sea since the 1960s (Blindheim et al., 2000). These time series include Russian surveys in the Norwegian Sea, Icelandic standard sections, Scottish and Faroese observations in the Faroe-Shetland region, and measurements made at Ocean Weather Station Mike (OWS M). This weather station is situated at 66°N 2°E is over the 2000□m isobath on the slope to the deep Norwegian Basin. Daily and weekly hydrographic stations have been made since 1948 to monitor both the deep Norwegian Sea and the front between the Atlantic and Arctic type waters. The reason for the upper layer decrease in temperature and salinity is mainly an increased freshwater supply from the East Icelandic Current. Blindheim et al. (2000) suggested the change in water mass structure is manifested by the development of a layer of Arctic intermediate waters, deriving from the Greenland and Iceland Seas and spreading over the Norwegian Sea, and a freshening of the Atlantic waters above. In the Norwegian Basin this has resulted an eastwards shift of the Arctic front, which in general terms divides the cold Arctic type waters from the warm Atlantic type waters, and widespread cooling of the upper layers. The high correlation between the eastward extent of the NAC and the NAO winter index suggest large-scale wind forcing. The principal cause of the freshening seems to be this wind induced eastward advection of Arctic waters.

Many studies of the overflow through Denmark Strait (sill depth 650□m) have shown it to have characteristic short term variability both in thickness and hydrographic properties (Mann, 1969; Worthington, 1969). Novel measurements were made in the overflow during autumn 1997, using instantaneous velocity profiles (Girton et al., 2001). Results from this work support the view of the DSO as an unchanging flow on timescales longer than a few days, with current meter studies within the DSO unable to identify significant seasonal or interannual variability (Aagaard and Malmberg,

1978; Dickson and Brown, 1994). Similarly, no observational evidence has so far identified a systematic seasonal signal in the Iceland-Scotland overflows (Østerhus et al., 1999).

(iv) Circulation of the Arctic Ocean and Barents Sea

The circulation of the Nordic Seas is linked to that of the remainder of the Arctic Mediterranean. Thus, to consider the main exchanges of the Nordic Seas with the Arctic Ocean and the Barents Sea it is worth understanding the general circulation of these regions.

The severe climatic conditions and perennial ice cover of the Arctic Ocean mean that the region is relatively inaccessible. The first measurements were made over a hundred years ago during the drift of the research vessel *Fram* (Nansen, 1902), and although coverage since then has been patchy both spatially and temporally, considerable advances in understanding have been made during the past three decades. The International Arctic Buoy Programme (IABP) has provided ice motion data since January 1979 (e.g. Zhang et al., 2003). Ice breaker cruises have provided oceanographic data (e.g. Anderson et al., 1989; Swift et al., 1997). Submarine expeditions have also provided information on both the oceanography and ice thickness and extent. The historical declassified data from military expeditions is mainly acoustic (upward looking sonar) data (Wadhams, 1992); between 1958 and 2000 there were about 63 cruises under the sea ice by US Navy submarines and there is also data available from some British naval submarine cruises. During the 1990's there were also six unclassified Scientific Ice Expeditions (SCICEX submarine cruises; Dickson, 1999) with civilian scientists participating in the cruise planning. Since the 1970's there has also been continually improving satellite data from the Arctic regions, with extended coverage, improved methods and more advanced technology. Interpretation of the data is, however, not always straightforward, with difficulty in distinguishing melt ponds from open water in summer, for example. The latest developments in satellite technology are the missions of ICESat (Ice, Cloud and land Elevation Satellite) and CryoSat[1]. The former is a laser altimeter system to measure changes in the elevation of the Greenland and Antarctic ice sheets (Kwok et al., 2004; Zwally et al., 2002). CryoSat is a three-year radar altimetry mission to be launched in early 2005. The primary objective of the mission is to test the prediction of thinning arctic ice due to global warming by determining variations in the thickness of the Earth's continental ice sheets and marine ice cover.

The water column of the Arctic Ocean can be considered as a three-layer system composed of surface waters, intermediate waters formed from the inflow of warm, salty Atlantic water, and deep waters. Waters of Atlantic origin (>□°C and salinity > 34.9) enter the Arctic in an extension of the Norwegian Atlantic Current, through Fram Strait and the Barents Sea. They are modified by cooling as they release heat to the atmosphere, forming the Atlantic layer with a core identified by a temperature maximum and relatively high salinity between depths of 200□800m over much of the

[1] Further information on the missions of ICESat and CryoSat is to be found at http://icesat.gsfc.nasa.gov and http://www.esa.int/export/esaLP/cryosat.htm.

Arctic basin. A fundamental change in the circulation of the Arctic Ocean has been noted since the early 1990s, with the front between waters of Atlantic and Pacific character shifting from over the Lomonosov Ridge to roughly over the Alpha and Mendeleyev Ridges (Morison et al., 1998). The surface layer consists of cold, fresh Polar Water (PW) (<0°C and salinity < 34.4) which occupies the upper 200m and forms the surface outflows within the East Greenland Current and Canadian Archipelago. A cold, salty halocline insulates this cold, fresh surface layer from the underlying warm, salty Atlantic layer. A combination of mechanisms may contribute to the formation of this halocline including winter advective intrusion of cold, salty shelf waters, winter convection in the deep basins, and year round injection of relatively fresh shelf waters in some regions (Steele and Boyd, 1998). The Arctic shelf waters have greater variability in salinity than open ocean surface waters at corresponding depths. This is due to the freshwater influence of summer river runoff and brine enrichment during winter ice formation (although shelf waters remain less saline than Atlantic Water in the open ocean). Waters of Pacific Origin enter the Arctic Ocean via the shallow Bering Strait (50m) with an average northward flow driven by sea level slope down towards the north, caused by the pressure difference between the Pacific and Atlantic oceans. This relatively cold and fresh water, which often enters the deep basin in shelf slope plumes, is high in silicate concentrations. The deep waters are divided between Canada Basin Deep Water (CBDW at ~-0.5°C and salinity of >34.95) and the colder, fresher Eurasian Basin Deep Water (EBDW at ~-0.7ºC and salinity of ~34.94).

The surface circulation of the central Arctic Ocean reflects the mean sea level pressure field, with the wind-driven motion alternating between anticyclonic and cyclonic regimes each persisting for 5-7 years (Proshutinsky and Johnson, 1997). The circulation of the halocline waters is likely to be some combination of the ice circulation and the flow of the underlying Atlantic layer with additions of waters of Pacific origin from the Chukchi shelf. In general terms, the Fram Strait and Barents Sea branches of the Atlantic Layer flow in a cyclonic boundary current dividing at the Lomonsov Ridge with some waters following the ridge north, and some waters continuing in a boundary current into the Canadian Basin (Aksenov and Coward, 2001). The flow of deep and bottom waters below 1700m is less well known. Deep waters in the Eurasian Basin could be formed by a mixture of deep waters entering through Fram Strait and an input of dense shelf waters from the Barents and Kara Seas. Deep waters in the Canadian Basin are mostly waters from the Eurasian Basin which spill over the Lomonsov Ridge (gaps extend to a depth of 2400m). Below the sill depth of the ridge CBDW is warmed and made more saline by dense water gravity currents carrying heat and salt to the deep ocean. The slow circulation of these deep waters is presumed to be cyclonic.

The Barents Sea is of particular importance among the Arctic shelf seas since the main oceanic inflows of heat and salt to the Arctic Ocean occur across its continental shelf (Schauer et al., 2002). Water masses are significantly modified before they enter the Arctic through interactions with ice and atmosphere, and mixing within the region. This contrasts to the AW entering the Arctic Ocean

through Fram Strait which, although cooled and freshened, is relatively unchanged. There is large seasonal variability in the conditions within the Barents Sea, the northern part being largely ice covered in winter. Cooling and brine rejection increase the density of the surface layer, and together with wind mixing lead to vertical homogenization of the water column. The dense water formed fills the northern Barents Sea; some flowing north into the Arctic Ocean sinking to depth in the St Anna Trough, some flowing southwards through the Barents Sea Opening into the Norwegian Sea (Ingvaldsen et al., 2004a). In summer, a fresh warm surface layer forms due to ice melt and summer heating. This increases the stability of the water column thus inhibiting vertical mixing and insulating the deeper water from the atmosphere. In this way, the properties of the water masses created in the winter are preserved.

2.3.2 Atmosphere

The prominent features of the atmospheric surface pressure field for the northern high latitudes are two low pressure cells, the Icelandic and Aleutian lows located at ~60°N in the North Atlantic and North Pacific respectively, and two high pressure cells, the Siberian and McKenzie highs located at approximately 70°N on either side of the Canada Basin. The Nordic Seas are influenced primarily by the Icelandic low pressure system and secondarily by the high pressures over the Arctic Ocean (Hopkins, 1991). In addition, there are strong pressure gradients around Greenland due to the anomalously cold temperatures over the Greenland ice sheet (Proshutinsky and Johnson, 1997).

The Nordic Seas are divided by the Arctic Front (Figure 2.4), with respect to climatic conditons. The mean position of this front (nominally running northeast from Iceland to Bear Island) approximately separates the Norwegian Sea from the Greenland and Iceland Seas, and divides the region of polar easterlies from that of the westerlies (Hopkins, 1991). Northwest of the front there is little seasonal variation in the prevailing easterlies. The mean wind speed is ~5 ms^{-1} with a light seasonal signal of ± ms^{-1}. In contrast, to the southeast, winds are dominated by cyclonic storms travelling towards the Barents Sea. There is strong seasonality with high winds in early winter and light winds in early summer. The mean wind stress curl (Jonsson, 1991) is positive over most of the Nordic Seas with two maxima in the Greenland Sea (over the southern part of the Greenland Basin, and over the Boreas Basin). In comparison with other regions (for example, the North Atlantic with a maximum of 0.1 Pa per 1000 km, and the North Pacific with a maximum of 0.2 Pa per 1000km) the wind stress curl over the Nordic Seas is extremely large. In January, the wind stress curl over much of the Greenland Sea is greater than 0.4 Pa per 1000 km, with a maximum exceeding 0.8 Pa per 1000 km. However, there is strong seasonality with near zero wind stress curl for the entire region during the summer (May to August).

The atmospheric variability of the northern high latitudes has a number of major features, with both local and widespread modes of variability. The Arctic Oscillation (AO; also known as the Northern Annular Mode) has been described as the leading mode of Northern Hemisphere sea level pressure

variability, and reflects an exchange of atmospheric mass between the Arctic Ocean and the mid latitudes (Thompson and Wallace, 1998). This pattern is highly correlated with the North Atlantic Oscillation (NAO), another robust recurrent mode of atmospheric behaviour involving a large-scale alternation of atmospheric mass centred on the Iceland low and the Azores high. The index of NAO activity is commonly defined as the pressure difference between these two cells. The NAO focuses on a coupled Atlantic high and Icelandic low variability, whereas the AO focuses on a coupled Arctic high and circumpolar low. Whether one or other of the AO and NAO are considered to be a 'real' atmospheric mode depends on the perspective taken, and the interpretation given (Serreze et al., 2003). A study by Ambaum et al. (2001) suggests that the NAO paradigm might be more physically relevant and robust for Northern Hemisphere variability than the AO paradigm.

Oceanic circulation is partly driven by the atmospheric forcing, including the wind speed and air-sea heat and freshwater exchanges. The NAO, as an atmospheric mode of variability, might therefore be expected to modify the oceanic circulation of the Nordic Seas and North Atlantic. The NAO alternates between a 'high index' pattern (NAO+), characterised by strong mid-latitude westerly winds, and a 'low index' pattern (NAO-) with weakened westerly winds over the Atlantic. The recent positive trends in the winter indices of both the AO and NAO have been linked to atmospheric warming over the Arctic Ocean and sub-Arctic land mass, warming of the Arctic Ocean's Atlantic layer and reductions in winter sea level pressure (Thompson and Wallace, 1998). These trends have been accompanied by an intensifying storm track through the Nordic Seas with greatly increased winter precipitation, an increase in both volume and temperature of the inflow of Atlantic Water to the Arctic Ocean via the Barents Sea and WSC, a decrease in the extent of sea ice throughout the European sub-arctic, and an increase in the annual volume flux of ice from Fram Strait (Dickson et al., 2000).

2.3.3 Ice

Ice is an important component of the Arctic environment and is influenced by conditions in both the atmosphere and oceans (Deser et al., 2000). In turn it affects climate through modification of the albedo, ocean-atmosphere exchanges, oceanic freshwater flux and the upper ocean stratification.

The central Arctic Ocean is ice-covered throughout the year. Seasonal variability affects mainly the margins of the Arctic Ocean; the seas north of Siberia (the Kara, Laptev, East Siberian and Chukchi Seas), the Canadian Archipelago and the region influenced by the East Greenland Current. Typically the average ice extent (the area covered by ice, including leads and other openings) varies from ~7 x 10^6 km^2 in summer to ~10 x 10^6 km^2 in winter (Polyakov et al., 1999). The offshore motion of sea ice is primarily wind driven with the two dominant features of the ice circulation in the Arctic Basin being the Beaufort Sea Gyre (anticyclonic circulation) and the Transpolar Drift which transports ice across the basin towards Fram Strait (Morison et al., 1998). Significant decreases in recent decades have been observed in the extent and thickness of Arctic sea ice

(Rothrock et al., 2003; Vinnikov et al., 1999). Laxon et al. (2003) qualify these earlier results and suggest that the high interannual variability in mean Arctic ice thickness is dominated by changes in the amount of summer melt. This would lead to further thinning of the Arctic sea ice if the length of the melt season continues to increase.

The ice cover in the Nordic Seas (Figure 2.5) reflects the east-west contrast in hydrographic characteristics. To the east, the Norwegian Sea and much of the Barents Sea remain largely ice free throughout the year (Mauritzen, 1996a). However, in the Greenland and Iceland Seas there is large seasonal and interannual variability in the ice cover. The major sources of sea ice within the Nordic Seas are the export of multiyear ice (typically 3-4m thick) from the Arctic Ocean through Fram Strait, and local sea ice production driven by air-sea fluxes (Brandon and Wadhams, 1999).

Over the region of the Nordic Seas, the areal extent of the sea ice varies seasonally by up to 6×10^5 km^2, a local variation of almost 200% (Gloersen et al., 1992). However, the shelf region of north-east Greenland in the vicinity of Belgica Bank at the western end of Fram Strait, is nearly permanently ice-covered. The ice thins and breaks up in summer, but seldom disperses, although the ice-edge does retreat. Further south, the nearshore bathymetry of East Greenland is too steep for extensive landfast-ice to develop. The marginal ice zone (MIZ) between the pack ice and open water can be ~100 km, consisting of various forms of pancake ice, ice cakes and floes.

A winter ice feature, known as the Odden (Wadhams, 1981), often develops across the southern part of the Greenland Sea, extending eastwards from the East Greenland Current. It develops as an ice tongue in winter over the cold, fresh Jan Mayen Current, which forms the southern limb of the Greenland Sea gyre. Depending on the degree of salinity stratification and atmospheric conditions, the Odden can grow across the entire Greenland Sea. A region of open water, Nordbukta, often exists to the northwest of the Odden, remaining ice free throughout the winter. Depending on conditions, ice formation in the Nordbukta region may eventually lead to brine rejection and deep water formation whereas in the southern part of the Greenland Sea gyre, the ice has been found to be stable and melt water returned locally (Brandom and Wadhams, 1999). Although a regular feature, in recent years there have been some winters in which the Odden has not formed (Comiso et al., 2001).

Vinje et al. (1998) estimate the mean annual ice flux through Fram Strait to be 2850 km^3 yr^{-1}, corresponding to an annual export of 10-20% of the sea ice within the Arctic. During periods of high cyclonic activity in Fram Strait (particularly in winter) it has been suggested that this ice export may be increased by up to 50% of the average (Brummer et al., 2001; Vinje, 2001). The net ice flux may depend as much on the drift speed (due to surface currents and wind fields) as actual ice thickness. An anomalously high export of ice through Fram Strait may have been the cause of the 'Great Salinity Anomaly' (Dickson et al., 1988; Hakkinen, 1993). This was a widespread freshening of the upper 500-800 m of the northern North Atlantic, traceable, as a largely advective

event, around the Atlantic subpolar gyre for over 14 years, from its origins north of Iceland to its return to the Greenland Sea.

Terrestrial ice cover is also an important component of the Arctic environment. The Greenland ice sheet contains the second largest amount of the Earth's ice-locked water (Bigg, 1999) and is relevant to the freshwater balance of the Arctic Ocean and Nordic Seas through the meltwater runoff and calving of icebergs (see section 2.3.4). Recent advances in airborne laser altimetry and global positioning system (GPS) have made possible large-scale assessment of elevation change characteristics of the entire Greenland ice sheet. Krabill et al. (2000) found widespread thinning of the ice sheet below elevations of 2000 m, with rates exceeding 1 m per year close to the coast. The net loss of ice per year from the entire ice sheet is estimated to be ~51 km^3, sufficient to raise sea level by 0.13 mm per year.

2.3.4 Freshwater

The flux of freshwater, influenced by the processes of ice formation and melt, evaporation and precipitation and river runoff, has a central role in ocean circulation and climate change. At high latitudes the density structure is controlled mainly by salinity, and the freshwater flux is of particular significance to the vertical stratification. From the equation of state for seawater at low temperatures, it follows that temperature stratification has very little effect on the density structure (since the thermal expansion coefficient is so small). The introduction of fresh water in the high latitudes can therefore prevent convective overturning even in the case of substantial surface cooling (Aagaard and Carmack, 1989).

The surface layers of the Arctic Ocean receive considerable input of freshwater both from oceanic sources of sea ice melt and continental sources of rivers and glacial melt. Both sources are seasonal, but there is a zero net freshwater contribution from sea ice (due to the melt/freeze cycle) and a positive net contribution from the continental sources. They provide an average freshwater input of 4650 km^3 yr^{-1} although there is significant variability on both annual and interannual time scales. Of this, an estimated 3300 km^3 yr^{-1} is from river runoff (Aagaard and Carmack, 1989; Treshnikov, 1985). There is significant annual and interannual variations in the flows from these Arctic rivers (Cattle, 1985), with the interannual flow variability in individual rivers typically 5–20% of the annual mean. In addition to these inputs, 1500–2000 km^3 yr^{-1} enters as the freshwater fraction of the Bering Strait inflow (Coachman and Aagaard, 1974). A number of studies have used hydrographic and tracer data (salinity, nutrients, dissolved oxygen and $\delta^{18}O$), to quantify the components of Arctic freshwater: river runoff, sea ice meltwater and Pacific water (Bauch et al., 1995, Ekwurzel et al., 2001). The remaining component of the Arctic freshwater balance is the estimated input from precipitation less evaporation (P–E). There is considerable uncertainty in estimates of this flux, but is suggested to be in the region of 900 km^3 yr^{-1} (Aagaard and Carmack, 1989).

The export of freshwater from the Arctic Ocean through Fram Strait provides the largest contribution of freshwater to the Nordic Seas. It is linked to the northern hemisphere thermohaline circulation particularly in its influence on, and potential control of, deep water formation. This contribution (through both ice and liquid water) is estimated to be in the region of 4000 $km^3 yr^{-1}$ (Aagaard and Carmack, 1989). Meredith et al., (2001) used hydrographic and $\delta^{18}O$ sections across Fram Strait (August - September 1997, 1998) to examine the freshwater contributions to the EGC. They derived meteoric water fluxes of ~3680 $km^3 yr^{-1}$ in 1997, and ~2000 $km^3 yr^{-1}$ in 1998. They found the ratio for the mean summer fluxes through Fram Strait of meteoric water to sea ice to be ~2:1. In this, they differ from the Aagaard and Carmack (1989) annual budget of the Arctic and Nordic seas which included sea ice as the largest contribution to the freshwater export through Fram Strait. Interannual variability and apparent correlation with processes such as the NAO and changing cyclonicity of the Arctic circulation could be a factor in this discrepancy (Proshutinsky and Johnson, 1997; Vinje et al., 1998). Meredith et al. (2001) also found a large volume of meteoric water on the East Greenland shelf which may prove to be a significant contributor to the overall freshwater flux through Fram Strait. Given the importance of the Fram Strait freshwater flux to the regional and global climates, it is important to understand the variability in both the solid and liquid phases of export (ice and water) and to determine the relative contributions of sea ice and meteoric water to the overall freshwater flux.

The land masses of Norway, Greenland and Iceland contribute a total runoff to the Nordic Seas of ~545 $km^3 yr^{-1}$. This estimate is based on ~350 $km^3 yr^{-1}$ runoff along the Norwegian coast (Aagaard and Carmack, 1989), ~133 $km^3 yr^{-1}$ from iceberg calving along the east Greenland coast (Hardy et al., 2000), and ~62 $km^3 yr^{-1}$ runoff from the north coast of Iceland (Stefansson, 1962). The contribution to the annual fresh water flux from P-E is not well quantified but is estimated to be in the region of 790 km^3 from the Gorshkov (1983) atlas. Although not a dominant factor, it does represent ~13% of the total freshwater input to the Nordic Seas. The final contribution is the input of freshwater from the Baltic Seas through the Skagerrak via the Norwegian Coastal Current. This is estimated to be ~950 $km^3 yr^{-1}$ (Aagaard and Carmack, 1989).

Although the exchanges of freshwater in the Nordic Seas are known to be important processes, large-scale estimates of oceanic transports of freshwater north of the Greenland-Scotland Ridge are rare. Estimates have been limited mainly to budget calculations (e.g. Aagaard and Carmack, 1989), although Oliver and Heywood (2003) estimated a summer freshwater transport between Norway and Greenland of 0.10 ±0.05 Sv away from the Arctic, and Bacon (1997) derived an estimate of the freshwater flux between Greenland and the European continental shelf which calculates an estimated net freshwater gain by the Arctic of 0.17±0.06 Sv.

2.4 Circulation Hypotheses

Various scenarios have been proposed for the circulation of the Nordic Seas and Arctic Ocean, and for the consequent production of deep water and formation of overflow waters, but the precise pathways and mechanisms remain largely undetermined.

To begin with, in order to adequately describe the circulation of the Nordic Seas and to consider the formation mechanisms of the overflows, it is important to differentiate between the different water masses. As Mauritzen (1999a) discussed, this can be problematic in the Nordic Seas. In particular, high interannual variability means that waters from the same source will not necessarily have the same characteristics each year. Swift and Kolterman (1988) observed that Norwegian Sea Deep Water (NSDW), not all of which actually enters the Norwegian Sea, was "*named by virtue of characteristics rather than location*". The situation is further complicated by the lack of a consensus in the conventions used to name water masses within the Nordic Seas, with different terms being used to describe waters with the same hydrographic characteristics. Mauritzen (1999a) based her water mass definitions on persistent extrema apparent in hydrographic profiles. These extrema are observed within the same density range in different data sets and years and the existence of a core implies circulation (an advective supply). To make a synthesis of terms found in the literature, initial divisions into Atlantic Water (AW), Polar Water (PW), Intermediate Water (IW) and Deep Water (DW) are followed here. A full description of these water masses is given in Table 2.1, and the conventions followed in thesis are specified in Chapter 5 (Table 5.1).

2.4.1 Atlantic Waters

Atlantic Water (AW) can be recognised by maxima in temperature and salinity (Table 2.1a). This core includes the waters entering the Nordic Seas in the Norwegian Atlantic Current and Irminger Current, the Atlantic waters recirculating in Fram Strait, and the Atlantic layer found in the Arctic Ocean. In the vicinity of the Faroe Islands (i.e. in the region of the major inflows across the Greenland-Scotland Ridge) AW has temperatures between about 8 and 10°C and salinities between about 35.2 and 35.34 (Fogelquist et al., 2003). Saunders (2001) also defines a North Atlantic Water (NAtlW; 9.5 < θ < 10.5°C and 35.35 < S < 35.45) and a slightly cooler and fresher Modified North Atlantic Water (MNAW; 7.0 < θ < 8.5°C and 35.10 < S < 35.3) in the region of the Greenland-Scotland Ridge. These Atlantic waters are significantly cooled during their passage through the Nordic Seas. Within the Atlantic domain of the Nordic Seas (Norwegian and Lofoten Basins) the core of these waters is characterised by a maximum temperature of >3.0°C and a maximum salinity >35 (Mauritzen, 1996a). Although a salinity of >35 is the common definition of AW in the Nordic Seas (Helland-Hansen and Nansen, 1909), it requires a fresher definition in the Barents Sea Opening since the temperature and salinity of AW decrease along its northward path. Within Bjørnøyrenna and Storfjordrenna (the channels connecting to the Barents Sea), the core of AW is identified as the

salinity maximum (salinity > 34.95) with □□□□2°C. The density of AW increases to about □$_0$□□27.9 before it reaches Fram Strait, and is found at a temperature range of 1.5□□2.5°C in the West Spitsbergen Current (Rudels and Quadfasel, 1991).

Return Atlantic Water (rAW) (0□□□□2°C; S□□34.9) is water of Atlantic origin which has recirculated into the EGC from both within Fram Strait and via the Atlantic layer in the Arctic Ocean. It is found at depths between 300□and 500m in the EGC underlying the Polar Water (PW), and exits the Nordic Seas through Fram Strait (Mauritzen, 1996a). Rudels and Quadfasel (1991) also defined this water mass as the recirculating Atlantic signal in Fram Strait (0□□□□1°C; S□□34.91). Swift (1986) defined the same water mass as lower Intermediate Arctic Water (lIAW; □□0°C and S□□34.9) again found at depths between 100 and 800m in the EGC.

A third Atlantic type water mass is defined as Arctic Atlantic Water (AAW; 0□□□□0.5°C; 34.8□□S□□34.9), an intermediate water mass of Arctic origin formed from the transformation of AW within the Arctic Ocean (Mauritzen, 1996a). It is found in the EGC, again below the PW, with properties between PW and rAW, but as a distinct outflow rather than the product of mixing. This water mass, originating from the Atlantic Layer in the Arctic Ocean, was also defined by Rudels and Quadfasel (1991), but called Modified Atlantic Water (MAW; 0□□□□1°C; 34.4□□S□□34.91).

2.4.2 Polar Waters

Polar Waters (PW) are the cold, fresh Arctic surface waters which eventually exit the Nordic Seas in the East Greenland Current via Denmark Strait (Table 2.1b). They are characterised by temperatures below 0°C and a minimum in salinity (S□□34.4) (Aagaard and Coachman, 1968; Mauritzen, 1999a; Rudels and Quadfasel, 1991; Swift and Aagaard, 1981). The actual salinities are variable due to the influence of melting ice and the contribution of Arctic Ocean surface water (Malmberg, 1972), although there is little seasonal variation when found in the Iceland and Greenland Seas (Swift and Aagaard, 1981).

Swift and Aagaard (1981) defined a further water mass, Arctic Surface Water (ASW), which overlies the Arctic Intermediate Water in summer. They describe it as being formed by summer heating and freshened by mixing with PW (□□0°C; 34.4□□S□□34.9).

2.4.3 Intermediate Waters

Intermediate Waters (IW) (Table 2.1c) are characterised by a minimum in salinity and a maximum in oxygen. It is in these waters masses at intermediate depths where some of the greatest confusion lies.

Polar Intermediate Water (PIW) is represented by a temperature minimum (□□0.0°C; 34.4□□S□□34.7) and is found beneath the upper waters of the EGC. It is distinguished from other Nordic Sea intermediate water masses mainly by its geographic distribution (Fogelqvist et al.,

2003). Malmberg et al. (1972) described it as being formed by mixing between PW and AIW at the Polar Front as far north as the Greenland Sea, and Swift and Aagaard (1981) differentiated it from upper Arctic Intermediate Water (uAIW) by virtue of its location in the western Iceland Sea.

Arctic Intermediate Water (AIW), in particular, has been subject to a range of definitions by different authors. Stefansson (1962) defined it as the water mass lying above Norwegian Sea Deep Water (NSDW; 0□□ < 2°C, 34.8□□□□35.0), formed by the cooling of saline AW and mixing with NSDW and the fresh PW. Ross (1984) gave it a cooler and narrower definition (-0.1□□ < 0.9°C, 34.65□□□□34.95). A similar, but fresher, definition was given by Mann (1969) to the IW to the north of Denmark Strait (0.0□□ < 1.0°C, 34.5□□□□34.94). Similarly, Aagaard and Coachman (1968) described an Atlantic IW, to the north of Denmark Strait, below the PW in the EGC (□□0.0°C, S□□35.0). The upper Arctic Intermediate Water (uAIW; (□ < -1.0°C, 34.7□□□□34.9) of Swift et al. (1980) is the Iceland Sea Arctic Intermediate Water (ISAIW) of Fogelqvist et al., (2003), mainly formed by winter convection in the northern and central part of the Iceland Sea and mixed with similar intermediate water derived from the Greenland Sea. The warmer part of this IW water mass, lower Arctic Intermediate Water (lAIW; 0.0□□ < 3.0°C, S□□34.9) is found above NSDW at the sill of Denmark Strait (Swift et al., 1980), and corresponds to previous definitions of rAW. Norwegian Sea Arctic Intermediate Water (NSAIW; -0.5□□ < 0.5°C, 34.87□□□□34.9) (Saunders, 2001) is advected from the Greenland and Iceland Seas into the Norwegian Sea where it occurs in a layer characterised by a salinity minimum between the Atlantic Water and the Deep Waters. Saunders (2001) also defined a Modified East Icelandic Water (MEIW; 1.0□□ < 3.0°C, 34.7<□□□□34.9) in the southern part of the Norwegian Sea. The IW of Mauritzen (1996a), with salinity < 34.9, is characterised by a high oxygen content and originates in the gyres of the Greenland and Iceland Seas. It is sandwiched between AW and DW in the Atlantic domain of the Nordic Seas (central/eastern Norwegian Sea) (corresponding to other definitions of NSAIW and MEIW) and also between rAW and DW to the west of the Greenland Sea at depths of about 1000m in the EGC, too deep to exit via Denmark Strait (corresponding to definitions of uAIW).

2.4.4 Deep Waters

Deep Waters (DW; Table 2.1d) with temperatures < 0.0°C, are generally characterised by a maximum in salinity and minimum in oxygen (Aagaard and Coachman, 1968; Mauritzen, 1996a). According to Mauritzen (1996a) the source of these deep waters is AW, cooled during its passage through the Barents Sea, and further modified during its circulation of the Arctic Ocean. They are found in the Atlantic domain (central/eastern Norwegian Sea) and underlying IW in the Greenland Sea (at depths too great to enter the Iceland Sea).

Greenland Sea Deep Water (GSDW; 1.2□□ <□1.0°C) is described as a uniform water mass formed by deep winter convection, and confined to the central Greenland Sea Gyre and found at depths

below 500m (Mauritzen, 1996a; Metcalf, 1960; Swift, 1986). Swift (1986) also noted its high oxygen content (7.26 ml/l; θ ~ -1.242°C; S ~34.895).

True NSDW (θ ~ -1.03°C; S ~34.91) is found at depths greater than ~2500m in the Norwegian Sea (Fogelqvist et al., 2003). However, Aagaard et al. (1985) defined NSDW as a mixture of Arctic Ocean Deep Water (AODW) and GSDW. Similarly, Swift and Kolterman (1988) described it as a 2:1 mixture of Eurasian Basin Deep Water (EBDW) and GSDW, with a fairly high oxygen content (6.76 ml/l), and suggested that some, but not all, of this water mass enters the Norwegian Sea through gaps in Mohns Ridge. NSDW appears to be a widespread water mass and not confined to the Norwegian Sea; it was described at Fram Strait by Quadfasel et al. (1988), in the Iceland Sea by Swift et al. (1980) (θ ≤ 0.0°C; 34.90 ≤ S ≤ 34.92), and on a section to the north of Denmark Strait near the sill by Mann (1969) and Swift et al. (1980) (S ~ 34.925 ± 0.01). Swift et al. (1980) also described it as Arctic Bottom Water (ABW), which fills the Iceland Sea up to a depth of 500m, and whose ultimate source is the Greenland Sea. Iceland Sea Deep Water (ISDW) is described as a similar water mass to NSDW, but with higher salinity due to a larger admixture of deep water from the Arctic Ocean (Buch et al., 1996).

Arctic Ocean Deep Water (AODW; θ ≤ 0.8°C; 34.90 ≤ S ≤ 34.94) is described by Dickson et al. (1996) to be formed by slope convection as dense waters on the Arctic shelves (formed by brine rejection during ice formation) entrain the intermediate AW layer. Strass et al. (1993) described a modified AODW (-1.2 ≤ θ ≤ -0.5°C; S ~ 34.9) in the EGC on the continental slope at depths between 1000 and 2500m, which has been advected from the Arctic Ocean through Fram Strait. This water mass of Arctic origin, found in Fram Strait below 2000m, is also known as Upper Polar Deep Water (UPDW; -0.5 ≤ θ ≤ 0.0°C; 34.90 ≤ S ≤ 34.92) (Rudels and Quadfasel, 1991), and subdivided into EBDW (-0.8 ≤ θ ≤ -0.5°C; S ~ 34.92) (Rudels and Quadfasel, 1991; Swift and Koltermann, 1988) and Canadian Basin Deep Water (CBDW) (Rudels and Quadfasel, 1991).

2.4.5 Overflow Waters

The characteristics of the waters forming the Greenland-Scotland overflows are considered in Table 2.1e. Denmark Strait Overflow Water (DSOW) is an intermediate water mass that exits the Nordic Seas via Denmark Strait and then entrains the ambient waters of the North Atlantic as it sinks to depth in the Irminger Basin. It is generally defined as θ ≤ 2.0°C and S ≤ 34.94 (Mann, 1969). Rudels et al. (1999) and Dickson et al. (1990) refer to waters with σ_0 ≥ 27.85 and σ_0 ≥ 27.80, respectively. Swift et al. (1980) assigned a tighter definition (0.0 ≤ θ ≤ 1.0°C; 34.8 ≤ S ≤ 34.9; 27.95 ≤ σ_0 ≤ 28.0), and described its primary source as uAIW. There is, as yet, no consensus on the formation of DSOW. Strass et al. (1993) have suggested it to be formed by isopycnal mixing in the EGC, with a 50% contribution from AW (recirculated within Fram Strait) and a 50% contribution from AIW. Mauritzen (1996b) proposed 85% to be derived from rAW and 15% from waters in the Greenland and Iceland Sea gyres. The Iceland-Scotland Overflow Water (ISOW; 2.7 ≤ θ ≤ 2.9°C;

S□34.92) flows mainly through the Faroe Bank Channel (Fogelqvist et al., 2003) and is transported into the Irminger Basin around the Reykjanes Ridge, mainly through the Charlie-Gibbs Fracture Zone (Saunders, 2001). Mauritzen (1996b) suggested ISOW originates mainly from the lightest NSDW in the Norwegian Sea, itself formed from AW cooled in the Barents Sea which subsequently exits the Arctic Ocean through Fram Strait and circulates the Greenland Sea without interacting with the gyre.

2.4.6 DSOW formation mechanisms

Traditional circulation schemes suggest that uAIW forms the major component of DSOW (Strass et al, 1993; Swift et al., 1980). Swift et al. (1980) were among the first to realise that DSOW is an intermediate water mass. They identified water masses just upstream of Denmark Strait as uAIW, lAIW and NSDW. Considering property comparisons they reasoned that only uAIW, formed during deep winter mixing in the Iceland Basin, was exported through Denmark Strait. Smethie and Swift (1989) proposed the densest part of the overflow originated from intermediate waters in the Greenland Sea, rather than the Iceland Sea, due to its greater age.

Aagaard et al. (1991) noted that the less dense deep waters of the Arctic Ocean present in Fram Strait are carried into the western Iceland Sea in the EGC. Similarly, Buch et al. (1996) observed Arctic Ocean deep waters in Denmark Strait, and suggested they may contribut to the formation of DSOW.

Strass et al. (1993) proposed that DSOW is formed by mixing of return Atlantic Water (rAW) recirculated in Fram Strait and Arctic Intermediate Waters, between the eastern edge of the EGC and the western edge of the Greenland Sea gyre. This scenario supports the argument put forward by Swift (1997) that the oxygenation of the EGC between the Fram and Denmark Straits can only be explained by an input of AIW from the convective gyres.

A radical alternative was proposed by Maurizen (1996a and 1996b), who presented a picture of Nordic Sea circulation in which the northward flowing Atlantic waters undergo major transformations during winter heat loss until their density is sufficient to provide the DSOW. She suggests that cooled North Atlantic Water (NAW) contributes to 85% of the DSOW, the remaining 15% being provided by intermediate waters formed in the convective gyres of the Greenland and Iceland Seas. Her argument is that the steadiness of the overflow over long time periods requires a source more constant than the varying convection of the Greenland and Iceland Seas, and her study showed that the air-sea fluxes could not sustain the required conversion rates of Swift and Aagaard (1981). Some NAW is described as following an extended loop through the high Arctic, while some recirculates westwards within Fram Strait. Both branches return southwards in the fast flowing EGC, as Arctic Atlantic Water (AAW) and rAW respectively. The primary component of DSOW would therefore be AAW, whose properties would have been set during its circulation of the Nordic Seas and Arctic Ocean. In other words, NAW is transformed by a major increase in density in the

Norwegian Sea, while its salinity is reduced either by freshwater input in the Arctic, or by interaction with AIW as it flows south in the EGC.

Another alternative was given by Rudels et al. (1999), who suggested that DSOW is composed of NAW, AIW and Arctic Ocean Deep Water (AODW) in equal parts. In this case, of the waters contributing to North Atlantic Deep Water, 40% would be supplied by the Arctic Ocean and 60% by the Nordic Seas. They proposed that most of the recirculating Atlantic Water is transformed by winter cooling and freezing, in the Greenland and Iceland Seas, into dense but less saline AIW. Rudels et al. (2002) revise these earlier thoughts, proposing that the EGC supplies most of the DSOW, with the remainder is derived from the Iceland Sea, and mixes with the EGC water masses to the north of Denmark Strait. Under these circumstances, two water masses would be created in the EGC by isopycnal mixing, firstly between rAW and AAW, and secondly between UPDW and AIW. These would be homogenised by diapycnal mixing at the sill in Denmark Strait. The last component of the upper part of DSOW would then be PIW, whose source is the thermocline at 150□□250□m in the Arctic Ocean.

There is evidence that the balance of horizontal and vertical exchanges within the Nordic Seas has changed over time (Dickson et al., 1996). It is therefore possible that the various scenarios proposed have all been implicated to some degree in the general circulation of the Nordic Seas and that their contributions have changed with time.

2.5 High Latitude Climate Change

There have been significant changes in the ocean climate of the North Atlantic and Arctic regions over recent decades, such as the freshening of the deep North Atlantic Ocean (Dickson et al., 2002) and decreased deep overflow in the Faroe Bank Channel (Hansen et al., 2001). The relationship between polar oceanography and climate suggest that the Arctic and sub-arctic regions may be particularly sensitive to global climate; climate models indicate global warming may occur more rapidly in the northern high latitudes due to complex feedback mechanisms in the atmosphere-ocean-ice system (Bengtsson et al., 2004; Johannessen et al., 2004).

The predicted warming in high latitude regions by the end of the century is of the order 3–4°C, at least 40% greater than the global mean (Johannessen et al., 2004). This estimate was made by the Intergovernmental Panel on Climate Change (IPCC, 2001), which also predicts that the central Arctic Ocean might be nearly ice-free during summer by the end of the century. Indeed, recent late summer research cruises have found surprisingly little ice in some areas of the Arctic Ocean (Woodgate, 2002, pers. comms.) and a record minimum Arctic sea ice extent was observed in 2002 (Serreze et al., 2003).

There is mounting observational evidence for significant climate change within the northern high latitudes. Recent overviews of such data indicate a coherent picture of recent change, including sea

ice, snow cover, river discharge, glaciers, permafrost and air temperature (Serreze et al., 2000). Since the late 1980s the Arctic Ocean has undergone major changes in surface pressure field, wind stress and surface heat exchange (Walsh et al., 1996). Significant decreases have also been observed in the extent and thickness of Arctic sea ice (Rothrock et al., 2003; Vinnikov et al., 1999). Laxon et al. (2003) find that the high interannual variability in mean Arctic ice thickness is dominated by changes in the amount of summer melt suggesting that continued increase in melt season length will lead to further thinning of the Arctic sea ice.

Comparison of ice flux variability with the evolution of the mean salinity structure in Greenland Sea Gyre in 1990s suggested the salinity distribution in the upper 800m of the convective region has been influenced by the ice flux variability (Bonisch et al., 1997). Within the Greenland Sea, reductions in deep water formation have been suggested by tracer data (Schlosser et al., 1991) and within the western Norwegian Sea a long trend of freshening within the upper layers since the 1960's has been detected (Blindheim et al., 2000).

It remains open to debate whether recent warming is a consequence of natural climate variability or a response to external factors such as anthropogenic greenhouse gas forcing (Polyakov et al., 2002). Johannessen et al. (2004) concluded, however, that there are strong indications that neither the recent warming trend nor the decrease in ice extent and volume over the past two decades can be explained by natural processes alone. Their study used multi-decadal data (surface air temperature, sea-ice extent, area and thickness) in combination with coupled atmosphere-ice-ocean simulations (using state of the climate models ECHAM4 and HadCM3) to investigate the degree to which changes in the Arctic might be attributed to natural variability or anthropogenic external factors, and the degree to which anthropogenic forcing may induce the Arctic sea-ice cover to decrease.

Modelling studies suggest that global warming may result in amplified temperature increases and enhanced precipitation at high latitudes, resulting in a freshening of the upper Arctic Ocean (Manabe et al., 1991). Numerical simulations have suggested such upstream freshwater anomalies can perturb the North Atlantic thermohaline circulation (Griffies & Bryan, 1997). It is possible that a weakening of the THC may be implicated in the response of the climate system to greenhouse warming (Rahmstorf, 1996). Simulated water transport for a range of global warming scenarios in a wide range of general circulation climate models (GCM's) have shown significant weakening of the flow associated with the THC. At present, at a latitude of 25°N, the North Atlantic Ocean carries $1.2 \pm 0.2 \square 10^{15}$ W of heat northwards (Hall and Bryden, 1982). This provides western Europe with its relatively mild climate (5 to 10 degrees warmer than elsewhere at the same latitude) (Rahmstorf, 1999). Rhamstorf (1995 and 1996) suggested that even local changes in the freshwater flux may shut down local deep convection and induce transitions between different climatic equilibrium states.

High latitude climate change may have significant implications extending beyond the central Arctic. The energy balance and atmospheric and oceanic circulations of the high latitudes may be affected

by a reduction in albedo through increased areas of open water. Large-scale changes in the marine ecosystems may occur due to a reduction in ice cover and a resultant increase in the freshwater flux would impact on arctic and subarctic marine biodiversity. Changes in the pathways and spreading of melt water and in the stratification in the Nordic Seas, and the effects of reduced deep-water formation in the Greenland Sea on the global thermohaline circulation could greatly alter the regional (and European) climate of the northern latitudes.

2.6 Aims of this Thesis

The circulation of the Nordic Seas is a key element of the global climate system. If high latitude warming and subsequent ice melt can 'cap' the deep water formation processes and slow down the THC, this would have severe consequences for the global climate, and European climate in particular. Elucidating the variability in water mass properties and circulation of the Nordic Seas and the implications for the formation and long-term variability of the dense northern overflows will enhance understanding of the possible effects of high latitude climate change for both ocean-atmosphere heat exchange and freshwater influence on the thermohaline circulation.

The current understanding of the Nordic Seas circulation is based on information from a variety of sources; one-time and repeated hydrographic sections, long-term current meter measurements in specific regions, surface drifters and satellite coverage (SST, sea-level height, ice extent and motion). Some aspects of the circulation have been relatively well characterised, for example the seasonal fluxes through Denmark Strait and Fram Strait, across the Iceland-Scotland Ridge, and between the Nordic Seas and the Barents Sea. Sections off the Norwegian coast (Svinøy and Gimsøy) and at 75°N have also quantified the fluxes within the NAC and EGC respectively. Measurements made at the Norwegian Ocean Station Mike, for example, also give some an indication of the long-term trends in temperature and salinity within the Norwegian Sea.

This thesis uses a combination of synoptic hydrographic measurements and concurrent direct velocity measurements, across the entire Nordic Seas, together with inverse methods, to provide a novel quantification of the mean summer flux field (volume, heat and freshwater) over the entire region of the Nordic Seas. In particular, the exchanges between the Nordic Seas and the Arctic Ocean to the north, the Barents Sea to the east, and North Atlantic to the south, via the North Atlantic Current inflow and the Denmark Strait and Iceland-Scotland overflows are determined. From these synoptic flux estimates some details of the interior circulation of the Nordic Seas can be resolved. In addition, the combination of these new mean summer flux estimates and the winter data (over a reduced region) allows an estimate of true annual mean circulation to be made.

There are still many outstanding questions concerning the circulation of the Nordic Seas; the importance of deep convection within the Nordic Seas, the formation mechanisms of the dense northern overflows, the annual heat loss over the Nordic Seas, the annual freshwater flux between

the Nordic Seas (and Arctic) and the North Atlantic. While not providing conclusive answers, this thesis is able to address these questions and shed light on the interior circulation of the Nordic Seas.

Atlantic Waters of the Nordic Seas				
Water Mass	**Potential Temperature (°C)**	**Salinity**	**Author**	**Location or Source** [σ_0]
Atlantic Water (AW)	maximum (>3.0)	maximum (>35.0)	Mauritzen (1996a)	Atlantic Domain [27.4 to 27.8] cooled by coastal waters in NS before reaching FS [27.9]
	1.5 to 2.5	35.0 to 35.1	Rudels and Quadfasel (1991)	in West Spitsbergen Current
	6.0 to 8.0 (expanded to > 3.0)	35.1 to 35.3 (expanded to >□4.0)	Swift and Aagaard (1981)	
North Atlantic Water (NAW) *Modified North Atlantic Water (MNAW)*	9.5 to 10.5 7.0 to 8.5	35.35 to 35.45 35.10 to 35.30	Saunders (2001) Saunders (2001)	
Arctic Atlantic Water (AAW)	0.0 to 0.5	34.8 to 34.9	Mauritzen (1996a)	defines **IW** of AO origin (whereas **AIW** is formed in GS & IS); formed from transformation of **AW** in AO along isopycnals; flows in EGC below **PW**; properties are between **PW** and **rAW** but is distinct outflow rather than product of mixing
Modified Atlantic Water (MAW)	0.0 to 1.0	34.4 to 34.91	Rudels and Quadfasel (1991)	Atlantic Layer in AO
return Atlantic Water (rAW)	maximum	> 34.9	Mauritzen (1996a)	**AW** from FS recirculation; GCS Domain; 300 to 500m depth in EGC underlying **PW**; exits DS (no signal in IS)
	0.0 to 1.0	> 34.91	Rudels and Quadfasel (1991)	FS (recirculating Atlantic Signal)
lower Arctic Intermediate Water (lAIW)	core > 0.0	core > 34.9	Swift (1986)	100 to 800m depth in EGC; **AW** cooled in NS and GS

Table 2.1a: Atlantic Waters of the Nordic Seas.

NS is Norwegian Sea; GS is Greenland Sea; DS is Denmark Strait; FS is Fram Strait; AO is Arctic Ocean; EGC is East Greenland Current;
GCS Domain is off the shelf of Greenland, west of the Greenland Sea Gyre, from Fram Strait to the Jan Mayen Fracture Zone; Atlantic Domain is the Norwegian Sea east of Mohns Ridge
IW is Intermediate Water, **AIW** is Arctic Intermediate Water, **PW** is Polar Water, **rAW** is return Atlantic Water

Polar Waters of the Nordic Seas				
Water Mass	**Potential Temperature (°C)**	**Salinity**	**Author**	**Location or Source** [σ_θ]
Polar Water (PW)	n/a	minimum (<34.5)	Mauritzen (1996a)	cold, fresh surface layer from AO; surface layer of EGC; GCS Domain; high oxygen [<27.8]
	< 0.0	any water < 34.4	Swift and Aagaard (1981)	little seasonal variation when in IS and GS; advected south in EGC from AO
	n/a	< 34.4	Rudels and Quadfasel (1991)	surface waters in EGC north of DS
	< 0.0	n/a	Aagaard and Coachman (1968)	
Arctic Surface Water (ASW)	> 0.0 > 2.0	34.4 to 34.7 34.7 to 34.9	Swift and Aagaard (1981)	formed from summer heating and freshened by mixing with **PW**; overlies **AIW** in summer

Table 2.1b: Polar Waters of the Nordic Seas

AO is Arctic Ocean; EGC is East Greenland Current; IS is Iceland Sea; GS is Greenland Sea; DS is Denmark Strait;
GCS Domain is the Greenland Continental Slope, off the shelf of Greenland, west of the Greenland Sea Gyre, from Fram Strait to the Jan Mayen Fracture Zone;
AIW is Arctic Intermediate Water

Intermediate Waters of the Nordic Seas				
Water Mass	**Potential Temperature (°C)**	**Salinity**	**Author**	**Location or Source** [σ_θ]
Polar Intermediate Water (PIW)	< 0.0	34.4 to 34.7	Malmberg et al. (1972)	formed by mixing between **PW** and **AIW** at Polar Front as far north as GS
	< 0.0	34.4 to 34.7	Swift and Aagaard (1981)	western IS; distinguished from **uAIW** by location
	< 0.0	< 34.7	Stefansson (1962) Malmberg et al. (1972)	less saline than **AIW**
Arctic Intermediate Water (AIW)	0.0 to 2.0	34.8 to 35.0	Stefansson (1962)	defined as water above **NSDW**; formed by cooling of saline **AW** and mixing with **NSDW** (and fresh **PW** to lesser extent)
	-0.1 to 0.9	34.65 to 34.95	Ross (1984)	
	0.0 to 1.0	34.5 to 34.94	Mann (1969)	**Intermediate Water**; just north of DS
	> 0.0	up to 34.88 to 35.0	Aagaard and Coachman (1968)	**Atlantic IW** below **PW** in EGC, north of DS
Norwegian Sea AIW (NSAIW) *Modified East Icelandic Water(MEIW)*	-0.5 ± 0.5 1.0 to 3.0	34.87 to 34.90 34.70 to 34.90	Saunders (2001)	**Norwegian Sea AIW** **Modified East Icelandic Water**
see(**rAW**) *lower AIW (lAIW)* *upper AIW (uAIW)*	< 2.0 (warmer part; 0.0 to 3.0) (colder part □ -1.0)	34.7 to 35.0 > 34.9 34.7 to 34.9	Swift et al. (1980)	at DS sill; from EGC and central IS above **NSDW** at sill; from EGC; **AW** cooled in NS and GS in EGC and central IS (principle winter product of IS)
Intermediate Water (IW)	n/a	minimum (<34.9)	Mauritzen (1996a)	source is interior of GS and IS gyres, high oxygen content; Atlantic Domain between **AW** and **DW** [~28.0] west of GS between **rAW** and **DW**; - exit GS to west, ~1000m in EGC so cannot exit DS - exit GS to east, in NS above FBC sill depth

Table 2.1c: Intermediate Waters of the Nordic Seas

GS is Greenland Sea; IS is Iceland Sea; DS is Denmark Strait; EGC is East Greenland Current; NS is Norwegian Sea; FBC is Faroe Bank Channel; Atlantic Domain is the Norwegian Sea east of Mohns Ridge; Atlantic Domain is the Norwegian Sea east of Mohns Ridge;

PW is Polar Water, (**r**)**AW** is (return) Atlantic Water; **DW** is Deep Water; **NSDW** is Norwegian Sea Deep Water

Deep Waters of the Nordic Seas				
Water Mass	**Potential Temperature (°C)**	**Salinity**	**Author**	**Location or Source [σ_0]**
Deep Water (DW)	n/a	maximum	Mauritzen (1996a)	Atlantic Domain; GCS Domain underlying **IW**; too deep to enter IS (cyclonic flow round GS); minimum in oxygen source is **AW** cooled through Barents Sea before entering AO
	< 0.0	34.87 to 34.95	Aagaard and Coachman (1968)	below 800m in EGC north of DS
Greenland Sea Deep Water (GSDW)	-1.242	34.895	Swift and Kolterman (1988)	high oxygen (7.26 ml/l)
	-1.2 to -1.0	34.88 to 34.9	Swift (1986)	all depths below 500m in deep GS; uniform water mass formed by deep winter convection in GS gyre
	< -1.0	n/a	Metcalf (1960)	confined to central GS gyre
	-1.2	34.89	Mauritzen (1996a)	GG Domain; [28.0 almost to surface even in summer]
Norwegian Sea Deep Water (NSDW)	< 0.0	~34.92	Swift et al. (1980)	
	-0.1	34.95	Ross (1984)	
	< - 0.5	34.91	Saunders (2001)	
	< 0.0	34.92 to 34.93	Mann (1969)	from section to north of DS
	n/a	n/a	Aagaard et al. (1985)	formed from **AODW** and **GSDW**
	-1.048	34.910	Swift and Kolterman (1988)	fairly high oxygen (6.76 ml/l); formed from 2:1 isopycnal mixing of **EBDW** and **GSDW**; some, not all, enters NS through Mohns Ridge; *"named by virtue of characteristics rather than location"*
	< 0.0 < 0.0	34.90 to 34.94 34.90 to 34.92 34.925 ± 0.01	Swift et al. (1980)	narrow salinity range; also known as **Arctic Bottom Water**; ultimate source is GS; fills IS up to depth of 500m characteristics at DS sill characteristics in IS
	-1.0	34.9	Rudels and Quadfasel (1991)	

Arctic Ocean Deep Water (AODW)	< -0.8	34.92 to 34.94	Dickson et al. (1996)	formed by 'slope convection' as dense shelf water (from brine rejection during ice formation) entrain intermediate **AW** layer
Modified (AODW)	-1.2 to -0.5	> 34.9	Strass et al. (1993)	1000 to 2500m in EGC on western side of continental slope; advected from AO through FS
(UPDW)	-0.5 to 0.0	34.90 to 34.92	Rudels and Quadfasel (1991)	**Upper Polar Deep Water**; AO origin; found in FS
Eurasian Basin Deep Water (EBDW)	-0.186	34.925	Swift and Kolterman (1988)	from AO; found below 2000m in FS
	-0.8 to -0.5	> 34.92	Rudels and Quadfasel (1991)	in FS; of AO origin
Canadian Basin Deep Water (CBDW)	-0.8 to -0.5	> 34.92	Rudels and Quadfasel (1991)	in FS; of AO origin

Table 2.1d: Deep Waters of the Nordic Seas

GS is Greenland Sea; AO is Arctic Ocean, EGC is East Greenland Current; DS is Denmark Strait; NS is Norwegian Sea; IS is Iceland Sea, FS is Fram Strait;
Atlantic Domain is the Norwegian Sea east of Mohns Ridge;
GG Domain is the Greenland Gyre Domain, the abyssal plain bounded by Mohns Ridge, the Greenland Slope and the Jan Mayen Fracture Zone
GCS Domain is the Greenland Continental Slope, off the shelf of Greenland, west of the Greenland Sea Gyre, from Fram Strait to the Jan Mayen Fracture Zone;
IW is Intermediate Water; AW is Atlantic Water

Overflow Waters of the Nordic Seas				
Water Mass	**Potential Temperature (°C)**	**Salinity**	**Author**	**Location or Source [σ_0]**
Denmark Strait Overflow Water (DSOW)	0 to 1.0	34.8 to 34.9	Swift et al. (1980)	primary contribution is **uAIW** [27.95 to 28.0]
	< 2.0	n/a	Rudels et al. (1999)	[> 27.85]
	n/a	n/a	Dickson et al. (1990)	[≥ 27.80]
	0.4 to 2.0	34.8 to 34.9	Mauritzen (1996a)	formed from 85% **rAW** and 15% waters from GS & IS gyres
	to 1.0	34.8 to 34.9	Strass et al. (1993)	formed by isopycnal mixing in EGC (50% **AW** from FS recirculation; 50% **AIW**)
	< 2.0	< 34.94	Mann (1969)	
Faroe Bank Channel Overflow Water	2.7 to 2.9 S	~34.92	Fogelqvist et al. (2003)	
	-0.7 to 3.0	34.9 to 35.1	Saunders (2001)	
	n/a	n/a	Mauritzen (1996a)	lightest **NSDW** in NS; formed from **AW** cooled in Barents Sea, exits AO through FS, circulates GS without interacting with the gyre
North Icelandic Winter Water (NIWW)	n/a	n/a	Stefansson (1962)	**North Icelandic Winter Water**; formed from cooling of **AW** entering IS through DS, enters NS via East Icelandic Current

Table 2.1e: Overflow Waters of the Nordic Seas

GS is Greenland Sea; IS is Iceland Sea, EGC is East Greenland Current; NS is Norwegian Sea; FS is Fram Strait; AO is Arctic Ocean; DS is Denmark Strait;
(r)AW is (return) Atlantic Water; (u)AIW is (upper) Arctic Intermediate Water; NSDW is Norwegian Sea Deep Water

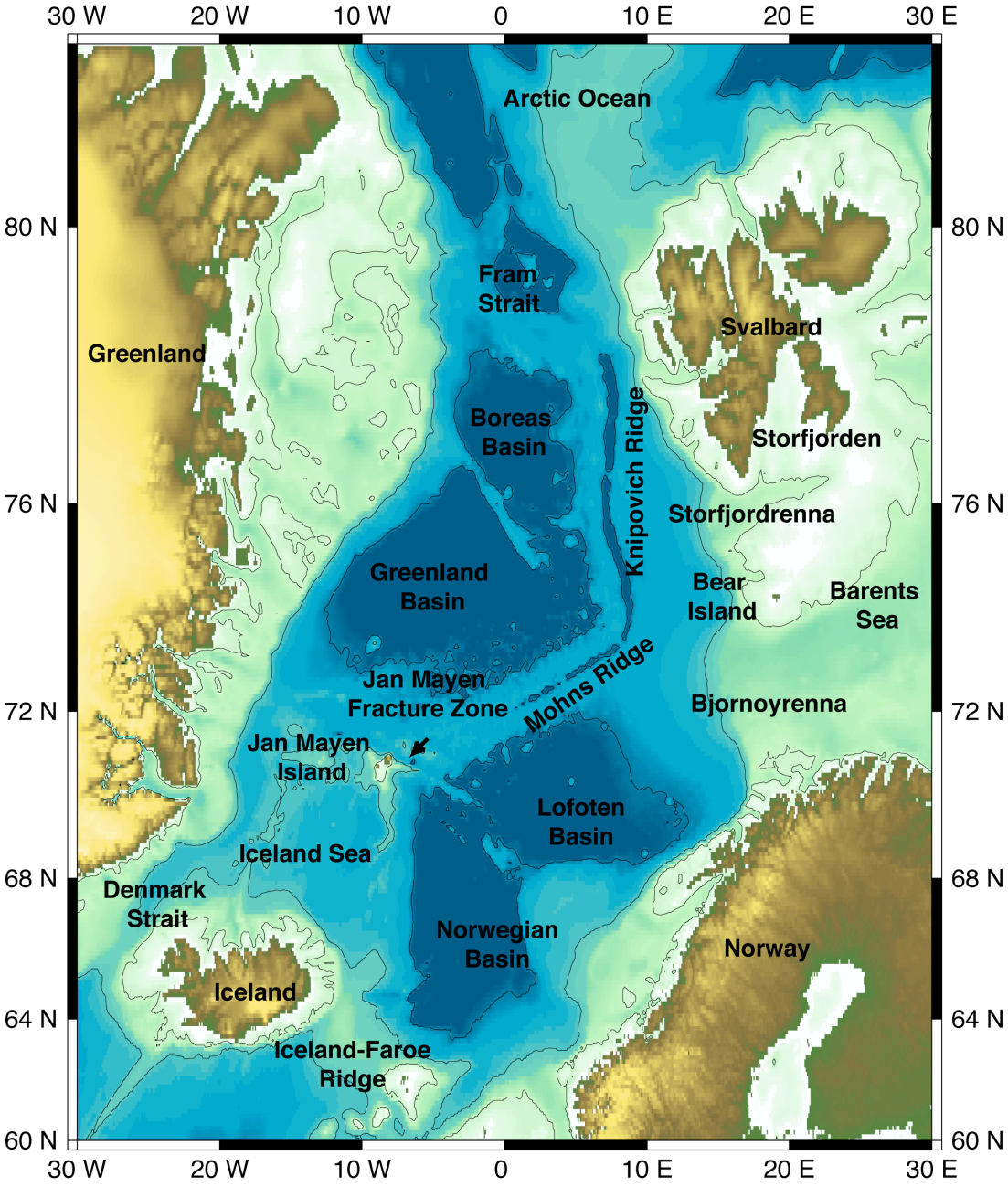

Figure 2.1: Bathymetry and geographic features of the Nordic Seas (contours at depths of 200m, 1000m and 2800m).

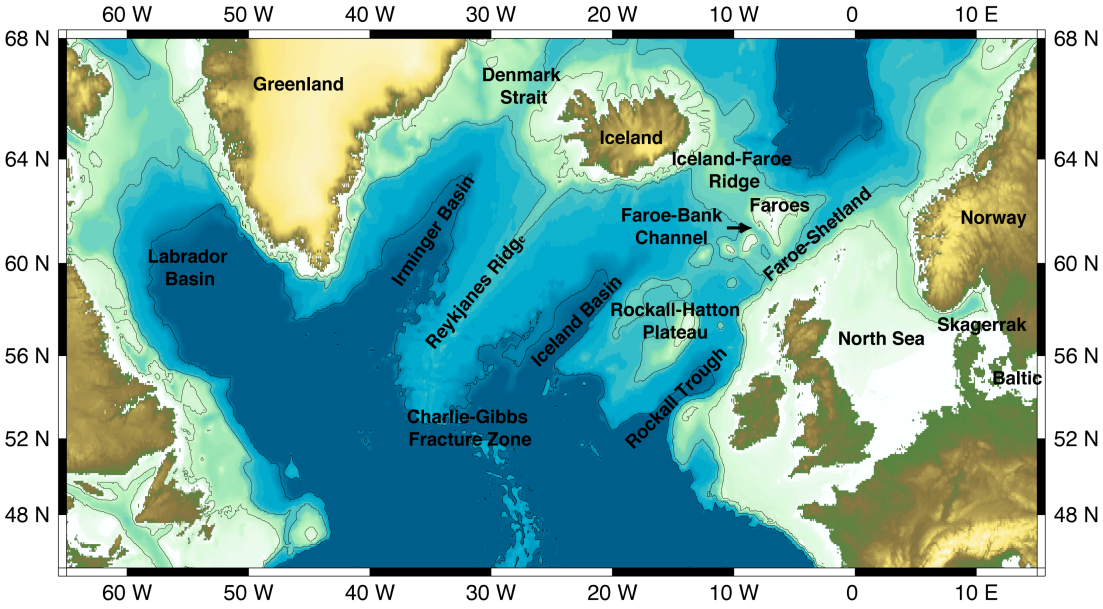

Figure 2.2: Bathymetry and geographic features of the Greenland - Scotland Ridge and the Northern North Atlantic (contours are marked at depths of 200m, 1000m and 2800m).

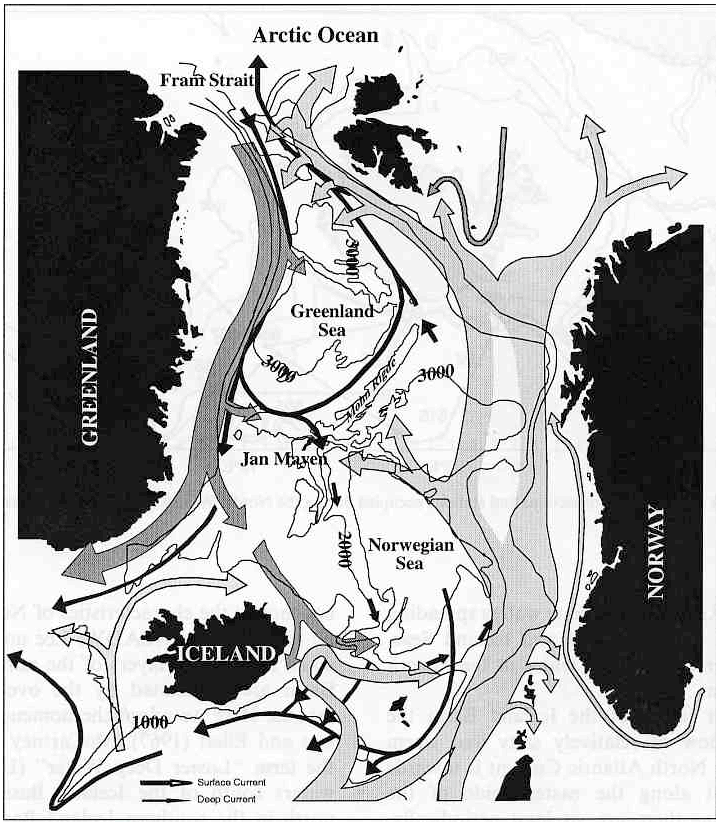

Figure 2.3: Schematic showing the general circulation of the Nordic Seas (from Fogelqvist et al., 2003). The surface circulation is represented by the pale arrows, and the deeper circulation by the dark arrows.

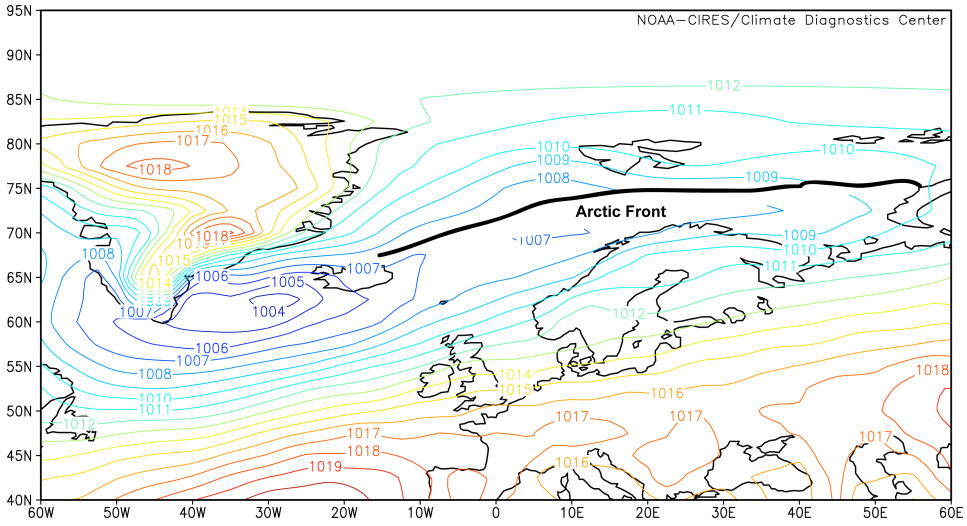

Figure 2.4: Annual mean sea level pressure from NCEP / NCAR Reanalysis data provided by the NOAA-CIRES Climate Diagnostics Center, Boulder, Colorado, USA, from their Web site at http://www.cdc.noaa.gov/. The Arctic Front is indicated by the trough of low pressure which continues from Iceland northeast across the Nordic Seas to the Barents Sea, and its position is marked by the solid black line.

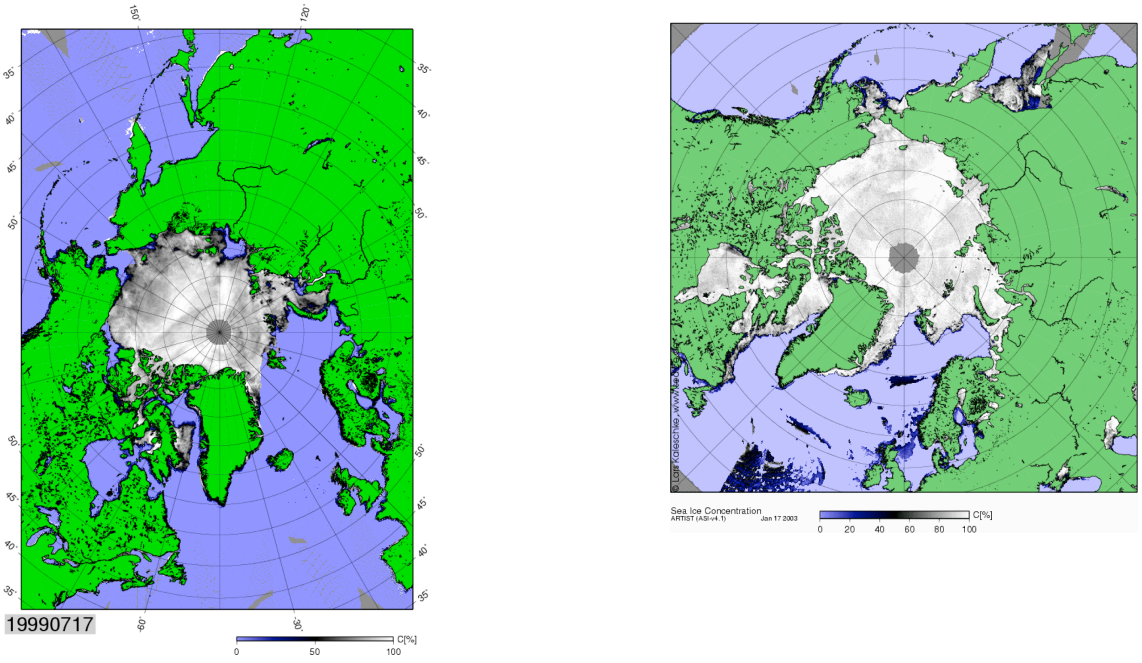

Figure 2.5: High resolution sea ice maps of the Arctic Ocean derived from satellite (passive microwave) sensors (DMSP-SSM/I) (Kaleschke et al. 2001). Figures are taken from http://www.seaice.de. The panel on the left illustrates the summer ice cover (July 17th 1999), and the panel on the right illustrates the winter ice cover (January 17th 2000).

Chapter Three

Data

3.1 Introduction

The data which provided the framework and motivation for this PhD were collected under the auspices of the NERC thematic programme ARCICE (Arctic Sea Ice and Environmental Variability) within the theme of Sea Ice-Atmosphere-Ocean Interactions. This was a multi-disciplinary research programme (1998–2001) aiming to enhance the understanding of and capacity to predict the fluctuations of Arctic sea-ice and glaciers, which influence climate and sea levels in North West Europe.

This chapter describes the hydrographic data and initial analysis, further data sources employed and the details of the setup of the boxes for flux calculations. The main hydrographic characteristics are discussed in Chapter 5.

3.2 Experiment Design

The aims of this thesis (section 2.2) are to use hydrographic observations to estimate the volume, heat and freshwater fluxes between the Nordic Seas and the North Atlantic to the south, Arctic Ocean to the north, and the Barents Sea to the east. Inverse methods have become a commonly used tool for the analysis of oceanographic data, and in this thesis the 'box inverse' method (section 4.6; Wunsch, 1996) was applied to the hydrographic data.

The majority of the hydrographic data used in this thesis was collected during the summer 1999 ARCICE cruise JR44. The cruise was specifically planned so that the hydrographic sections would provide data suitable for use with the 'box inverse' method. This technique is applied to a closed circuit (which may include coastline) of station pairs about a volume of ocean. The hydrographic sections conducted as part of the summer phase of the ARCICE programme, supplemented by additional data, were used to create four boxes in the Nordic Seas (illustrated in Figure 3.1 and fully described in section 3.7). These boxes are hereto referred to as the north, south, east and west boxes, and were configured such that fluxes (volume, heat, freshwater) over the region could be quantified.

To close the north, south and east boxes four additional hydrographic sections were used;

(i) Fram Strait: ice conditions prevented stations being occupied over the western part of Fram Strait and on the shallow East Greenland shelf during ARCICE cruise JR44 hence CTD data from a section conducted in September 1999, by the Alfred-Wegener-Institut were used to close the *north* box.

(ii) Barents Sea Opening: a section across the Barents Sea opening conducted in July 1999, as part of the Variability of Exchanges In the Northern Seas (VEINS) experiment, was used to close the *east* box.

(iii) Iceland to Scotland: a CTD and LADCP section conducted by the Southampton Oceanography Centre, as part of a cruise to study exchanges between the North Atlantic and the Norwegian Sea, was used to close the *south* box.

(iv) Skagerrak: data from an international investigation, the Joint Skagerrak Experiment (SKAGEX), was used to close the south box with respect to exchanges with the Baltic.

The winter phase of ARCICE (cruise JM3/2000) provided winter hydrographic data over a reduced region of the Nordic Seas.

3.3 Cruise Descriptions

3.3.1 JR44, Summer 1999

A detailed hydrographic survey of the Nordic Seas was made during the ARCICE research cruise JR44 (Bacon and Yelland, 2000) in summer 1999 on the *RRS James Clark Ross*, with a total of 165 stations (Figure 3.2a). The cruise, Circulation And Thermohaline Structure – Mixing, Ice And Ocean Weather (CATS-MIAOW), was conducted from 23rd July to 31st August 1999, with the survey completed during the period from 26th July to 27th August. Two long sections, the first from Norway to Greenland (ending deep in the ice over the north-east Greenland shelf) and the second from Svalbard to Iceland (passing over the Jan Mayen Fracture Zone and skirting the west of Jan Mayen Island) were conducted along the ground tracks of the ERS-2 satellite. Another section was conducted in Fram Strait following the line of an array of moorings deployed by the Alfred-Wegener-Institut, Bremerhaven, on about 78° 50' N (Fahrbach et al., 2001). This ran from the ice edge to the west of Fram Strait to the coast of Svalbard. A further section was conducted in the northern Denmark Strait, also under the path of an ERS-2 pass. This section was executed at high horizontal resolution with an average station spacing of 15 km, ending about 4 km off the Greenland coast. A repeat of this section was made at reduced resolution (using alternate station positions previously occupied). Stations were also made in the Marginal Ice Zone (MIZ) in the region of Fram Strait and Svalbard as part of the Meteorology phase of the cruise.

High quality CTD (conductivity-temperature-depth) data was collected from all stations along the sections described above (a total of 152 stations). A Neil Brown / General Oceanics (GO) Mk. IIIc CTD was used, with a 24 bottle Falmouth Scientific Instruments (FSI) rosette pylon. Pre-cruise CTD calibrations were provided by Ocean Scientific International Ltd. (OSIL) of Petersfield, Hampshire, U.K. The temperature calibration used a 5-point fit between 0.9°C and 29.1°C with an accuracy of ±0.002°C. The pressure calibration used a 10-point fit between 0 and 6000 dbar with an accuracy of better than ±0.1 dbar. Bottle samples, with a mean salinity difference of 0.0002 between 178 duplicate pairs, were used to derive a post-cruise empirical calibration for conductivities. The final CTD salinity accuracy was 0.002.

LADCP (lowered acoustic doppler curent profiler) data was also collected on the 152 CTD stations, in depths ranging from 110□m to 3756□m. The LADCP package, fitted centrally within the CTD rosette frame, consisted of an RDI 150□kHz BroadBand ADCP (Phase III) with a pressure case rated to 6000□m and four downward facing transducers with 20-degree beam angles. No data was processed from station 128, since there were no downcast data in the binary files extracted from the LADCP unit. It was noted that the CTD package was covered in marine detritus from this cast, and it was suspected that the LADCP may have been confused by returns from such a scatterer. There was a loss of upcast data at stations 121 and 122, possibly due to battery pack failure at low temperature. No data was processed on station 137 due to leakage on the first deployment of the battery pack replacement.

3.3.2 D242, Summer 1999

Cruise D242, Atlantic – Norwegian Exchanges, was conducted on the *RRS Discovery* between 7th□September and 6th□October 1999 (Cunningham, 2000). Its objectives were to measure the flux of warm, upper ocean water northward through the Iceland Basin and Rockall Trough to high latitudes, and to measure the returning flux of cold, deep water that flows through the Faroe Bank Channel into the North Atlantic. Two full depth hydrographic sections, comprising CTD and LADCP stations, were occupied between Scotland and Iceland. The first was made along the frequently occupied Rockall Trough section and its recent extension to Iceland (Figure 3.2b), and the second was made from southeast Iceland to Lousy Bank. Horizontal station spacing was ~□30□km in the Iceland Basin, with greater resolution over steep bathymetry and in the Rockall Trough.

An OTD Neil Brown MK IIIc was used as the CTD underwater unit, on a 24-way rosette frame. Two underwater units, DEEP03 and DEEP04, were used. The first 19 casts used the DEEP04 instrument. However, this was replaced by the DEEP03 instrument for the next 29 casts due to evidence of hysteresis present in the conductivity cell data on the upcasts. CTD DEEP03 experienced noise (fluctuations) in temperature readings between the depths of approximately 100 to 200□m on both upcasts and downcasts, although these spikes were not evident in the 1□Hz post-processed data. Calibrations and scaling were applied to correct the mismatch in the temperature and conductivity measurements between the two instruments. The raw conductivities were scaled and calibrated as described in (Cunningham, 2000). The offset and slope for the correction were determined using bottle samples and small offsets were applied to compensate for fluctuations in the CTD and in the bottle sampling. These were obtained by slightly different procedures according to the CTD used, largely due to the hysteresis problems affecting DEEP04.

A Self Contained Acoustic Doppler Current Profiler (SCADCP) on loan from the Woods Hole Oceanographic Institute (WHOI) was fitted to the CTD frame and used as a lowered ADCP (LADCP) during the stations used in this thesis. The instrument had a 30° beam angle. Although

the instrument was said to perform well (Cunningham, 2000), no LADCP data was processed on stations 13633, 13656, 13657, 13662, 13663 and no water track data processed on stations 13635 and 13654.

3.3.3 ARKTIS XV/3, Summer 1999

The Alfred-Wegener-Institut (AWI) conducted cruise ARKTIS XV/3 in the northern part of the Nordic Seas, on FS *Polarstern*, between 10th September and 15th October 1999 (Schauer, 2000). This was a multi-disciplinary cruise with physical, chemical and biological oceanographic programmes. The objectives of the physical oceanography component were to study the exchanges through Fram Strait, and the shelf plumes from the Storfjord, south of Svalbard. In this thesis, CTD data from the hydrographic section crossing Fram Strait, from the Svalbard shelf to the East Greenland shelf, was used (Figure 3.2c).

The CTD system used during the cruise was a Seabird Electronics SBE9*plus* probe, *SN 09P16392–0485*, in combination with a SBE32 Carousel Water Sampler, *SN 3217673–0202*, which operated 24 12-litre Ocean-Test-Equipment bottles. The CTD was equipped with standard conductivity, temperature and pressure sensors, *SN 03p2417* for temperature and *SN 042055* for conductivity. The temperature and conductivity sensors were calibrated by the manufacturer immediately before and after the cruise. The sensor accuracy was 1 db for the pressure sensor, 0.001ºC for the temperature sensor and 0.003 mS cm^{-1} for the conductivity sensor. In addition, salinity values derived from the CTD measurements were calibrated with the aid of water samples. During the cruise a total number of 548 samples were analysed with a Guildline Autosal 8400A salinometer, and IAPSO standard seawater Batch number P135, K15=0.99992. It was reported that it was difficult to achieve stable temperature conditions for the salinometer, but preliminary comparisons between sensor and bottle data indicated that the conductivity sensor measured values too low by 0.002-0.003 mS cm^{-1}. A more precise estimation of this error was made with further analysis of 70 salinity samples on return to AWI, and a suitable calibration applied.

3.3.4 VEINS/9911, Summer 1999

Station data for the section across the opening to the Barents Sea (Figure 3.2d) was obtained from the website of the International Council for the Exploration of the Seas (ICES)[1]. The stations formed part of the Variability of Exchanges In the Northern Seas (VEINS) experiment. The overall objective of this experiment was to measure and to model the variability of fluxes between the Atlantic and the Arctic Ocean. More specifically, the aims were:

[1] http://www.ices.dk/ocean/project/veins/htmls/summvein.htm

(i) to obtain time-series of heat, salt and water fluxes for the exchange routes through the Northern Seas, i.e. between the Atlantic Ocean and the Nordic Seas and between the Nordic Seas and the Arctic Ocean.

(ii) to quantify the magnitude of the variability of these fluxes

(iii) to improve the understanding of processes responsible for the variability

(iv) to develop a conceptual model of exchanges and water mass alterations between the Atlantic and the Arctic Ocean.

With these objectives VEINS contributed to a series of EU-MAST funded large-scale projects.

The data used here were collected on the 11th VEINS cruise[1] (VEINS/9911); conducted by the Norwegian Polar Institute on R/V *Lance* between July 18th 1999 and July 24th 1999. The hydrographic work was performed with a Seabird CTD and the data submitted to the ICES website were calibrated. No LADCP data was collected on this cruise.

3.3.5 SKAGEX II, Summer 1990

Station data for the section across the opening to the Baltic Seas (Figure 3.2e) was also obtained from the ICES website[2]. The stations used here formed part of SKAGEX, an international investigation under the auspices of ICES, carried out between spring 1990 and spring 1991. Its objectives were to identify and quantify the various water masses entering and leaving the Skagerrak area, and their variations over time; to investigate the mechanisms that drive the circulation in the area, and its links with biological processes; and to investigate the pathways of contaminants through the Skagerrak. The leader of the Project was Dr B. Dybern, and the ICES Data Centre acted as the Project Data Centre, collating most of the Oceanographic Data collected from the 2200 or so profiles. Four field phases (SKAGEX I-IV) were carried out, and 17 research ships from 7 countries participated. The relevant station data in the ICES oceanographic database were available for download directly from the website. The data used here included stations 469 to 479 made on 10th September 1990 on G.M. *Dannevig (LINW)* undertaken by the Floedevigen Marine Research Station, Arendal, (FRMS).

3.3.6 JM3/2000, Winter 2000

A second research cruise SCORESBY (Scientific Consideration of the Odden Response to a Benign Year) JM3 (Wadhams et al., 2000) was conducted on RV *Jan Mayen* in winter 2000. It was supported by Germany, the United Kingdom and Norway; the UK portion of which originated as part of the ARCICE project. The purpose was determine the winter 2000 hydrography of the central

[1] http://www.ices.dk/oceans/project/veins/crinfo/la99jul/la99jul.htm

[2] http://www.ices.dk/ocean/INDEX.HTM

Greenland Sea gyre region, including the location and depth of convective events and the structure of the Jan Mayen Current, especially where it emerges from the East Greenland Current. CTD stations were made between 16th February and 10th March, over a reduced region of the Nordic Seas, providing winter repeats of some of the summer ARCICE JR44 stations (Figure 3.2f).

A total of 81 CTD stations were occupied. Water samples were made on each CTD cast to take both temperature readings (protected and unprotected mercury thermometers), and water samples for a salinity calibration of the Seabird CTD. Salinity samples were measured on board with a Guildline salinometer.

During this cruise, deployments of Pancake Ice Motion Monitors (PIMMs floats) were made in addition to the CTD stations. These are an innovative type of freely drifting, expendable surface float capable of deployment within open ocean ice fields, which provide a novel approach to tracking ice motion. The design of the float was required to meet the conditions of stability and strength, and had to enable the float to be surface following. The slope of the float sides ensured the buoys would rise up to avoid crushing by ice pressure, the idea behind the design of Nansen's ship the SV *Fram*. The hull had a similar profile to ice pancakes in size (~1m in diameter), so that its drift would be comparable. ORBCOMM communications using the Low Earth Orbit Satellites allowed transmission of GPS position together with air and sea temperature data back to the Southampton Oceanography Centre (SOC). Platinum resistance thermometers were used to continuously measure both air and sea temperatures.

Deployments were made either on ice floes in the East Greenland Current, or with a drogue in the open ocean. Ten deployments were made using PIMMs with two different makes of satellite communicator (Stellar and Panasonic). Of the ten apparently successful deployments, data from five floats were received at the SOC, suggesting the remainder did not achieve satellite communication, or were somehow destroyed. Subsequent recovery of a failed float indicated that a flaw in the antenna design was responsible for the absence of communication from these floats. The Panasonic communicator appeared to have the best performance; its ability to communicate with more satellites allowed more messages to be sent per day. Of the successful floats, four were deployed on ice floes, and one was deployed in open water using a 20m drogue.

3.3.7 Svinøy section, Summer 1999 and Winter 2000

The Svinøy section runs northwestwards from the Norwegian coast at 62°N (Figure 7.1) and cuts through the Atlantic inflow just to the north of the Faroe-Shetland Channel (Orvik et al, 2001). It forms part of a long-term monitoring program undertaken by Norwegian scientists, and CTD stations along the section are occupied several times each year. High quality CTD data were made available and were used in this thesis to give an indication of the summer to winter changes in the upper part of the water column within the Norwegian Sea (Chapter 7). The annual 'Havets Miljø'

(Marine Climate) reports from the Norwegian Institute of Marine Research (Havforskningsinstituttet) describe the regular occupations of the section (e.g. Sjøtun, 2004).

3.4 Further Data Sources

3.4.1 Climatological Data

Wind stress fields from the adjusted SOC climatology (Josey et al., 1999) and the Hellerman and Rosenstein (1983) (HR) climatology were used for the calculation of Ekman fluxes (described in Chapter 4).

The SOC climatology is a new global air-sea heat flux climatology generated from an enhanced version of the Comprehensive Ocean Atmosphere Dataset 1a (COADS1a; Woodruff et al., 1993). It presents global wind stress fields on a one degree grid, based on in situ marine meteorological reports for the period 1980 to 1993. The individual ship meteorological reports have been corrected for biases arising from variations in the observing procedure Kent et al. (1993). This has improved on the flux estimates of, for example, the Silva et al. (1994) climatology. The choice of drag coefficient (incorporating the dependence of momentum transfer on atmospheric stability) is supported by recent observational analyses. The ice mask of Alexander and Mobley (1976) was used to exclude climatologically ice-covered regions resulting in missing values within the climatology for some periods of the year. The SOC climatology, in common with other flux climatologies, exhibits a substantial global mean heat gain by the ocean (of the order ~30 Wm^{-2}). An approach to resolving this problem is to adjust the individual components of the heat flux by using a linear inverse analysis technique, with independent measures of physical quantities such as ocean heat transport as constraints. The adjusted flux fields, used in this thesis, are a more balanced version of the SOC climatology, in which inverse analysis techniques have been used to reduce the global bias to within 5 Wm^{-2} (Grist and Josey, 2003).

The HR climatology presents wind stresses on a two degree grid, calculated using data from the period 1870 to 1976. Josey et al. (2000) suggested their drag coefficient was biased in the order of 25% too high.

Regional variations between the two climatologies might be expected as a result of the influence of decadal climate variability and the different data sets each is based on. At high latitudes, differences in the spatial representation of the Northern Hemisphere sub-polar gyres have been attributed to differences in the state of the North Atlantic and North Pacific Oscillations (Josey et al., 2000). The North Atlantic sub-polar gyre is more intense in the SOC analysis, higher winds leading to a doubling in strength of the Ekman pumping. In particular, the North Atlantic Oscillation has been in a predominantly positive state since the early 1980s, hence stronger features associated with the North Atlantic sub-polar gyre might be expected in the SOC analysis.

Further climatological data were not considered since the SOC and HR climatologies are the best available over the region of the Nordic Seas. Of the possible alternatives, the Trenberth et al. (1989) climatology is based on ECMWF (European Centre Medium-Range Weather Forecasts) reanalysis, rather than observational data and the Silva et al. (1994) climatology uses observations over an earlier time period (1945–1989) and does not incorporate the corrections to observational biases which are made in the SOC climatology.

3.4.2 Tidal Models

The OSU TOPEX/Poseidon global solution TPXO.5.1 (hereto referred to as the Egbert tidal model) and the Kowalik and Proshutinsky (1993) Arctic Ocean tidal model (hereto referred to as the Kowalik tidal model) were used to detide processed LADCP data (as described in Chapter 4). The geographical extent of the LADCP data made the use of two models necessary.

The Egbert tidal model is a global model of ocean tidal currents, obtained by inverting TOPEX/Poseidon sea surface height data between 66°S and 66°N. The methods are described by Egbert et al. (1994) and Egbert and Erofeeva (2000). The model provides complex amplitudes of earth-relative sea-surface elevation for eight primary harmonic constituents (M2, S2, N2, K2, K1, O1, P1, Q1) on a 0.5 degree grid between 85.75°S and 81.75°N. No Arctic data was incorporated, so the authors "*cannot guarantee TPXO.5.1 is good everywhere in the Arctic*" (Erofeeva, pers comm., June 2002), i.e. further north than 66°N. Their present work, which will incorporate ERS-2 (latitudinal limate of 81.5°N) and coastal tide gauge data, focuses on an Arctic inverse solution, but as yet is unavailable.

The Kowalik tidal model describes the distribution of the main semidiurnal and diurnal tide components of the Arctic Ocean and North Atlantic, covering latitudes from 61°N to 90°N. It incorporates computer model output and ground station and satellite data on sea level, currents and ice distribution. The system of tidal equations for the water and ice is solved on a stereographic map projection using a large scale model with a spatial resolution of ~14km. The final product of amplitude, phase, current ellipses and ice motion related to the eight tidal constituents (M2, S2, N2, K2, K1, O1, P1, Q1) are interpolated on to a spherical grid with a spatial resolution of one sixth of a degree.

Figure 3.3 illustrates the difference between the two models at two sites within the Nordic Seas. Since both these sites are north of 66°N the Kowalik model gives the better representation of the tides.

3.4.3 Bathymetric Data

For the presentation of topographic data in maps (for example, in Figure 3.1), use has been made of the recent International Bathymetric Chart of the Arctic Ocean (IBCAO) (Jakobsson et al. 2000).

This is the product of a project that was initiated to construct a modern, high resolution (2.5 km) digital data-base containing all available bathymetric data north of 64°N. The IBCAO bathymetry is currently only available north of 64°N. To extend the dataset further south World Ocean Elevation Data (ETOPO5) is used. This data is at lower resolution (10□km) and uses data merged from a number of sources on a 5□minute grid. These data sets were merged by Professor David Holland at the Centre for Atmospheric and Ocean Studies at the Courant Institute of Mathematical Sciences, New York University, for use in the Arctic Ocean Model Intercomparison Project (AOMIP). The IBCAO data (on a polar stereographic projection grid) and the ETOPO5 data (on a spherical coordinate grid) are merged to form one single data set in spherical coordinates on a 5 minute grid. The result is some loss in resolution of the IBCAO data, but is currently the best available data set over the region of the Nordic Seas and northern North Atlantic.

3.5 Hydrographic Data

The collection of the data are described in section 3.3, and further details are given in the respective cruise reports (Bacon and Yelland, 2000; Cunningham, 2000; Schauer, 2000; Wadhams et al., 2000) and project websites[1]. For all further analysis in this study, the calibrated hydrographic data (pressure, temperature, salinity) are projected onto a 5□db grid. The JR44 and D242 hydrographic measurements were made to WOCE (World Ocean Circulation Experiment) standard, and as such, accuracies were ±□.□□db in pressure, 0.001□°C in temperature and 0.002 in salinity, or better (Joyce, 1991). Further comments on the accuracy of salinity measurements are made by Bacon et al. (2000). Although the relevant cruise reports for the remainder of the hydrographic data did not explicitly report accuracies they can be expected to be in the region of ±□.□db in pressure, 0.002□°C in temperature and 0.003 in salinity, or better.

The International Committee for Weights and Measures approved the replacement of the International Practical Temperature Scale of 1968 (IPTS68) with the International Temperature Scale of 1990 (ITS90) which more closely approximates the thermodynamic temperature scale (Saunders, 1990b). Although there is relatively little difference between temperatures measured on the two scales, the effect on derived quantities, which require temperature for their determination, is non-negligible. All CTD temperatures used in this thesis are reported on the ITS90 scale but are converted to the IPTS68 scale for the computation of derived quantities following Saunders (1999b).

$$T_{68} = 1.00024 \cdot T_{90}. \qquad 3.1$$

Salinity is determined using the Pratical Salinity Scale 1978 (PSS78; Culkin and Ridout, 1989). On this scale it is a dimensionless quantity (e.g. S = 35.1 or 'salinity of 35.1') and the units of ppt (parts

[1] http://www.ices.dk/ocean/project/vein/htmls/summvein.htm
http://www.ices.dk/oceans/project/veins/crinfo/la99jul/la99jul.htm

per thousand) used in previous scales are no longer correct. For this thesis, salinities are expressed by a dimensionless number, although the units of psu (pratical salinity units) are sometimes used to denote salinities measured on PSS78. In the interest of clarity, salinity transport is reported using the units Sv psu in order to distinguish it from volume transport, which has units of Sv. 1 Sv is equal to 10^6 m^3 s^{-1}.

The CTD based conductivity measurements are calibrated by water samples taken at specific depths. In practise, the salinity of a water sample is calculated by comparing its electrical conductivity with that of a standard sample of known salinity at the same temperature. This measured conductivity ratio is converted to salinity using the PSS78 algorithm, which is valid for temperatures within the range -2°C to +35°C (measured according to IPTS-68), and salinities within the range 21 to 42. By definition, seawater of practical salinity 35 has a conductivity ratio of unity at 15°C with a potassium chloride (KCl) solution containing 32.4356 grams KCl per kilogram of solution.

3.6 Lowered Acoustic Doppler Current Profiler data

The analysis of Lowered Acoustic Doppler Current Profiler (LADCP) data is described in Chapter 4, but the basic steps of the initial processing are explained here. The LADCP data measurements were output in terms of depth (m). For the further analysis, depth was converted to pressure (Saunders, 1981) and the processed velocities were projected onto a 5 db grid, so as to be consistent with the CTD data.

The LADCP measures instantaneous scatterer relative velocities of the water column and these can be converted into profiles of absolute current by an elaborate processing path. The scatterer velocities are measured by utilising the Doppler frequency shift, phase changes and correlation between coded pulses transmitted and received by four transducers. Given the geometry of the transducer set, and the orientation/motion of the package, the along beam velocities are transformed into earth coordinates to give north, east and vertical current motion relative to the CTD package for each of the ensemble bins.

3.6.1 Processing

The raw velocity measurements are a combination of the true ocean currents and the motion of the instrument. Individual pings from the ADCP result in a number of overlapping velocity profiles within a range of 100–200 m from the instrument. These velocity profiles are relative to the unknown instrument velocity. Vertical differentiation produces a series of overlapping shear profiles. These are interpolated on to a uniform depth grid and averaged to give a composite shear profile. The data is then integrated up over the cast to produce a shear profile with zero net velocity. This process removes not only the unknown instrument velocity, but also the barotropic component.

This must be reinstated either from the ship displacement (recorded from differential GPS data) or from the relative motion of the package over the sea floor (bottom tracking). CTD data is used in the latter stages of the processing, firstly to correct the depths of the ensemble bins through the matching of the CTD data to the vertical velocity of the package as measured by the LADCP and secondly to provide in-situ sound speed values for these depths. The final velocity profile is therefore the sum of the baroclinic and barotropic components.

The method assumes that successive overlapping velocity profiles, individually covering a fraction of the water column, can be used to obtain full depth integrated profiles of absolute velocities. For all LADCP data used in this thesis the instrument was deployed as part of a CTD/rosette package and lowered through the water column during particular hydrographic casts. The data were processed using software created by Professor E. Firing of the University of Hawaii, following a now well-used method (Beal, 1997; Cunningham et al., 2003).

Following Beal (1997) the velocity measured by the LADCP can be written as three components: $U_{baroclinic}$, the baroclinic component (calculated from the velocity shear); $U_{barotropic}$, the unknown barotropic component of the ocean current; and U_{LADCP}, the unknown component from the motion of the LADCP through the water;

$$U_{measured\,(t)} = U_{barotropic} + U_{baroclinic\,[z(t)]} - U_{LADCP\,(t)} \qquad 3.2$$

The motion of the LADCP includes U_{ship}, the movement of the ship relative to the ground, and $U_{instrument}$, the motion of the instrument relative to the ship,

$$U_{LADCP} = U_{ship} + U_{instrument} \qquad 3.3$$

The first component of equation 3.3 (U_{ship}) is determined from the ship GPS positioning data. When equation 3.2 is integrated in time over the period of the whole cast T, the second (unknown) component of equation 3.3 ($U_{instrument}$) vanishes since the instrument must begin and end the cast at the ship. Hence,

$$U_{barotropic} = \frac{1}{T}\left[\int_0^T U_{measured\,(t)}\,dt - \int_0^T U_{baroclinic\,[z(t)]}\,dt + \int_0^T U_{ship}\,dt\right] \qquad 3.4$$

Finally, the absolute ocean current is given by,

$$U_{ocean\,(t)} = U_{baroclinic\,[z(t)]} + U_{barotropic} \qquad 3.5$$

These final velocity profiles are the sum of the baroclinic and barotropic components (over the full water column except the surface 50□m and the bottom 30□m) and are hereafter referred to as the Water Track (WT) data.

Bottom tracking was also used to obtain absolute velocity profiles when the bottom was within range of the instrument. As the LADCP approaches the ocean floor, the strong resulting backscatter

can be used to obtain a 'bottom velocity' which is essentially a direct measurement of the motion of the instrument relative to the stationary sea-bed. Each 2□second ensemble consists of a BT ping followed by a WT ping. BT pings are used to determine height off bottom and absolute velocity of the package; WT pings determine velocity of the water relative to the package. Absolute velocity of water over the ground is then a simple vector addition of the BT and WT velocities. Typically, near-bottom velocities can be determined between 50 and 250□m off bottom, in water depths greater than 3000m. The processing of bottom track data involves extracting the relevant position and magnetic variation from the standard LADCP data, and reading in the CTD data for that cast. The sound velocity is calculated from the CTD pressure, temperature and salinity data in order to correct the depth of the LADCP bins relative to the instrument, and to correct the measured velocities. The water depth is extracted from the LADCP processing files and the absolute near bottom water velocities are calculated by subtracting the bottom velocities from the water track velocities. All velocities are then averaged back onto the original bins (the bins are displaced by the sound speed correction). The magnetic declination is then used to correct the compass involving a simple vector rotation. The final velocity profiles are hereafter referred to as Bottom Track (BT) data.

3.6.2 Accuracy

LADCP velocities have an accumulative error which can be estimated by a random walk, if no instrument bias is assumed. This is derived when each shear profile is strung together over the depth of the cast (Firing and Gordon, 1990). A bad velocity measurement occurring in a bin at the centre of a profile will result in negatively correlated shear to either side of it (i.e. a peak). If a bad velocity occurs in the last bin of a profile, the shear is offset and doesn't recover. This offset will then affect the remaining shear data as more profiles are added.

For a 150 kHz ADCP over a profile range of around 160□m with 16□m bins, the average standard deviation of each WT and BT velocity measurement is quoted to be 1□cm□s^{-1} (RDinstruments, 1995).

For WT data, additional uncertainty is introduced by the determination of the barotropic component of the flow. This component was derived either from the displacement of the vessel as recorded by differential GPS (water-tracking) or, when the instrument was within ~□200□m of the bottom, from the motion of the LADCP relative to the ocean floor (bottom-tracking) (Fischer and Visbeck, 1993).

For BT data, if we assume that the absolute velocity error has a contribution from the bottom track and water track, and there are about 50 independent estimates of velocity in each 5□m bin, then the error of the near-bottom velocities, x, is approximately,

$$x = \frac{\sqrt{1^2 + 1^2}}{\sqrt{50}} = 0.2 \ cm\ s^{-1}. \qquad 3.6$$

This means that errors in the BT data are an order of magnitude less than the stochastic error in a typical top to bottom profile derived from water track shear estimates (Cunningham et al., 2003).

The characteristic accuracy of the barotropic component of the LADCP flow is estimated to be 3 cm s^{-1} by calculating the root-mean-square (rms) deviation between the WT and BT velocities over their common depth range. The mean deviation was 0.06 cm s^{-1}, which is not significantly different from zero at the 99% confidence limit.

3.7 Setup of Boxes for Flux Calculations and Inversion

As stated in section 3.2, summer hydrographic data is used to construct four boxes over the Nordic Sea region; north, south, east and west. The locations of the resulting station pair positions are illustrated in Figure 3.1 and detailed information is given in Table 3.1.

The data are gridded to form ten sections, and then joined to construct the four boxes. The *north* box is formed by sections 4, 5, and 6; the *south* by sections 2, 3, 7 and 10; the *east* by sections 3, 4, 8 and 9; and the *west* by sections 1, 6 and 7. The *south* box is thus configured such that it includes the area of the North Sea, but not the Baltic Sea.

The 'external sections' (Sections 1, 2, 5, 8, 9) are gridded such that positive velocities and transports are directed out of the Nordic Seas and towards the North Atlantic, Barents Sea and Arctic Ocean respectively. Section 1 uses data across Denmark Strait, from Greenland to Iceland, from the ARCICE cruise JR44. Section 2 uses data from Iceland to Scotland, from cruise D242. Section 5 uses AWI cruise ARKTIS XV/3 data across Fram Strait, from the coast of Svalbard to the ice edge off the East Greenland coast. Sections 8 and 9 use data from the 11th VEINS cruise across the Barents Sea Opening from the northern coast of Norway northwards towards Bear Island, and onwards to the coast of Svalbard. Section 10, using data from the SKAGEX experiment, is gridded such that positive velocities are directed out of the Baltic Sea into the Nordic Seas.

The 'internal sections' (Sections 3, 4, 6 and 7) use data from the ARCICE cruise JR44; with Section 3 formed by stations from the coast of Norway to the crossover station in the middle of the Greenland Sea Basin, Section 4 by stations from the crossover station in the middle of the Greenland Sea Basin to Svalbard, Section 6 by stations from the Greenland coast to the crossover station in the middle of the Greenland Sea Basin and Section 7 by stations between this crossover station and the northern coast of Iceland. Sections 3 and 4 are gridded such that positive velocities were directed into the *east* box (and out of the *south* and *north* boxes respectively). Sections 6 and 7 are gridded such that positive velocities are directed into the *west* box (and out of the *north* and *south* boxes respectively).

For consistency in all further discussion, sections will be referred to as: *Denmark Strait* (DS) comprised of section 1; *Barents Sea Opening* (BSO) comprised of sections 8 and 9; *Fram Strait* (FS) comprised of section 5; *Skagerrak* (Sk) comprised of section 10; *Iceland-Scotland* (IScot)

comprised of section 2; *Iceland-Svalbard* (ISval) comprised of sections 7 and 4 and *Greenland-Norway* (GN) comprised of sections 3 and 6.

During the first leg of the ARCICE cruise JR44 (Norway to Greenland) used in Section 6, one station was conducted out of sequence. Geographically the stations 039, 040, 041, 043, 042, 044, 045 proceed northwards along the section from the middle of the Greenland Basin up on to the continental shelf off the east coast of Greenland (Figure 3.4). If the section is gridded geographically (such that the station order is … 040, 041, 043, 042, 044, 045 …) then an apparent eddy like feature is created in the velocity field (Figure 3.5). This is an artefact of short-term variability in the boundary current, rather than a real feature, due to the stations being non-sequential in time. To treat the stations consistently with respect to time, in the Standard Model station 042 was excluded from the box setup (Table 3.1) for flux calculations.

Box Stn Pair #	Section	Box	Station Pair	Lat °N	Lon °E	Depth of shallow station of pair (m)	Mean depth of station pair (m)	Depth of 'bottom triangle' area (m)
1 (1/2)	1	*west*	150 149	69.31	-23.81	145	165	20
2 (2/3)	1	*west*	149 148	69.19	-23.65	185	225	40
3 (3/4)	1	*west*	148 147	69.07	-23.49	260	325	65
4 (4/5)	1	*west*	147 146	68.95	-23.33	390	615	225
5 (5/6)	1	*west*	146 145	68.83	-23.17	840	1120	280
6 (6/7)	1	*west*	145 144	68.71	-23.02	1400	1455	55
7 (7/8)	1	*west*	144 143	68.59	-22.86	1475	1495	20
8 (8/9)	1	*west*	143 142	68.47	-22.71	1395	1435	40
9 (9/10)	1	*west*	142 141	68.35	-22.56	1285	1340	55
10 (10/11)	1	*west*	141 140	68.23	-22.41	1175	1230	55
11 (11/12)	1	*west*	140 139	68.11	-22.26	875	1025	150
12 (12/13)	1	*west*	139 138	67.99	-22.11	795	835	40
13 (13/14)	1	*west*	138 137	67.87	-21.96	740	770	30
14 (14/15)	1	*west*	137 136	67.75	-21.82	675	710	35
15 (15/16)	1	*west*	136 135	67.63	-21.67	645	660	15
16 (16/17)	1	*west*	135 134	67.51	-21.53	530	590	60
17 (17/18)	1	*west*	134 133	67.83	-21.38	305	420	115
18 (18/19)	1	*west*	133 132	67.26	-21.24	275	290	15
19 (19/20)	1	*west*	132 131	67.14	-21.10	205	240	35
20 (20/21)	1	*west*	131 130	67.01	-20.96	170	190	20
21 (21/22)	1	*west*	130 129	66.89	-20.82	170	230	60
22 (22/23)	1	*west*	129 128	66.77	-20.69	285	320	35
23 (23/24)	1	*west*	128 127	66.64	-20.55	290	320	30
24 (24/25)	1	*west*	127 126	66.52	-20.42	165	230	65
25 (25/26)	1	*west*	126 125	66.40	-20.28	105	135	30
26 (26/27)	*LAND*	*LAND*	125 672	*LAND*	*LAND*	*LAND*	*LAND*	*LAND*
27 (27/28)	2	*south*	672 671	62.63	-20.00	200	1005	805
28 (28/29)	2	*south*	671 670	61.80	-20.00	1805	1915	110
29 (29/30)	2	*south*	670 669	61.46	-20.01	2020	2205	185
30 (30/31)	2	*south*	669 668	61.11	-20.01	2390	2410	20
31 (31/32)	2	*south*	668 667	60.76	-20.00	2425	2455	30
32 (32/33)	2	*south*	667 666	60.29	-20.00	2485	2615	130
33 (33/34)	2	*south*	666 665	59.84	-19.57	2700	2720	20
34 (34/35)	2	*south*	665 664	59.55	-18.78	2440	2570	130
35 (35/36)	2	*south*	664 663	59.37	-18.35	1935	2190	255
36 (36/37)	2	*south*	663 662	59.27	-18.08	1555	1745	190
37 (37/38)	2	*south*	662 661	59.17	-17.77	995	1275	280
38 (38/39)	2	*south*	661 660	59.04	-17.44	850	925	75
39 (39/40)	2	*south*	660 659	58.90	-17.12	850	1000	150
40 (40/41)	2	*south*	659 658	58.70	-16.59	1150	1185	35
41 (41/42)	2	*south*	658 657	58.40	-15.77	675	950	275
42 (42/43)	2	*south*	657 656	58.10	-15.00	470	575	105
43 (43/44)	2	*south*	656 655	57.83	-14.29	145	310	165
44 (44/45)	2	*south*	655 654	57.63	-13.79	110	130	20
45 (45/46)	2	*south*	654 653	57.56	-13.48	110	140	30
46 (46/47)	2	*south*	653 652	57.56	-13.16	170	235	65
47 (47/48)	2	*south*	652 651	57.55	-12.93	295	670	375
48 (48/49)	2	*south*	651 650	57.54	-12.75	1045	1350	305
49 (49/50)	2	*south*	650 649	57.52	-12.45	1650	1735	85
50 (50/51)	2	*south*	649 648	57.51	-12.04	1805	1810	5
51 (51/52)	2	*south*	648 647	57.49	-11.68	1805	1920	115
52 (52/53)	2	*south*	647 646	57.48	-11.42	735	1385	650
53 (53/54)	2	*south*	646 645	57.46	-11.19	585	660	75
54 (54/55)	2	*south*	645 644	57.42	-10.96	585	695	110
55 (55/56)	2	*south*	644 643	57.39	-10.75	800	1490	690
56 (56/57)	2	*south*	643 642	57.33	-10.51	2175	2205	30
57 (57/58)	2	*south*	642 641	57.26	-10.21	2115	2175	60
58 (58/59)	2	*south*	641 640	57.22	-9.94	1945	2030	85
59 (59/60)	2	*south*	640 639	57.17	-9.72	1785	1865	80
60 (60/61)	2	*south*	639 638	57.13	-9.53	1375	1580	205
61 (61/62)	2	*south*	638 637	57.10	-9.39	765	1070	305
62 (62/63)	2	*south*	637 636	57.07	-9.28	330	550	220
63 (63/64)	2	*south*	636 635	57.03	-9.11	120	225	105
64 (64/65)	2	*south*	635 634	56.98	-8.89	115	120	5

65	(65/66)	2	*south*	634	633	56.92	-8.65	115	115	0
66	(66/67)	2	*south*	633	632	56.86	-8.42	115	120	5
67	(67/68)	2	*south*	632	631	56.81	-8.18	115	120	5
68	(68/69)	*LAND*	*LAND*	631	003	*LAND*	*LAND*	*LAND*	*LAND*	*LAND*
69	(69/70)	3	*south, east*	003	004	64.89	9.98	340	350	10
70	(70/71)	3	*south, east*	004	005	65.18	9.69	285	320	35
71	(71/72)	3	*south, east*	005	006	65.49	9.39	285	365	80
72	(72/73)	3	*south, east*	006	007	65.81	9.07	295	370	75
73	(73/74)	3	*south, east*	007	008	66.13	8.74	295	310	15
74	(74/75)	3	*south, east*	008	009	66.43	8.42	310	320	10
75	(75/76)	3	*south, east*	009	010	66.69	8.14	310	380	70
76	(76/77)	3	*south, east*	010	011	66.93	7.88	445	735	290
77	(77/78)	3	*south, east*	011	012	67.15	7.63	1025	1250	225
78	(78/79)	3	*south, east*	012	013	67.38	7.36	1385	1430	45
79	(79/80)	3	*south, east*	013	014	67.65	7.05	1280	1335	55
80	(80/81)	3	*south, east*	014	015	67.93	6.72	1280	1400	120
81	(81/82)	3	*south, east*	015	016	68.13	6.46	1515	1745	230
82	(82/83)	3	*south, east*	016	017	68.37	6.17	1975	2245	270
83	(83/84)	3	*south, east*	017	018	68.60	5.88	2515	2785	270
84	(84/85)	3	*south, east*	018	019	68.82	5.59	3055	3155	100
85	(85/86)	3	*south, east*	019	020	69.12	5.18	3250	3260	10
86	(86/87)	3	*south, east*	020	021	69.42	4.76	3270	3275	5
87	(87/88)	3	*south, east*	021	022	69.72	4.34	3275	3275	0
88	(88/89)	3	*south, east*	022	023	70.02	3.91	3275	3275	0
89	(89/90)	3	*south, east*	023	024	70.32	3.46	3275	3275	0
90	(90/91)	3	*south, east*	024	025	70.62	2.98	3220	3250	30
91	(91/92)	3	*south, east*	025	026	70.91	2.53	3185	3205	20
92	(92/93)	3	*south, east*	026	027	71.20	2.05	2305	2745	440
93	(93/94)	3	*south, east*	027	028	71.50	1.53	2305	2355	50
94	(94/95)	3	*south, east*	028	029	71.80	1.01	2400	2420	20
95	(95/96)	3	*south, east*	029	030	72.09	0.47	2275	2360	85
96	(96/97)	3	*south, east*	030	031	72.38	-0.08	2275	2385	110
97	(97/98)	3	*south, east*	031	032	72.67	-0.64	2490	2845	355
98	(98/99)	3	*south, east*	032	033	72.95	-1.22	3170	3185	15
99	(99/100)	3	*south, east*	033	034	73.24	-1.81	3070	3120	50
100	(100/101)	3	*south, east*	034	035	73.52	-2.44	2955	3015	60
101	(101/102)	3	*south, east*	035	036	73.73	-2.91	2955	2990	35
102	(102/103)	3	*south, east*	036	037	73.95	-3.42	3025	3310	285
103	(103/104)	4	*east, north*	037	102	74.27	-3.41	3595	3615	20
104	(104/105)	4	*east, north*	102	101	74.60	-2.59	3635	3660	25
105	(105/106)	4	*east, north*	101	100	74.92	-1.72	3685	3710	25
106	(106/107)	4	*east, north*	100	099	75.23	-0.85	3735	3750	15
107	(107/108)	4	*east, north*	099	098	75.53	0.01	1860	2815	955
108	(108/109)	4	*east, north*	098	097	75.83	0.95	1860	2575	715
109	(109/110)	4	*east, north*	097	096	76.14	1.96	3170	3230	60
110	(110/111)	4	*east, north*	096	095	76.43	2.98	2775	2975	200
111	(111/112)	4	*east, north*	095	094	76.72	4.02	2775	2875	100
112	(112/113)	4	*east, north*	094	093	77.00	5.09	2565	2770	205
113	(113/114)	4	*east, north*	093	092	77.26	6.17	2390	2480	90
114	(114/115)	4	*east, north*	092	091	77.43	6.88	2390	2565	175
115	(115/116)	4	*east, north*	091	090	77.51	7.22	2735	3060	325
116	(116/117)	4	*east, north*	090	089	77.59	7.60	2990	3190	200
117	(117/118)	4	*east, north*	089	088	77.72	8.16	1905	2450	545
118	(118/119)	4	*east, north*	088	087	77.86	8.84	1075	1490	415
119	(119/120)	4	*east, north*	087	086	78.02	9.64	200	640	440
120	(120/121)	4	*east, north*	086	085	78.16	10.32	200	230	30
121	(121/122)	*LAND*	*LAND*	085	20901	*LAND*	*LAND*	*LAND*	*LAND*	*LAND*
122	(122/123)	5	*north*	20901	21301	78.83	8.33	215	655	440
123	(123/124)	5	*north*	21301	21401	78.83	6.85	1090	1765	675
124	(124/125)	5	*north*	21401	22101	78.83	5.05	2350	2395	45
125	(125/126)	5	*north*	22101	22501	78.83	3.31	2350	2430	80
126	(126/127)	5	*north*	22501	22601	78.86	2.11	2505	2530	25
127	(127/128)	5	*north*	22601	22701	78.92	1.19	2540	2545	5
128	(128/129)	5	*north*	22701	23801	78.97	-0.67	2540	2575	35
129	(129/130)	5	*north*	23801	24301	78.99	-2.88	2125	2365	240
130	(130/131)	5	*north*	24301	24601	78.99	-4.23	1465	1795	330
131	(131/132)	5	*north*	24601	24802	79.01	-5.80	270	870	600
132	(132/133)	5	*north*	24802	24901	79.01	-7.12	215	245	30
133	(133/134)	5	*north*	24901	25101	78.99	-7.72	190	205	15
134	(134/135)	5	*north*	25101	25201	78.94	-8.39	190	255	65
135	(135/136)	5	*north*	25201	25301	78.87	-9.19	195	260	65
136	(136/137)	5	*north*	25301	25401	78.85	-10.09	195	225	30
137	(137/138)	5	*north*	25401	25501	78.91	-10.95	75	165	90
138	(138/139)	5	*north*	25501	25601	78.99	-11.76	75	130	55
139	(139/140)	5	*north*	25601	25701	79.04	-12.58	130	160	30
140	(140/141)	*LAND*	*LAND*	25701	054	*LAND*	*LAND*	*LAND*	*LAND*	*LAND*
141	(141/142)	6	*north, west*	054	053	77.18	-13.49	245	250	5
142	(142/143)	6	*north, west*	053	052	76.94	-12.50	245	280	35
143	(143/144)	6	*north, west*	052	051	76.75	-11.94	305	310	5
144	(144/145)	6	*north, west*	051	050	76.62	-11.44	305	305	0
145	(145/146)	6	*north, west*	050	049	76.40	-10.50	270	290	20
146	(146/147)	6	*north, west*	049	048	76.18	-9.73	270	365	95
147	(147/148)	6	*north, west*	048	047	76.06	-9.33	460	700	240
148	(148/149)	6	*north, west*	047	046	75.96	-9.01	940	1215	275
149	(149/150)	6	*north, west*	046	045	75.83	-8.60	1490	1560	270
150	(150/151)	6	*north, west*	045	044	75.72	-8.26	2030	2275	245
151	(151/152)	6	*north, west*	044	043	75.56	-7.76	2515	2940	425
152	(152/153)	6	*north, west*	043	041	75.32	-7.02	3365	3435	70
153	(153/154)	6	*north, west*	041	040	75.06	-6.27	3505	3525	20
154	(154/155)	6	*north, west*	040	039	74.79	-5.53	3545	3560	15
155	(155/156)	6	*north, west*	039	038	74.51	-4.81	3570	3580	10
156	(156/157)	6	*north, west*	038	037	74.24	-4.11	3590	3595	5
157	(157/158)	7	*west, south*	037	104	73.94	-4.20	3430	3515	85
158	(158/159)	7	*west, south*	104	105	73.60	-5.02	2970	3200	230
159	(159/160)	7	*west, south*	105	106	73.24	-5.80	2635	2805	170
160	(160/161)	7	*west, south*	106	107	72.89	-6.54	2580	2610	30
161	(161/162)	7	*west, south*	107	108	72.54	-7.25	2580	2595	15
162	(162/163)	7	*west, south*	108	109	72.18	-7.93	2525	2570	45
163	(163/164)	7	*west, south*	109	110	71.81	-8.62	1070	1800	730
164	(164/165)	7	*west, south*	110	111	71.52	-9.13	1070	1700	630
165	(165/166)	7	*west, south*	111	112	71.34	-9.45	465	1395	930

166	(166/167)	7	*west, south*	112	113	71.05	-9.93	465	865	400
167	(167/168)	7	*west, south*	113	114	70.67	-10.55	1260	1425	165
168	(168/169)	7	*west, south*	114	115	70.30	-11.13	1590	1725	135
169	(169/170)	7	*west, south*	115	116	69.92	-11.69	1745	1805	60
170	(170/171)	7	*west, south*	116	117	69.53	-12.25	1745	1765	20
171	(171/172)	7	*west, south*	117	118	69.14	-12.79	1780	1820	40
172	(172/173)	7	*west, south*	118	119	68.77	-13.29	1820	1840	20
173	(173/174)	7	*west, south*	119	120	68.40	-13.77	1505	1665	160
174	(174/175)	7	*west, south*	120	121	68.02	-14.24	1155	1330	175
175	(175/176)	7	*west, south*	121	122	67.63	-14.70	865	1010	145
176	(176/177)	7	*west, south*	122	123	67.29	-15.10	185	525	340
177	(177/178)	7	*west, south*	123	124	66.96	-15.48	185	210	25
178	(179/180)	8	*east*	B1	B2	70.58	19.97	115	130	15
179	(180/181)	8	*east*	B2	B3	70.75	19.93	145	155	10
180	(181/182)	8	*east*	B3	B4	70.92	19.90	160	175	15
181	(182/183)	8	*east*	B4	B5	71.08	19.97	185	200	15
182	(183/184)	8	*east*	B5	B6	71.25	19.84	200	205	5
183	(184/185)	8	*east*	B6	B7	71.42	19.80	200	215	15
184	(185/186)	8	*east*	B7	B8	71.63	19.75	230	245	15
185	(186/187)	8	*east*	B8	B9	71.88	19.68	260	275	15
186	(187/188)	8	*east*	B9	B10	72.13	19.63	290	295	5
187	(188/189)	8	*east*	B10	B11	72.38	19.57	300	335	35
188	(189/190)	8	*east*	B11	B12	72.62	19.51	370	380	10
189	(190/191)	8	*east*	B12	B13	72.87	19.45	390	400	10
190	(191/192)	8	*east*	B13	B14	73.12	19.39	410	430	20
191	(192/193)	8	*east*	B14	B15	73.38	19.34	445	450	5
192	(193/194)	8	*east*	B15	B16	73.58	19.30	330	390	60
193	(194/195)	8	*east*	B16	B17	73.75	19.27	220	275	55
194	(195/196)	8	*east*	B17	B18	73.92	19.23	125	175	50
195	(196/197)	8	*east*	B18	B19	74.08	19.20	60	95	35
196	(197/198)	8	*east*	B19	B20	74.21	19.18	50	55	5
197	(198/199)	*LAND*	*LAND*	B20	B21	*LAND*	*LAND*	*LAND*	*LAND*	*LAND*
198	(199/200)	9	*east*	B21	B22	74.58	18.81	20	45	25
199	(200/201)	9	*east*	B22	B23	74.66	18.70	65	80	15
200	(201/202)	9	*east*	B23	B24	74.74	18.62	95	160	65
201	(202/203)	9	*east*	B24	B25	74.82	18.54	200	210	10
202	(203/204)	9	*east*	B25	B26	74.91	18.47	65	135	70
203	(204/205)	9	*east*	B26	B27	75.03	18.32	60	65	5
204	(205/206)	9	*east*	B27	B28	75.18	18.14	50	55	5
205	(206/207)	9	*east*	B28	B29	75.33	17.98	50	70	20
206	(207/208)	9	*east*	B29	B30	75.46	17.82	90	105	15
207	(208/209)	9	*east*	B30	B31	75.62	17.64	120	160	40
208	(209/210)	9	*east*	B31	B32	75.77	17.44	200	245	45
209	(210/211)	9	*east*	B32	B33	75.91	17.23	290	300	10
210	(211/212)	9	*east*	B33	B34	76.06	17.07	280	295	15
211	(212/213)	9	*east*	B34	B35	76.18	16.92	195	240	45
212	(213/214)	9	*east*	B35	B36	76.28	16.81	100	150	50
213	(214/215)	9	*east*	B36	B37	76.33	16.75	50	75	25
214	(215/216)	9	*east*	B37	B38	76.38	16.65	25	40	15
215	(217/218)	10	*south*	S1	S2	58.36	8.86	75	160	85
216	(218/219)	10	*south*	S2	S3	58.30	8.93	240	315	75
217	(219/220)	10	*south*	S3	S4	58.23	9.03	390	395	5
218	(220/221)	10	*south*	S4	S5	58.17	9.13	400	515	115
219	(221/222)	10	*south*	S5	S6	58.07	9.27	400	515	115
220	(222/223)	10	*south*	S6	S7	57.97	9.40	165	285	120
221	(223/224)	10	*south*	S7	S8	57.89	9.51	65	115	50
222	(224/225)	10	*south*	S8	S9	57.83	9.62	30	50	20
223	(225/226)	10	*south*	S9	S10	57.75	9.73	30	45	15
224	(226/227)	10	*south*	S10	S11	57.67	9.82	25	45	20

Table 3.1: Station Pairs used to create the *north*, *south*, *east* and *west* boxes (as shown in Figure 3.1). Depths refer to the deepest property measurement (on the shallowest station of the pair) interpolated onto a 5db grid.

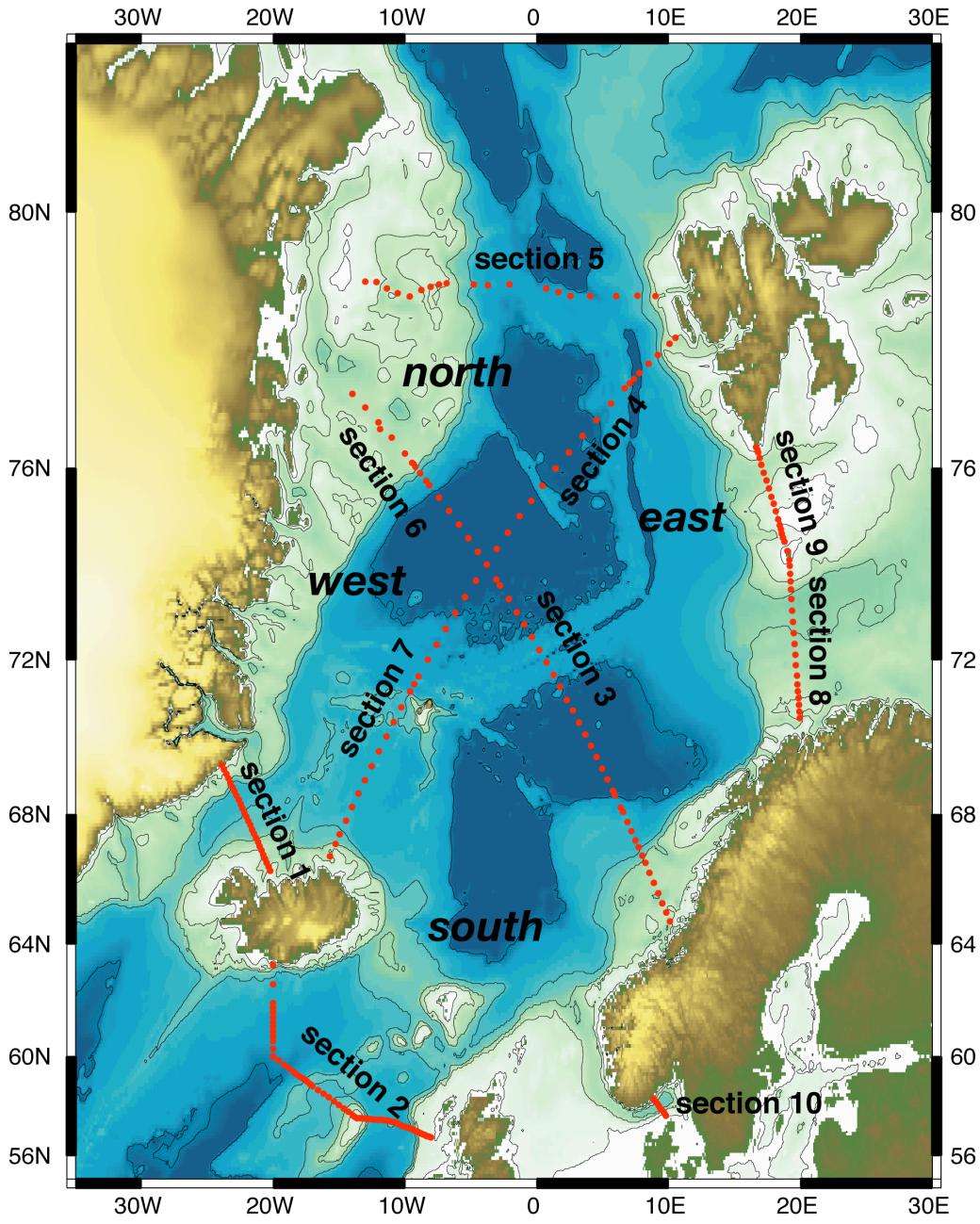

Figure 3.1: The Nordic Seas with station pair positions in red, showing the setup of boxes (*north*, *south*, *east*, *west*) used for the inverse calculation. The details of the box setup are described in section 3.7.

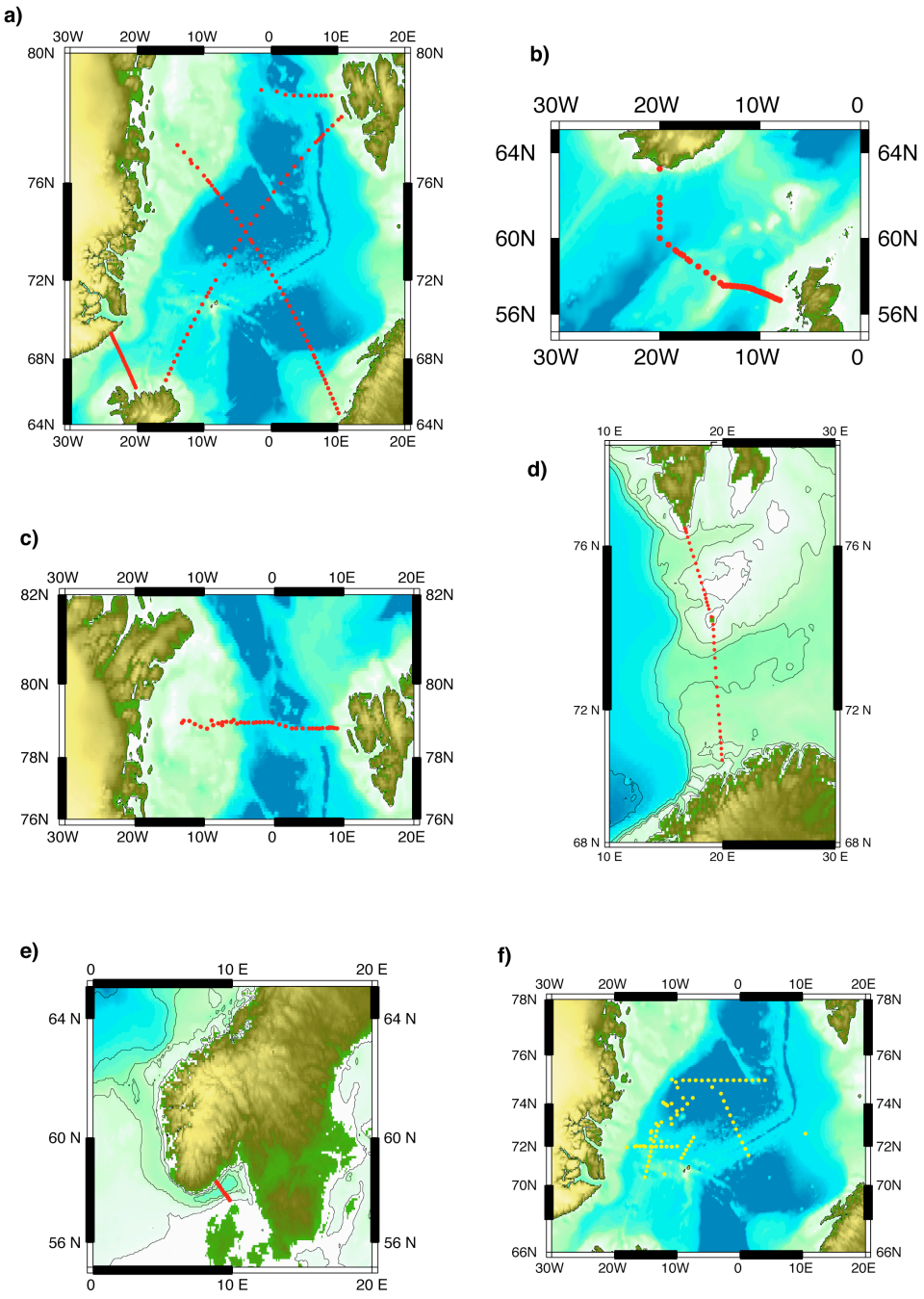

Figure 3.2: Hydrographic stations occupied during the individual cruises: a) JR44, Summer 1999; b) D242, Summer 1999; c) ARKTIS XV/3, Summer 1999; d) VEINS/9911, Summer; e) SKAGEX II, Summer 1990; and f) JM3/2000, Winter 2000.

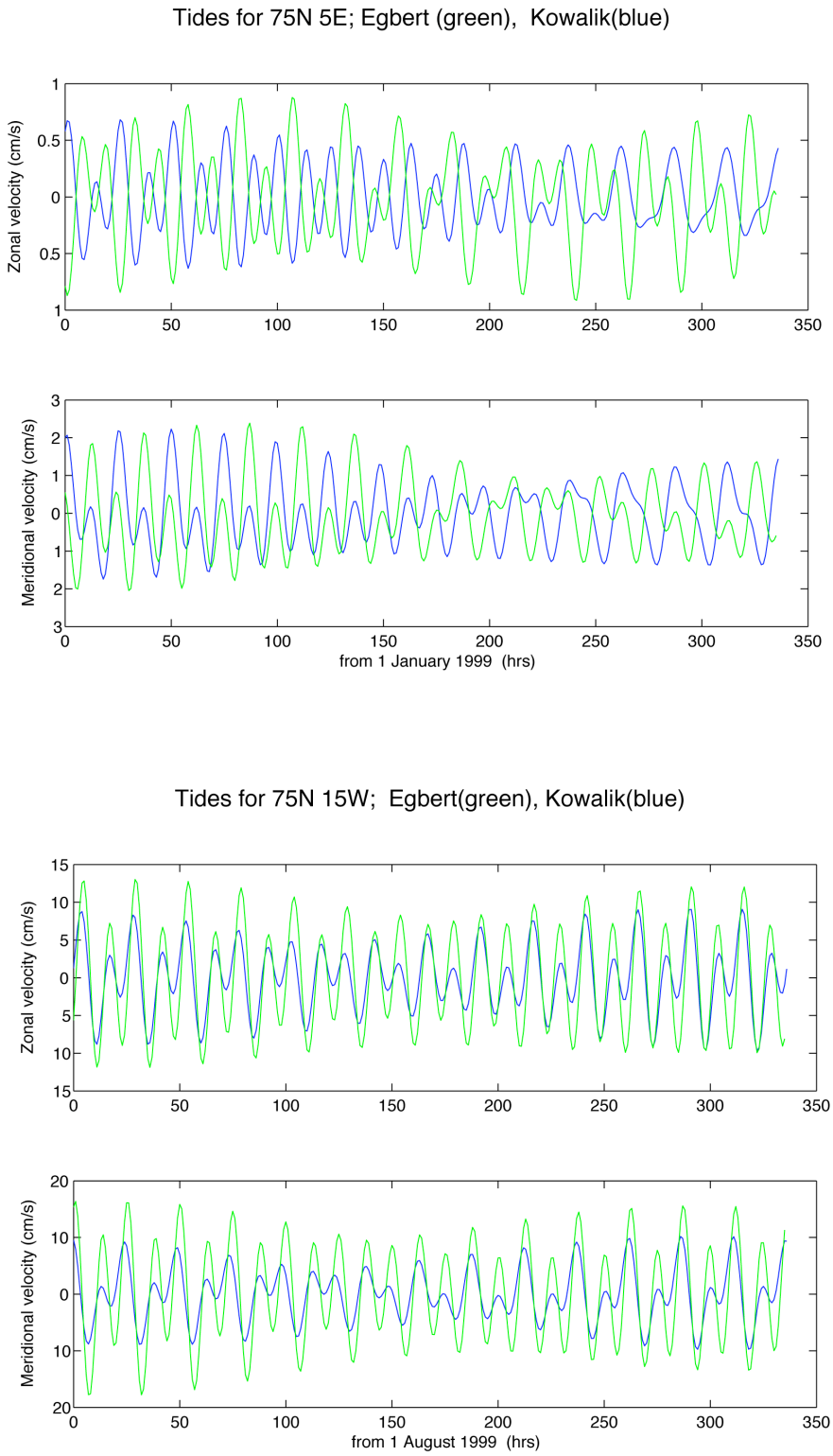

Figure 3.3: Comparison between the Egbert (green) and Kowalik (blue) tidal models at two sites within the Nordic Seas.

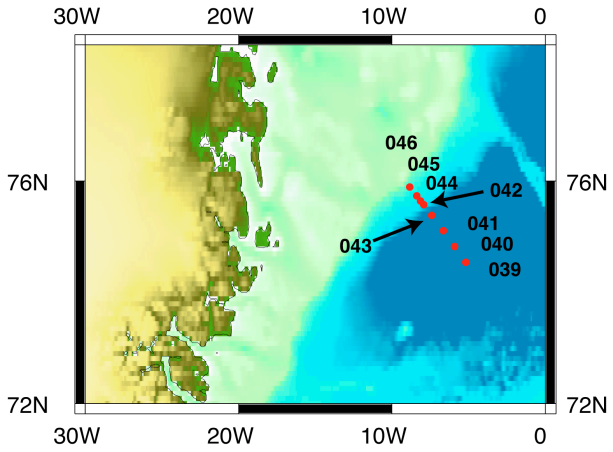

Figure 3.4: Station positions off the East Greenland coast on cruise JR44 showing the geographic locations of stations 042 and 043 in particular. Station 042 was conducted before station 043.

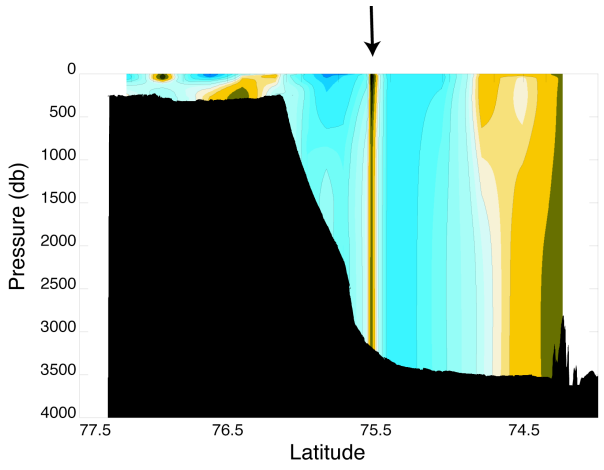

Figure 3.5: Geostrophic velocity (cm^{-1}) for section 6. Station 043 is included such that the stations are considered non-sequentially with respect to time. The apparent eddy like feature in this realisation is marked by the arrow. To eliminate this feature, station 042 is not used in the analysis.

Chapter Four

Methods

4.1 Introduction

The primary objective of this thesis is to determine the circulation of the Nordic Seas as it can be deduced from this unique data set of near-synoptic measurements obtained across the entire region during summer 1999. Specifically, the aim is to quantify the volume, heat and freshwater fluxes between the Nordic Seas and the Arctic Ocean to the north, the Barents Sea to the east, and North Atlantic to the south, via the Greenland-Scotland overflows.

In this Chapter the basic concepts of ocean circulation dynamics and flux calculations are first reviewed. The specific methods used in this thesis are then explained, including how LADCP data and inverse methods have been used to improve our estimates of the large-scale mean circulation.

4.2 Ocean Circulation Dynamics

The circulation of the ocean is governed by the laws of classical physics. Since the ocean can be considered as a fluid in a rotating frame of reference, geophysical fluid dynamics has created a dynamical and mathematical framework within which its circulation can be discussed.

4.2.1 The Geostrophic Method

The ocean tends towards a state of geostrophic equilibrium where the steady circulation is a balance between the local horizontal component of Coriolis force and the horizontal pressure gradient (Gill, 1982). This balance is a feature of the response of a rotating fluid to gravity and is described by the geostrophic approximation

$$-f v = -\frac{1}{\rho}\frac{\partial p}{\partial x} \qquad 4.1$$

$$f u = -\frac{1}{\rho}\frac{\partial p}{\partial y} \qquad 4.2$$

$$-\rho g = -\frac{\partial p}{\partial z} \qquad 4.3$$

where f is the Coriolis parameter ($f = 2\Omega \sin\phi$, with Ω as the angular speed of rotation of the earth (7.29×10^{-5} s^{-1}), and ϕ as the geographic latitude), u and v are the horizontal components of velocity in the x and y directions respectively (m s^{-1}), ρ is the density (kg m^{-3}) and p is pressure (Pa).

This geostrophic approximation can also be written in the form of the thermal wind relation

$$f\frac{\partial v}{\partial z} = -\frac{g}{\rho}\frac{\partial \rho}{\partial x} \qquad 4.4$$

$$f\frac{\partial u}{\partial z} = \frac{g}{\rho}\frac{\partial \rho}{\partial y} \qquad 4.5$$

which defines the velocity shear *(∂v/∂z* and *∂u/∂z)* at all depths. Integrating from z_0, the depth of the reference level, then

$$v_{(x,z)} = \frac{-g}{\rho_0 f} \int_{z_0}^{z} \frac{\partial \rho}{\partial x} dz + v_{(x,z_0)} = v_r + b \qquad 4.6$$

The first term of the R.H.S. of equation 2.6 is the relative velocity, v_r, which can be calculated from the density gradient. The second term is the unknown reference velocity, *b* (the constant of integration). To determine the absolute velocity some estimate of this unknown reference velocity must be made. Hydrographic data can thus be used to describe the circulation since the geostrophic shear (vertical velocity gradient) can be calculated from the horizontal density distribution computed from salinity and temperature profiles.

4.2.2 Time Dependence

The geostrophic method described above ignores the individual time derivatives. If time dependence is taken into account ('quasi-geostrophy', e.g. Gill, 1982) then equations 4.1 and 4.2 become

$$\frac{Du}{Dt} - f v = -\frac{1}{\rho}\frac{\partial p}{\partial x} \qquad 4.7$$

$$\frac{Dv}{Dt} + f u = -\frac{1}{\rho}\frac{\partial p}{\partial y} \qquad 4.8$$

where Du/Dt and Dv/Dt are the rate of change of u and v respectively. It follows that these terms would also be included in the conservation equations. The time derivatives describe the extent to which the system is not stationary, including variability on transient, seasonal, interannual and decadal time-scales. In practise, as here, the time derivatives are ignored and the conservation equations are applied in the steady state.

For a synoptic hydrographic survey of a couple of months duration, the rate of change of oceanic properties on a decadal timescale is not significant. For example, long term trends suggest a freshening within the Nordic Seas of the order ~0.01 per decade (Dickson et al., 2002). This implies a ~0.001 freshening per year, or ~0.00025 over the duration of the summer, and is insignificant. Curry and Mauritzen (2005) estimate that the Nordic Seas and Subpolar Basins have been diluted by an extra 19□000□km^3 of freshwater input between the years 1965 and 1995. Of this ~4000□km^3 remained in the Nordic Seas, accumulating at a rate of ~133□km^3 year^{-1} (i.e. 0.004□Sv) which is again less than the error bounds.

On an interannual timescale, numerous studies have given an indication of how interannual variability dominates over decadal variability. For example, observations from moored current meters, VM-ADCP and CTD data have suggested variability in the Atlantic inflow to the Nordic

Seas of the order 10% (Orvik et al., 2001). This would relate to a transport error of <0.1 Sv over a month long period, which is of the same order as the error bounds given to the fluxes (see Chapter 6).

Variability on seasonal timescales is also an issue. To try to determine its possible contribution the seasonality in the volumes of the isopycnal layers was estimated. Data from the National Oceanographic Data Center World Ocean Atlas 2001 (WOA01; (Conkright et al., 2002)) was used. This atlas provides objectively analysed fields of major ocean parameters at annual, seasonal and monthly timescales on a 1° by 1° grid. The annual and seasonal fields are full depth, while monthly fields are to a depth of 1500 m. The depth of each isopycnal was estimated at every grid point (over the area covered by the *north*, *south*, *east* and *west* boxes) by linear interpolation. Layer volumes were then calculated by integrating over the horizontal areas spanned by the isopycnals using the monthly mean fields over the upper 1500 m. Figure 4.1 illustrates the seasonal variability of the volume of light waters within the Nordic Seas and the separate inverse boxes, and the corresponding volume flux error. These light waters (layers 1–5) are defined by a density of 1027.6 kg m^{-3}. The variability is based on the monthly variations from the yearly mean volume of waters. There is a clear seasonal cycle in the volume of waters. However, taken over the whole of the Nordic Seas region during the summer period, the variability of these waters are in the order of 5% (the maximum deviation of individual summer months from the summer mean volume). This is sufficiently low for conservation within individual layers to be valid. Typically this would influence the fluxes calculated for the Nordic Seas to within ~1 Sv, which is in any case within the error bounds of the calculation (Table 4.1).

	Volume Flux Error (Sv)	**Freshwater Flux Error (Sv psu)**	**Heat Flux Error (TW)**
Maximum error	3.8	0.11	23
RMS mean error for Nordic Seas	0.8	0.02	5

Table 4.1: Flux errors due to seasonality in the volumes of the isopycnal layers. The maximum error within all layers (above 1500 m) and boxes, and the rms mean error for the Nordic Seas are quoted.

At the smallest end of the spectrum, short term variability such as internal waves (see section 4.2.6) do complicate the measurement of the density field by introducing fluctuations for which it is difficult to correct. Internal waves can occur at surfaces between different density layers within the ocean (Pond and Pickard, 1983). They can be a major source of error in flux calculations since they produce a wave motion with no associated mass transport. They may lift a density surface for the duration of their passing; apparent as internal wave noise in velocity space.

These estimates of the individual time derivatives suggest that the use of 'steady state' conservation equations is justified.

4.2.3 Volume Transports

Volume flux is calculated as the area integral of velocity across each section

$$\textit{Volume flux} = \int v \, dx \, dz \qquad 4.9$$

where dx is the station pair separation (m), dz is the mean station pair depth (m) and v is the velocity ($m\,s^{-1}$). Oceanographers commonly quote volume transports in the convenient non-SI (International System of Units) unit of Sverdrups (Sv), with 1 Sv equal to $1 \times 10^6\ m^3\,s^{-1}$.

To simplify interpretation of the circulation, the water column can be divided into layers defined by pressure, density, temperature or salinity. This allows the transport of various water masses (as described by hydrographic characteristics) to be calculated. For this work, the sections have been split into fourteen layers defined by potential density, subdividing the main water masses (Table 4.2). These isopycnals were chosen such that the range of water masses within the domain of the Nordic Seas and north of the Iceland-Scotland section were resolved while keeping to a reasonable number of layers. Neutral density, γ^n (a function of salinity, temperature, pressure, longitude and latitude), is not yet defined for the Nordic Sea and Arctic Ocean regions and so it could not be used in this thesis.

When computing geostrophic transports it is necessary to allow for the missing triangle at the bottom of each station pair (the triangular area below the deepest observation of the shallower station of each pair). Uncertainty arises from the interpolation or extrapolation of the property gradients since the geostrophic profile extends only to the deepest common depth of the temperature and salinity profiles for each station pair. Various extrapolation techniques have been employed (Fiadero and Veronis, 1983): linear decrease in vertical shear, continuation of constant vertical shear, and continuation of constant velocity from the deepest common level to the bottom. The method of extrapolation can strongly affect transports where there is a large difference between the depths of two stations in a pair. A simple procedure has been used here whereby the current at the greatest common depth is extended at a constant value to the mean pair depth. The full station pair separation is used so that the areas are correct. An alternative method of calculation was also investigated (Chapter 6) where the velocity shear at the deepest common depth was extrapolated through the bottom triangle area of each station pair.

Layer	Layer Boundaries	Section						
		DS	**BSO**	**FS**	**GN**	**ISval**	**IScot**	**Skag**
1	$\theta_0 < 26.5$	13 (27)	11 (21)	27 (54)	16 (31)	- -	20 (40)	18 (35)
2	$26.5 < \theta_0 < 27.0$	26 (17)	19 (20)	38 (17)	31 (17)	11 (21)	33 (65)	44 (9)
3	$27.0 < \theta_0 < 27.3$	42 (13)	33 (23)	40 (9)	37 (21)	12 (23)	131 (128)	54 (15)
4	$27.3 < \theta_0 < 27.5$	58 (19)	48 (27)	48 (13)	55 (38)	21 (10)	422 (437)	137 (151)
5	$27.5 < \theta_0 < 27.6$	81 (26)	58 (27)	58 (26)	88 (34)	29 (9)	881 (153)	308 (177)
6	$27.6 < \theta_0 < 27.7$	105 (26)	71 (50)	81 (27)	96 (49)	38 (8)	1063 (199)	- -
7	$27.7 < \theta_0 < 27.8$	122 (30)	116 (63)	111 (35)	158 (74)	44 (11)	1524 (706)	- -
8	$27.8 < \theta_0 < 27.95$	175 (83)	201 (88)	237 (228)	277 (175)	86 (72)	2111 (374)	- -
9	$27.95 < \theta_0 < 28.0$	295 (181)	320 (39)	533 (259)	423 (101)	171 (107)	- -	- -
10	$\theta_0 > 28.0$ and $\theta_1 < 32.73$	459 (128)	328 (6)	725 (123)	528 (73)	274 (90)	- -	- -
11	$32.73 < \theta_1 < 32.76$	636 (185)	228 (7)	868 (159)	648 (169)	408 (194)	- -	- -
12	$32.76 < \theta_1 < 32.78$	776 (114)	272 (11)	1030 (163)	854 (249)	640 (265)	- -	- -
13	$\theta_1 > 32.78$ and $\theta_2 < 37.45$	1165 (360)	279 (1)	1538 (852)	1506 (1058)	1284 (1026)	- -	- -
14	$37.45 < \theta_2$	- -	- -	2313 (286)	2581 (870)	2487 (871)	- -	- -

Table 4.2: Layers defined by θ_0, θ_1 and θ_2 surfaces (potential density minus 1000 kg m^{-3}, referenced to the surface, 1000 m and 2000 m, respectively), with mean layer depth and thickness (in brackets) for each section, and each layer.

Following Naveira Garabato et al. (2002) the uncertainty in volume transport calculations is estimated by applying random barotropic perturbations to individual velocity profiles, and calculating the root-mean-square deviation of 50 realizations of the resulting transport. The perturbations followed a normal distribution with a standard deviation of 3 cm s^{-1}, the characteristic accuracy of the barotropic component of the LADCP flow (section 3.6.2). This assumes that the dominant source of error is in the barotropic component of the LADCP flow, and that errors are horizontally uncorrelated. These transport error estimates do not include the sampling error due to regions of steep topography being poorly resolved (leading to large discrepancies in the depths of the stations making up a station pair). These *a priori* errors are used in the weighting scheme for the standard inverse model (see sections 4.6.3 and 5.6.2) and are summarised in Table 6.1.

4.2.4 Heat Fluxes

An understanding of the mechanisms by which oceanic energy transport occurs is of prime importance since changes in these mechanisms provide indicators of the oceanic response to climate change. The primary mechanisms of heat transport described by Bryden and Imawaki (2001) are: the large scale overturning thermohaline circulation, the shallow wind-driven Ekman transport, the horizontal circulations associated with the basic horizontal ocean gyres (driven by the curl of the wind stress in the interior and closed by a boundary at the western coast) and eddy fluxes.

For ocean heat transport, analysis of the basin-scale circulation can focus on the net flow in a set of layers defined by isopycnal surfaces. Heat fluxes due to ocean currents can only be calculated for an area of ocean where volume is conserved, for example, within each of the inverse boxes:

$$Heat\ Flux = \int\int \left(\rho C_p \theta v \right) dx\, dz \qquad 4.10$$

where ρ is the density, C_p is the specific heat capacity, θ is the potential temperature, v is the component of velocity normal to the section, dx is the station pair separation and dz is the mean station pair depth.

Following Bryden and Imawaki (2001), to determine the mechanisms and process by which heat is transported across a hydrographic section, the flux calculations can be further divided into the barotropic component due to the net transport across the section at the section averaged temperature, the baroclinic transport due to the overturning circulation, and the horizontal component due to the large scale gyre circulation and smaller-scale eddies. This gives:

$$Heat\ Flux = \left(\rho C_p V < \theta > \right) \int L_{(z)}\, dz + \int \left(\rho C_p \bar{\theta}\, \bar{v}\, L_{(z)} \right) dz + \int\int \left(\rho C_p \theta' v' \right) dx\, dz \qquad 4.11$$

The first term refers to the net transport across the section, V, at the section averaged temperature, $<\theta>$, where $\int L_{(z)}\, dz$ is the area of the section. The second term refers to the baroclinic heat transport where $\bar{\theta}$ and $\bar{v}$ refer to the average temperature and velocity over a density surface, and L is the horizontal length of that surface. The third term refers to the horizontal heat transport, where $\theta' = \theta - \bar{\theta}$ and $v' = v - \bar{v}$.

4.2.5 Freshwater Fluxes

Direct estimates of oceanic freshwater fluxes can be determined using hydrographic sections enclosing a volume of ocean, for which budget equations can be written (Wiffels, 2001). Over a region of ocean there is generally an imbalance between freshwater inputs and evaporation, resulting in non-zero convergence or divergence of freshwater. In contrast, salinity is conserved since it cannot be exchanged across the free surface of the ocean, and has no significant sources or sinks (Brown et al., 1989).

For a volume of ocean enclosed by hydrographic sections, where volume is conserved, the freshwater flux, F, is defined as

$$F = P - E + R \qquad 4.12$$

where P is the precipitation over the region, E is the evaporation and R represents the contribution of freshwater inputs from river runoff and glacial melt. The volume flux for the region is defined as

$$V + F = \int v\, dx\, dz + F = 0 \qquad 4.13$$

and the corresponding salinity flux is defined as

$$Salinity\ Flux = \int (S\,v)\,dx\,dz = 0 \qquad 4.14$$

where S is the salinity and v is the component of velocity normal to the section. An areal average salinity, $\bar{S}$, and its deviation, S', over the region can be calculated following:

$$\bar{S} = \frac{\int S\,dx\,dz}{\int dx\,dz} \qquad and \qquad S' = S - \bar{S} \qquad 4.15$$

The salinity flux can then be written as

$$V\,\bar{S} + \int S'v'\,dx\,dz = 0 \qquad 4.16$$

From equation 4.11

$$V\,\bar{S} + F\,\bar{S} = 0 \qquad 4.17$$

so the freshwater flux divergence over the region can be written as the product of the salinity deviations and the velocity field:

$$F = -\frac{\int S'v'\,dx\,dz}{\bar{S}} \qquad 4.18$$

This calculation of the freshwater flux assumes the measured salinity and velocity fields are representative of the long-term mean (Wiffels, 2001). Since the errors in the measured volume and salinity fluxes are highly correlated they largely cancel when combined as in equation 4.16. The accuracy of modern salinity measurements, allows then the derivation of freshwater (fractions of a Sv) despite net volume fluxes being measured only to within a few Sv. If an accuracy of ±0.01 in salinity were to be assumed then, for a mean salinity of 35 and a volume flux of 15Sv for example, the freshwater flux would be determined to an accuracy of ±0.0003 (Bacon, 1996).

4.2.6 Ageostrophic components of the circulation

(i) Wind driven Ekman Transport

The near-surface layer of the ocean does not have a purely geostrophic flow, rather it is directly influenced by the winds. Historically, Nansen noted that icebergs drifted to the right of the wind in the north. Ekman (1905) showed this behaviour to be caused by the Coriolis force, ie the effect of the rotation of the earth. This results in a depth integrated Ekman transport to the right of the wind in the northern hemisphere, and to its left in the southern hemisphere. The resultant flow can give rise to vertical motion (upwelling and downwelling), depending on the divergence or convergence of the wind driven Ekman transports. This Ekman transport associated with the direct wind forcing is an important component of the surface transport of the overturning circulation.

At high latitudes the seasonal heating and cooling of the Ekman layer drives a component of the time dependent heat transport in those regions. Ekman transport thus has a strong impact on the

time-dependent heat transport. This variability, however, does not affect estimates of the time-mean heat transport made by hydrographic surveys if the Ekman layer contribution is estimated from the time-mean wind stress (Jayne and Marotzke, 2001).

In this thesis, Ekman transports were calculated using the SOC (Josey et al., 1999) and Hellerman and Rosenstein (1983) climatologies. The climatological wind stress fields (projected onto station pair positions) are used to estimate the cross-track Ekman fluxes:

$$Ekman\,Volume\,Transport = \frac{\Delta\tau^{x}\,\Delta x}{\rho f} \qquad 4.19$$

where τ is the wind stress along the section (Nm^{-2}), Δx is the distance between stations (m), f is the Coriolis parameter and ρ is the density (kgm^{-3}).

The Ekman transport estimates are then combined with property measurements to calculate the property fluxes. Although Ekman volume transport does not depend on the thickness of the Ekman layer, the Ekman flux of other properties does. The depth scale of the Ekman layer is proportional to the wind friction velocity and is a function of latitude, being inversely proportional to the square root of the Coriolis parameter (Niiler, 2001). This depth, theoretically the depth at which the direction of the wind-driven current is directly opposite to its direction at the surface, is ~50m at mid-latitudes. Hence, for the calculation of property fluxes the vertical mean of the property concentration over the upper 50m at each station is used.

(ii) Internal Waves

Internal waves can occur at surfaces between different density layers within the ocean (Pond and Pickard, 1983). The possible cause of internal waves is an instability of flow where there is strong vertical shear of velocity (eg strong tidal currents over rough topography). In the upper layers of coastal waters, internal waves may have periods of a few minutes and amplitudes of several metres, while in oceanic waters (where density differences are typically smaller) periods of up to 12 hours and amplitudes of 10 to 300m have been observed. Internal waves can be a major source of error in flux calculations since they produce a wave motion with no associated mass transport. They may lift a density surface for the duration of their passing; apparent as internal wave noise in velocity space.

4.3 Analysis of Direct Velocity Measurements

Following the initial processing of the LADCP data (described in Chapter 3), for each station where the LADCP was successfully deployed, there are two sources of direct velocity measurements; Water Track and Bottom Track (hereto referred to as WT and BT respectively). WT data consists of full depth velocity profiles (except the surface 50m and the bottom 30m). BT data consists of

velocity profiles over the bottom few hundred metres of the water column. These final velocity profiles are the sum of the baroclinic and barotropic components.

4.3.1 Detiding

The absolute velocities derived from LADCP data include a deterministic ageostrophic component of the current due to barotropic tides. These tidal currents can be removed from the measured currents by use of a suitable tidal model. The processed JR44 LADCP data are detided using the Kowalik tidal model, while the D242 LADCP data, which is all south of 64°N, are detided using the Egbert tidal model. These models were both described in section 3.4.2. For consistency, it would be preferable to use one tidal model for all the data, however this was not possible due to the geographical extent of the models and data. The Egbert model does not extend beyond north of 65°N with any confidence, and the Kowalik model is only applicable north of 61°N.

Tidal velocities are calculated every 10 minutes over the duration of the cast, or period of bottom tracking. The mean tide between the start and end of a cast is usually negligibly different from the tide at the bottom of the cast (Torres, pers com., 2002). In this study, the mean difference between the tide estimates is 0.001 $cm\,s^{-1}$, which is not statistically significantly different from zero to the 95% confidence limit. The mean tidal velocities for the period of bottom tracking are thus used as the tidal correction. These are applied as a barotropic offset to both the full depth and bottom track velocity profiles. The directions and magnitudes are illustrated in Figure 4.2. Over most of the region the tides are small, in the region of 1 to 2 $cm\,s^{-1}$. There are, however, significantly larger tides on Section 1, to the north of Denmark Strait. This is consistent with current meter measurements in the region, which found substantial tides reaching up to 25 $cm\,s^{-1}$ (Girton, 2001).

4.3.2 Full-depth profile and near-bottom velocities

Figures 4.3, 4.4, 4.5 and 4.6 illustrate the direct velocity field derived from the detided full-depth LADCP measurements made on the Denmark Strait, Fram Strait, Greenland-Norway and Iceland-Svalbard sections. A velocity field is created for the hydrographic section across Fram Strait using the LADCP measurements made in Fram Strait during ARCICE cruise JR44. These profiles are interpolated on to the box station positions 122 to 130 (Table 3.1) created from the AWI CTD data (section 3.5).

To allow a comparison between the LADCP data and the geostrophic (CTD-derived) flow between two stations, the full depth detided WT profiles from adjacent stations are averaged onto the midpoint position for each station pair and rotated to along-track and across-track components. The differences between the geostrophic profiles and the across-track component of the WT profiles are calculated at each depth, and the mean difference is then taken to be the WT offset, with one value for each station pair. Near surface LADCP measurements include an ageostrophic component due

to wind-driven Ekman flow. To take this into account, for stations deeper than 2000 m, the depth mean difference is calculated over the water column below the surface 2000 m.

Estimates of the near-bottom velocity are also obtained from the two independent sources of LADCP data (WT and BT). The BT bottom velocity is estimated by averaging the detided BT data. The top and bottom 200 db of the profile are excluded from this calculation to minimise bias caused by greater instrument error at maximum range (Cunningham et al., 2003). The WT bottom velocity is estimated by averaging the detided WT data over the same depth range. These near-bottom velocities are averaged on to the mid-point positions for each station pair and rotated to along-track and across-track components.

The WT offset and WT and BT near bottom velocities provide three alternative estimates of the reference velocity and are used to derive the initial velocity field (section 4.5).

4.4 Geostrophic and Direct Velocities

This section gives a short discussion of the velocity fields for each section, contrasting the geostrophic field (referenced to a level of no motion at the seabed) with the direct velocity field, where measurements were available. This inspection prepares the ground for the derivation of the initial velocity field (section 4.5). Regions are identified where measurements are in agreement, and where the greatest discrepancies are to be found. Where appropriate, comparison is also made to typical velocities quoted in the literature. These values are generally based on yearly mean currents reported by various field programmes, and so may not be representative of a summer mean circulation. Here, velocities are referred to as barotropic when there is no velocity shear in the vertical throughout the water column.

4.4.1 Nordic Seas Openings

(i) Denmark Strait

On the shallow shelf off Greenland the mean flow is southward, with some northward flow at the surface. Geostrophic velocities up to 10 cm s^{-1} are observed. LADCP velocities (Figure 4.3) are generally stronger with stronger flow at the bottom, except for some apparent northward flow on station pair 3 (JR44 stations 147–148; station pair details are described in Table 3.1). On the shelf slope, the LADCP velocities are largely barotropic with southward flow of 12–15 cm s^{-1} throughout the water column. The geostrophic field clearly shows the flow of the East Greenland Current, with strong velocities (up to >40 cm s^{-1}). Over the deeper part of the Strait the circulation is complex with evidence of large–scale cyclonic eddies, the mean flow being southward on the western flanks, and northward on the eastern flanks. The geostrophic field shows a stronger flow at

the surface, although the LADCP velocities suggest the flow at depth within the large-scale eddies may reach strengths between 15 cm s^{-1} southward and 10 cm s^{-1} northward. There is mean southward flow in the deeper waters over the continental slope off Iceland on the eastern part of the section, but northward flow in the upper waters. Over the Icelandic shelf itself the flow is mainly northward; evidence of the continuation of the Irminger Current carrying Atlantic Water through Denmark Strait and along the northwestern coast of Iceland. Measurements of the annual mean direct flow (Jonsson, 1999; Kristmannsson, 1998) suggest a somewhat less complex picture with fairly weak southward currents (2 cm s^{-1}) to the west, stronger southward currents (10–20 cm s^{-1}) on the western flanks of the sill and moderate northward currents (5 cm s^{-1}) on the eastern flanks of the sill (Isachsen, 2003).

(ii) Barents Sea Opening

No synoptic direct velocity measurements (LADCP) were available for this section, so the geostrophic field is discussed here. A fairly strong westward jet is apparent at the tip of Svalbard with flow of up to 30 cm s^{-1} at the surface. There is also mainly westward flow on the northern flanks of Storfjordrenna showing apparent surface-intensification to the north, but greater velocities at depth on the southern flanks. Over the very shallow shelf in the vicinity of Bear Island there is evidence of only very weak recirculating flow. The main inflow of Atlantic Water to the Barents Sea occurs between 72°N and 73°N through the southern part of Bjørnøyrenna. Velocities of ~10 cm s^{-1} are associated with the core of the inflow and some return westward flow is found on the northern slope off Bear Island. On the shelf off the northern coast of Norway there are strong eastward currents of up to ~20 cm s^{-1} into the Barents Sea. O'Dwyer et al. (2001) presented a similar picture of the velocity field, dominated by barotropic tidal currents, using vertically averaged ADCP velocities. They find the flow on the southern flanks of Bjørnøyrenna to be characterised by weak to moderate eastward velocities of 2–5 cm s^{-1}, with a return westward flow of 3–10 cm s^{-1} along the northern slope. To the north of Bear Island, weak (0–2 cm s^{-1}) eastward flow is described on the southern slope of Storfjordrenna with strong westward flow (10–30 cm s^{-1}) on the northern slope. Ingvaldsen et al. (2004b) using 4-year long records from moored current meters between 71°30'N and 73°30'N, found that although the mean velocity field of the Barents Sea Opening shows the Atlantic inflow as a wide core between these latitudes it is dominated by large and frequent fluctuations.

(iii) Fram Strait

To the west in Fram Strait, over the Greenland shelf, the geostrophic velocity field is very weak. Towards the shelf break, southward flow is apparent in the upper waters (~ surface 50 m) with fairly strong currents (>20 cm s^{-1}) on some station pairs. Over the Greenland continental slope the geostrophic field suggests weak currents throughout most of the water column with stronger

southward flow at the surface, peaking at ~10 cm s^{-1}. The LADCP data (Figure 4.4) suggest southward surface flow and moderate barotropic southward currents (~5–10 cm s^{-1}) below about 500 m. The apparent weak northerly flow between these layers may be waters of Atlantic origin recirculating within Fram Strait. This general picture is consistent with the annual mean description of the East Greenland Current (Fahrbach et al., 2001). Over the relatively smooth, deep, central part of the strait, the geostrophic field suggests very weak southward flows below about 1000 m, and stronger southward flow in the upper layers to the west. The LADCP data show some apparent cyclonic recirculation within the deep part of Fram Strait and with indication of moderate bottom velocities (5–10 cm s^{-1}) on some station pairs. In the eastern part of Fram Strait, over the continental slope off Svalbard, the mean flow is northward. This northward flow continues onto the continental shelf region with geostrophic velocities up to ~10 cm s^{-1} and stronger flow in the direct velocity field (~20 cm s^{-1}). Fahrbach et al. (2001) discussed a strongly barotropic West Spitsbergen Current with strong northward bottom flow (5–20 cm s^{-1}) based on annual mean currents. However, they described a clear seasonal signal, with a minimum volume transport in August, which is consistent with the weaker currents observed here.

(iv) Skagerrak

The geostrophic velocities indicate that the outflow from the Baltic Seas to the North Sea shelf region is confined to the northern part of the channel. The outflowing surface currents are very strong, peaking at velocities of 1 m s^{-1} to the very north of the section. The outflow is balanced by a recirculating inflow in the deeper parts of the channel, and on its southern slope. These exchanges are dominated by alternating barotropic inflows and outflows (Winsor et al., 2001), with the instantaneous flow typically of the order 10 times the net outflow.

4.4.2 Nordic Seas

(i) Greenland-Norway

Over the East Greenland continental shelf the circulation is variable, with evidence of some local recirculation, but the mean flow is southward. There is little flow below ~100 m, but surface velocities of >20 cm s^{-1} are observed on one station pair. On the shelf slope the EGC is evident with surface velocities of 20–25 cm s^{-1}. Over much of the Greenland basin there is weak bottom flow, although on some station pairs there are bottom velocities in the order of 5 cm s^{-1}. Within the deep basin there is a generally cyclonic circulation at all depths, except over the bottom 1000 m where flow is mainly southward. In the vicinity of the Polar Front, roughly over Mohns Ridge, there is a northeastward surface current and southward flow below about 1000 m. Within the Lofoten basin in the Norwegian Sea a strong cyclonic circulation is observed with the LADCP data (Figure 4.5) suggesting moderate bottom velocities (5–10 cm s^{-1}) in places. Over the Norwegian

continental slope and shelf the flow is mainly northward with some return southward flow between the 1500□m isobath and the foot of the slope. It is interesting that on some deep stations in the Greenland and Norwegian Seas the LADCP data show moderate bottom flow (up to ~5□cm□s^{-1}) whereas the classic picture is of weak (around zero) geostrophic flow in the deep basins. Although there is no evidence of the long-lived penetrating eddies observed in the Greenland Basin by Gascard et al. (2002) and Wadhams et al. (2004), the LADCP data does suggest some circulation within the deeper waters.

(ii) Iceland-Svalbard

The majority of the flow off the north Icelandic coast and in the southern part of the Iceland Sea is to the southeast. This is likely to be formed in part from the continuation of Atlantic Inflow in the Irminger Current as the Northeast Icelandic Current and cyclonic circulation within the Iceland Sea. Over the deep basins of the Greenland Sea there is again evidence of a broadly cyclonic circulation, with fairly weak flow in the geostrophic velocity field. Offshore of the Svalbard continental slope there is mostly northward flow, except for some small recirculations, with weak currents at depth and significantly stronger currents towards the surface in both the geostrophic and LADCP velocity fields (Figure 4.6). On the slope itself there is a mainly northward flow. These northward currents are, in the upper waters, the continuation of the Norwegian Atlantic Current (carrying waters of Atlantic origin towards Fram Strait), and are at depth, the flow carrying remnants of the dense winter water formed in the northern Barents Sea and in the Storfjorden.

4.4.3 Northeast Atlantic

(i) Iceland-Scotland

On the shelf slope off the south coast of Iceland there is very weak flow in the geostrophic field but the direct velocities suggest moderate (~5□cm□s^{-1}) flow to the west. On descent to roughly the 2000□m isobath the geostrophic shear remains fairly weak throughout the water column, however, the direct velocities again suggest a strong westerly flow (10–40□cm□s^{-1}), stronger at depth. Further south into the Iceland Basin there is indication of northeasterly flow in the upper waters (surface 500–1000□m), but southwesterly flow at depth. Ascending the slope towards the Hatton Bank region, the apparent flow is mainly towards the southwest with moderate (10–20□cm□s^{-1}) barotropic flow in the upper 1000□m. Very weak flow (~zero) is evident from geostrophy on some stations pairs, whereas the LADCP data suggest moderate southward flow for these station pairs. In the shallow waters of the Hatton Bank and Rockall Plateau region the flow is variable but mainly weak (<5□cm□s^{-1}). Towards the east of this region there is a complex circulation as the bathymetry steepens. For the first few station pairs the geostrophic velocity field suggests mainly northward flow (up to ~20□cm□s^{-1} towards the surface), but the LADCP data suggest weak southward flow. On

the next few station pairs, the flow is apparently reversed, with geostrophy giving southerly flow, and the LADCP data giving northerly flow. Over the shallower region before the final descent into the Rockall Trough the flow is broadly northward. Within the trough itself there is variable flow, with generally stronger velocities in the upper waters (above ~1000□m). Over the slope towards the Scotland continental shelf there is moderate to strong northward flow, with mainly (weak) northward flow on the shallow shelf region. For this section, shipboard ADCP data over the upper 500□m was available in addition to the LADCP data. The ADCP data provided continuous coverage of the velocity field of the upper water column, whereas the LADCP data provided only on-station measurements. Examination of this alternative estimate of the velocity field suggests that the inflow of the Atlantic Water was confined to the Rockall Trough to the east of the Hatton-Plateau (see section 4.5.2).

4.5 Derivation of the Initial Velocity Field

4.5.1 General Principles

The accurate calculation of fluxes and transports require an absolute velocity field. Volume flux, for example, is calculated as the area integral of velocity across each section. Since the velocity shear calculable from hydrographic data represents only the relative velocity between two depths, the absolute geostrophic velocity profile for any station pair is defined as the sum of the geostrophic and reference velocities. This reference velocity is an offset derived either from some known velocity at some known depth or an estimate of the barotropic (depth averaged) velocity. The classical technique is to use a level of no motion defining the velocity to be zero at some depth as suggested by water mass boundaries or the absence of velocity shear. An alternative technique is the use of direct velocity measurements (from current meters, for example) to reference the flow. These various methods inevitably result in different absolute geostrophic velocity fields (Pickart and Lindstrom, 1993).

Traditional methods of referencing geostrophic velocities based upon water mass distributions do not always accurately represent the velocity field (Donohue et al., 2000), since the density structure alone is insufficient to fully describe the ocean circulation. The circulation of the Nordic Seas is strongly influenced by topography (Chapter 2), and much of the flow is concentrated over slopes with a strong barotropic component. In many regions, levels of no motion either do not exist, or there is no objective way of determining them (Hansen and Østerhus, 2000).

LADCP measurements made on hydrographic stations have successfully been used as a referencing method (Beal and Bryden, 1997; Cunningham et al., 2003; Naveira Garabato et al., 2002). The question remains as to whether direct, instantaneous velocities are typical of the long-term mean. However, LADCP measurements can identify robust features of the circulation that may not be

apparent from the hydrographic data alone. For example, using full-depth LADCP profiles Beal and Bryden (1999) discovered that the Agulhas Current velocity signal extends to the sea-bed and that there exists an equatorward Agulhas Undercurrent. These features had never been inferred from hydrographic measurements alone, and since they were found in three different LADCP velocity sections they are considered to form part of the long term mean circulation (Donohue et al., 2000).

The direct velocity field can be rather difficult to interpret since it is a 'snapshot' of the currents, and an exact agreement between the direct (LADCP) and geostrophic velocity fields cannot be expected (Joyce et al., 2001). Firstly, actual LADCP velocities will include ageostrophic components throughout the water column due to inertial oscillations, internal waves, and internal tides. Secondly, the station pair LADCP profiles are the average of two sets of instantaneous velocity measurements. Thirdly, there are errors associated both with the measurement of LADCP data (see section 3.6.2), and with the calculation of the geostrophic velocity field (see section 3.5 for accuracy of the hydrographic data).

There is, as yet, no consensus on the best technique by which LADCP data can be used to reference geostrophic velocities. With the data available for this thesis, the alternatives are:

(i) use of a near-bottom velocity derived from BT data

(ii) use of a near-bottom velocity derived from WT data

(iii) use of an offset derived from the full depth WT data.

The WT offset, together with the WT and BT near-bottom velocities, provide three estimates of the reference velocity. Over the full dataset, the differences between the WT and BT near-bottom velocities (Figure 4.7) have a mean of 0.45 cm s^{-1}, and an RMS deviation of 2.5 cm s^{-1}. The mean difference is not significantly different from zero at the 98% confidence limit. The normal probability plot shows that, excepting outliers greater than about 4 cm s^{-1}, the differences between estimates follow a normal (random) distribution.

However,

(i) on some station pairs there are large differences between the LADCP derived estimates of the reference velocity;

(ii) the shears of the geostrophic and WT profiles differ greatly in some regions;

(iii) over steep topography station pairs have large differences in bottom depth of their constituent stations leading to uncertainty in the interpolation of the WT and BT near-bottom velocities on station pair positions.

For this thesis, alternative initial velocity fields were created using a 'best guess' of the reference velocity (a subjective choice between the LADCP alternatives and no adjustment). For this, a subjective selection of reference velocity was made on a station by station basis. The choice was

made by inspection of the WT and BT profiles for each station in the pair, together with the station pair geostrophic profile (section 4.4). An exact agreement between the LADCP and geostrophic velocity fields cannot be expected (Joyce et al., 2001). Firstly, actual LADCP velocities include ageostrophic components and secondly, the station pair LADCP profiles are an average of two sets of instantaneous velocity measurements. For each station pair, a constant velocity offset was sought such that when added to the geostrophic estimate, the difference between the two profiles over some depth range is minimised. Hence, although BT data is more accurate than WT data over their common depth range (section 3.6.2) it was often desirable to use the full depth WT data over the full duration of the cast, rather than the shorter BT record. The WT offset was used here on the majority of stations, although the BT near-bottom velocity was selected for some shallow water station pairs. For shallow station pairs with particularly noisy LADCP/CTD comparisons (due to large ageostrophic effects), and for those station pairs where there was large divergence in the shear between the WT and geostrophic profiles, no adjustment was made.

The initial geostrophic velocity field was referenced to zero velocity at the bottom (see section 4.5.2 for the Iceland-Scotland section). Over much of the Nordic Seas there are strong barotropic currents (Cisewski et al., 2003) with significant bottom velocities, hence in many regions a zero bottom velocity is an unreasonable assumption. The LADCP derived reference velocity for each station pair was then applied as a barotropic offset to the full depth geostrophic profile creating the velocity fields used in the initial flux calculations (section 5.5). For station pairs without LADCP data, the reference velocity was set to the average of the LADCP derived reference velocities for the adjacent station pairs. The reference velocity was set to zero for those station pairs where it was decided to make no adjustment. Across the Barents Sea Opening, O'Dwyer et al. (2001) use vertically averaged ADCP velocities to study the velocity field. Since the thermal wind shear is weak, these can also be taken as an initial estimate of near-bottom reference velocities and were used in this work to reference the geostrophic field due to the absence of LADCP data.

To give an example of the alternative velocity fields created, Figure 4.8 illustrates station pair 81 at 68.1°N 6.5°E in the Norwegian Sea (Table 3.1). The geostrophic profile (referenced to zero at the bottom), full depth WT profile, and the geostrophic profiles adjusted to the WT LADCP are shown. On this station pair the shears of the geostrophic and full-depth WT profiles are well matched.

4.5.2 Iceland-Scotland section

The Iceland-Scotland section runs south from Iceland, southeast across the Iceland Basin to the Rockall-Hatton Plateau, and continues across Rockall Trough to the coast of Scotland (see Figures 3.1 and 3.2b). The entire section is south of the Greenland-Scotland Ridge and so lies within the northeast North Atlantic rather than the Nordic Seas. An estimated level of no motion at 1400□m was suggested by Saunders (2001) and this is used as the initial reference for the geostrophic

velocities. A first guess of the initial velocity field is derived by applying the LADCP derived reference velocities as a barotropic offset to these geostrophic velocities, following the procedure employed for the other sections.

The initial fluxes derived from the LADCP data indicated there was an imbalance within the initial circulation. The cumulative volume transports in the upper part of the water column suggest a 2□Sv inflow of Atlantic Waters across the section into the Nordic Seas (dashed black line in Figure 4.9). This was confined mainly to the Iceland Basin, and is low compared to the widely accepted values of 6.7□-□7.4□Sv (Hansen and Østerhus, 2000). Initial runs of the inverse also revealed imbalances with extremely low heat transports across the Greenland-Scotland Ridge and inconsistent results particularly when salinity conservation was required within the south box in the layers relating to the Atlantic inflow. In effect, the NAtlC and Atlantic inflow was 'missing' from the initial circulation.

To find the cause of the problem the hydrographic properties along the section are examined together with the alternative velocity field provided by the shipboard ADCP data. During this section an alternative estimate of the direct velocities in the upper water column was made by shipboard ADCP. This provided continuous coverage of the velocity field in the upper 500□m, with high spatial (1□-□2□km) and temporal resolution (2 minute ensembles), whereas the LADCP data provided only on-station measurements. The cumulative transports over the upper 500□m of the water column calculated from the average ADCP currents (solid black line in Figure 4.9) show the inflow of Atlantic Water to be confined to the Rockall Trough to the east of the Rockall-Hatton plateau. Turning to the hydrographic properties, the position of the warm and saline NAtlW can be seen to the right of the contoured salinity plot (Figure 5.7b), within the upper waters of the Rockall Trough. This evidence points to the major pathway of the inflow to the Nordic Seas at the time of the section being via the Rockall Trough.

Although the station spacing was such that a reasonable representation of the hydrographic properties along the section can be described, the LADCP data did not adequately capture the circulation of the upper part of the water column. One probable reason for this was that the length scales of variability in the water mass properties are greater than those for variability in the currents. To adjust the initial field to give a reasonable circulation, a further barotropic correction of 0.5□ms^{-1} directed into the Nordic Seas is applied to station pairs east of the Rockall-Hatton plateau. This adjustment ensured that the transports within the upper part of the water column are comparable to those suggested by the shipboard ADCP data (solid black line in Figure 4.9). The final input field for the inverse model was thus the geostrophic velocity field with a level of no motion at 1400m, with a northwards barotropic correction of 0.5□ms^{-1} to station pairs east of the Rockall-Hatton plateau.

The circulation of the sub-polar gyre is usually such that the major pathway for the inflow of Atlantic Water to the Nordic Seas is via the Iceland Basin to the west of the Rockall-Hatton plateau (Orvik and Niiler, 2002). However, the data from this section show the inflow to be confined to the Rockall trough during September 1999. This is known to be a second pathway by which warm North Atlantic upper water reaches the Norwegian Sea (Holliday et al., 2000). Although it is unusual for the entire inflow to be via this pathway, considerable variability in this Rockall input has been noted on inter-annual to decadal timescales. Holliday et al. (2000) and White and Heywood (1995) showed how in winter 1993/1994 the "NAtlC zone" moved from the Iceland Basin and entered the Rockall Trough.

The unusual circulation described by the hydrographic data can be attributed to the anomalous wind field in September 1999, at the time of the Iceland-Scotland section. This wind field influenced the circulation of the upper waters of the Iceland Basin so there was no net northwards flow west of the Rockall-Hatton Plateau. Figure 4.10 is a map of the long-term climatological mean sea level pressure for September from NCEP reanalysis (National Center for Environmental Prediction, US National Oceanographic and Atmospheric Administration). It shows the prevailing atmospheric conditions, with westerly winds and an area of low pressure to the southwest of Iceland and an area of high pressure off the west coast of Spain. Figures 4.11 and 4.12 show the mean sea level pressure for September 1999, and the anomaly in sea level pressure for September 1999 from the long term mean (Septembers 1968□□1996), respectively. These figures show how in September 1999, the region of low pressure had shifted southeast from its mean position and was situated directly over the Rockall Trough region. Figure 4.12 indicates that the range of the anomaly in sea level pressure was greater than the range of the climatological mean for the entire region. Regions of low pressure give rise to cyclonic winds in the northern hemisphere such that the Ekman transport (circulation of the wind-driven layer of the upper ocean) causes divergence of the upper waters and upwelling of the underlying waters. The position of the area of low pressure in September 1999 was such that Ekman pumping caused northward movement of waters in the Rockall Trough region, manifested in the transport of warm Atlantic Waters into the Nordic Seas via the North Atlantic Current. This shift in the atmospheric conditions of the sub-polar gyre forced the northwards flow of the NAtlW to the east from the Iceland Basin into the Rockall Trough.

4.6 The Box Inverse Method

Inverse methods encompass a wide range of statistical techniques which combine observations with dynamical information to estimate unknown features of the ocean circulation (McIntosh and Rintoul, 1997). They have been used to address the classical problem of physical oceanography; the determination of a reference level velocity (which must be added to the thermal wind velocity to give the absolute velocity) (Wunsch, 1978).

The 'box inverse' method (the Wunsch formulation of the inverse problem) has become a commonly used tool for the anaylsis of oceanographic data. In this thesis, this technique is applied to hydrographic data to compute the unknown reference velocities. These are then applied as a barotropic correction to the initial velocity field to give an improved estimate of the circulation. The method itself may be adapted to address a variety of unknown aspects of the circulation (e.g. Naveira Garabato et al., 2002; Sloyan and Rintoul, 2000), and its strength is essentially that any prior information can be incorporated as a constraint.

The method may be applied to a closed circuit (which may include coastline) of station pairs about a volume of ocean divided into horizontal layers defined by pressure, density, potential temperature or salinity. The system is set up as a set of linear simultaneous equations and suitable constraints are applied by requiring conservation of property and volume fluxes in some or all layers (Wunsch, 1996). In particular, it can be ensured that flow through a closed volume is reasonable by requiring zero net mass flux (Hall and Bryden, 1982).

The method assumes that the ocean is in geostrophic balance and that mass and salt are conserved (Bacon, 1996; Wunsch and Grant, 1982). It also assumes that instantaneous hydrographic sections can be used to represent the long-term mean flows. These assumptions are the major limitations or weaknesses of the method. However, if the reality of the oceanic system is to be understood, there is a responsibility to seek the best possible interpretation of the data.

The solution is used to provide valuable information about the reference velocity. If a highly divergent 'first guess' is chosen (such as zero velocity at the bottom), the solution will be large. If a more responsible initial state is used (such that the 'first guess' is as nearly non-divergent as possible) the solution is typically small. There are many possible solutions to an underdetermined problem such as this. To find a solution that departs minimally from the assumed initial state, singular value decomposition (SVD) may be used (Lanczos, 1961). This is a cost function based method where a small solution is 'good', and a large solution 'bad'. It seeks a least squares fit where the 'best' answer is the minimum cost function.

If more than one constraint is used it is necessary to truncate the SVD such that the preferred solution degree is selected (e.g. McDonagh and King, 2002). As the solution degree increases the flow field becomes less divergent (according to the constraints being applied by the inversion) at the cost of becoming increasingly noisy. If the full rank solution is chosen a large change in the solution may be forced by small changes in noise. If all constraints are independent (as, for example, when the water column is subdivided into a small number of layers representing distinct water masses) then all of the few resulting eigenvalues contribute to the solution. If, however, there is an overlap of information then the solution will become unreasonable after a certain solution degree. When both salt and volume are conserved, for example, then there is inherent redundancy

since these conditions are not independent. A variety of approaches may be employed for the selection of the best solution degree (see section 5.6.2).

4.6.1 Setup of the Standard Model

For this thesis a closed circuit (including coastline) of 224 station pairs was considered (Figure 3.1). These form four boxes, north, south, east and west, divided into 14 layers defined by isopycnal surfaces (Table 4.2). The layer divisions selected were based on the characteristic water masses of the Nordic Seas such that as much information was extracted from the system as possible (section 5.6.2).

Full depth and layer-specific (all layers) conservation of volume and salinity (for salt) was required for each of the four boxes (north, south, east, west). The conservation of potential temperature (for heat) was also required in all layers that did not outcrop at the surface (i.e. layers 6 to 14), since heat can be exchanged with the atmosphere at the surface. Layer anomalies (for example, salinity minus the average salinity for the Nordic Seas) rather than absolute properties were used to reduce the dependence of the solution on the size of the units of the property equations.

To obtain an accurate set of reference velocities it is necessary to include some form of inter-layer exchange (Naveira Garabato et al., 2003; McIntosh and Rintoul, 1997). Here, diapycnal fluxes (volume, heat, salinity) were explicitly included for the relevant layer interfaces such that layer-specific conservation was physically consistent. The inclusion of independent diapycnal fluxes for each property represents the net diapycnal flux that results from all mixing processes which transfer mass, heat, or salinity between water masses in the ocean interior (Sloyan and Rintoul, 2001a). The vertical velocities and mixing were combined into an 'effective' diapycnal velocity which represents both advective and diffusive components:

$$w^* = w + \kappa_C \frac{\partial C}{\partial z} \qquad 4.20$$

where w^* is the effective diapycnal velocity, w is the actual diapycnal velocity, κ_C is the property diffusion coefficient and $\partial C/\partial z$ is the vertical gradient of the property C. The interfacial flux unknowns are here defined to have units of velocity and are referred to as effective interfacial velocities. For volume, the effective diapycnal velocity is the advective velocity, but for heat and salinity it has contributions from both advection and diffusion, and can be defined as the velocity that gives the total flux when multiplied by the interface area and mean property concentration. It is important to calculate separate effective transfer velocities for heat and salinity since there is asymmetry in the molecular behaviour of heat and salt (thermal diffusivity is 1.4×10^{-7} m^2 s^{-1} and the diffusivity of salt in water is 1.5×10^{-9} m^2 s^{-1}).

The resulting conservation equations are of the form

$$\sum_{j=1}^{N} \Delta x_j \int_{h_m}^{h_{m+1}} (v_r + b)_j C_j \, dp - (w_c A C)_m + (w_c A C)_{m+1} + n_{c,m+1} = 0 \qquad 4.21$$

where j and m refer to the station pair and layer interface indices respectively, N is the total number of station pairs, Δx is the station spacing, C is the property concentration, v_r is the baroclinic or relative velocity, b is the barotropic velocity, w_c is the effective interfacial velocity for each property C, and A is the layer interface area within the domain. Thus for a layer, m, the equation represents the conservation of a property by summing around the sides of the layer (1st term), through the bottom of the layer (2nd term) and through the top of the layer (3rd term). Noise in the constraint, i.e. the extent to which exact conservation is not achieved, is represented by n. Noise is inherent in inverse problems involving the real ocean due in part to measurement problems with the data, and in part to the asynopticity of measurements.

Additional constraints are included to take into account prior knowledge of the circulation. Conservation of the volume transports within the deep basins below sill depth (~2800 m) is required in the Greenland and Lofoten Basins of the Greenland and Norwegian Seas. The volume flux between the Baltic and the rest of the Nordic Seas is constrained to zero (negligible effective volume exchange). Also, conservation of waters within the density range of Labrador Sea Water ($36.8 < \sigma_2 < 36.95$) in the south box is required on the section between Iceland and Scotland, and then over the remainder of the box, since the Iceland-Scotland Ridge effectively restricts exchange of these water masses within the domain of the box. Similarly the deep transports within the Rockall Trough (below 1200 m) are conserved, since the topography restricts communication of those waters with the rest of the south box.

The conservation equations were solved for a total of 364 unknowns. These comprised the 224 reference velocities (for each station pair) and the diapycnal fluxes for mass, salt (w_m, w_s; 13 layer interfaces), and heat (w_h; 8 layer interfaces) for each box. The resulting system of 165 equations and 364 unknowns was set up as a matrix equation after McIntosh and Rintoul (1997) and Wunsch (1978).

$$\mathbf{Ax} = \mathbf{b} \qquad 4.22$$

The (M x N) matrix, **A**, contains information about the geometry of the system; station pair layer areas multiplied by property concentrations, and layer interface areas multiplied by average interfacial property concentrations. The (1 x N) vector, **x**, contains the unknown reference velocities and the unknown interfacial 'fluxes' for mass, heat, and salt anomaly (w_m, w_h and w_s respectively) such that $\mathbf{x} = [\mathbf{v}\ \mathbf{w_m}\ \mathbf{w_h}\ \mathbf{w_s}]^T$. The ($M$ x 1) vector, **b**, contains information about the divergence due to the horizontal baroclinic property flux and the Ekman flux (i.e. the values to which the system is to be constrained). The system is underdetermined since there are fewer constraints (M) than unknowns (N), ie $M < N$.

The inverse problem was solved using truncated SVD. Otherwise known as the 'natural inverse' this was introduced to solve such underdetermined systems by Lanczos (1961). Two sets of eigenvectors $\mathbf{u_i}$ and $\mathbf{v_j}$ may be found such that

$$\mathbf{A}\,\mathbf{v}_j = \lambda_j \mathbf{u}_j \quad \text{and} \quad \mathbf{A}^T \mathbf{u}_i = \lambda_i \mathbf{v}_i \qquad 4.23$$

or $$\mathbf{A}^T \mathbf{A}\,\mathbf{v_j} = \lambda_j^2 \mathbf{v}_j \quad \text{and} \quad \mathbf{A}\,\mathbf{A}^T \mathbf{u}_i = \lambda_i^2 \mathbf{u}_i \qquad 4.24$$

for j = 1,…,N and i = 1,…,M. The eigenvalues (with corresponding eigenvectors) are ranked in decreasing order of magnitude, forming a diagonal matrix such that

$$\lambda_i = \lambda_j \quad \text{if } i = j \text{ and } i \le q \qquad \text{and} \qquad \lambda_i = 0,\ \lambda_j = 0 \quad \text{if } i,j > q \qquad 4.25$$

for some integer q such that $q \le \min(M,N)$. The matrix **A** can be factored into the product

$$\mathbf{A} = \mathbf{U}\Lambda\mathbf{V}^T \qquad 4.26$$

such that the solution vector was given by

$$\mathbf{x} = \mathbf{V}\,\Lambda^{-1}\,\mathbf{U}^T\,\mathbf{b} \qquad 4.27$$

where **U** was a $(M \times q)$ matrix whose columns were the eigenvectors $\mathbf{u_i}$, $i=1,\ldots,q$; $\mathbf{V}^T$ was a $(q \times N)$ matrix whose columns were the eigenvectors $\mathbf{v_i}$, $i=1,\ldots,q$; and Λ was the diagonal matrix of q eigenvalues (λ_i). There remain (M-q) eigenvectors $\mathbf{u}_i$ and (N-q) eigenvectors $\mathbf{v_i}$ which correspond to zero eigenvalues; these are also assembled into matrices $\mathbf{U_0}$ ($M \times \{M\text{-}q\}$) and $\mathbf{V_0}$ ($N \times \{N\text{-}q\}$). If q=M, then **U** contains the complete set of eigenvectors of the symmetric matrix $[\mathbf{A}\,\mathbf{A}^T]$ and is therefore an orthonormal modal matrix; similarly, if q=N, then **V** contains the complete set of eigenvectors of the symmetric matrix $[\mathbf{A}^T\mathbf{A}]$, and is therefore an orthonormal modal matrix. Were **A** square and of full rank (q=M=N), the system would be fully determined. However, since there are fewer constraints than unknowns, no information is provided about the part of the solution x that lies in the so-called 'null space'.

The SVD solution seeks a least squares fit to simultaneously minimize the size of the solution **x** and the size of the residuals $\mathbf{A}\,\mathbf{x} - \mathbf{b}$. It is the simplest solution in the sense that it introduces the minimum correction to the initial model required to satisfy the constraints. If the full rank solution were used then all the equations would be exactly satisfied. However, since the equations are known to contain errors, this would introduce noise for which there is no justification. There is also inherent redundancy in the equations since, for example, the equations for salinity conservation are not entirely independent of the equations for volume conservation. Increasing the rank of the solution reduces the size of the residuals, but at the cost of adding noise.

Recent inverse models have explicitly included ocean-atmosphere exchanges in the form of a heat flux at the ocean surface (Naveira Garabato et al., 2002; Sloyan and Rintoul (2001a). Here, only conservation below the thermocline was considered since there is a high degree of uncertainty in the climatologies available for the high latitude region of the Nordic Seas, and the magnitude of the

signals are at the level of the *a priori* error estimates (for example, as discussed further in Chapter 5).

4.6.2 Initialisation of the Standard Model

The model was initialised by a 'best guess' velocity field (section 4.5), containing as much prior knowledge of the circulation as possible. The hydrographic data used (Chapter 3) were from summer 1999 (July to September). The exception to this were the stations across the opening to the Baltic Sea which were made in September 1991. However, the volume transport exchanges between the Baltic and the Nordic Seas are negligible, and these stations were included mainly to allow representation of the freshwater input of the Baltic to the Nordic Seas. The flow was also assumed to be in geostrophic balance with a wind-driven Ekman component in the upper water column. Ekman property fluxes were calculated (section 4.2.5), and incorporated into the surface layer at each station pair. The unknown diapycnal velocities were initialised to zero, and the mean potential temperature and salinity at each interface were extracted from a hydrographic atlas, the National Oceanographic Data Center World Ocean Atlas 2001 (WOA01; Conkright et al., 2002). The inversion modified this velocity field such that the specified constraints were satisfied.

4.6.3 Weighting scheme for the Standard Model

The importance of scaling the system has been noted and investigated by numerous authors (McIntosh and Rintoul, 1997; Wunsch, 1978).

Column scaling was required to avoid each element of the solution vector being scaled by the cross sectional area of its station pair, and to allow for the relative sizes of reference level and effective diapycnal velocities. This involved postmultiplying $\mathbf{A}$ by a matrix $\mathbf{W}_c$ and premultiplying $\mathbf{x}$ by the inverse of $\mathbf{W}_c$. The square of this matrix, $\mathbf{W}_c^2$, is the formal prior solution covariance matrix. In the absence of prior estimates of the full covariance matrix it is typically taken to be diagonal (Wunsch, 1996), with the size of the diagonal elements chosen to reflect the relative magnitude of the elements of $\mathbf{x}$. Effectively, each column of the matrix is normalised and weighted by the typical uncertainty in the initial estimate of the velocity. For the reference and diapycnal velocities this is equivalent to multiplying by the square root of the uncertainty, σ, and dividing by the square root of the station pair or layer interface area, respectively, such that $\mathbf{W}_{cii} = (\sigma_i / \mathbf{area}_i)$. The *a priori* uncertainty in the reference velocities is chosen to be 5 cm s^{-1} for all station pairs. The effect of varying this uncertainty is discussed in Chapter 6. The *a priori* uncertainty in the diapycnal velocities is chosen as 10^{-5} m s^{-1}, near the upper end of observed deep ocean mixing values.

Row weighting was also applied such that each property transport equation is not weighted by the magnitude or range of values of the property being transported. This required $\mathbf{A}$ and $\mathbf{b}$ to be premultiplied by $\mathbf{W}_r$. The square of this matrix, $\mathbf{W}_r^2$, is formally the inverse of the equation error

covariance matrix. Effectively, each row equation is multiplied by the reciprocal of the *a priori* uncertainty for that constraint. For volume transports this is the standard deviation of 50 realisations of the transport (section 4.2.2 and Table 6.1). For property equations other than volume, this uncertainty is estimated as double the product of the *a priori* error in volume conservation and the standard deviation of property variations within the relevant layer. This *ad hoc* best guess was proposed by Ganachaud and Wunsch (2000) where the factor of 2 accounts for possible correlations between the section-averaged and mesoscale components in the property conservation equation.

Following the notational conventions above, the matrix equation thus became

$$\mathbf{A}\,\mathbf{x} = \mathbf{b} \qquad 4.28$$

where,

$$\mathbf{A} = \mathbf{W}_r\,\mathbf{A}\,\mathbf{W}_c\,, \quad \mathbf{x} = \mathbf{W}_c^{-1}\,\mathbf{x} \quad \text{and} \quad \mathbf{b} = \mathbf{W}_r\,\mathbf{b} \qquad 4.29$$

and was solved by SVD, such that

$$\mathbf{A} = \mathbf{U}\,\Lambda\,\mathbf{V}^T \qquad 4.30$$

and the solution was then recovered by

$$\mathbf{x} = \mathbf{V}\,\Lambda^{-1}\,\mathbf{U}^T\,\mathbf{b} \quad \text{or} \quad \mathbf{x} = \mathbf{W}_c\,\mathbf{V}\,\Lambda^{-1}\,\mathbf{U}^T\,\mathbf{W}_r\,\mathbf{b}. \qquad 4.31$$

4.6.4 Uncertainties

The prior covariance matrices for the solution and equation errors, $\mathbf{C}_{xx}$ and $\mathbf{C}_{nn}$ respectively, are related to the row and column weighting matrices such that

$$\mathbf{C}_{xx} = \mathbf{W}_c^{2} \qquad \text{and} \qquad \mathbf{C}_{nn} = \mathbf{W}_r^{-2} \qquad 4.32$$

The model posterior covariance matrix, $\mathbf{P}_{xx}$, and the noise covariance matrix, $\mathbf{P}_{nn}$, can be calculated in the framework of the Gauss-Markov formulation of the inverse problem as described by McIntosh and Rintoul (1997), and following the method of Wunsch (1996, chp. 3). The details of the calculations are given in Appendix I. $\mathbf{P}_{xx}$ is an updated version of the model prior covariance matrix, taking into account the introduction of new information represented by the vector **b**, and gives an indication of the accuracy of the model estimates of the reference and effective diapycnal velocities.

$$\mathbf{P}_{xx} = \mathbf{C}_{xx} - \mathbf{C}_{xx}\mathbf{A}^T\left(\mathbf{A}\,\mathbf{C}_{xx}\,\mathbf{A}^T + \mathbf{C}_{nn}\right)^{-1}\mathbf{A}\,\mathbf{C}_{xx} \qquad 4.33$$

The main assumption is that the initial estimate of the solution is zero, consistent with the inverse being set up with an initial state as close to the solution as possible. This statistical interpretation of the inverse problem provides a formal error estimate. The posterior noise covariance matrix, $\mathbf{P}_{nn}$, is computed following Ganachaud (1999).

$$\mathbf{P}_{nn} = \mathbf{A}\,\mathbf{P}_{xx}\,\mathbf{A}^T \qquad 4.34$$

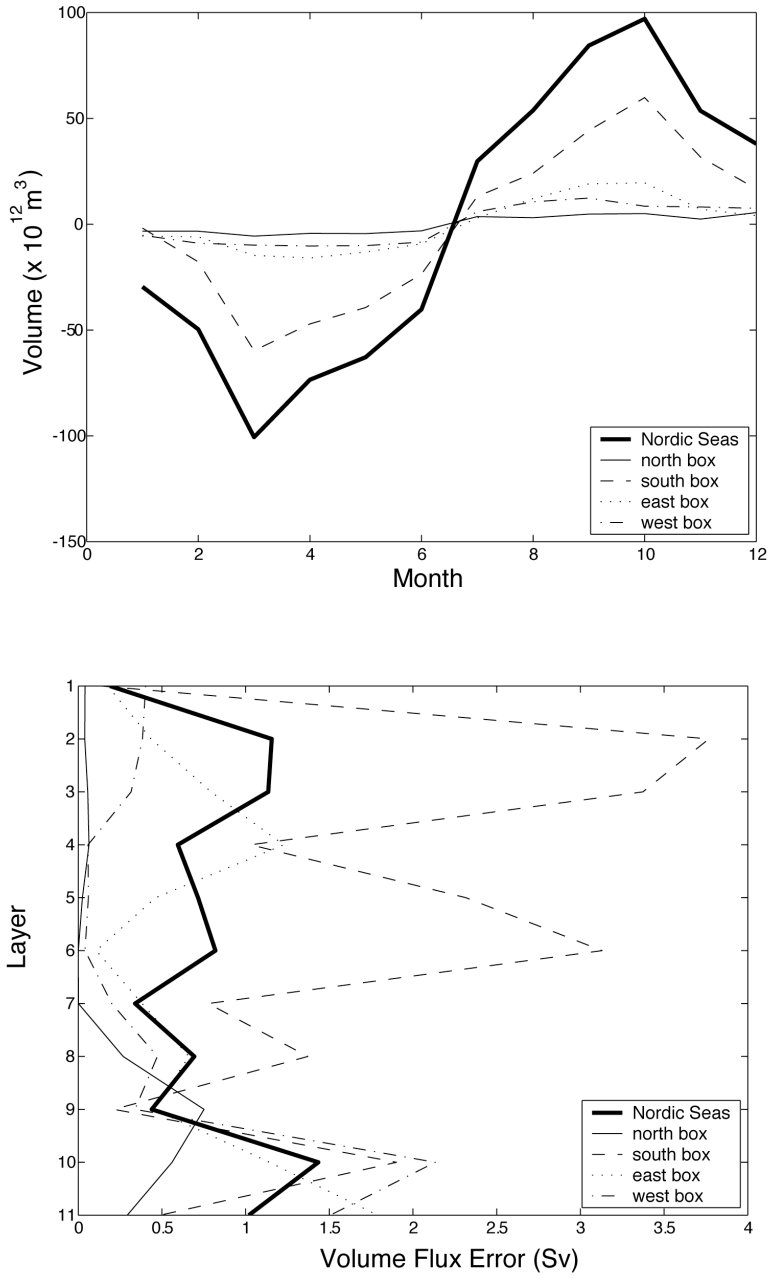

Figure 4.1: The seasonal variability of the volume of light waters, with a density of less than 1027.6 kg m^{-3} (layers 1 to 6), is illustrated in the upper panel for the Nordic Seas and the separate inverse boxes. The variability is based on the monthly deviations from the yearly mean volume of waters. The corresponding volume flux error is illustrated in the lower panel for all layers above 1500 m.

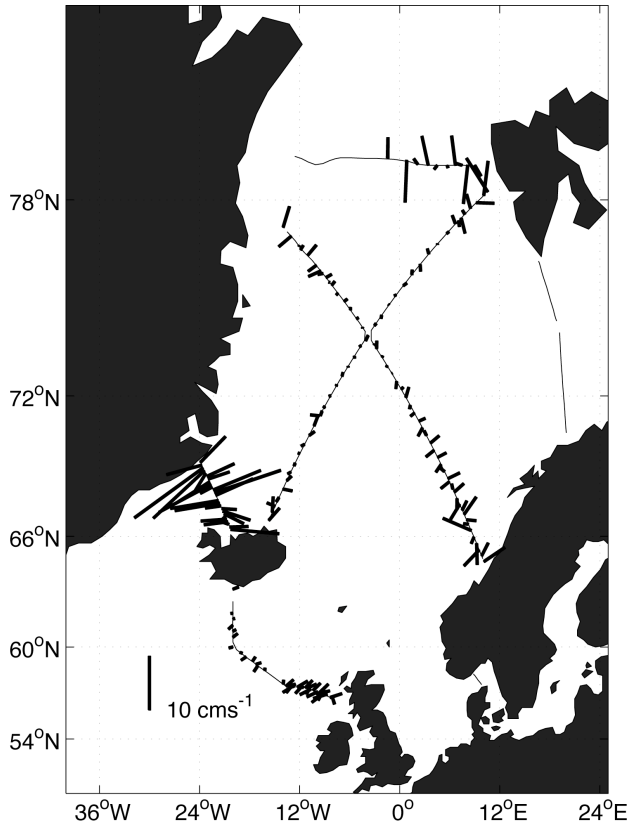

Figure 4.2: Average tidal velocity (cm s^{-1}) over the duration of the hydrographic cast, applied as a barotropic correction to the on station WT and BT LADCP profiles. Direction is indicated by the orientation of the sticks, and stick length represents magnitude (a black stick representing a velocity of 10 cm s^{-1} in a northward direction is also shown, for scale).

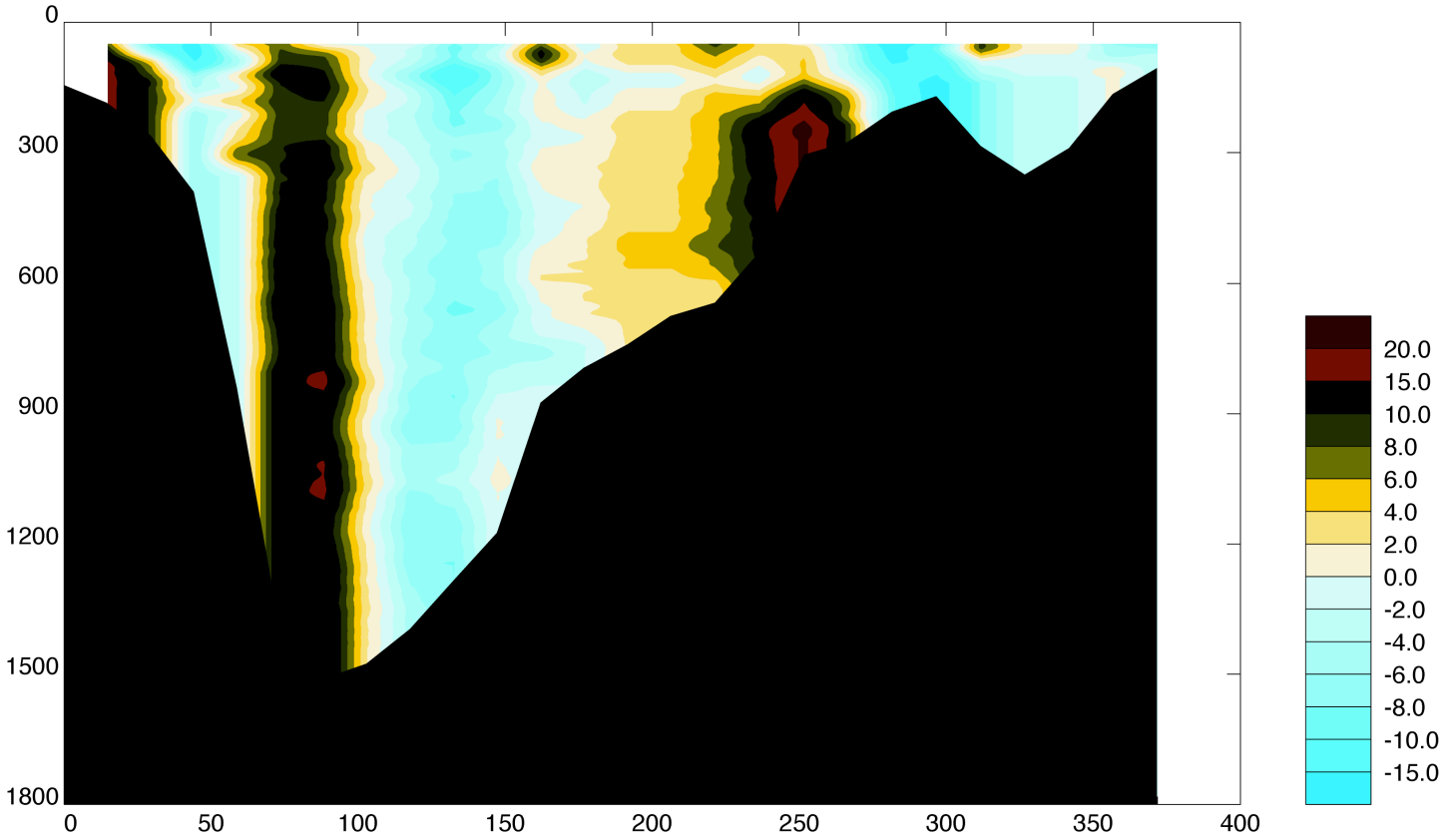

Figure 4.3: Contoured section of the LADCP velocity field (cm^{-1}) for Denmark Strait, from Greenland on the left, eastwards to Iceland on the right. The x and y axes represent distance from the start of the section (km) and pressure (db) respectively. Positive velocities are directed northwards into the Nordic Seas.

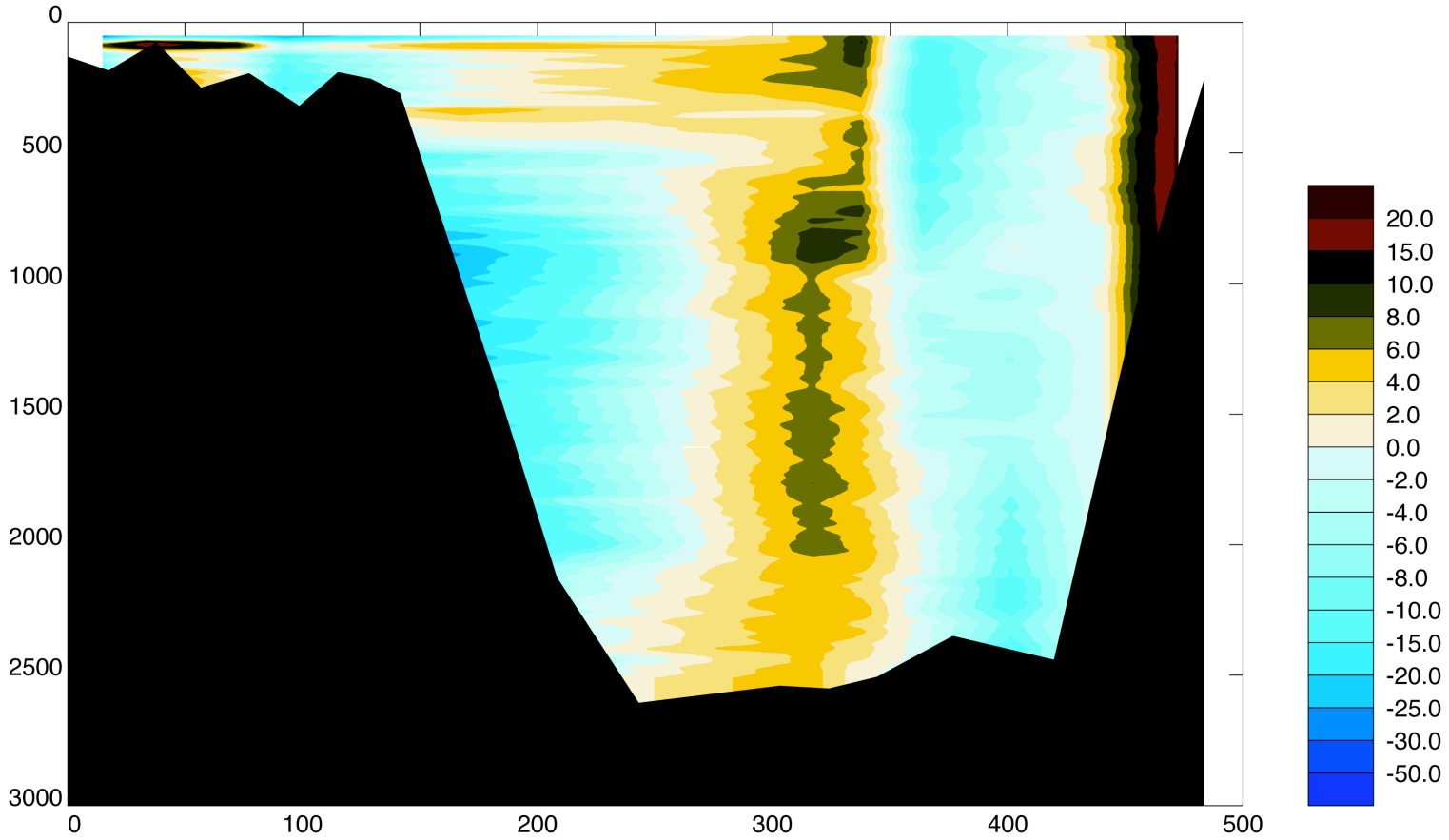

Figure 4.4: Contoured section of the LADCP velocity field (cm^{-1}) across Fram Strait, from Greenland on the left, eastwards to Svalbard on the right. The x and y axes represent distance from the start of the section (km) and pressure (db) respectively. Positive velocities are directed northwards into the Arctic Ocean.

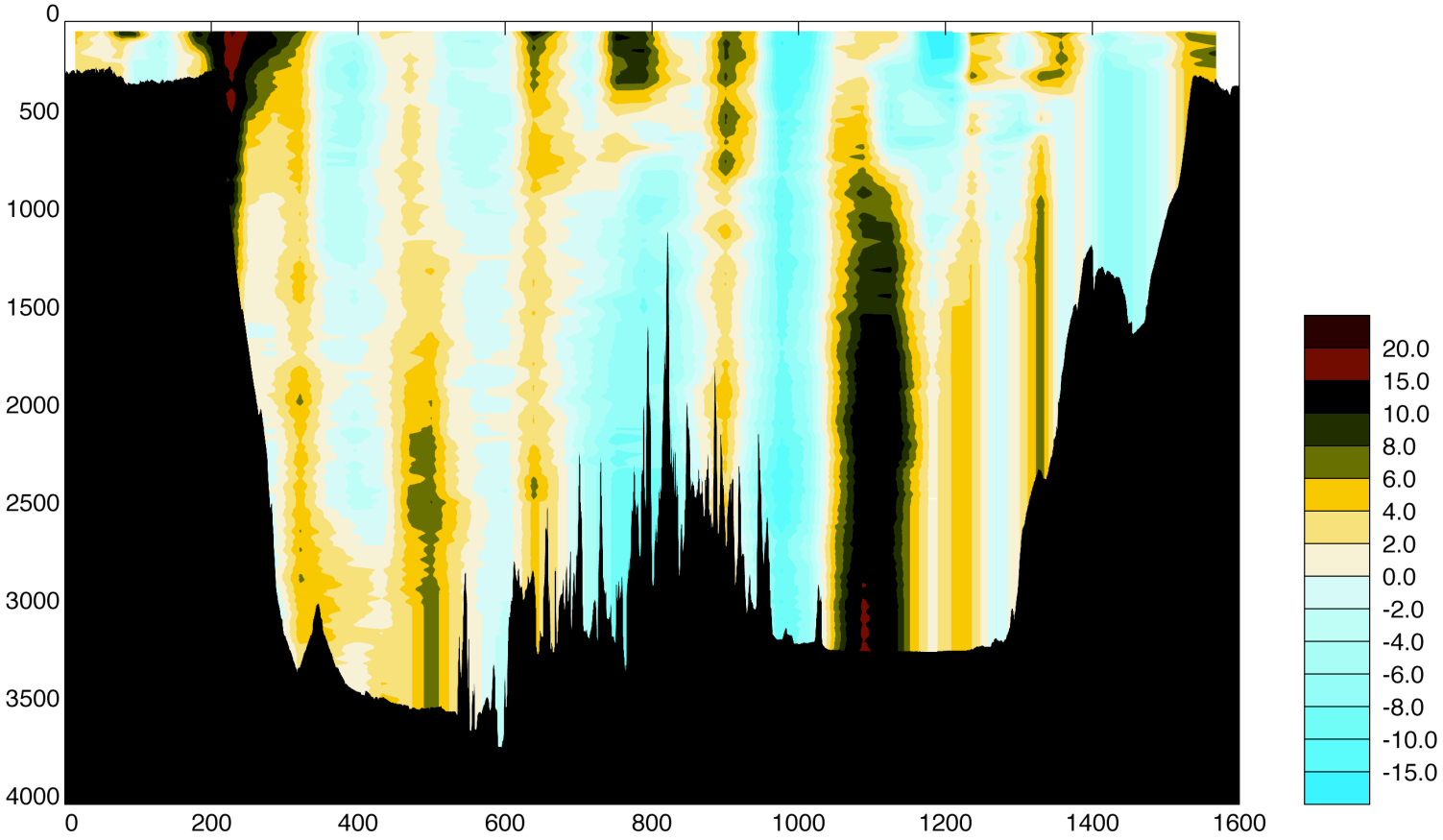

Figure 4.5: Contoured section of the LADCP velocity field (cm^{-1}) for the Greenland to Norway section, from Greenland on the left, eastwards to Norway on the right. The x and y axes represent distance from the start of the section (km) and pressure (db) respectively. The sharp vertical contours in the velocity field are artefacts of the contouring.

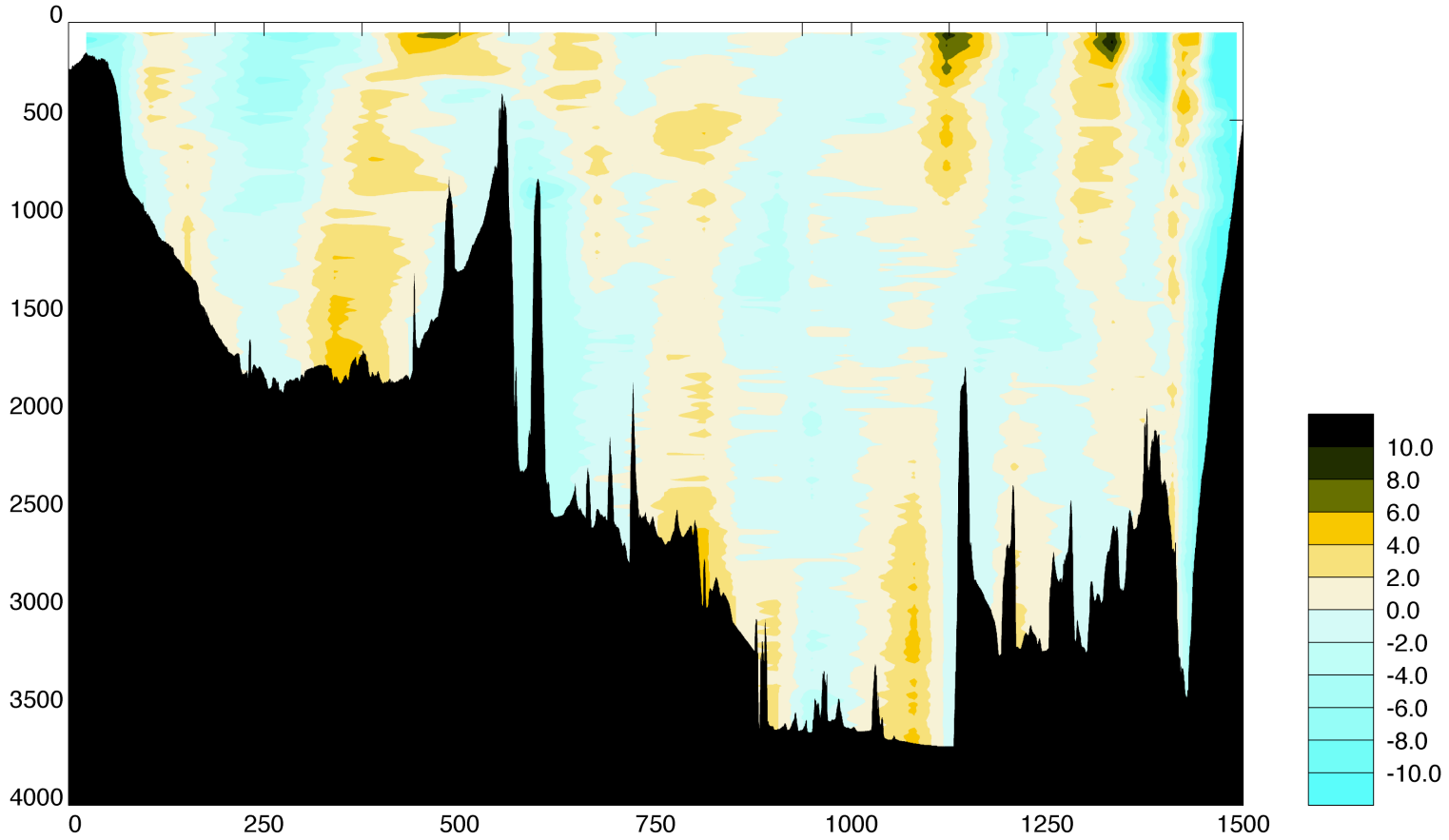

Figure 4.6: Contoured section of the LADCP velocity field (cm^{-1}) for the Iceland to Svalbard section, from Iceland on the left, eastwards to Svalbard on the right. The x and y axes represent distance from the start of the section (km) and pressure (db) respectively. Positive velocities are directed northwest across the section.

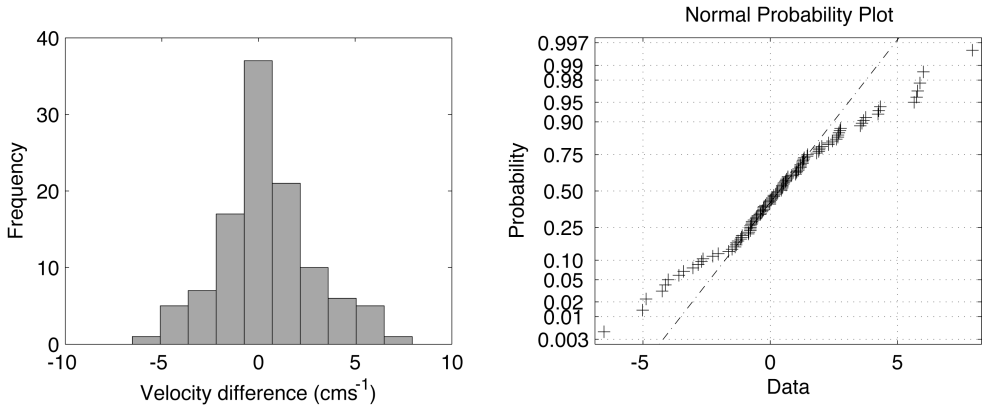

Figure 4.7: The left panel shows the differences (cm^{-1}) between the WT and BT near-bottom velocities. The right panel shows the normal probability plot.

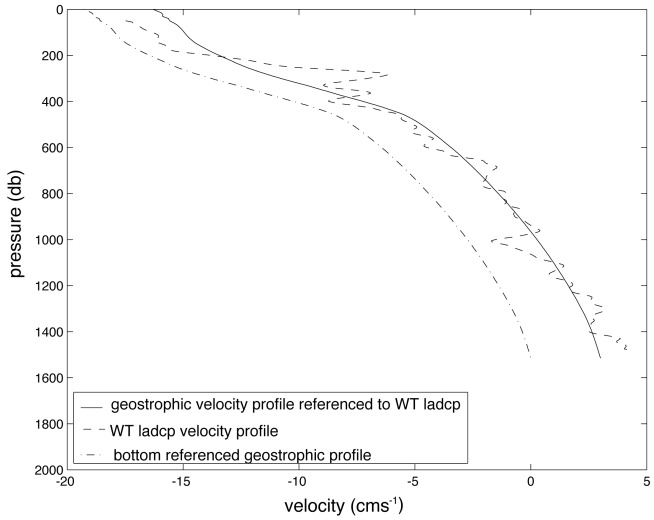

Figure 4.8: Velocity profiles for station pair 81 at 68.1°N 6.5°E in the Norwegian Sea (see section 4.5). The geostrophic profile (dash-dot line), full-depth WT ladcp profile (dashed line) and the geostrophic profile referenced to the WT ladcp (solid line) are shown.

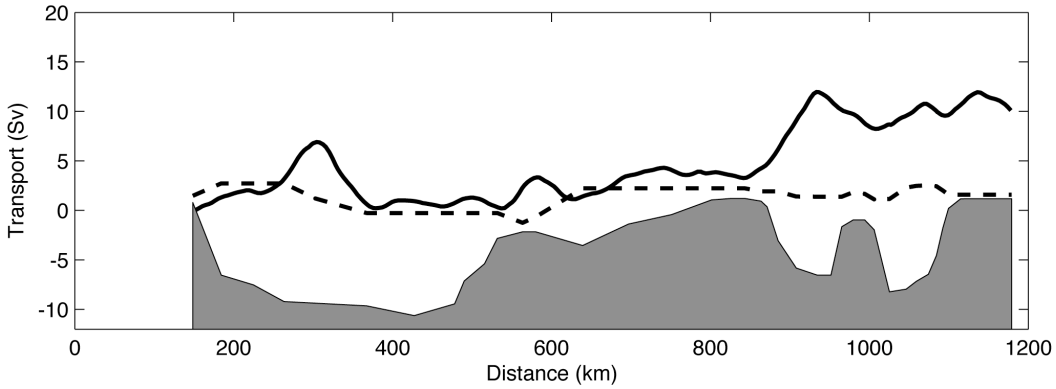

Figure 4.9: Cumulative volume transports (Sv) from shipboard ADCP data (black solid line) and LADCP data (black dashed line), in the upper 500□m of the water column for the Iceland to Scotland section. Transports are accumulated from zero on the Icelandic coast (on the left).

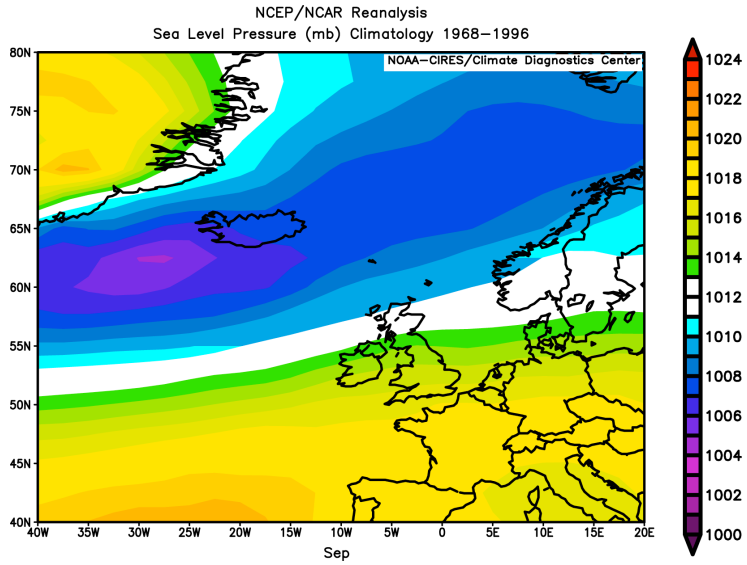

Figure 4.10: Long term mean Sea Level Pressure for September (millibars), for 1968□□1996. Image provided by the NOAA-CIRES Climate Diagnostics Center, Boulder, Colorado, from their website at http://www.cdc.noaa.gov.

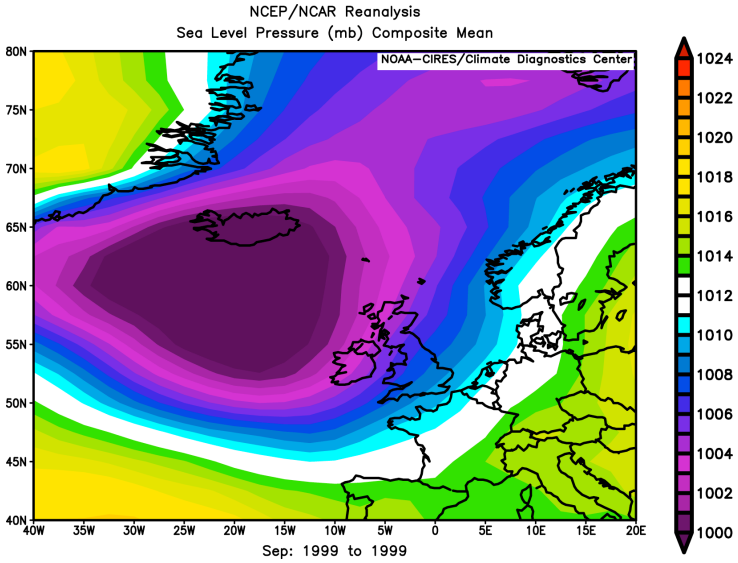

Figure 4.11: Mean Sea Level Pressure for September 1999 (millibars). Image provided by the NOAA-CIRES Climate Diagnostics Center, Boulder, Colorado, from their website at http://www.cdc.noaa.gov.

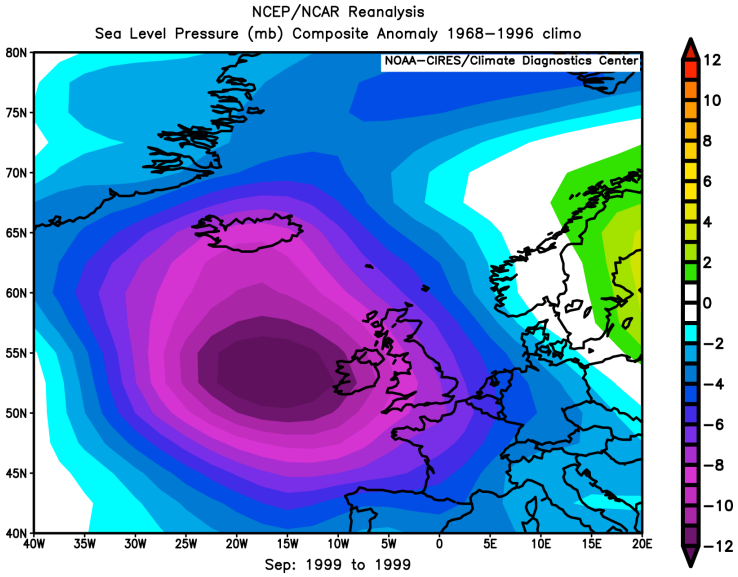

Figure 4.12: Anomaly in Sea Level Pressure (millibars) for September 1999 from the long term mean (Septembers 1968□□1996). Image provided by the NOAA-CIRES Climate Diagnostics Center, Boulder, Colorado, from their website at http://www.cdc.noaa.gov.

Chapter Five

Summer Circulation and Fluxes in the Nordic Seas

5.1 Introduction

This chapter presents results from the inverse study of the summer circulation and fluxes of the Nordic Seas, which has formed the major part of this thesis. To set the stage the chapter begins with a description of the hydrography of each section, describing the presence and location of the water masses observed. The direct velocity field of the region (from LADCP measurements), the wind-driven circulation and the ocean-atmosphere exchanges are then discussed. The chapter goes on to describe the determination of the velocity field using the box inverse method, including the choice of initial reference level, constraints and selection of the appropriate solution. The circulation given by the standard solution is discussed in detail, presenting a summer picture of the fluxes and exchanges of the Nordic Seas. A study of the sensitivity of the inverse and a discussion of errors are the subject of Chapter 6.

5.2 Hydrographic Characteristics

To fully describe the circulation of a particular oceanic region it is first necessary to define the water masses present (identifying temperature and salinity properties). Oceanic waters are not randomly distributed with respect to temperature and salinity. A water type is defined as occupying a particular location in temperature/salinity (θ/S) space (i.e. with particular characteristics of θ and S). An area in θ/S space is defined as a water mass (an envelope of water types). The specification of a water mass, however, is arbitrary and can be particularly problematic within the Nordic Seas. This is partly due to the range of terminology used in the literature (discussed in section 2.4.1), and partly due to high interannual variability in the characteristics of water masses from the same source. This section discusses the main features of the water masses observed in the sections forming the inverse boxes used in this study (see Chapters 3 for a description of the data).

The water column can be divided into surface, intermediate and deep waters. However, although the general vertical differentiation can be made on the basis of density, geographic variation means that a particular isopycnal cannot always be used to divide surface and intermediate waters, for example (Hopkins, 1991). In the winter many surface water types converge with the intermediate water types. Aagaard et al. (1995) used $27.75 \leq \sigma_0 \leq 27.90$ to differentiate between the surface and intermediate waters, and $\sigma_1 = 32.785$ to differentiate between the intermediate and deep waters.

	Water Mass	Properties and Description
Surface Waters	Norwegian Atlantic Water (NAW) or North Atlantic Water (NAtlW) south of the GS Ridge	□ > 3.0°C; S□35.0 S□34.9 in FS
	Norwegian Coastal Water (NCW)	S□35.0.
	Polar Water (PW)	□ < 0.0°C; S□34.4
	Arctic Surface Water (ASW)	□ > 0.0°C; 34.7 < S□34.9 and □ > 2.0°C; 34.4 < S□34.7 surface waters overlying AIW formed by summer heating and freshened by mixing with PW
	Greenland Sea Shelf Water (GSSW)	□□-1.5°C; S□32 locally formed on shelf off coast of northeast Greenland
	Knee Water (KW)	□ < 0.0°C; S□34 Arctic Water of Atlantic origin found on continental shelf off northeast Greenland
Intermediate Waters	Return Atlantic Water (rAW)	0□□□2.0°C; S□34.9
	Greeland Sea Arctic Intermediate Water (GSAIW)	-1.0□□□0.0°C; 34.8□S□34.9
	Norwegian Sea Arctic Intermediate Water (NSAIW)	□ < -0.5°C; S□34.89
	Iceland-Scotland Overflow Water (ISOW)	□ > 2.0°C; S□34.89
	Denmark Strait Overflow Water (DSOW)	□□1.0°C; 34.8□S□34.9
	Labrador Sea Water (LSW)	□□3.0°C; S□34.9
	Eastern North Atlantic Water (ENAW)	□□8.0°C; S□35.2
	Western North Atlantic Water (WNAW)	□□8.0°C; S□35.2
	Modified North Atlantic Water (MNAW)	7.5□□□8.0°C; S□35.2
Deep Waters	Arctic Ocean Deep Water (AODW)	-0.8□□□-0.5°C; S□34.90
	Greenland Sea Deep Water (GSDW)	□□-1.0°C; 34.9□S□34.94 found in Greenland Sea
	Norwegian Sea Deep Water (NSDW)	formed by mixing of GSDW with saline deep inflows of AODW through FS; found in Fram Strait and Norwegian and Iceland Seas

Table 5.1: Conventions used in this thesis to identify water masses. **FS** denotes Fram Strait, **AIW** denotes Arctic Intermediate Water.

Following the review of the Nordic Seas water masses made in section 2.4, this thesis follows the conventions described in Table 5.1. The surface waters are subdivided into Atlantic Waters and Polar Waters together with the shelf surface water masses. The Norwegian Atlantic Water (NAW) is defined as □□3.0°C and S□35.0, increasing to S□34.9 in the northern part of the Nordic Seas and Fram Strait. The Atlantic Waters south of the Greenland-Scotland Ridge, as present on the Iceland-Scotland section, are referred to as North Atlantic Waters (NAtlW). Norwegian Coastal Water (NCW) is defined as the surface waters off the Norwegian coast with S□35.0. The cold, fresh Polar Waters (PW) from the Arctic are defined as the surface waters found in the western

Nordic Seas with $\theta < 1.0$°C and $S < 34.7$. Arctic Surface Water (ASW) with $\theta > 0.0$°C and $34.7 < S < 34.9$ (and also $\theta > 2.0$°C and $34.4 < S < 34.7$) overlies the Arctic Intermediate Waters and is formed by summer heating and freshened by mixing with PW. Greenland Sea Shelf Water (GSSW) is a very cold and fresh surface water mass locally formed on the shelf off the coast of northeast Greenland with $\theta < 1.5$°C and $S < 32.0$. Also present on the Greenland shelf in the region of Belgica Bank is Knee Water ($\theta < 0$°C and $S < 34.0$), a cold, fresh surface Arctic Water of Atlantic origin (Bourke et al., 1987).

The intermediate waters are subdivided into the modified Atlantic Waters, Arctic Intermediate Waters, the Overflow Waters, and the intermediate waters found in the northeast North Atlantic. Return Atlantic Water (rAW) is used to refer to intermediate waters found in the western domain of the Nordic Seas with $0 < \theta < 2.0$°C and $34.5 < S < 35.0$. These are waters of Atlantic origin that have been cooled on their passage through the Nordic Seas. The Arctic Intermediate Waters include Greenland Sea Arctic Intermediate Water (GSAIW) with $-1.0 < \theta < 0.0$°C and $34.8 < S < 34.9$, and Norwegian Sea Arctic Intermediate Water (NSAIW) with $\theta < 0.5$°C and $S < 34.89$. Denmark Strait Overflow Water (DSOW) is defined as waters with $\theta < 2.0$°C and $34.8 < S < 34.9$ and Iceland-Scotland Overflow Water (ISOW) is given the definition of $\theta > 2.0$°C and $S > 34.89$. Within the northeast North Atlantic, south of the Greenland-Scotland Ridge, the major water masses present are Labrador Sea Water (LSW) ($\theta < 3.0$°C and $S < 34.9$), Eastern North Atlantic Water (ENAW) ($\theta > 8.0$°C and $S < 35.2$), Western North Atlantic Water (WNAW) ($S < 35.2$) and Modified North Atlantic Water (MNAW) ($7.5 < \theta < 8.0$°C and $S < 35.2$).

The deep waters are subdivided into Arctic Ocean Deep Water (AODW), Greenland Sea Deep Water (GSDW) and Norwegian Sea Deep Water (NSDW). AODW is defined to be waters within the range $-0.8 < \theta < 0.5$°C and $S < 35.2$ and is present mainly in Fram Strait region. GSDW is the deep water mass of the Greenland Sea with $\theta < 1.0$°C and $34.9 < S < 34.94$. NSDW ($\theta < 0.0$°C and $34.9 < S < 34.92$) is formed by mixing of GSDW with the saline deep inflows of AODW through Fram Strait, and is present in Fram Strait, and the Norwegian and Iceland Seas.

Figures 5.1 to 5.7 show contour plots of potential temperature (°C) and salinity and θ/S (potential temperature /salinity) diagrams for each section. These figures illustrate the hydrography discussed here. The isopycnals (represented by σ_0 surfaces) used to define the layers for flux and inverse calculations are also illustrated on the θ/S diagrams, and the major water masses are marked. The general characteristics of the different layers for each section are summarised in Table 5.2, which gives their area-weighted layer-average potential temperatures and salinities. The mean depths and thicknesses of each layer are summarised in Table 4.2.

Layer	Layer Boundaries	Section						
		DS	**BSO**	**FS**	**GN**	**ISval**	**IScot**	**Skag**
1	$\sigma_0 < 26.5$	2.188 32.23	10.290 34.172	-1.6244 32.031	5.138 32.824	- -	13.488 35.212	14.851 33.181
2	$26.5 < \sigma_0 < 27.0$	3.931 33.790	8.760 34.602	-0.806 33.317	6.384 34.358	8.774 34.524	11.740 35.204	10.233 34.833
3	$27.0 < \sigma_0 < 27.3$	2.943 34.201	7.779 34.820	0.729 33.923	7.633 34.881	6.598 34.659	9.746 35.296	8.509 35.008
4	$27.3 < \sigma_0 < 27.5$	3.967 34.608	6.846 34.968	1.117 34.321	6.613 34.993	5.434 34.762	8.675 35.277	7.682 35.139
5	$27.5 < \sigma_0 < 27.6$	4.327 34.831	6.305 35.057	2.878 34.650	6.418 35.101	5.369 34.895	6.912 35.151	7.529 35.234
6	$27.6 < \sigma_0 < 27.7$	3.067 34.769	5.692 35.087	1.855 34.649	5.346 35.061	4.484 34.905	5.574 35.064	- -
7	$27.7 < \sigma_0 < 27.8$	1.550 34.717	4.777 35.061	2.056 34.768	4.390 35.035	3.349 34.898	3.779 34.936	- -
8	$27.8 < \sigma_0 < 27.95$	0.545 34.778	3.359 35.036	2.578 34.970	2.870 34.983	1.881 34.913	2.961 34.949	- -
9	$27.95 < \sigma_0 < 28.0$	0.194 34.860	2.288 35.032	1.107 34.924	0.666 34.893	0.426 34.877	- -	- -
10	$\sigma_0 > 28.0$, $\sigma_1 < 32.73$	-0.031 34.878	0.780 34.951	0.192 34.895	0.106 34.889	-0.010 34.881	- -	- -
11	$32.73 < \sigma_1 < 32.76$	-0.218 34.890	0.019 34.926	-0.180 34.896	-0.336 34.882	-0.329 34.881	- -	- -
12	$32.76 < \sigma_1 < 32.78$	-0.465 34.896	-0.072 34.953	-0.453 34.900	-0.653 34.881	-0.672 34.880	- -	- -
13	$\sigma_1 > 32.78$, $\sigma_2 < 37.45$	-0.688 34.907	-0.164 34.955	-0.794 34.909	-0.843 34.904	-0.846 34.900	- -	- -
14	$37.45 < \sigma_2$	- -	- -	-0.958 34.915	-1.045 34.908	-1.070 34.906	- -	- -

Table 5.2: Layers defined by σ_0, σ_1 and σ_2 surfaces (potential density minus 1000 kg m^{-3}, referenced to the surface, 1000 m and 2000 m, respectively). The area-weighted layer-average potential temperature (°C) and salinity are given by the upper and lower of each pair of numbers per layer and per section, respectively. Sections are denoted by; **DS** for Denmark Strait, **BSO** for the Barents Sea Opening, **FS** for Fram Strait, **GN** for the Greenland-Norway section, **ISval** for the Iceland-Svalbard section, **IScot** for the Iceland-Scotland section and **Skag** for the section across the Skagerrak.

5.2.1 Nordic Seas Openings

The Nordic Seas openings include the exchanges across the Greenland-Scotland Ridge to the North Atlantic, the exchanges across the Barents Sea Opening between Norway and Svalbard, the exchanges through Fram Strait into the Arctic Ocean and the exchanges into the Baltic Sea via the Skagerrak.

(i) Denmark Strait (Figure 5.1 a to c)

This section extends from the east coast of Greenland to the northwest coast of Iceland, lying to the north of the sill in Denmark Strait. The deepest station has a depth of ~1400 m. Since the actual sill depth of the strait is ~600 m some of the water masses present are too deep to form part of the overflow waters and so they only circulate within the Iceland Sea. The very surface layer (the upper 50 m) shows evidence of summer heating. For example, on the shelf region off the coast of Greenland the surface waters reach a temperature of ~2.4°C. Immediately below this warm 'skin', very cold, fresh Polar Waters (θ < 1°C; S < 34.5) are observed over the western part of the continental slope. Below depths of ~50 m this water mass is isothermal, but salinities increase with

depth. Further to the east, as the shelf steepens, there is a clear signal of the rAW, described by Mauritzen (1996a), between depths of about 200–500 m and with temperatures up to ~1°C and salinities of ~34.5. A signal of rAW is present over the entire shelf slope and in the deeper parts of the strait (between 200–300 m), to a distance of about 120 km offshore. Underlying the eastern extent of the rAW and filling the deeper parts of the basin below ~300 m are intermediate waters ($-1 \leq \theta < 0$°C; S > 34.85). Over the Icelandic continental slope are the warm Atlantic waters flowing northward in the Irminger Current (above ~200 m depth). On the shelf itself, the upper 100 m of the water column is near-isothermal (~6°C) and very fresh (S ≤ 33.8).

(ii) Barents Sea Opening (Figure 5.2 a to c)

This section runs north at a longitude of about 19°E to Bear Island and then slightly west of north to the southern tip of Svalbard. Flow between the Nordic Seas and the Barents Sea occurs in the channels on either side of Bear Island: Bjørnøyrenna, to the south, with maximum depth ~500 m, and Storfjordrenna, to the north, which has a maximum depth of ~300 m but shoals to the east, and is blocked by Svalbard further north (Figure 2.1). Throughout the section there is a warm, fresh surface layer showing evidence of freshening and summer heating. The warmest waters, reaching a maximum of >1°C are over the continental slope off Norway extending across the Bjørnøyrenna. Atlantic Water can be identified as a warm salinity maximum ($\theta \geq 2$°C; S ≥ 35) with its main core on the southern slope of Bjørnøyrenna roughly between depths of 150–250 m, and a shallower core in the Storfjordrenna (~50–150 m). The NAW in Storfjordrenna is cooler and fresher than that in Bjørnøyrenna since it has undergone more mixing with the surrounding cold, fresh Arctic water masses. The colder waters present in the bottom of Storfjordrenna ($0.5°C \leq \theta \leq 2°C$) are likely to be remnants of winter water formed in the northern Barents Sea and in the Storfjorden, a shallow fjord south of Svalbard (Schauer, 1995).

(iii) Fram Strait (Figure 5.3 a to c)

Across Fram Strait the section extends from the shallow shelf (Belgica Bank) off the east coast of Greenland to Svalbard at a latitude of ~79°N. To the west, the shallow surface waters (~0–50 m) on the Greenland shelf, which are largely locally formed, are very cold and fresh ($\theta \leq -1.5$°C; S ≤ 32). Underlying these are slightly warmer, saltier waters ($\theta \leq 0$°C; S ≤ 34). This intermediate layer of Knee Water is the Arctic Water of Atlantic origin described by Bourke et al. (1987). Over the deepest part of the bank (<depths of 150–200 m) there is evidence of rAW ($0°C \leq \theta \leq 2°C$; $34.5 \leq S \leq 35$). On the shelf slope this warm, salty core is apparent as a temperature maximum between depths of ~250–500 m. The colder Deep Waters lie over the central part of the strait. Below 2000 m the temperature and salinity properties lie within the ranges $-0.97°C \leq \theta \leq -0.82°C$ and $34.91 \leq S \leq 34.92$. Between ~1000–2000 m the waters are slightly warmer and fresher ($\theta \leq -0.15$°C; $34.89 \leq S \leq 34.92$). These deep waters correspond to typical definitions of NSDW

and are probably a mixture of the colder, fresher GSDW and the saltier AODW. A clear signal of AODW (Aagaard et al., 1991) is apparent in the salinity section (Figure 5.3b) at about 2000m on the slope off Greenland. The very surface layer (< ~50m) remains very fresh. On the shelf off Svalbard (~220m) there are warm, fresh waters (3<θ<3.2°C; 34.3<S<S< 35.0). This salinity stratified surface water is influenced by the freshwater supply from the glaciers and fjords of Svalbard (Saloranta and Svendsen, 2001). The warm core of Atlantic Water (in the West Spitsbergen Current) is confined to the upper continental slope and extends to ~150km off shore. It has a temperature maximum of 6.1°C at a depth of ~65m (comparable with the temperature maximum of 5.9°C at 30m observed by Schauer (1995). At the deeper stations, below the Atlantic Water, the temperature decreases monotonically towards the bottom and a salinity minimum is apparent ~600m depth. The common definition of NAW in the Nordic Seas is S>34.95 (Helland-Hansen and Nansen, 1909) but a fresher definition is required in Fram Strait since the temperature and salinity of NAW decrease along its northward path towards the Arctic. At this latitude the 34.9 isohaline can typically be used to demarcate the more saline AW from fresher Arctic Waters (Swift, 1986).

(iv) Skagerrak (Figure 5.4 a to c)

The section across the opening to the Baltic Seas extends southwards from Norway to Denmark with the deepest part of the channel having a depth of just over 500m. This section is characterised by very warm waters with a mean potential temperature of 11.8°C, and ranging between 7.4°C and 16.4°C. Similarly, the section is characterised by very fresh, low salinity surface waters, including fresh Norwegian Shelf Water (NSW), originating within the Baltic Sea. The Baltic Sea itself has an average salinity of 8 (Rodhe and Winsor, 2003; Winsor et al., 2001). The section has a mean salinity of 31.6 ranging from a minimum of 24.4, due to waters of Baltic Sea origin, to a maximum of 35.3, due to the recirculating North Sea inflow in the deeper parts of the channel.

5.2.2 Nordic Seas

The interior circulations of the Nordic Seas are covered by the two long sections from Greenland to Norway and Iceland to Svalbard.

(i) Greenland-Norway (Figure 5.5 a to c)

Over the East Greenland shelf there are very cold, fresh waters, influenced by melting ice (probably both sea and glacial ice). At the edge of the shelf slope, both cold, fresh Polar Waters (PW), and warmer, salty recirculated waters of Atlantic origin (rAW) are apparent as they are carried south in the East Greenland Current. The Polar Waters have a minimum salinity of 30.6 at the surface, and a minimum temperature of –1.7°C at ~60m. The rAW forms a saline (S > 34.9) wedge with a maximum thickness of ~400m within 50km offshore of the shelf break, and thinning to about ~100m thick by ~350km offshore of the shelf break. The majority of the Greenland Sea basin is

filled with the cold, dense, relatively saline water (–1.5°C < θ < 0°C; 34.9 < S < 34.94; σ_0 > 28.05) characteristic of GSDW (Aagaard et al., 1991; Carmack and Aagaard, 1973; Strass et al., 1993). Overlying this deep water at depths of 1000–1500m are slightly fresher intermediate waters (θ < 0°C; 34.8 < S < 34.9). Throughout the Greenland Sea the surface layer (~100m thick) has been warmed by summer heating, and freshened. The Arctic Frontal Zone (AFZ) separating the warm, saline NAW to the east and Arctic Water from the Greenland Sea Gyre to the west is clearly evident at a distance of ~800km off the Norwegian coast, approximately over Mohns Ridge. At this front there is an increase in sea surface temperature of ~1.64°C and in sea surface salinity of ~0.20 over a distance of 38km, from the Polar to Atlantic side. Within the Norwegian Sea the 35.0 isohaline has typically been used to define the lower boundary of NAW (Oliver and Heywood, 2003; Orvik et al., 2001). In the Lofoten Basin this boundary lies at ~640m (θ = 3°C) and rises to ~250–450m over the continental slope (with the corresponding temperature increasing to ~4°C). Also in the Lofoten Basin there is a salinity minimum of 34.89 (θ = 0.1°C) at ~950m. This intermediate water mass is commonly defined as NSAIW advected from the Iceland and Greenland Seas (Hansen and Østerhus, 2000). The deep waters have θ < 0°C and salinities ~34.9, corresponding to the common definition of NSDW. Over the Norwegian Shelf the fresh NCW (S < 35.0) forms a layer with a mean thickness of 70m.

(ii) Iceland-Svalbard (Figure 5.6 a to c)

This section runs northeast through the Nordic Seas from the northeast coast of Iceland to Svalbard. It first crosses the Iceland Sea, then passes to the west of Jan Mayen Island before crossing both the Greenland and Boreas basins of the Greenland Sea. An inflow of Atlantic Water, originating in the Irminger Current through Denmark Strait, follows the northwest coast of Iceland (Stefansson, 1962). This is probably the source of the warm, salty waters observed over the north Icelandic continental shelf. In the Iceland Sea (south of the Jan Mayen fracture zone at 71°N) water characteristic of NSDW is present below depths of ~1200m. This water mass is 'generally named by virtue of characteristics rather than location' (Swift and Koltermann, 1988) but falls within the broad definition of θ < 0°C and 34.9 < S < 34.94 (Swift et al., 1980). Further north in the Greenland Sea the deep waters below 2000m are characteristic of GSDW (θ < –1°C; mean salinity of 34.9). Over the upper ~250m of the water column within both the Iceland and Greenland Basins, there is a fresher surface water with an average salinity of ~34.82. On the southwestern shelf off Svalbard (the extreme top right of Figure 5.6b) there is a very fresh surface layer (to a depth of ~25m) probably freshened by runoff or local meltwater. Below this are warm salty waters of Atlantic origin (θ > 3°C; S > 34.89). Offshore over the continental slope above ~600m this water mass is evident as a saline wedge (0.5 < θ < 6.7°C; 34.89 < S < 35.09). Below the salinity minimum (~600m) there are intermediate waters characteristic of NSAIW with average temperatures of –0.5°C and salinities of 34.9.

5.2.3 Northeast Atlantic

(i) Iceland-Scotland (Figure 5.7a to c)

The last section used to close the inverse boxes lies well to the south of the Iceland-Scotland Ridge (see section 3.3.2). This means that the water masses present (Pollard et al., 2004) are somewhat different in character to those that would be found along the ridge itself. The section runs from the southern coast of Iceland due south at 20°W to a latitude of ~60°N in the Iceland Basin of the Northeast Atlantic. It then continues southeast across Hatton Bank, Rockall Plateau and the northern end of the Rockall Trough to the continental shelf off Scotland.

The shelf waters off southern Iceland are warm and saline ($8 < \theta < 9$°C; S ~35.2) and are separated from the warm surface layer ($\theta > 10$°C; S ~35.0) by a thermocline between ~50–70 m. On the slope a slight salinity minimum is apparent at ~1400 m (S = 34.91), with temperatures decreasing monotonically to 2.7°C. The salinity minimum deepens to ~1900 m further south into the Iceland Basin. This signal is indicative of LSW (Lazier et al., 2002), identified by a salinity minimum and temperature minimum or stad at depths between 1000–1800 m. This is formed from the cold fresh intermediate waters which spread from the Labrador Sea, crossing the Mid Atlantic Ridge south of 54°N, into the Iceland Basin and Rockall Trough (Read, 2001). Below ~2000 m within the Iceland Basin there is evidence of ISOW with the signal defined by a light salinity maximum. As these overflow waters flow south in the Iceland basin they mix with the surrounding deep waters (Saunders, 1996). The coldest and freshest waters on the section are observed within the Iceland Basin, with a minimum temperature of 2.0°C at 2400 m and minimum salinity of 34.89 at 1800 m. The deepest station within the Iceland Basin was in water of ~2740 m since the section did not extend far enough to the southwest to cover the abyssal basin. At ~200 m there is a slight salinity maximum (S ~35.3) across the basin. These upper waters overlying LSW are subpolar mode waters, a complex mixture of warm, saline water from the south and cold, fresh water from the northwest (Pollard et al., 2004).

Over the slope onto Hatton Bank the salinity maximum remains evident as a wedge between about 200–600 m. Below this maximum and below the seasonal thermocline both temperature and salinity decrease monotonically. Potential temperatures above 800 m are between 8–9°C. Over the shallow Rockall Plateau (below the slightly warmer, fresher ~50 m thick surface layer) salinities are > 35.3 and $\theta > 9$°C. Throughout this region ENAW overlies the deeper MNAW (Holliday, 2003).

The section crosses the northern end of the Rockall Trough with the deepest station in depths of about 2200 m. The upper waters are warm and saline, with a salinity maximum evident at ~300 m (S ~35.4). These lie within the temperature–salinity range of ENAW and are substantially more saline than the subpolar mode waters of the Iceland Basin (Holliday et al., 2000). The signal of

LSW is apparent at depths of ~1800m as a salinity minimum (S=34.92), becoming warmer and more saline eastwards along its path. The maximum temperature (13.5°C) and salinity (S=35.43) for the section occur on the Scotland continental shelf.

5.3 Wind Driven Circulation

The wind–driven circulation of the Nordic Seas is relatively weak during the summer months. In this thesis, the Ekman fluxes were calculated using climatological wind stress fields (see section 3.4.1). A comparison was made between the SOC (Josey et al., 1999) and Hellerman and Rosenstein (1983) (HR) climatologies. Errors were estimated by considering the variability between the annual and summer average fluxes for the two climatologies.

	Volume Transports (Sv)		**Temperature Transport (Sv °C)**		**Salinity Transport (Sv psu)**	
	SOC	HR	SOC	HR	SOC	HR
Denmark Strait	-0.05	-0.06	-0.25	-0.22	0.05	0.07
Barents Sea Opening	-0.03	-0.05	-0.20	-0.35	0.00	0.00
Fram Strait	-0.01	-0.01	-0.02	-0.01	0.01	0.01
Skagerrak	-0.01	-0.02	-0.12	-0.32	0.01	0.03
Greenland-Norway	-0.10	-0.12	-0.43	-0.84	0.03	0.03
Iceland-Svalbard	0.20	0.21	0.93	0.98	-0.04	-0.04
Iceland-Scotland	-0.20	-0.21	-2.43	-2.56	-0.07	-0.07
Nordic Seas	**-0.20**	**-0.26**	**-2.52**	**-3.32**	**-0.01**	**0.03**

Table 5.3: Ekman Volume (Sv), Temperature (Sv °C) and Salinity (Sv psu) Transports calculated from the SOC and HR summer average climatologies. For the Nordic Seas positive transports indicate a convergence over the region. For the Denmark Strait, the Barents Sea Opening, Fram Strait and the Iceland-Scotland section, positive transports are directed polewards. For the Greenland-Norway and Iceland-Svalbard sections, positive transports are directed northwards (northeastward and northwestward respectively). Salinity and temperature transports are calculated relative to a salinity of 34.93 and a temperature of 0°C, respectively.

Table 5.3 and Figure 5.15 summarise the Ekman transports over the Nordic Seas region. The fluxes presented here are calculated from the SOC summer average wind stress field (Figure 5.16). The SOC climatology is available over the region of the Nordic Seas, however data is very sparse. It uses in situ marine reports for the period 1980–1993 and a drag coefficient supported by recent observational analyses (see Chapter 3 for a discussion of the merits of the various climatologies available). The use of the summer average minimises problems with missing data due to ice covered regions. These values give a net divergence over the Nordic Sea region (as enclosed by the inverse boxes) of 0.2 Sv for volume transport, 2.52 Sv°C for temperature transport, and 0.01 Sv psu for salinity transport. Salinity transports are calculated relative to a mean salinity over the Nordic Seas of 34.93 and temperature transports are calculated relative to 0°C. This is consistent with the

characteristic low wind stress curl over the entire region during the summer months (Jonsson, 1991). The variability between the summer and annual average fluxes calculated from the SOC and HR climatologies over the domain of each box is of the order 20%. This is taken to be the error associated with the fluxes.

5.4 Atmosphere - Ocean Exchanges

The summer atmosphere - ocean heat flux exchanges were investigated using the adjusted SOC (Grist and Josey, 2003; Josey et al., 1999) climatology (see section 3.4.1). The atmospheric heat budget consists of four terms with the net atmospheric heat flux, Q_{net}, given by

$$Q_{net} = (1 - \alpha)\, Q_{sw} + \varepsilon\left(Q_{lw} - \sigma T_{sfc}^{4}\right) + Q_h + Q_e \qquad 5.1$$

where Q_{sw} is the short wave radiation, Q_{lw} is the long wave radiation, Q_h is the sensible heat, Q_e is the latent heat of evaporation, α is the surface albedo, ε is the emissivity of water, σ is the Stefan–Boltzmann constant (5.67×10^{-8} Wm^{-2}K^{-4}), and T_{sfc} is the surface air temperature. In the SOC climatology a positive Q_{net} indicates heating of the ocean surface while a negative Q_{net} indicates a heat loss from the ocean to the atmosphere.

Table 5.4 presents a summary of the results. The annual average values can be compared to those found by Mauritzen (1996b) and Isachsen (2003).

Isachsen (2003) using the SOC climatology (Josey et al., 1999) and the NOAA 1994 climatology of surface marine data (SMD94; Silva et al., 1994) found an average annual mean heat loss from the ocean to the atmosphere over the Nordic Seas of 130 TW. This gives an average heat loss per unit area of 16 Wm^{-2} based on an area of 8×10^{12} m^2. This total is low when compared a heat loss of ~200 TW (Table 5.4). This discrepancy is due to the use of the adjusted SOC climatology (see section 3.4.1) in this thesis. Allowing for an average ocean heat gain of 30 Wm^{-2} in the original SOC climatology, then the total heat loss over the Nordic Seas would be adjusted to 124 TW (similar to the estimate of Isachsen, given above). The exact area included in Isachsen's definition of the Nordic Seas is unclear, since he uses a surface area nearly three times larger than that used for the present study. The results of Isachsen's inverse calculation adjusted the total annual mean heat transport convergence within the Nordic seas to 146 ± 21 TW (~20 Wm^{-2}).

Mauritzen (1994) used three atlases of net annual heat flux (Budyko, 1974; Bunker, 1976; Gorshkov, 1983) to calculate air–sea heat fluxes. All show a tendency towards high heat fluxes in the Norwegian and Barents Seas over the North Atlantic Current, with smaller heat fluxes further to the east over the Greenland and Iceland Seas. She set her initial estimates to 70 Wm^{-2} over the majority of the Nordic Seas and 0 Wm^{-2} over the ice covered region of the East Greenland Current, with large uncertainties of ±30 Wm^{-2} and ±10 Wm^{-2} (due to insulating properties of ice)

respectively. Her inverse calculation reduced the heat flux over the Greenland and Iceland Seas to 27±22 Wm^{-2} and 48±34 Wm^{-2}, respectively, while the solution remained unchanged over the North Atlantic Current (68±7.5 Wm^{-2}) and the East Greenland Current (0±31 Wm^{-2}). She argued that no heat loss over the EGC is reasonable since little exchange with the atmosphere can be expected, a consequence of ice cover during part of the year. Interestingly, when the heat flux over the Norwegian Sea was reduced from 70 Wm^{-2} to 0 Wm^{-2} in her model, the solution remained unchanged (68 Wm^{-2}), suggesting her inverse was insensitive to the actual heat flux with which it was initialised.

	nordic seas		***north* box**		***south* box**		***east* box**		***west* box**	
	Wm^{-2}	TW	Wm^{-2}	TW	Wm^{-2}	TW	Wm^{-2}	TW	Wm^{-2}	TW
Annual	-76	-207	-82	-15	-68	-102	-114	-74	-40	-16
Summer	28	76	4	1	38	57	16	10	19	8
late Summer	17	48	-1	-0.3	24	36	5	3	22	9
July	78	214	53	10	88	132	78	50	57	23
August	27	79	10	2	32	48	13	8	51	21
September	-55	-150	-67	-13	-48	-72	-77	-50	-41	-16
Surface Area (m^2)	2.7×10^{12}		1.9×10^{11}		1.5×10^{12}		6.5×10^{11}		4.1×10^{11}	

Table 5.4: Air-Sea Heat fluxes per unit area (Wm^{-2}), and total (TW; 1 TW = 10^{12} W), over the both the Nordic Sea region and the inverse boxes. The annual, summer (May to September), late summer (July to September), July, August and September averages are given for comparison. Negative values indicate a net heat loss from the ocean to the atmosphere. The surface areas for each region (used in the per unit area calculations) are also quoted.

Mauritzen's initial annual average heat flux over the Nordic Sea region (70 Wm^{-2}; 2.2×10^{12} m^2) was similar to the present calculations (76 Wm^{-2}; 2.7×10^{12} m^2; Table 5.4). For comparison, Aagaard and Carmack (1989) defined the Nordic Sea region as an area of 2.55×10^{12} m^2, and Simonsen and Haugan (1996) defined it to be 2.71×10^{12} m^2 (for the Arctic Mediterranean excluding the Arctic Ocean, Barents Sea and North Sea).

5.5 Initial Fluxes

The determination of the initial velocity field has been the subject of much angst. The solution of an inverse calculation is highly dependent on the starting point, so it is important that the initial velocity field is as close to 'reality' as possible. It is no simple matter, however, to come to this point.

The individual velocity fields (geostrophic and LADCP) are discussed in section 4.2, and the specific details of how the LADCP data were used to reference the geostrophic velocity field are described fully in section 4.5. The resultant initial velocity field is illustrated in Figures 5.8 to 5.14 (i.e. the geostrophic velocity field referenced to LADCP data, where applicable). The transports calculated from this initial velocity field are discussed here. They are summarised in Table 5.5 and provide initial estimates for the inverse model. These estimated fluxes are comparable to those in the literature, indicating that the initial velocity field is most probably a reasonable starting point for the inverse.

The total inflow of AW to the Nordic Seas ($\sigma_0 < 27.6$) of 7.4 Sv is similar than the 8 Sv reported by Turrell et al. (1999) which was based on the net flow after accounting for some recirculation. The 6.8 Sv inflow across the Iceland-Scotland Ridge ($\theta > 7$°C and $S > 35.15$) is within the range (6.7–7.4 Sv) given by Hansen and Østerhus (2000), but the inflow through the eastern part of Denmark Strait ($\sigma_0 < 27.7$, $\theta > 4$°C) of 0.6 Sv is lower than the 1.5 Sv suggested by Kristmannsson (1998).

Within the southern part of the Norwegian Sea, at a latitude of 62°N on the Greenland to Norway section, the net northward flow of NAW above 600–800 m is 1.6 Sv, comparable to the 2.0 Sv reported by Orvik et al. (2001). Further inshore towards the Norwegian coast there is a net northward flow of 0.6 Sv NCW, the same as noted by Robitaille et al. (1995). Continuing northwards the NAW has been cooled and become more dense. There is a net outflow of NAW ($\sigma_0 < 27.95$, $\theta > 2$°C), into the Barents Sea of 1.1 Sv, compared to the estimate of 1.6 Sv proposed by O'Dwyer et al. (2001).

Continuing further north, the present study finds a net northward flow of NAW through Fram Strait in the WSC of 2.2 Sv, which is comparable to the 2 Sv estimate given by Schlichtholz and Houssais (1999). The strength of the WSC, considering the total northward flow, is 4.3 Sv.

The southward flow of the EGC through Fram Strait is 7.4 Sv estimated from the initial velocity field. This compares to the 7 Sv estimate of Schlichtholz and Houssais (1999). Included within the transport of the EGC is 1.2 Sv of PW ($\sigma_0 < 27.5$, $\theta < 1$°C, $S < 34.3$), close to the Hansen et al. (2003) estimate of 1.1 Sv and the Mauritzen (1996b) estimate of 1.5 Sv.

In the present study, a 4.3 Sv flow in the WSC and a 7.4 Sv flow in the EGC suggest a total net southward flow from the Arctic into the Nordic Seas, through Fram Strait of 3.1 Sv. This is divided between 1.1 Sv in the deep waters and 2.0 Sv in the surface and intermediate waters. A higher estimate was given by Schlichtholz and Houssais (1999), with a total net outflow of 5.2 Sv divided between 2.6 Sv of deep waters and 2.6 Sv of intermediate and surface waters.

A study in Fram Strait (Fahrbach et al., 2001) using current meter measurements suggested the volume transports within Fram Strait, in the years 1997-1999, were significantly larger than earlier

estimates given in the literature, with an estimated northward transport in the WSC of 9.5±1.4Sv (or 7.2±1.3Sv), and an estimated southward transport in the EGC of 13.7±1.7Sv (or 8.9±1.6Sv). These values are the average of monthly northward and southward transports. For comparison the annual northward and southward transports calculated from the annual mean at each current meter are given in brackets. It should be noted that there is a large difference (2-4Sv) between these calculations, and too that these are the annual estimates. The monthly mean fields revealed marked velocity variations over seasonal and annual time scales, and within the spatial structure of the northward flowing WSC and the southward flowing EGC, with a maximum in spring and minimum in summer. Inspection of the monthly averages gives values of 5.0Sv (WSC) and 10.0Sv (EGC) for August 1999.

The recirculation within Fram Strait is an issue that needs to be addressed. In the Fahrbach et al. (2001) study, to compensate for change in latitude half way across the mooring line, the southward transports in the EGC were referred to 78°50'N by adding the recirculation between two moorings (F8 and F9). The magnitude of this recirculation was quoted as ~2.6±0.1Sv. This error on the recirculation is rather low, and of the same order as the magnitude as the transport (Woodgate, pers. Comm., 2003; since an Aanderaa RCM current meter has a systematic error of 1cms^{-1}, and the error in the mean velocity is also ~1cms^{-1}, then multiplied by the area between the morrings an error of ~1Sv is obtained). If the recirculation is ignored then the initial velocity field used in this thesis is the same order as the Fahrbach et al. (2001) study; with a total northward flow of 4.3Sv (c.f. the 5.0Sv attributed to the WSC) and a total southward flow of 7.4Sv (c.f. the 10.0−2.6=7.4Sv attributed to the EGC).

The EGC increases in strength as it flows further south, with Woodgate et al. (1999) noting a summer transport of ~11Sv from moored current meters at 75°N. The initial velocity field suggests a comparable transport within the EGC on the western part of the Greenland-Norway section (between latitudes of 77°N and 75°N) ranging from 9.0Sv to 14.9Sv taking the eastern extent of the EGC to be 7.0°W (308km offshore) or 6.3°W (344km offshore).

The total transport of intermediate waters (σ_0>27.8) over the Greenland-Scotland Ridge was estimated to be 5.6±0.7Sv by Hansen and Østerhus (2000), with 2.9Sv of DSOW through Denmark Strait (σ_0>27.8, θ<2°C; Ross, 1984) and 3.4Sv of ISOW across the Iceland-Scotland Ridge (Hansen and Østerhus, 2000). The initial velocity field gives similar estimates with a total of 5.8Sv, including 2.6Sv of DSOW and 3.3Sv of ISOW. It also gives an surface flux estimate of PW (σ_0<27.6, θ<1°C, S<34.3) through Denmark Strait into the North Atlantic of 1.1Sv, compared to the 1.5Sv of Hansen and Østerhus (2000) and Maurtizen (1996b).

Table 5.6 summarises the heat fluxes over the Nordic Seas. The initial velocity field gives a total oceanic heat flux of 241TW across the Greenland-Scotland Ridge towards the Arctic. This agrees with the 245±17TW suggested by Isachsen (2003) and the 200±30TW put forward by Oliver

and Heywood (2003). The total heat flux into the Arctic Ocean, through Fram Strait and the Barents Sea Opening, is 76 TW, compared to the 99±12 TW estimated by Isachsen (2003). The majority of this heat flux (69 TW) is into the Barents Sea. The remaining heat flux into the Arctic Ocean through Fram Strait of 7 TW is within the range 4.3–10.9 TW suggested by Schlichtholz and Houssais (1999). These estimates give a total heat convergence within the Nordic Seas of 165 TW and an average flux of 35 Wm^{-2} (using a surface area of 2.7×10^{12} m^2). This is in agreement with the total heat flux estimate of 146±21 TW suggested by Isachsen (2003), although his 20 Wm^{-2} estimate of the average flux is lower since he uses an area of 8×10^{12} m^{-2}.

The full depth volume transports across each section used to form the inverse boxes are illustrated in Figure 5.17. These suggest a net inflow to the Nordic Seas from the Arctic Ocean (through both Fram Strait and the Barents Sea Opening) of 1.5 Sv and a comparable net southwards transport across the Greenland to Norway section of 1.4 Sv. There is also, however a net northwards inflow to the Nordic Seas from the North Atlantic of 1.0 Sv across the Greenland-Scotland Ridge. This results in a convergence of 2.5 Sv over the entire region enclosed by the inverse boxes. As a comparison, the unreferenced geostrophic field (referenced to zero at the bottom everywhere except the Iceland-Scotland section where it is referenced to zero at a depth of 1400 m) gives a convergence of 3.6 Sv.

Although the flux estimates derived from the initial velocity field are reasonable and consistent with previous studies, as discussed above, there are imbalances over the individual regions enclosed by the *north*, *south*, *east* and *west* boxes. These imbalances are summarised in Table 5.7 and suggest that the initial velocity field does not accurately describe the internal circulation of the Nordic Seas.

	Total volume transport into the region (Sv)
north	-7.5
south	-9.0
east	7.6
west	11.4
Nordic Seas	**2.5**

Table 5.7: Full depth volume transports (Sv) for each of the inverse boxes and the entire Nordic Seas region from the initial state of the standard model. Positive transports indicate a convergence into the region.

The imbalances for the individual inverse boxes are relatively large (of the order 9 Sv). However, if the Nordic Seas are considered as a northeast (comprising the *north box* and *east box*) and a southwest (comprising the *south box* and *west box*) sector, then they are reduced to 0.1 Sv and –2.4 Sv respectively (positive transports denote a convergence into the region). Similarly if the Nordic Seas are considered as a northwest (comprising the *north box* and *west box*) and a southeast

(comprising the *south box* and *east box*) sector then the imbalances are reduced to 3.9 Sv and –1.4 Sv. This implies that the initial imbalances are to some extent 'internal' to the Nordic Seas.

The volume transports indicate that the imbalances occur primarily within waters with $\sigma_0 > 27.8$ (i.e. layers 8 to 14); with large southwards transports in the Greenland Sea, and large northwards transports in the Norwegian Sea. The initial field is additionally unbalanced by a net transport of deep waters from the Norwegian Sea into the Iceland Sea across the Iceland-Svalbard section. This is inconsistent with the estimates of Carmack and Aagaard (1973) and Soelen (1986) who proposed a flow of bottom waters from the Greenland Sea to the Norwegian Sea of the order 1 Sv and 0.1 Sv, respectively. The flow is thought to occur through a deep connection within the Jan Mayen Fracture Zone with a minimum depth of 2000 m. This inflow to the Nordic Seas then follows a cyclonic path on the deep slopes of the basin.

5.6 The Standard Model and Solution

The inverse methods used in this thesis and the setup of the standard model are explained in detail in Chapter 4 (see section 4.6). This section describes the particular constraints applied to the standard model, the selection of a reasonable solution, and then that resultant solution with its resolution matrices.

5.6.1 Constraints

The constraints applied to the standard model are summarised in Table 5.8. The primary constraint is the conservation of net volume transport (including Ekman transport) within each of the inverse boxes and thus over the Nordic Seas as a whole, such that there is no net transport into or out of each of the boxes. Volume fluxes are thus conserved over the full depth of the water column, and within each layer individually. Since the model includes diapycnal mixing (strictly speaking, transports across density surfaces) individual layer conservation is justified.

The standard model also requires the conservation of salinity fluxes over the full depth of the water column and within each layer individually, and temperature fluxes within all but the surface layers. Anomaly conservation equations were written for salinity and temperature since it has been found this reduces the sensitivity of the inversion to errors (removing the effect of properties having small variations about a large mean) (McDougall, 1991). McIntosh and Rintoul (1997) found that it is not important for the reference salinity to exactly equal the mean value of salinity. In this thesis the salinity anomaly is defined as $S' = S - 34.93$, where S is salinity and 34.93 is the mean salinity over the entire data set.

The standard model is row and column weighted, as described in Chapter 4. The effects of this weighting are explored and discussed in Chapter 6.

Constraint Number	Constraint Description		Station Pairs constraint applied to
1 - 4	full depth	volume	*north*, *south*, *east*, *west boxes*
5 - 8	full depth	salinity	*north, south, east, west boxes*
9 - 22	individual layers 1 - 14	volume	*north box*
23 - 36	individual layers 1 - 14	volume	*south box*
37 - 50	individual layers 1 - 14	volume	*east box*
51 - 64	individual layers 1 - 14	volume	*west box*
65 - 78	individual layers 1 -14	salinity	*north box*
79 - 92	individual layers 1 - 14	salinity	*south box*
93 - 106	individual layers 1 - 14	salinity	*east box*
107 - 120	individual layers 1 - 14	salinity	*west box*
121 - 129	individual layers 6 - 14	temperature	*north box*
130 - 138	individual layers 6 - 14	temperature	*south box*
139 - 147	individual layers 6 - 14	temperature	*east boxt*
148 - 156	individual layers 6 - 14	temperature	*west box*
157 - 159	deep transports	volume	deep stations in Greenland and Lofoten Basins
160	Labrador Sea Water	volume	Iceland-Scotland section
161	Labrador Sea Water	volume	*south box* (except Iceland-Scotland)
162	full depth	volume	Skagerrak
163	deep transports below 1200□m	volume	Rockall Trough
164	full depth	volume	entrances to the Nordic Seas (sections 1, 2, 5, 8, 9,10)
165	full depth	volume	Greenland to Norway section (sections 2 and 6)

Table 5.8: Details of the constraints applied in the standard inverse model. Each constraint represents a conservation equation with the flux (volume, temperature or salinity) constrained to zero.

5.6.2 Selection of Solution Degree

The inverse is setup as an underdetermined problem, as discussed previously, hence there are many possible solutions. The SVD method seeks a solution with minimum square length. Since there are errors in both the model and the data, the full rank solution can magnify these errors and produce large, variable reference velocities, which may lead to an unrealistic circulation. The solution is therefore truncated to balance the requirements for the constraints to be satisfied while introducing as little noise as possible into the solution. There is no definitive method to determine the preferred solution degree, and a number of approaches may be taken. These include the tapered least squares solution (Wunsch, 1996), which involves introducing an assumed noise level, and the withholding of data from the inverse to use as an independent measure to aid solution choice (Bacon, 1996). Together with the approaches explained below, they all seek a solution with an acceptable level of noise.

In this thesis, the preferred solution for the standard model was chosen such that the residuals are required to be zero to within three standard deviations of the error estimate (Table 6.1, see explanation in section 4.6.3) (McDonagh and King, 2002). The uncertainties within the *a priori* error estimate include the small contributions to the budget from river input, exchanges with the atmosphere (precipitation and evaporation) and sea ice export. These errors are discussed in Chapter 6 (and summarised in Table 6.1). Also, the solution was required to be within one standard deviation of the *a priori* error estimate.

The above considerations lead to the selection of solution degree 43 as the preferred solution degree for the standard model. The variance explained by each mode (solution degree) is revealed when the contribution of each eigenvector to the answer is considered (the square of the eigenvalues for that mode). This gives the percentage variance of the total velocity. For the standard model, solution degree 43 explains 87% of the total variance (Figure 5.18). It is likely that after this point, additional eigenvectors add noise without making a significant contribution to the solution. For each constraint the residual generally decreases with increasing solution degree, with the first few solution degrees resulting in some constraints having unacceptably large residuals.

The behaviour of the inverse solution in the presence of error is largely determined by the ratio of the largest to smallest singular value kept in the inversion (McIntosh and Rintoul, 1997). This ratio is the condition number (Figure 5.19), and indicates the amount by which relative errors in **b** might be amplified to become relative errors in the solution (**x**). Rank 43 of the standard model has a condition number of 4. This is well within the range (<100) that McIntosh and Rintoul (1997) suggest indicates that an inversion is well conditioned and tolerant to some error (in contrast, a large condition number of the order 1×10^5 would indicate the inversion is sensitive to even small errors in the data). The concept of a condition number as an approach to solution choice is a form of optimization explored by Bacon (1996) and Barth and Wunsch (1990).

Other common methods do suggest that a high rank solution (close to full rank) should be chosen as the preferred solution. However, solutions near to full rank can be assumed to be correspondingly noisy, and the examination of a near full rank solution demonstrates how it implies an unrealistic circulation (see section 5.6.4). For example, the simplest test is to examine the relative magnitude of the eigenvalues and to choose a solution degree before a sharp decrease in size, on the assumption that the noise will significantly increase after this point. The nature of the standard model is such, however, that its eigenvalues are on a continuum from high (significant) to low (insignificant) ones, with no sudden decrease in size before solution degree 160 (Figure 5.20). This is near full rank, and so it may be assumed to be correspondingly noisy. Levenburg-Marquardt analysis (Lawson and Hanson, 1974) provides an alternative method, in which the constraint residuals are considered as a function of solution magnitude. The 'best' solution (i.e. one which incorporates most of the ‘information’ obtained from the constraints) can be interpreted as a point just prior to where solution magnitude increases rapidly with little or no reduction in residual magnitude. For the standard

model this doesn't happen until solution degree 159 (Figure 5.21), which again is very near to full rank.

Some authors have supported their choice of solution by considering how particular results vary with solution degree (e.g. Tsimplis et al., 1998). Although there is an element of arbitrariness to this method, examination of the variability between results from the different solution degrees for the standard model does show rank 43 to give a reasonable circulation. This gives further support to the choice of rank for the standard solution, which was based primarily on requiring the residuals to be within three standard deviations of the error estimate, and the solution to be within one standard deviation of the *a priori* error estimate.

5.6.3 Standard Solution

Figures 5.22 and 5.23 show the reference and effective diapycnal velocities for the standard solution, respectively (rank 43 of the standard model).

Inverse box	**Barotropic Corrections to Reference Velocities (cms^{-1})**		
	mean	**std**	**peak**
Denmark Strait	0.45	0.32	1.46
Barents Sea Opening	-0.17	0.96	4.39
Fram Strait	0.46	0.50	1.70
Skagerrak	0.02	1.74	2.40
Greenland-Norway	0.07	0.42	0.94
Iceland-Svalbard	-0.11	0.29	1.07
Iceland-Scotland	0.25	0.41	1.42
Nordic Seas	**0.01**	**0.66**	**4.39**

Table 5.9: Mean, peak and standard deviations of the barotropic corrections (cms^{-1}) to the reference velocities from the standard solution.

The barotropic correction to the reference velocities suggested by the first eigenvector is of the order 0.001cms^{-1}, with peak values of the order 0.1cms^{-1}. The correction given by the standard solution (rank 43) is summarised in Table 5.9. The inverse puts the largest peak corrections on the Barents Sea Opening and Skagerrak sections, neither of which had direct velocity measurements to reference the initial velocity field (Figure 5.22). Elsewhere the largest corrections are near to the coasts at section ends. Along the Greenland-Norway section, consistently southwards corrections are made to the Norwegian end of the section, and similarly, northwards corrections are made to the Greenland end. These are in response to the imbalances discussed in section 5.6.

Inverse Box		Corrections to Effective Diapycnal Velocities (x10^{-5} cms^{-1})		
		mean	**std**	**peak**
Volume:	*north*	-0.763	3.485	-9.407
	south	1.623	7.734	23.852
	east	–2.295	8.183	-26.995
	west	-0.449	2.660	-4.312
Temperature:	*north*	–0.023	0.212	0.303
	south	–0.045	0.240	-0.456
	east	–0.024	1.366	2.764
	west	–0.054	0.338	0.583
Salinity:	*north*	–0.165	0.715	1.379
	south	–0.068	0.142	-0.377
	east	–0.366	3.587	-11.089
	west	–0.037	1.105	-2.118

Table 5.10: Mean, peak and standard deviations of the corrections (x10^{-5} cms^{-1}) to the effective diapycnal velocities from the standard solution.

The corrections to the diapycnal velocities are of the order 1x 10^{-5} cms^{-1} (Figure 5.22), and are summarised in Table 5.10. For the effective diapycnal volume velocities, the largest corrections are made in the surface layers in the *south* and *east* boxes, and in the lower layers in the *north* and *west* boxes. For salinity, the largest corrections to the effective diapycnal velocities are made in the upper layers, particularly in the *east* box. For heat, the largest corrections are also made within the *east* box.

5.6.4 Near full rank solution

As the solution degree increases and smaller eigenvalues are added the structure of the solution becomes increasingly complex, with increasingly 'noisy' velocities (i.e. large amplitude and rapidly alternating sign) resulting. This is illustrated in Figure 5.24, which shows how the norm of the solution vector increases with solution degree. As described previously (section 5.6.3) the standard solution gives a barotropic correction to the reference velocities of the order 0.01cms^{-1}, with peak values of ~4cms^{-1}. In contrast, the full rank solution gives a barotropic correction to the reference velocities of the order 1cms^{-1}, with peak values of the order 7cms^{-1}.

The selection of a high (near full rank) solution (for example, rank 140), results in an unreasonable circulation (Table 6.3). To begin with, the solution is no longer within one standard deviation of the *a priori* error estimate. It is significantly noisier than the standard solution with large amplitude and rapidly alternating sign. Across individual sections the fluxes are greatly reduced. In particular, the magnitude of the Atlantic inflow across the Greenland-Scotland Ridge is reduced to 2.5Sv (i.e. to a third). The magnitude of the East Greenland Current is roughly halved, as are the magnitudes of the dense overflows into the North Atlantic. The resultant heat fluxes across the Greenland-Scotland

Ridge are reduced by almost a factor of 3, such that the total heat convergence of the Nordic Seas is reduced to 6 TW (i.e. 2□W□m^{-2}). None of these consequences is plausible. For example, Osterhus et al. (2005) found no collapse of the Atlantic inflow in their measurements of the volume, heat and salt fluxes across the Greenland-Scotland Ridge (based on moorings and CTD cruises between the mid 1990's and 2001).

The variability of the circulation resulting from different rank solutions is discussed further in Chapter 6 (section 6.4.2).

5.6.5 Resolution Matrices

The observation resolution matrix is defined as $U_k \square U_k^T$, where k is the rank of the chosen solution. The diagonal elements of this matrix are illustrated in Figure 5.25. The columns of this matrix show the information content in each equation, with a diagonal element of 1 indicating that the corresponding constraint is completely independent of other constraints. The overall mean value for the diagonal elements is 0.5; with 0.2 for full depth volume equations, 0.5 for layer volume equations, 0.4 for layer salinity equations and 0.8 for layer temperature equations. This suggests that there is linear dependence between many of the equations. This applies in particular to the volume and salinity equations, with the temperature conservation constraints contributing rather more independent information. This relationship between tracers was explored by Fukumori and Wunsch (1991) who used the large–scale temperature, salinity, oxygen and nutrient distributions to describe the general circulation and dominant physical characteristics of the North Atlantic Ocean They found significant redundancy among the data, with temperature being highly correlated with salinity and also with the three nutrients, and only oxygen providing independent information. The tight relationship between temperature and salinity underpins the □□S plot of classical hydrography (Warren and Wunsch, 1981).

Figure 5.26 illustrates the diagonal elements of the solution resolution matrix, $\mathbf{V}_k \square \mathbf{V}_k^T$, where k is the rank of the chosen solution. If all solution elements are perfectly resolved then the diagonal of this matrix is unity. For rank 43 of the standard model the diagonal elements for the reference velocities have mean and peak values of 0.1 and 0.4, respectively, while those for the effective diapycnal velocities reach peak values of 0.9. This suggests that while the resolution of the effective diapycnal velocities is generally satisfactory, the individual reference velocities are poorly resolved. This means that the ability of the model to accurately determine the lateral fluxes, as for many inverse studies, is restricted to the larger scales (Naveira Garabato et al., 2003). McIntosh and Rintoul (1997) do note, however, that

"… the strategy of choosing the column weight to resolve the interfacial fluxes at the expense of the reference level velocities generally produces the most accurate horizontal fluxes in addition to the most accurate interfacial velocities: Decreasing the relative weight to redirect

information to the determination of the reference level velocities generally degrades the estimate of the lateral fluxes ….."

The use of direct current measurements to initialise the velocity field does mean, however, that the initial estimate of the solution is close to satisfying the model equations within *a priori* uncertainties. The initial volume residuals are typically <4 Sv in individual layers.

5.7 Net fluxes of the Nordic Seas

The standard solution adjusts the unknown reference level velocities and the effective diapycnal velocities to ensure that the resulting flow field is consistent with the constraints applied to the model. Consistency in the flow field is attained since the residuals of this solution are required to be equal to or smaller than the uncertainty ascribed to the conservation equations (three times the standard deviation in the transport estimate).

5.7.1 Volume Fluxes

The standard solution is not full rank, so the residual norms are not exactly zero. This results in small volume imbalances in each box (-0.7 Sv for the *north* box, 0.4 Sv for the *south* box, -0.6 Sv for the *east* box and 0.1 Sv for the *west* box), and thus a divergence over the Nordic Seas of 0.8 Sv. Although this is smaller than the ascribed uncertainty, the calculation of heat and freshwater fluxes require zero net volume transport. To achieve this, the inverse is applied for a second time, but requiring only full depth volume conservation within each inverse box. The full rank solution of this second inverse provides a further small barotropic correction for each station pair, of the order 0.03 $m s^{-1}$. The resultant flux field, with zero net volume transport into each inverse box, and the Nordic Seas, is illustrated in Figure 5.27.

The volume transports across each of the sections are summarised in Table 5.11. The transports are given for each layer, for surface waters (e.g. NAW and PW; $\sigma_0 <$ 27.8), for water the same density as the overflows (27.8 $< \sigma_0 <$ 28.0), for denser intermediate waters ($\sigma_0 >$ 28.0 and $\sigma_1 <$ 32.76), for the deep waters ($\sigma_1 >$ 32.76) and for the full water column. The isopycnal $\sigma_0 =$ 27.8 is selected since, within the domain of the Nordic Seas, it generally implies the separation of the North Atlantic Water (NAW) and the lighter Polar Waters from the denser Intermediate and Deep Waters. Similarly, the isopycnal $\sigma_0 =$ 28.0 separates the overflow waters from the denser intermediate and deep waters. The volume transports within these layers are illustrated in Figure 5.28.

Layer	Layer Boundaries	Section						
		DS	**BSO**	**FS**	**GN**	**ISval**	**IScot**	**Skag**
1	$\sigma_0 < 26.5$	-0.47	0.20	-0.60	-0.03	0.00	0.00	0.26
2	$26.5 < \sigma_0 < 27.0$	-0.22	0.27	-0.19	-0.12	-0.02	0.59	0.02
3	$27.0 < \sigma_0 < 27.3$	-0.13	0.32	-0.02	0.18	-0.03	2.28	-0.12
4	$27.3 < \sigma_0 < 27.5$	-0.06	0.23	0.03	0.54	0.15	2.22	-0.16
5	$27.5 < \sigma_0 < 27.6$	0.00	0.18	0.00	0.67	0.12	0.49	-0.06
6	$27.6 < \sigma_0 < 27.7$	-0.13	0.29	-0.11	-0.17	-0.02	0.43	0.00
7	$27.7 < \sigma_0 < 27.8$	-0.13	0.20	-0.12	0.29	-0.08	- 0.12	0.00
8	$27.8 < \sigma_0 < 27.95$	-0.51	-0.41	-0.36	0.37	0.73	-3.07	0.00
9	$27.95 < \sigma_0 < 28.0$	-0.88	-0.27	-0.72	-1.26	0.36	0.00	0.00
10	$\sigma_0 > 28.0, \sigma_1 < 32.73$	-0.37	-0.03	-0.35	-1.03	-0.03	0.00	0.00
11	$32.73 < \sigma_1 < 32.76$	-0.62	-0.16	-0.34	-0.71	-0.03	0.00	0.00
12	$32.76 < \sigma_1 < 32.78$	-0.13	-0.02	-0.18	0.20	-0.04	0.00	0.00
13	$\sigma_1 > 32.78, \sigma_2 < 37.45$	-0.40	-0.04	0.60	-1.01	0.87	0.00	0.00
14	$37.45 < \sigma_2$	0.00	0.00	0.29	0.78	0.00	0.00	0.00
1-7	$\sigma_0 < 27.8$	-1.14	1.69	-1.01	1.36	0.12	5.89	-0.06
8-9	$27.8 < \sigma_0 < 28.0$	-1.39	-0.68	-1.08	-0.89	1.09	-3.07	0.00
10-11	$\sigma_0 > 28.0, \sigma_1 < 32.76$	-0.99	-0.19	-0.69	-1.74	-0.06	0.00	0.00
12-14	$\sigma_1 > 32.76$	-0.53	-0.06	0.71	-0.03	0.83	0.00	0.00
1-14	**Full Depth**	**-4.05**	**0.76**	**-2.07**	**-1.33**	**1.98**	**2.82**	**-0.06**

Table 5.11: Volume transports (Sv) for each section, and for each layer, for surface waters (e.g. NAW and PW; $\sigma_0 \leq$ 27.8), for water the same density as the overflows ($27.8 \leq \sigma_0 \leq 28.0$), for denser intermediate waters ($\sigma_0 >$ 28.0 and $\sigma_1 <$ 32.76), for the deep waters ($\sigma_1 > 32.76$) and full depth. Positive transports are directed northwards towards the Arctic (see text). Sections are denoted by; **DS** for Denmark Strait, **BSO** for the Barents Sea Opening, **FS** for Fram Strait, **GN** for the Greenland-Norway section, **ISval** for the Iceland-Svalbard section, **IScot** for the Iceland-Scotland section and **Skag** for the section across the Skagerrak.

These net fluxes can be given a crude separation (see Table 5.7) to give an idea of the various exchanges. A total of 6.1 Sv Atlantic Water flows into the Nordic Seas (0.5 Sv through eastern Denmark Strait, and the remainder across the Iceland-Scotland Ridge). Over half this inflow (3.6 Sv) flows directly to the Arctic via Fram Strait and the Barents Sea (becoming denser through ocean-atmosphere exchanges, rather than through interaction with the gyres of the Iceland and Greenland Seas). An inflow of 1.0 Sv Polar Water through Fram Strait, together with modified Atlantic Waters (some of which have circuited the Arctic Ocean, and some of which have recirculated within Fram Strait), contribute to a southward flow of 5.1 Sv in the EGC. The addition of intermediate waters from the Greenland Sea gyre increase the strength of the EGC to 13.2 Sv at ~75°N. The net inflow of 6.8 Sv to the Nordic Seas through Fram Strait is divided almost equally between the surface and intermediate waters and the deep waters. There is a total outflow of 4.1 Sv through Denmark Strait, with an inferred overflow of 2.9 Sv (intermediate waters) and a surface outflow of 1.2 Sv Polar Waters. The total flow of dense water across the Iceland-Scotland Ridge is 3.2 Sv.

5.7.2 Heat and Freshwater Fluxes

The net fluxes of heat and freshwater are calculated for zero net volume transport in each of the inverse boxes; effectively zero net volume transport between the Nordic Seas and the North Atlantic and Arctic Ocean. The details of the calculations are explained in section 4.2.3 and 4.2.4. The fluxes are summarised in Figures 5.29 and 5.30.

(i) Heat fluxes

The standard solution gives an oceanic poleward heat flux between the North Atlantic and the Nordic Seas of 188 TW, and 57 TW between the Nordic Seas and the Arctic Ocean (through Fram Strait and the Barents Sea Opening). This suggests a total heat convergence within the Nordic Seas of 137 TW, giving an average flux of 51 Wm^{-2} (using a total surface area of 2.7×10^{12} m^2).

This can be divided further into a mean summer heat flux to the atmosphere over the domain of each of the inverse boxes. The greatest average heat flux is 70 Wm^{-2} over the south box (surface area of 1.5×10^{12} m^2), suggesting that the NAC interacts with the atmosphere most strongly over the southern part of the Nordic Seas (over the Norwegian and Lofoten Basins of the Norwegian Sea). The corresponding heat fluxes are -2 Wm^{-2} over the north box, 35 Wm^{-2} over the east box and 10 Wm^{-2} over the west box (surface areas of 1.9×10^{11} m^2, 6.5×10^{11} m^2 and 4.1×10^{11} m^2, respectively).

(ii) Freshwater fluxes

Following the method described in section 4.2.4, the volume transport balance for the Nordic Seas, is given by

$$V_N + V_S + F = 0 \qquad 5.2$$

where F is the freshwater gain of the Nordic Seas, V_N is the net volume transport into the Nordic Seas across the northern boundaries (ie Fram Strait and the Barents Sea Opening), and V_S is the net volume transport into the Nordic Seas across the southern boundaries (ie the Greenland - Scotland Ridge). The subscripts S and N denote the southern and northern boundaries, respectively.

When taken around the boundary of the Nordic Seas the salinity flux is given by

$$\oint (S\,v)\,dx\,dz = 0 \qquad 5.3$$

where S is the salinity, v is the component of velocity normal to the section, dx is the station pair separation and dz is the mean station pair depth. In terms of the salinity flux across the southern and northern boundaries this becomes:

$$\int_S (S_S\,v_S)\,dx\,dz + \int_N (S_N\,v_N)\,dx\,dz = 0 \qquad 5.4$$

Following equations 4.13 and 4.14, equation 5.4 can be written in terms of the average salinity $\overline{S}$ and its deviation S' over each boundary:

$$\overline{S}_S V_S + \int (S'_S v_S)\, dx\, dz + \overline{S}_N V_N + \int (S'_N v_N)\, dx\, dz = 0 \qquad 5.5$$

Multiplying equation 5.2 by $\overline{S_S}$

$$\overline{S}_S V_N + \overline{S}_S V_S + \overline{S}_S F = 0 \qquad 5.6$$

Putting equations 5.5 and 5.6 equal to each-other,

$$\overline{S}_S V_N + \overline{S}_S V_S + \overline{S}_S F = \overline{S}_S V_S + \int (S'_S v_S)\, dx\, dz + \overline{S}_N V_N + \int (S'_N v_N)\, dx\, dz \qquad 5.7$$

re-arranging,

$$\overline{S}_S V_N + \overline{S}_S F - \int (S'_S v_S)\, dx\, dz - \overline{S}_N V_N - \int (S'_N v_N)\, dx\, dz = 0 \qquad 5.8$$

isolating the freshwater term,

$$\overline{S}_S F = \left(\overline{S}_N - \overline{S}_S\right) V_N + \int (S'_S v_S)\, dx\, dz + \int (S'_N v_N)\, dx\, dz \qquad 5.9$$

and dividing by the $\overline{S}_S$ term, then the expression for the freshwater gain of the Nordic Seas is given by

$$F = \frac{1}{\overline{S}_S}\left\{\left(\overline{S}_N - \overline{S}_S\right) V_N + \int (S'_S v_S)\, dx\, dz + \int (S'_N v_N)\, dx\, dz\right\} \qquad 5.10$$

The salinity fluxes, S_S and S_N, are 4.3×10⁶ Sv psu northwards between the North Atlantic and the Nordic Seas, and 2.5×10⁶ Sv psu northwards between the Nordic Seas and the Arctic Ocean, respectively, with mean salinities across the southern and northern boundaries of $\overline{S}_S = 34.963$ and $\overline{S}_N = 34.853$. Following equation 5.10, these equate to southward freshwater fluxes of 0.121×10⁶ Sv and 0.068×10⁶ Sv respectively, and give a net input of freshwater over the Nordic Seas of 0.053×10⁶ Sv.

This input of freshwater is due in part to an estimated freshwater input of 0.030×10⁶ Sv from the Baltic Seas (Figure 5.30).

5.7.3 Effective Diapycnal Fluxes

Independent diapycnal fluxes for each property (volume, heat and salinity) are explicitly included in the inverse for the relevant layer interfaces. These fluxes represent the net diapycnal flux resulting from all mixing processes in the ocean interior. The effective diapycnal volume velocities, representing the advective velocities, are illustrated in Figure 5.31 for each of the north, south, east and west boxes. The associated diapycnal volume transports are also shown.

Over most of the Nordic Seas the interior diapycnal volume velocity is typically less than 0.5×10^{-6} m s^{-1}. Within the north box the magnitude of the diapycnal velocity is not significantly

different from zero below σ_0=27.95, and only a relatively large downwelling rate of 1.0×10^{-6} m s^{-1} towards the surface across σ_0=26.5. In the south box there is significant upwelling of waters with density above σ_0=27.3, but typically low diapycnal velocities throughout the deeper water column. Within the east box, there is significant downwelling of waters lighter than σ_0=26.5, below which are only low velocities. Typically the velocities within the west box are low and not significantly different from zero.

The interlayer fluxes implied by these solution vertical velocities are typically of the order 0.5 Sv, which are no greater than the individual layer residuals. However, it should be noted that the inverse is initialised with the diapycnal volume velocity as zero (based on a lack of prior knowledge of the regional properties of the mixing). This may introduce a bias towards a minimum mixing solution. Although the inclusion of diapycnal fluxes was necessary for the inverse model to be physically consistent, it may be the case that the fluxes diagnosed from the inverse are of limited value, since they appear to show little diapycnal mixing within the Nordic Seas.

5.8 Summer Circulation of the Nordic Seas

A circulation scheme for the Nordic Seas, as illustrated in Figure 5.39, can be derived from the net fluxes described in section 5.7. These calculations are based on the standard solution of the inverse model. The investigation of the errors and sensitivity of the inverse (Chapter 6) allows an estimation of the errors that should be assigned to the standard solution. The study demonstrates that net fluxes are relatively robust within the error bounds suggested. Hence, although the details depend to some extent on a subjective choice of water mass definitions, the scenario described here can be assumed to give insight to the summer circulation of the Nordic Seas.

To assemble a circulation the water column is considered in three parts; upper, mid-depth and deep. Analysis is based on the water masses defined in Table 5.1. The upper part includes the surface waters of the inflowing North Atlantic Water, the cold Polar Waters, Arctic Surface Water and the Shelf Waters (NCW, GSSW and KW). The mid-depth part includes the Intermediate Waters (rAW, GSAIW, NSAIW), the overflows, and the waters found in the northeast Atlantic (LSW, WNAW and MNAW). The deep part includes the deep outflow from the Arctic Ocean (AODW) and the deep waters of the Nordic Seas (GSDW and NSDW).

To ascertain the magnitude and pathways of the circulation, the cumulative transports along each section are derived for the layers defined for the inverse calculations (based on σ_0, σ_1 and σ_2), and also for layers defined by pressure. These are illustrated in Figures 5.32 to 5.38.

Rather than describing each section in turn and in isolation, the pathways and modifications of the major water masses are traced as they circuit the Nordic Seas. The discussion focuses mainly on the

circulation presented here since the net fluxes derived from previous studies were considered within the description of the initial velocity field (section 5.5).

5.8.1 Upper Waters

The logical starting point is to trace the path of the warm inflowing Atlantic Waters, and to track them from their source in the eastern North Atlantic as they circuit the Nordic Seas. Looking first to the Iceland-Scotland section, and then to the section just to the north of Denmark Strait, the total inflow of Atlantic Waters across the Greenland-Scotland Ridge is 8.2 Sv, defined to be within the density range $26.5 \leq \sigma_0 \leq 27.6$ (layers 2–5). The cumulative transport plot for the Iceland-Scotland section (Figure 5.38) shows the inflow to be concentrated in waters with $27.0 \leq \sigma_0 \leq 27.5$ (layers 3 and 4). At the time of the section the inflow was confined to a pathway through the Rockall Trough (described in detail in section 4.5.2). The standard solution, however, prefers to divide the inflow between the Rockall pathway and the pathway through the Iceland Basin. The Atlantic Water in the Irminger Current enters the Nordic Seas to the west of Iceland, through Denmark Strait. The northern extension of the Irminger Current has a magnitude of 0.4 Sv at the location of the Denmark Strait section where it is known as the North Icelandic Irminger Current. This warm inflowing Atlantic Water, defined as $\theta > 4$°C (with $\sigma_0 < 27.7$, and mostly within the range $26.5 \leq \sigma_0 \leq 27.3$), is confined to the Icelandic Shelf region to the east of the section. Considering the salinities of this inflow it should be noted that; the surface waters (~0.06 Sv) have been freshened ($32 \leq S \leq 34$), there is ~0.12 Sv of water fresher than the typical definition of AW with salinity $34.8 \leq S \leq 34.9$, and the remainder of the inflow has a salinity between $34.94 \leq S \leq 35.2$. This suggests that the character of the inflow has been partially modified by local meltwater or river discharge. The total inflow is towards the lower end of reported transports, which are of the order 1 Sv, but vary from 0.7 to 2.7 Sv (Kristmannsson, 1998). It continues to follow the Icelandic coast to flow eastward into the Norwegian Basin, and close in to the coast it can be traced across the Iceland-Svalbard section, although modified such that $S < 34.9$.

As the Atlantic Waters cross the Greenland-Norway section two main branches can be discerned within the flow. At this latitude the Atlantic inflow has been modified through heat loss to the atmosphere, hence the definition of AW on this section is extended to include waters with temperatures above 3°C and salinities above 35.92 ($\sigma_0 < 27.95$). The western branch is a continuation of the Faroe Current and is steered initially by the Vøring Plateau, and then continues northwest toward the Greenland Basin, crossing the Greenland-Scotland section to the east of Mohns Ridge. The eastern branch takes the form of a barotropic slope current which follows the continental slope of Norway. These branches are separated by the cyclonic circulation within the Lofoten Basin, but give a combined transport of 4.3 Sv towards the Arctic. The near-surface circulation is complicated by the presence of mesoscale eddies. Since 4.3 Sv of the Atlantic inflow continues north across the Greenland–Norway section, it implies that 3.9 Sv of Atlantic Water is

cooled and mixed into the intermediate waters of the Norwegian Sea south of the section. To the far east of the section, along the Norwegian coast, there is a buoyant coastal current known as the Norwegian Coastal Current (NCC). This is created by the freshwater supply to the Nordic Seas from the Baltic and coastal river discharge. This low-saline flow is confined over the shelf region near in to the coast and has a magnitude of ~0.6 Sv as it crosses the Greenland–Norway section.

Further north, there is a transport of 1.4 Sv from the Nordic Seas into the Barents Sea, across the Barents Sea Opening. At this latitude AW can be defined as having temperatures >2°C and σ_0<27.95 to account for the heat loss and densification that occur further to the south within the Norwegian Sea. Within Bjørnøyrenna, to the south of Bear Island, ~2.5 Sv flow eastwards into the Barents Sea, including a less saline component derived from the NCC (~0.7 Sv). Of this, ~0.5 Sv recirculate back into the Nordic Seas on the northern slope of Bjørnøyrenna. Since the magnitude of the NCC (~0.6 Sv) remains roughly constant between the Greenland–Norway section and the Barents Sea Opening, this coastal current does not seem to significantly interact with the warm Atlantic flow. To the north of Bear Island, 1.2 Sv flows back through Storfjordrenna into the Nordic Seas. This includes a contribution of ~0.2 colder Arctic water, ~0.7 Sv of dense winter waters formed in the northern Barents Sea and Storfjorden, and ~0.3 Sv recirculating AW. There is thus a net transport of ~1.4 Sv AW from the Nordic Seas to the Arctic through the Barents Sea Opening.

The remaining pathways of the Atlantic inflow recombine to cross the Iceland-Svalbard section as a single branch (~2.9 Sv), with the majority of the transport between the northern edge of the Boreas Basin and the continental slope off Svalbard. At this latitude the density of the Atlantic waters has been further increased (σ_0<28.0) through continued heat loss. There is a net transport of ~1.7 Sv through the eastern part of Fram Strait into the Arctic Ocean within the West Spitsbergen Current. This suggests that ~1.2 Sv of NAW recirculates to the south of Fram Strait. A further 0.1 Sv of fresh (S<34.7) surface waters also flow north on the shelf break off Svalbard.

Having considered the surface flow of Atlantic Waters and coastal waters in the eastern sector of the Nordic Seas, the surface flow of Polar Waters and cold Shelf Waters are now traced through the Nordic Seas from Fram Strait, along the coast of Greenland and into the North Atlantic via Denmark Strait. First considering the Greenland shelf region to the west of Fram Strait, a broadly southward flow is noted with a net transport of 0.6 Sv of Greenland Sea Shelf Water (GSSW), and ~0.3 Sv of Knee Water (KW). GSSW is a locally formed water mass (θ<-1.5°C and S<34), while the slightly warmer KW (-1.5<θ<0°C) is Arctic surface water of Atlantic origin. The core of the East Greenland Current is concentrated over the shelf break and shelf slope and carries a further ~0.6 Sv of cold, fresh Polar Waters. The total surface flow of Polar Waters through the western part of Fram Strait is therefore 1.5 Sv. This southward surface flow can be traced as it crosses the Greenland–Norway section between latitudes of 75°N and 77°N. Of this ~0.3 Sv is GSSW (θ<-1.5°C), and the remainder is PW (~1.9 Sv). Continuing southwards this cold, fresh surface flow exits the Nordic

Seas into the North Atlantic carried in the EGC through Denmark Strait. At the Denmark Strait section, a southward flow of 1.2±0.5Sv of cold Polar Waters is observed. This is defined as $\theta < -1.0$°C and $\sigma_0 < 27.5$. There is no evidence of the colder GSSW ($\theta < -1.5$°C), indicating that these waters are confined to the broad shelf region off the Greenland coast further north.

In addition to the surface inflows and outflows, the surface layers within the interior of the Nordic Seas are to be considered. Within the Greenland Basin a thin surface layer of relatively warm Arctic Surface Water (ASW) is present ($2 < \theta < 6$°C). It can be observed on both the Greenland-Norway and Iceland-Svalbard sections and its circulation is broadly cyclonic (~0.5±0.5Sv). These surface waters overlying the intermediate waters of the Greenland Sea are formed by summer heating and freshened by mixing with PW. There is also a warm surface layer of ASW type waters in the Iceland Sea, with a net transport to the southeast towards the Norwegian Sea of ~0.7±0.5Sv.

5.8.2 Mid-depth Waters

Having traced the Atlantic Waters in their circuit of the Nordic Seas, the next step is to look for evidence of waters of Atlantic origin whose character has been modified during their passage through both the Nordic Seas and their longer circuit through the Arctic Ocean. This water mass, is referred to as return Atlantic Water (rAW), and is defined as being all water with $S > 34.9$ and $0 < \theta < 2$°C (i.e. $\sigma_0 > 27.95$ and $\sigma_1 < 32.73$). The net southward flow of rAW within the EGC in Fram Strait is 3.5±0.5Sv. Further to the east there is a recirculating flow of about 0.9±0.5Sv, which may be formed partly from rAW and modified Atlantic Waters carried in the extension of the NAC.

The water mass defined here as rAW is observed in the EGC crossing the Greenland-Norway section between 77°N and 75°N. At this latitude ~3.3±0.5Sv can be traced, since this is only 0.2±0.5Sv less than the 3.5±0.5Sv flow of rAW within the EGC in Fram Strait, the implication is that there is little interaction between this water mass and the intermediate waters within the Greenland Sea gyre to the east. As the EGC continues to flow south along the coast of Greenland into the North Atlantic, rAW can be observed crossing the Denmark Strait section as a cooler, dense layer beneath the outflowing surface Polar Waters. The net southward flow of rAW is 1.2±0.5Sv (if defined as $0 < \theta < 2$°C). This suggests that ~2±0.5Sv of rAW leaves the EGC south of the Greenland-Scotland section, and flows eastward into the interior of the Nordic Seas, perhaps partly within the Jan Mayen Current (JMC) along the Jan Mayen Ridge, and partly within the East Icelandic Current further south.

Intermediate waters of fresher character are defined as Arctic Intermediate Water with $S < 34.9$ and $-1 < \theta < 3$°C (i.e. $\sigma_0 < 28.0$ and $\sigma_2 < 37.45$). These are termed Greenland Sea Arctic Intermediate Water (GSAIW) within the Greenland Sea, and Norwegian Sea Arctic Intermediate Water (NSAIW) within the Norwegian and Iceland Seas. At the latitude of the Greenland-Norway section, 5.0±0.5Sv are carried south in the EGC below the Polar Waters and rAW. Within the Greenland Sea Basin most

of the transport is within waters colder than $\theta = 0$°C. The net transport of GSAIW in the northward limb of the cyclonic gyre is 5 Sv, balancing the southward flow in the EGC which forms the southward limb of the gyre. This suggests that there is no discernible transport of GSAIW out of the Greenland Sea.

Across the Lofoten Basin in the Norwegian Sea there is a strong cyclonic circulation of 15 Sv (full depth). Over the width of the basin there is a net southward flow of NSAIW balancing the net northward flow of AW. Within the Iceland Sea (to the south of Jan Mayen Island and the Jan Mayen Fracture Zone) there is a weaker cyclonic circulation of 4 Sv (full depth). There is net flow to the southeast across the Iceland-Svalbard section within water masses characteristic of NSAIW.

The overflow through Denmark Strait (DSOW) is defined as $\theta < 2$°C and $34.8 < S < 34.9$ (giving $\sigma_0 > 27.8$ and $\sigma_1 < 32.78$). Using this definition the strength of the overflow is 2.5 Sv as it crosses the Denmark Strait section. The source of these waters is likely to have a contribution both from rAW and other intermediate waters derived from the Greenland and Iceland Seas. Since 1.2 Sv of rAW were observed on the section, it would suggest a 50% contribution from rAW and a 50% contribution from other intermediate waters.

Dense water also overflows the Iceland-Scotland part of the Ridge. Iceland-Scotland Overflow Water is defined as $\theta < 2$°C and $34.94 < S < 35.0$ (giving $27.8 < \sigma_0 < 27.95$). Figure 5.38 shows it to be confined to the south of Iceland implying the overflows through the Faroe Bank Channel and the notches in the Iceland-Faroes Ridge join together and follow a cyclonic pathway through the northern part of the Iceland Basin.

5.8.3 Deep Waters

The circulation of the deep waters is confined to the interior of the Nordic Seas and the deep exchanges through Fram Strait, due to the topographic restrictions of the Greenland–Scotland Ridge and the shallow Barents Sea Opening.

Although the northern part of the Barents Sea Opening is shallow (the Storfjordrenna) 0.7 Sv of dense water flow into the Nordic Seas. These waters are the probable remnants of winter water formed in the northern Barents Sea and in the Storfjorden, a shallow fjord south of Svalbard. These dense waters continue to sink to depth in the Nordic Seas as they flow parallel to the coast of Svalbard. They can be traced crossing the northern end of the Iceland-Svalbard section, and form the deep northward part of the WSC in the eastern part of Fram Strait.

In the deep part of Fram Strait (below 1000 m) a total southward flow of 1.5 Sv in the west of the section is partly balanced by ~1 Sv of recirculating deep waters. This results in a net deep southward flow of 0.5 Sv ($\sigma_1 > 32.73$), implying a 0.5 Sv upwelling of the deep waters. These deep waters are composed of AODW, defined as $\theta < -0.5$°C and $S > 34.92$ (giving $\sigma_2 > 37.45$), and NSDW. Most of these waters are NSDW, with a small southward flow of AODW of ~0.1 Sv.

The Greenland–Norway section cuts across the Greenland Basin of the Greenland Sea. Within the basin, the deepest waters are GSDW (θ<-1.0°C, 34.9<S<34.94 and σ_2>37.45). These have a cyclonic circulation (southward flow to the west of the basin and northward flow to the east) of 2.0±1Sv. The centre of the gyre does not appear to be in the central part of the basin, instead it is offset to the west. Similarly, the centre of the gyre in the Lofoten Basin of the Norwegian Sea seems to be offset to the south of the basin. The deep waters within this basin are characteristic of NSDW (θ<0°C and S~34.9), and follow a cyclonic circulation with a strength of ~2±1Sv. The small net flow of deep waters in the Greenland Basin is to the north, while the small net flow of deep waters in the Lofoten Basin is to the south, partly balancing the dominant surface flows within the western and eastern parts of the Nordic Seas. The deep cyclonic circulation of the Greenland Basin is also observed on the Iceland-Svalbard section, with a small (~0.6±1Sv) net flow of GSDW to the southeast. Within the Boreas Basin and the deep trench to the north, there is a small (~0.8±1Sv) net flow of GSDW towards the northwest.

Within the Iceland Sea there is a cyclonic circulation in the deep waters (NSDW) of <0.1±1Sv. There is a net southward flow of these deeper waters of 0.7±1Sv to the southeast, suggesting some deep flow between the Iceland Sea and the Norwegian Basin of the Norwegian Sea.

5.9 Summary

Table 5.12 summarises the exchanges between the Nordic Seas and the North Atlantic (across the Greenland–Scotland Ridge) and the Arctic Ocean (through Fram Strait and the Barents Sea Opening). Since the constraints required by the standard model imply zero net transport between the Nordic Seas and both the Arctic and the Atlantic oceans, when the sections are combined in this way the net fluxes illustrate the water mass transformations occurring between them.

The σ_0=27.8 isopycnal is taken to define the density of waters overflowing the Greenland-Scotland Ridge into the North Atlantic, and the net transport of waters above this level is towards the Arctic. Between the Greenland–Scotland Ridge and the openings to the Arctic Ocean, 4±1Sv of the warm, saline inflow are converted to more dense waters. The majority of this transformation occurs between the Greenland–Scotland Ridge and the Greenland–Norway section. This suggests that most of the ocean–atmosphere heat loss occurs over the southern part of the Nordic Seas.

It is also interesting to look for the transformations within particular temperature and salinity classes. Throughout the Nordic Seas there is a net northward flow of warm waters with θ>4°C, and a net southward flow of all waters cooler than this. A total of 3.8±1Sv of waters warmer than 4°C are cooled, and again most of this heat loss occurs between the Greenland-Scotland Ridge and the Greenland-Norway section. To balance this there is a 1.8±1Sv net increase of waters within the range 0<θ<4°C, all of which occurs between the Greenland-Norway section and the Greenland-

Scotland Ridge, and a net increase of cold waters with $\theta < 0$°C (a third of this transformation occurs to the north of the Greenland-Norway section).

Layers	Exchanges to North Atlantic (across GS Ridge and into Skagerrak) Volume Transport (Sv)	Exchanges across GN section Volume Transport (Sv)	Exchanges to the Arctic Ocean (via FS and BSO) Volume Transport (Sv)
$\sigma_0 < 27.8$	4.7	1.4	0.7
$27.8 < \sigma_0 < 28.0$	-4.5	-0.9	-1.8
$\sigma_0 > 28.0$, $\sigma_1 < 32.76$	-1.0	-1.7	-0.9
$\sigma_1 > 32.76$	-0.5	-0.0	0.7
Full Depth	**-1.3**	**-1.3**	**-1.3**
$\theta < 0$°C	-2.8	-1.4	-0.8
$0 < \theta < 4$°C	-4.7	-2.9	-2.9
$\theta > 4$°C	6.2	3.0	2.4
S < 34.9	-3.8	-0.5	-2.0
34.9 < S < 35.0	-4.5	-3.0	-0.7
S > 35.0	7.1	2.2	1.3
0 – 400m	0.8	1.8	-0.6
400 – 800m	1.0	-1.5	-0.8
800 – 1200m	0.6	-1.0	-0.4
1200 – 2000m	-1.7	-0.9	0.2
2000 – 4000m	-2.0	0.2	0.4

Table 5.12: Volume transports (Sv) summarised from Table 5.11, for exchanges between the Nordic Seas and the North Atlantic across the Greenland–Scotland (GS) Ridge, across the Greenland–Norway (GN) section, and into the Arctic Ocean through Fram Strait (FS) and the Barents Sea Opening (BSO). Positive transports are directed towards the Arctic.

There is a net northward flow of saline waters (S > 35.0) throughout the Nordic Seas, with 4.1 Sv of these waters being freshened on their passage through the Nordic Seas (again mainly south of the Greenland-Norway section). There is net southward flow of all waters less saline than S < 35.0. This is divided between a 2.7 Sv increase in waters within the range 34.9 < S < 35.0, and a 4.6 Sv increase in waters with S < 34.9.

The total volume transports from the standard solution suggest an input of 1.3 Sv into the Nordic Seas from the Arctic Ocean. Similarly, there is a net export of 1.2 Sv across the Greenland-Scotland Ridge into the North Atlantic from the Nordic Seas. The error estimates of this circulation scheme are the subject of the following chapter (Chapter 6).

Water Mass	Transport estimate (Sv)	*(author)*	Transport Estimate (Sv) Initial Velocity Field	Transport Estimate (Sv) Standard Solution
Total AW inflow across GS Ridge $26.5 < \sigma_0 < 27.6$	8 (based on net flow accounting for some recirculation)	*Hansen & Østerhus, 2000*	7.4	6.1
AW inflow through eastern Denmark Strait $\sigma_0 < 27.7$; $\theta > 4°C$	1.5 ± 0.7	*Kristmannsson, 1998*	0.6	0.5
AW inflow across Iceland-Scotland Ridge $\sigma_0 < 27.6$; $\theta > 7°C$; $S > 35.15$	6.7□□.4	*Hansen & Østerhus, 2000*	6.8	5.6
net northward flow of AW above 600-800m at 62°N (GN section)	2.0	*Orvik et al., 2001*	1.6	1.8
Net northward flow of NCW (GN section)	0.7	*Robitaille, 1995*	0.6	0.6
net outflow of AW into Barents Sea $\sigma_0 < 27.95$; $\theta > 2°C$	1.6	*O'Dwyer, 2001* *Ingvaldsen, 2002*	1.1	1.0
net northward flow in WSC through FS	2	*Schlichtholz and Houssais, 1999*	2.2	2.6
net inflow from the AO to NS via FS	5.2□(total) 2.6□(deep waters) 2.6□(surface/intermediate waters)	*Schlichtholz and Houssais, 1999*	3.1□(total) 1.1□(deep waters) 2.0□(surface/intermediate)	6.8□(total) 3.2 (deep waters) 3.6 (surface/intermediate)
PW inflow through western FS $\sigma_0 < 27.5$; $\theta < -1°C$; $S < 34.3$	1.5 1.1	*Mauritzen, 1996b* *Hansen et al., 2003*	1.2	1.0
net southward flow in EGC in FS	7	*Schlichtholz and Houssais, 1999*	5.7	5.2
Transport in EGC at ~75°N	11	*Woodgate et al., 1999*	9.0 (to 308□km offshore) 14.9 (to 344□km offshore)	8.1 (to 308□km offshore) 13.0 (to 344□km offshore)
PW surface outflow in western Denmark Strait $\sigma_0 < 27.6$; $\theta < -1°C$; $S < 34.3$	1.5	*Mauritzen 1996b* *Hansen & Østerhus, 2000*	1.1	1.2
Total IW/DW overflow over GS Ridge $\sigma_0 > 27.8$	5.6 ± 0.7	*Hansen & Østerhus, 2000* *Dickson & Brown, 1994*	5.8	6.0
IW/DW overflow through Denmark Strait $\sigma_0 > 27.8$; $\theta < 2°C$	2.9	*Ross, 1984* *Dickson & Brown, 1994*	2.6	2.9
IW/DW overflow across Iceland-Scotland Ridge $\sigma_0 > 27.8$; $\sigma_1 < 32.73$	3.4	*Hansen & Østerhus, 2000*	3.3	3.1

Table 5.5: Transport estimates (Sv) for the Nordic Seas, from the literature, the initial velocity field, and the standard solution of the inverse model. **GS Ridge** Greenland-Scotland Ridge; **IS Ridge** Iceland-Scotland Ridge; **GN** section Greenland-Norway section ; **FS** Fram Strait; **AO** Arctic Ocean; **NS** Nordic Seas; **DS** Denmark Strait; **AW** Atlantic Water; **NCW** Norwegian Coastal Water**; PW** Polar Water; **IW** Intermediate Water; **DW** Deep Water; **WSC** West Spitsbergen Current; **EGC** East Greenland Current.

Water Mass	Heat Transport Estimate (TW)	*(author)*	Transport Estimate (TW) Initial Velocity Field	Transport Estimate (TW) Standard Solution
Oceanic poleward heat flux across GS Ridge	245 ± 17 200 ± 80	*Isachsen, 2003* *Oliver & Heywood, 2003*	241	187
Heat flux through FS into AO	4.3 to 10.9	*Schlichtholz and Houssais, 1999*	7	9
Total heat flux into AO (via FS and BSO)	99 ± 12 average flux of 10 Wm^{-2} (using surface area of 9 x 10^6 km^2)	*Isachsen, 2003*	76	64
Total heat flux convergence in NS	146 ± 21 average flux of 20 Wm^{-2} (using surface area of 8 x 10^{12} km^2)	*Isachsen, 2003*	165 average flux of 35 Wm^{-2} (using surface are of 2.7□x□10^{12}□km^2)	123 average flux of 45 Wm^{-2} (using surface are of 2.7□x□10^{12}□km^2)

Table 5.6: Heat Flux estimates (TW) for the Nordic Seas, from the literature, the initial velocity field, and the standard solution of the inverse model. Some estimates are also quoted as W□m^{-2}, and the respective surface areas (km^2) are also stated. **GS Ridge** Greenland-Scotland Ridge; **FS** Fram Strait; **AO** Arctic Ocean; **BSO** Barents Sea Opening; **NS** Nordic Seas.

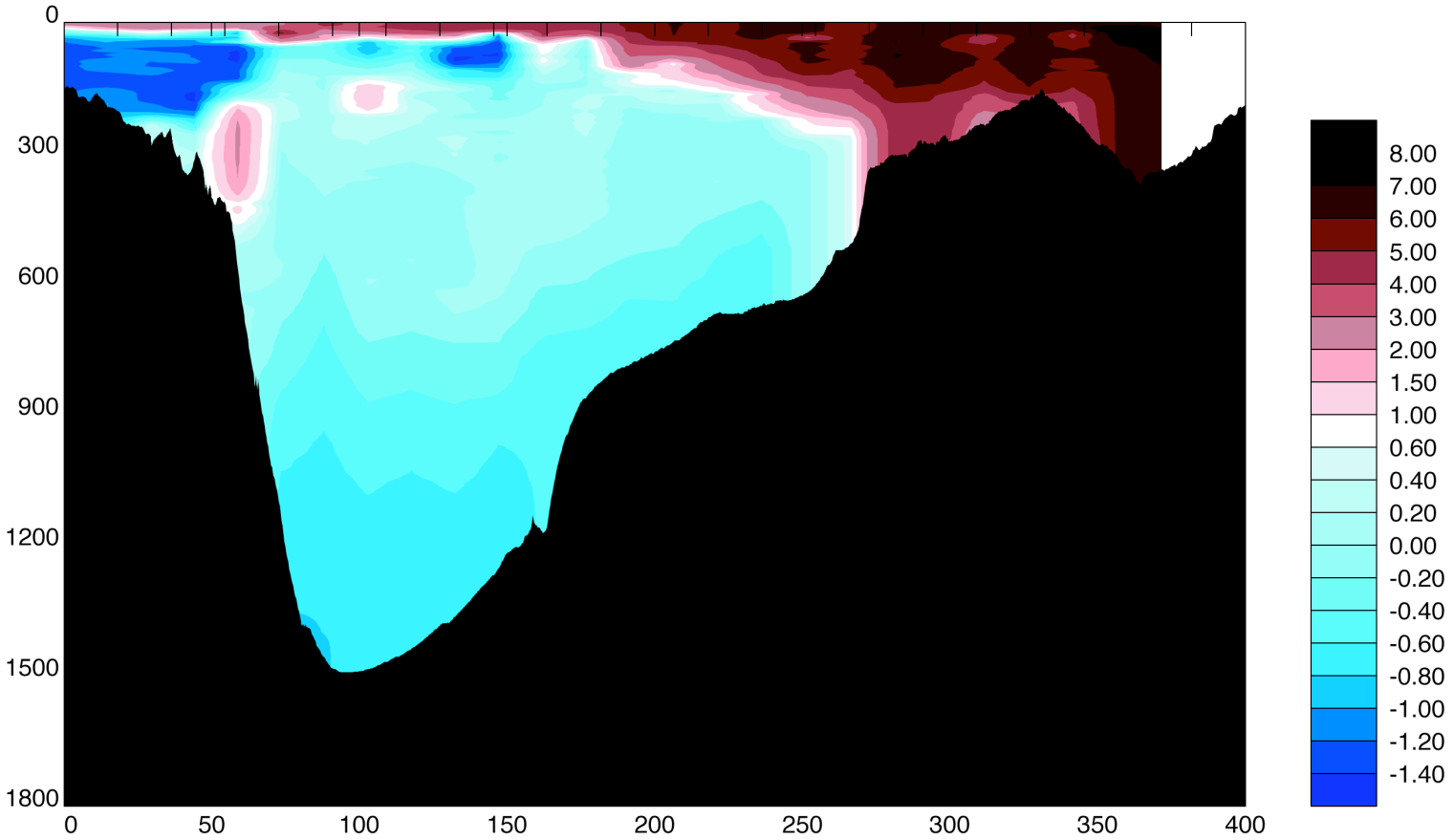

Figure 5.1a: Contoured potential temperature (°C) section across Denmark Strait, from Greenland on the left, eastwards to Iceland on the right. The x and y axes represent distance from the start of the section (km) and pressure (db) respectively. The sharp vertical contours in the temperature field are artefacts of the contouring.

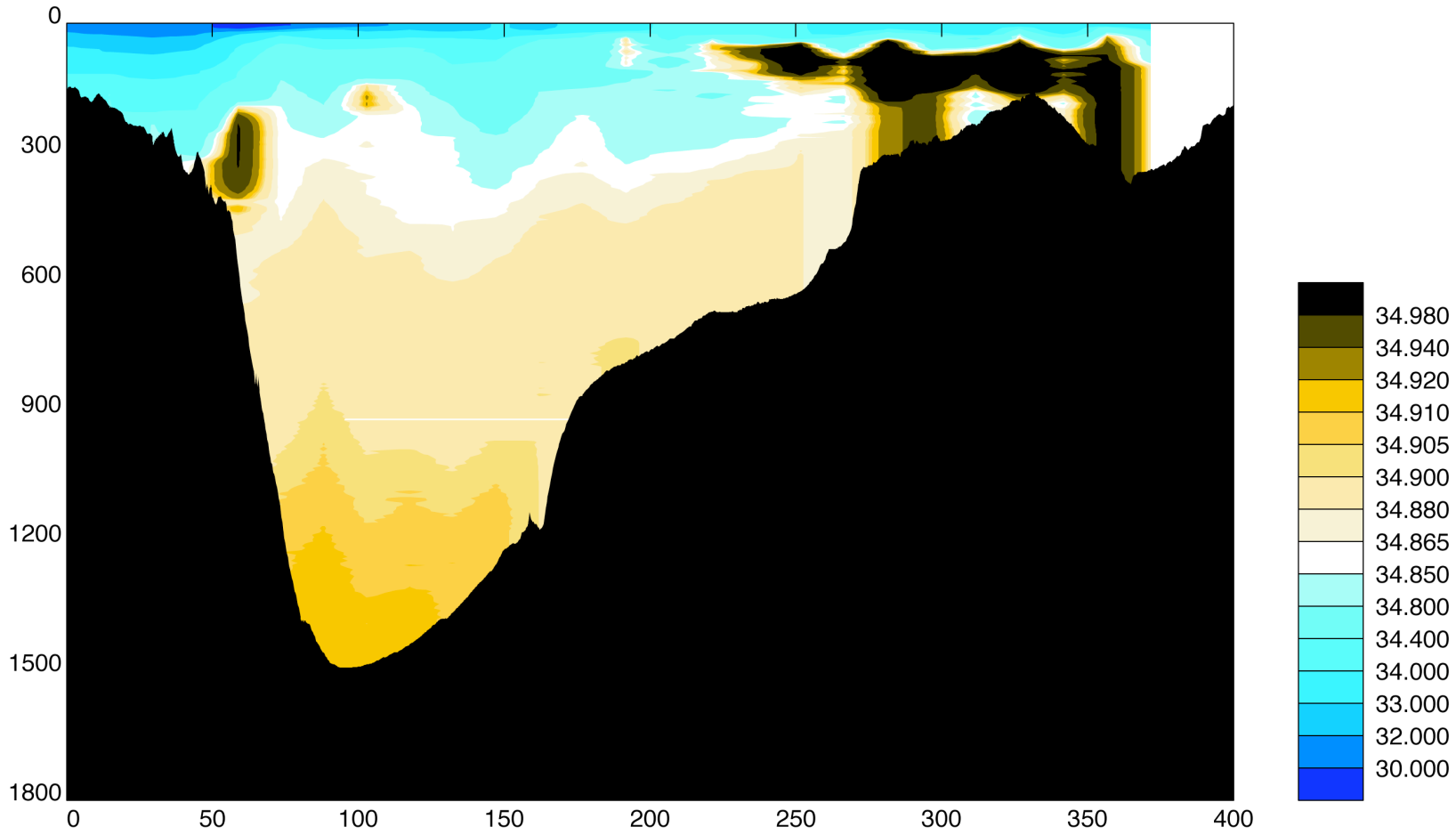

Figure 5.1b: Contoured salinity section across Denmark Strait, from Greenland on the left, eastwards to Iceland on the right. The x and y axes represent distance from the start of the section (km) and pressure (db) respectively. The sharp vertical contours in the salinity field are artefacts of the contouring.

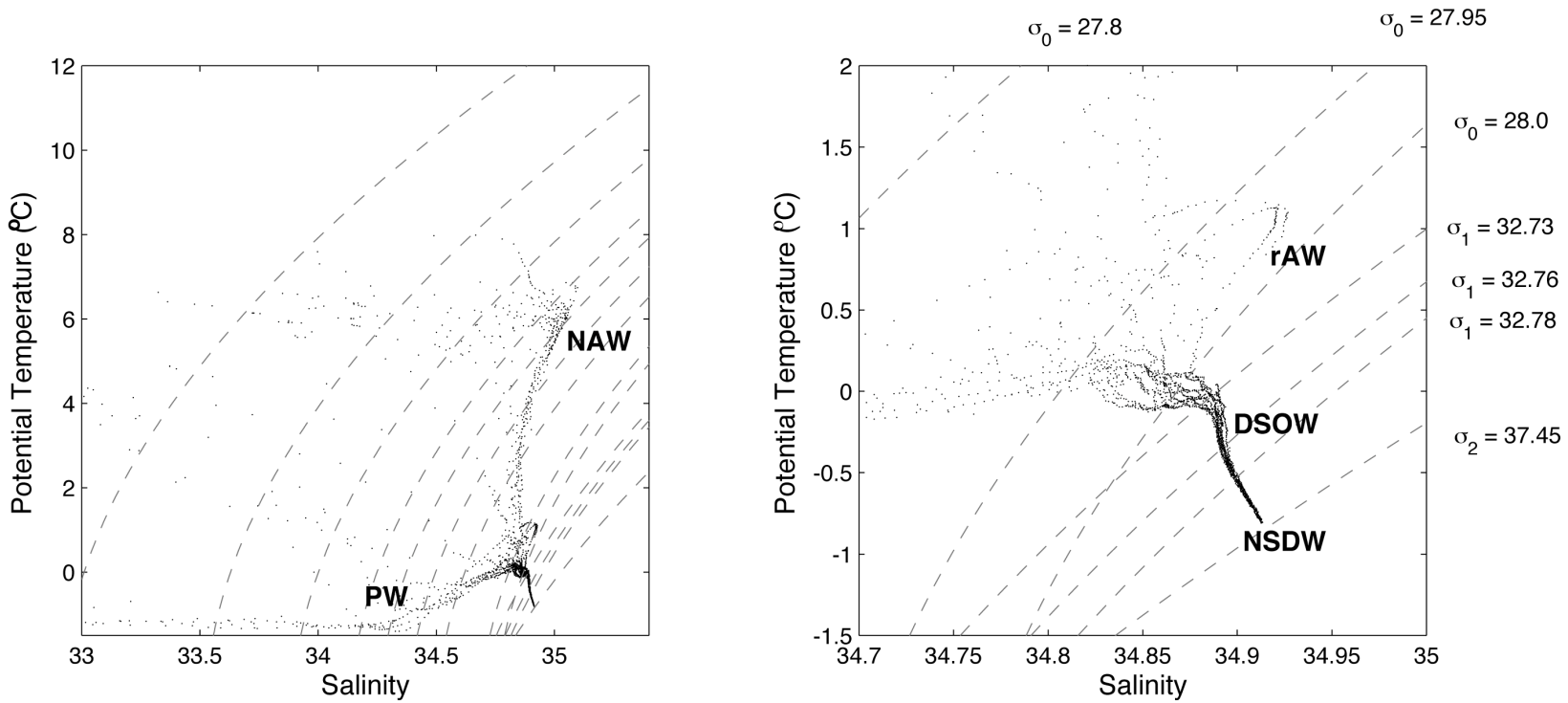

Figure 5.1c: □□S diagram (potential temperature / salinity plot) for the Denmark Strait section. The isopycnals used to define layers for the flux and inverse calculations are also illustrated. The scale for the panel on the left is the same for all sections to allow inter-comparison, the scale for the panel on the right is chosen to best illustrate the water masses present on this section. Some of the major water masses are marked; **PW** Polar Water, **NAW** Norwegian Atlantic Water, **rAW** return Atlantic Water, **NSDW** Norwegian Sea Deep Water, **DSOW** Denmark Strait overflow water.

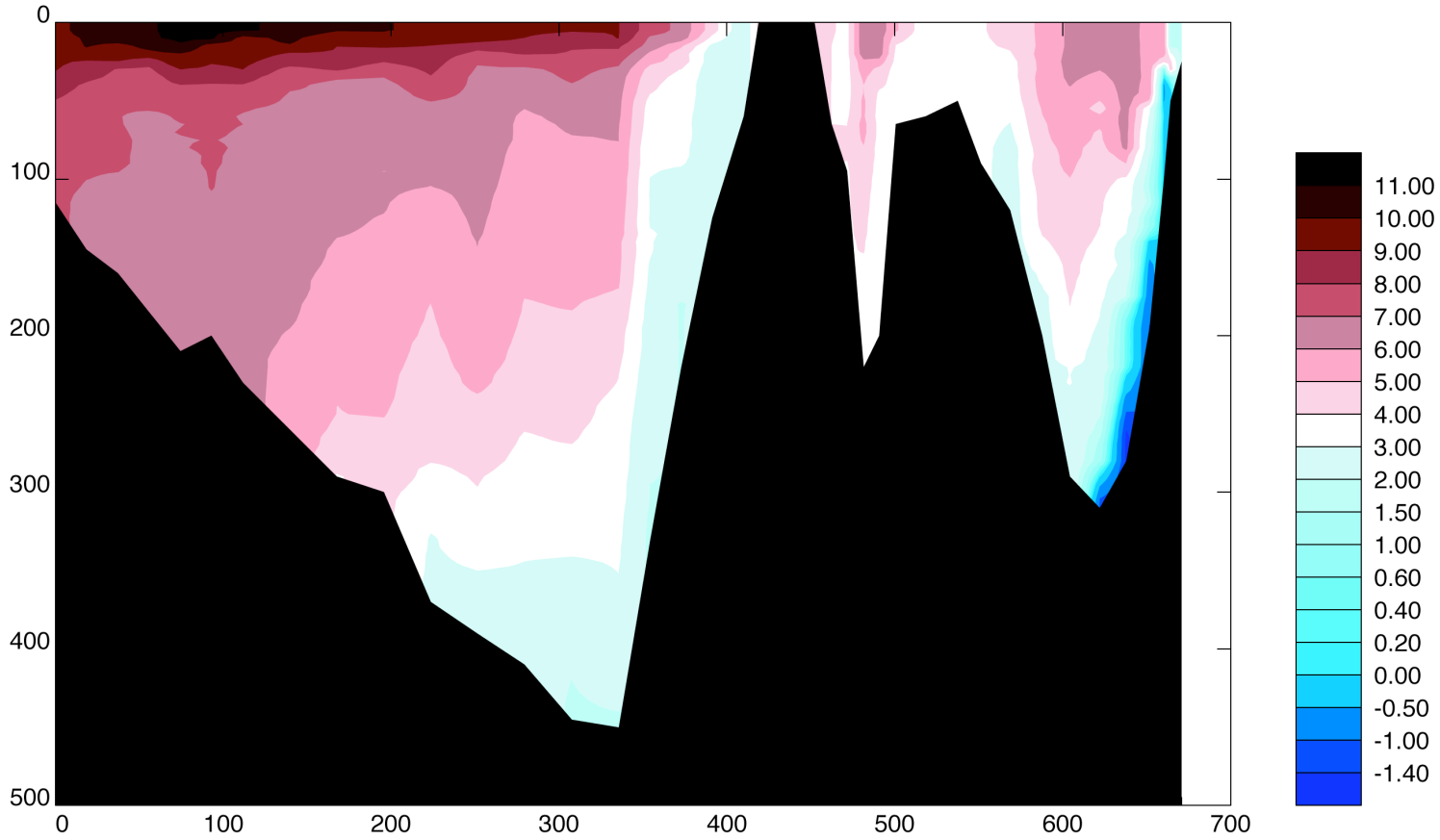

Figure 5.2a: Contoured potential temperature (°C) section across the Barents Sea Opening, from Norway on the left, northwards to Svalbard on the right. The x and y axes represent distance from the start of the section (km) and pressure (db) respectively. The sharp vertical contours in the temperature field are artefacts of the contouring.

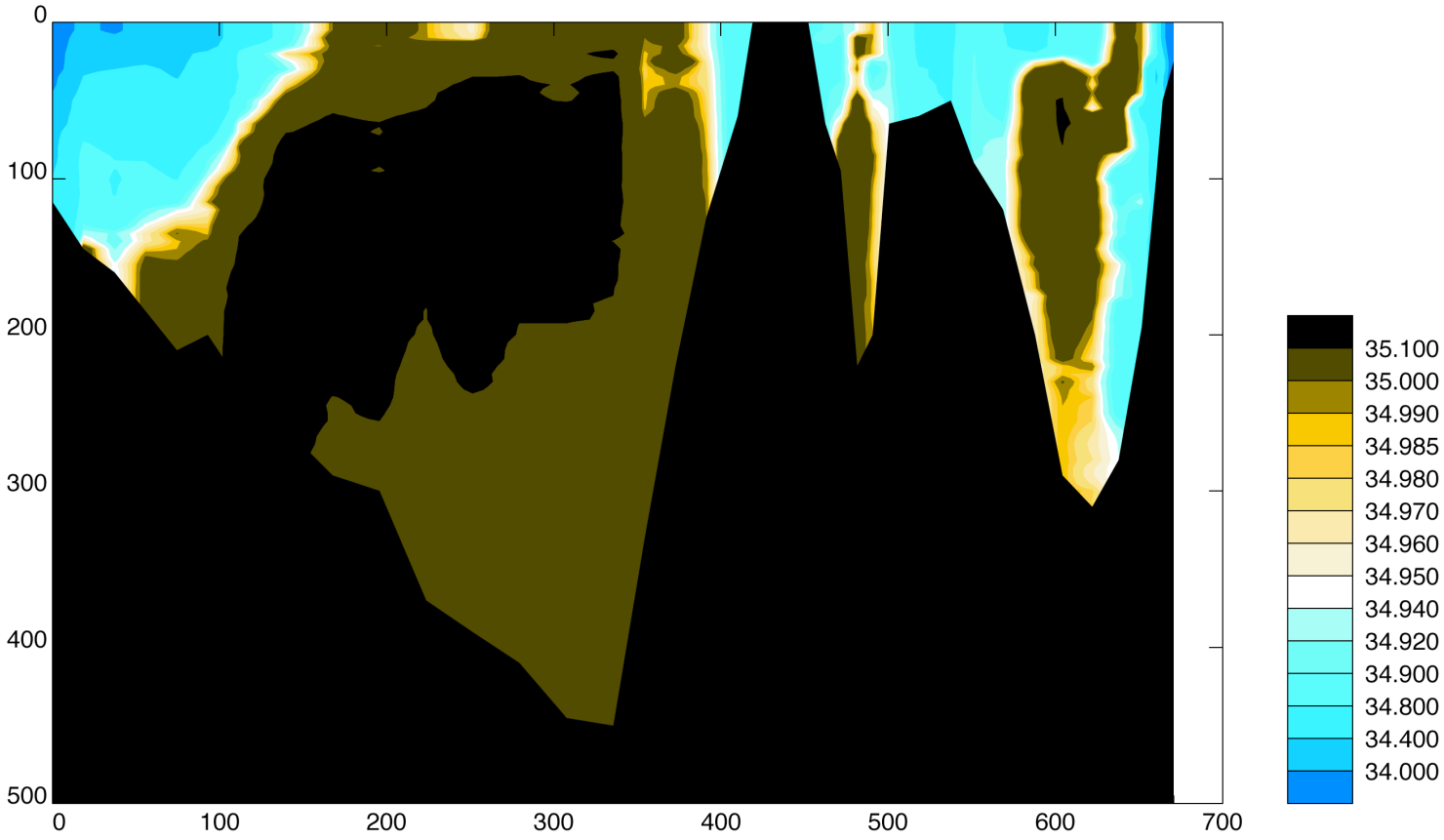

Figure 5.2b: Contoured salinity section across the Barents Sea Opening, from Norway on the left, northwards to Svalbard on the right. The x and y axes represent distance from the start of the section (km) and pressure (db) respectively. The sharp vertical contours in the salinity field are artefacts of the contouring.

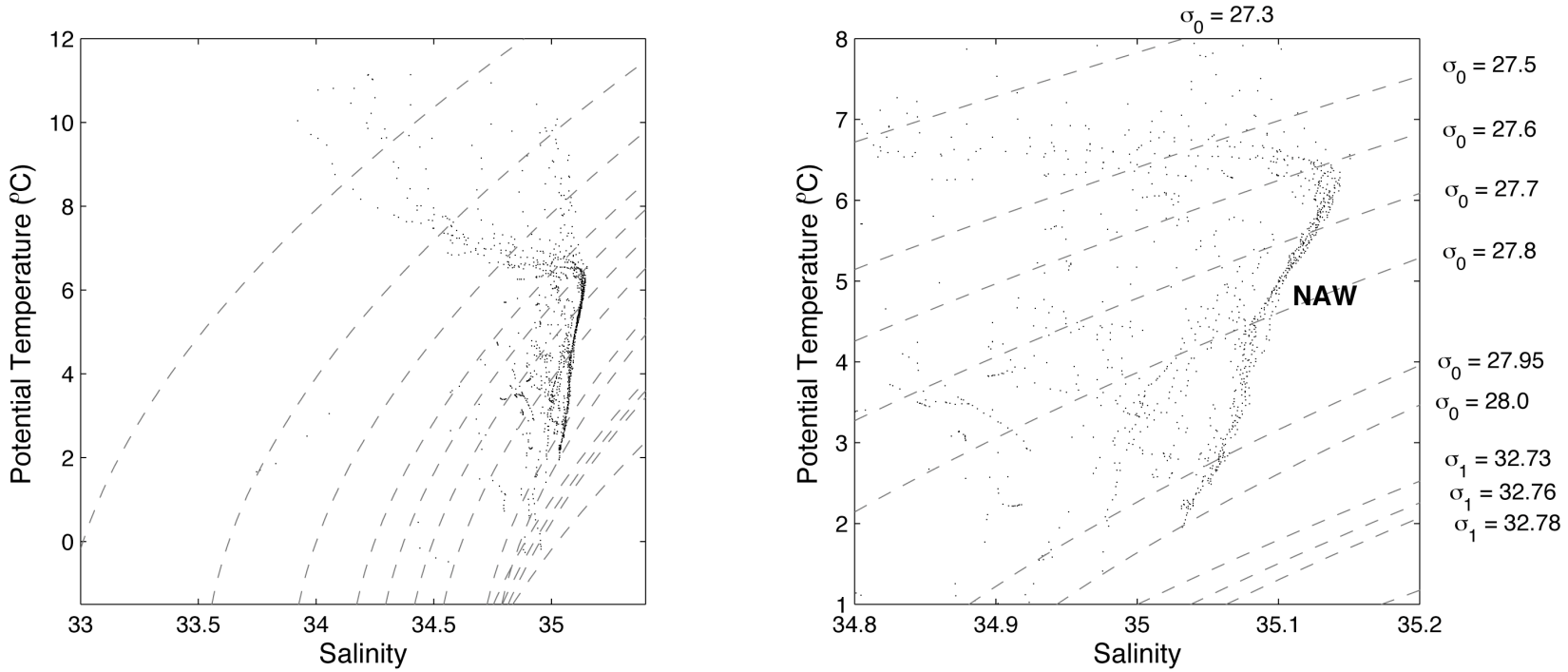

Figure 5.2c: □□S diagram (potential temperature / salinity plot) for the section across the Barent Sea Opening. The isopycnals used to define layers for the flux and inverse calculations are also illustrated. The scale for the panel on the left is the same for all sections to allow inter-comparison, the scale for the panel on the right is chosen to best illustrate the water masses present on this section. Some of the major water masses are marked; **NAW** Norwegian Atlantic Water.

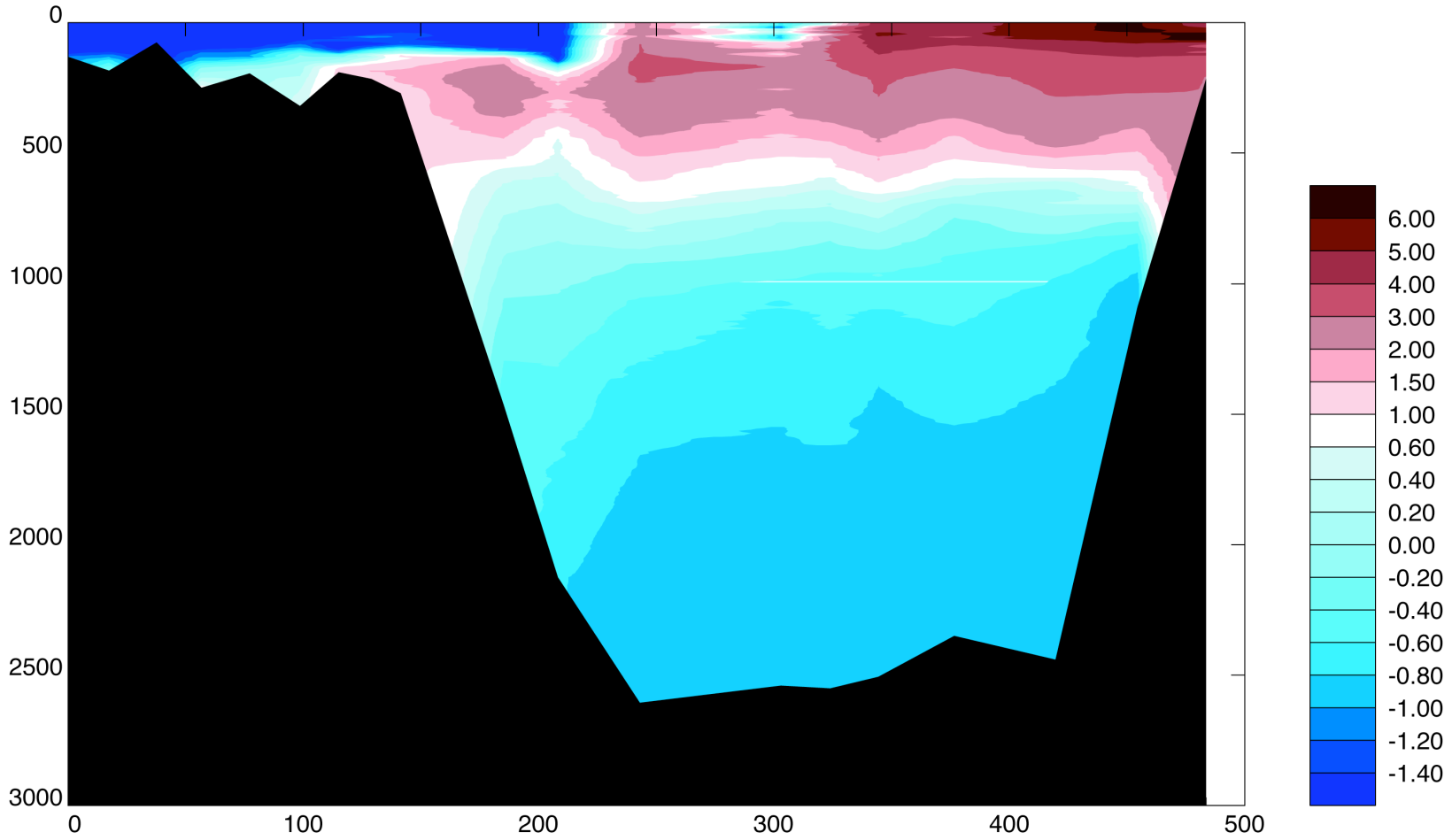

Figure 5.3a: Contoured potential temperature (°C) section across Fram Strait, from Greenland on the left, eastwards to Svalbard on the right. The x and y axes represent distance from the start of the section (km) and pressure (db) respectively. The sharp vertical contours in the temperature field are artefacts of the contouring.

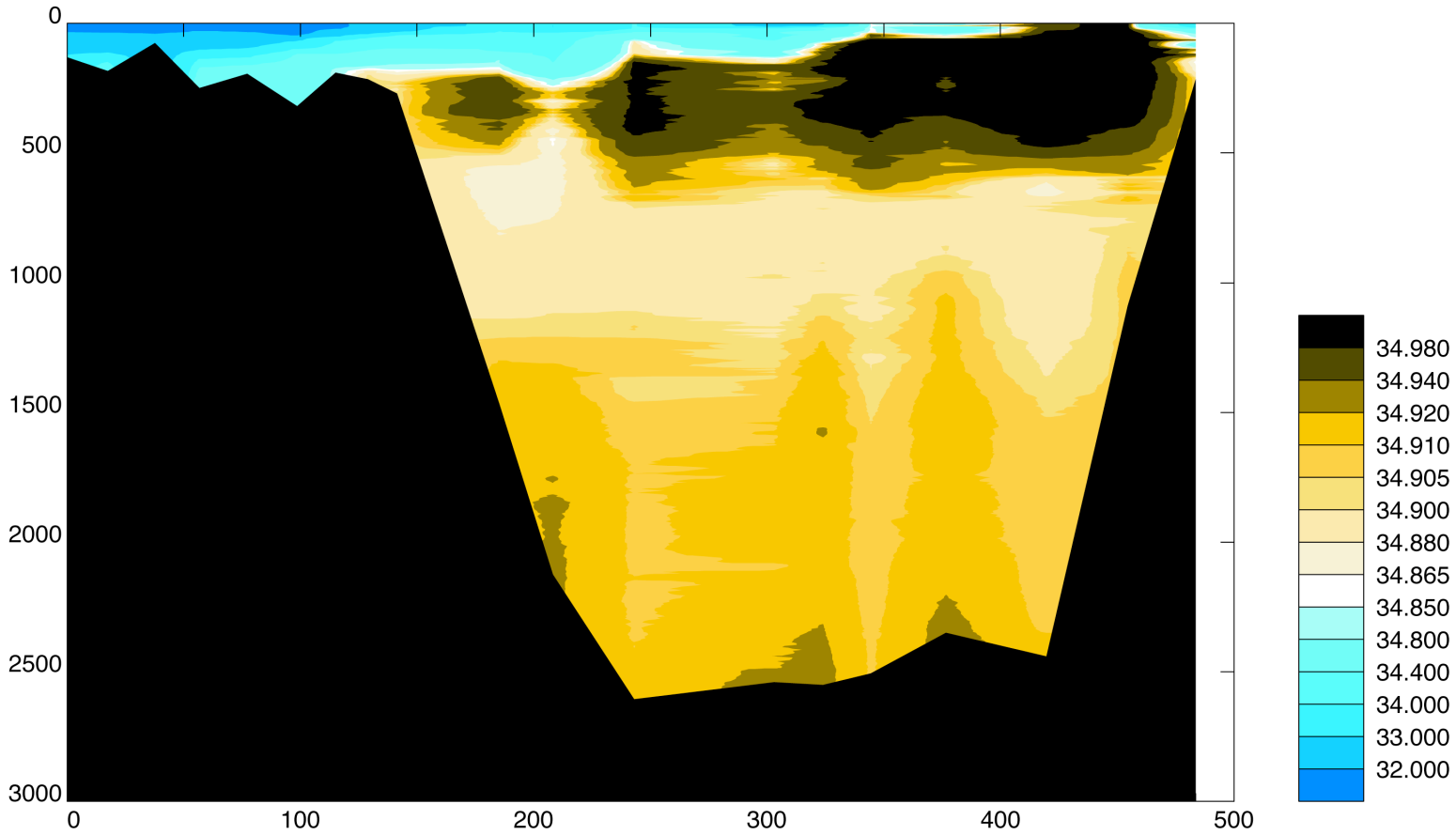

Figure 5.3b: Contoured salinity section across Fram Strait, from Greenland on the left, eastwards to Svalbard on the right. The x and y axes represent distance from the start of the section (km) and pressure (db) respectively. The sharp vertical contours in the salinity field are artefacts of the contouring.

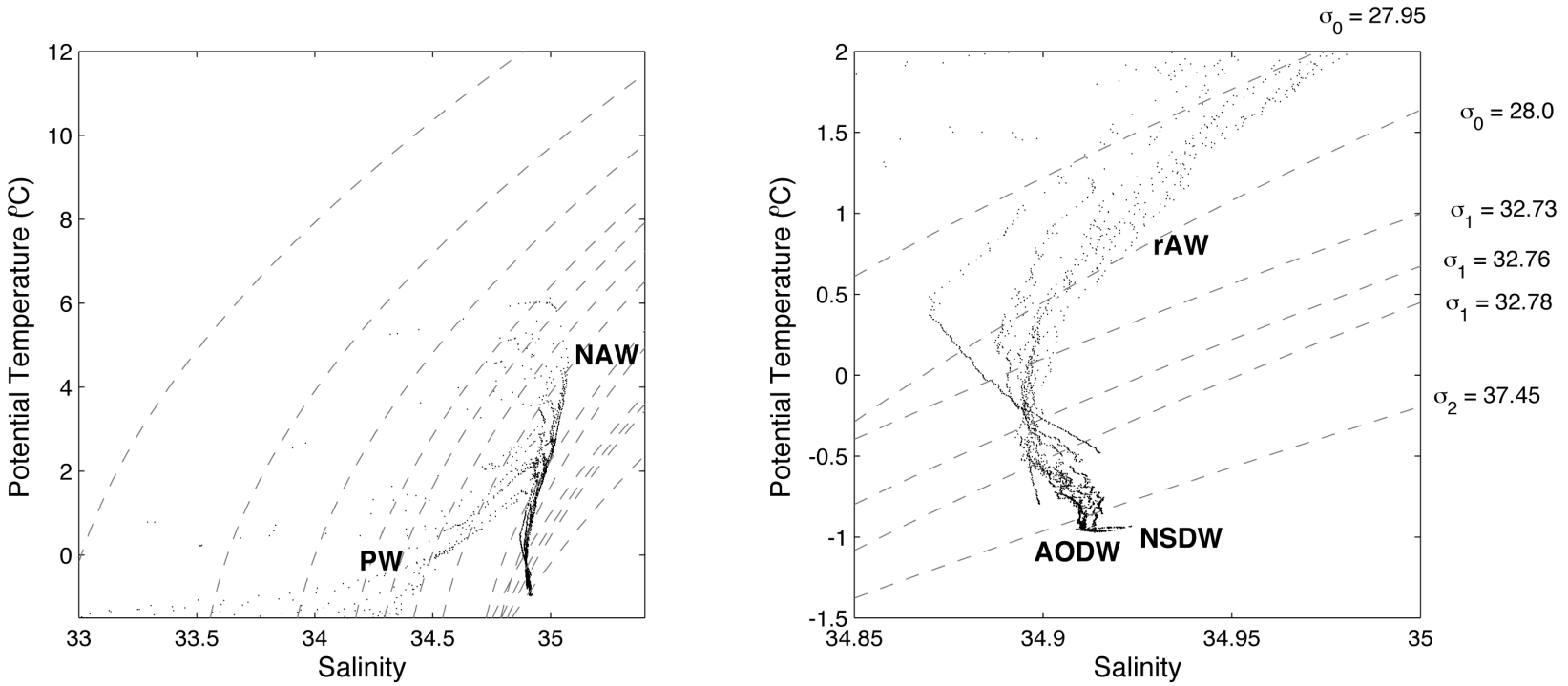

Figure 5.3c: □□S diagram (potential temperature / salinity plot) for the section across Fram Strait. The isopycnals used to define layers for the flux and inverse calculations are also illustrated. The scale for the panel on the left is the same for all sections to allow inter-comparison, the scale for the panel on the right is chosen to best illustrate the water masses present on this section. Some of the major water masses are marked; **PW** Polar Water, **NAW** Norwegian Atlantic Water, **rAW** return Atlantic Water, **NSDW** Norwegian Sea Deep Water, **AODW** Arctic Ocean Deep Water.

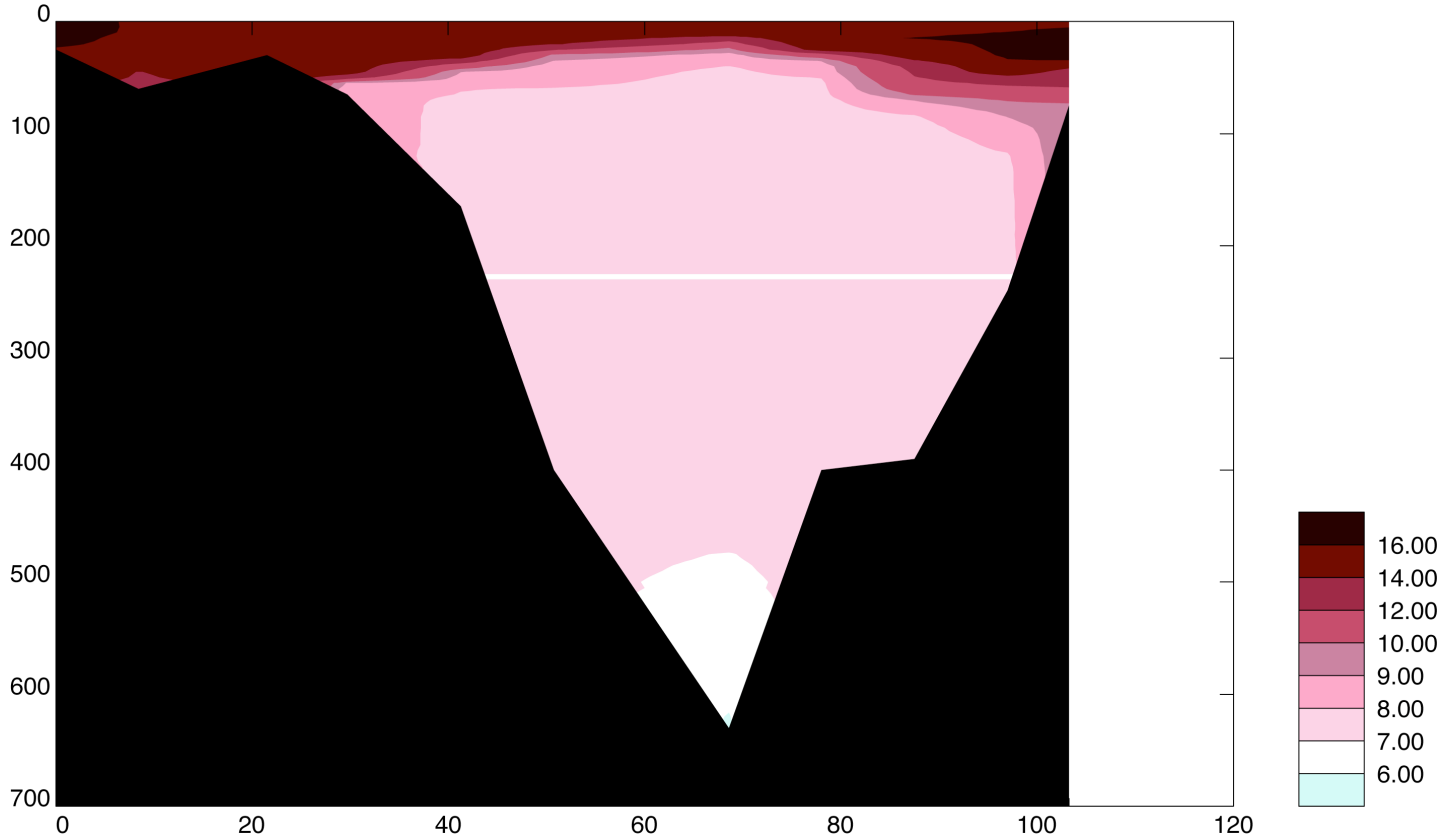

Figure 5.4a: Contoured potential temperature (°C) section across the Skagerrak (the opening to the Baltic Seas), from Denmark on the left, northwards to Svalbard on the right. The x and y axes represent distance from the start of the section (km) and pressure (db) respectively. The sharp vertical contours in the temperature field are artefacts of the contouring.

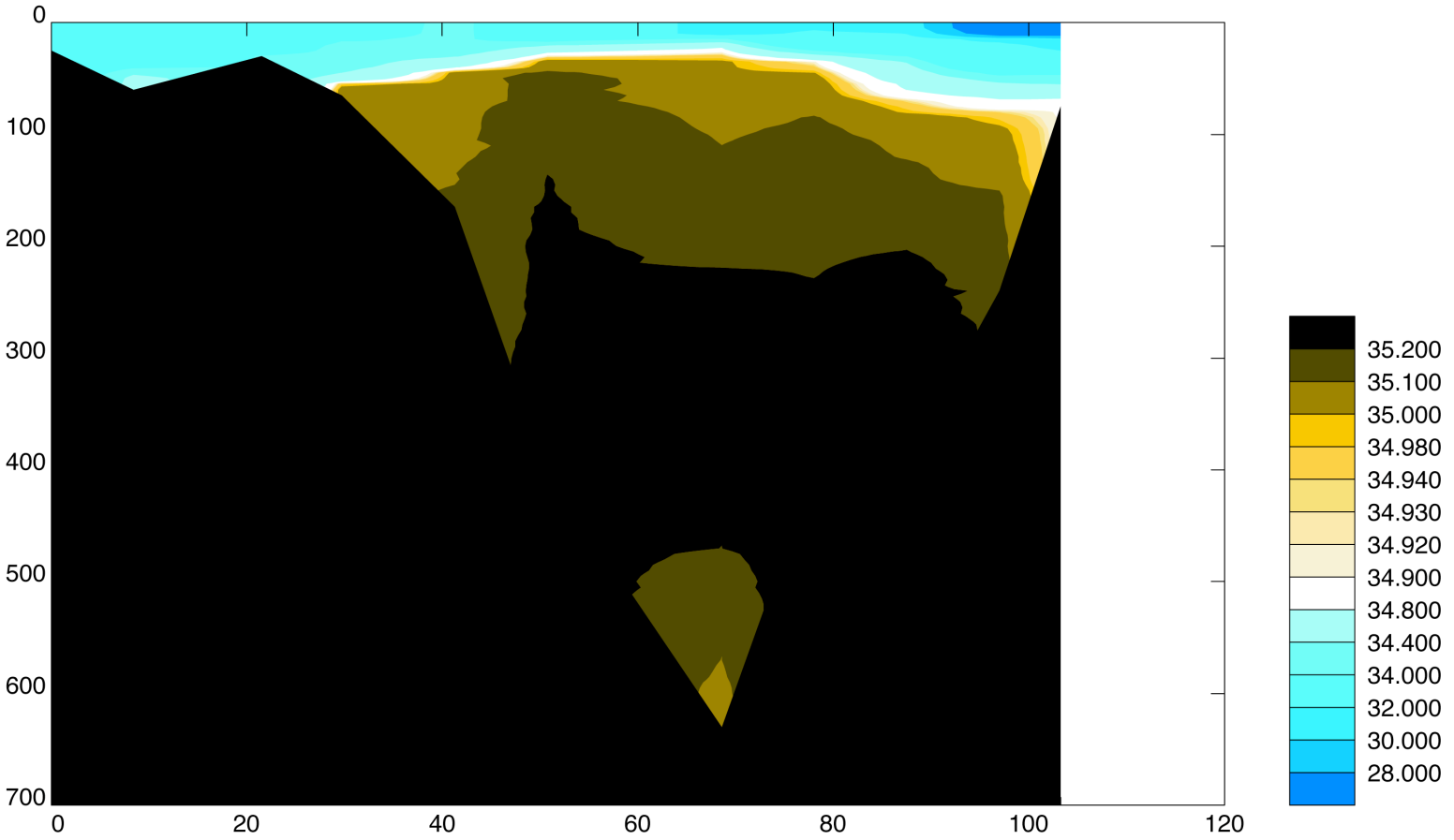

Figure 5.4b: Contoured salinity section across the Skagerrak (the opening to the Baltic Seas), from Denmark on the left, northwards to Svalbard on the right. The x and y axes represent distance from the start of the section (km) and pressure (db) respectively. The sharp vertical contours in the salinity field are artefacts of the contouring.

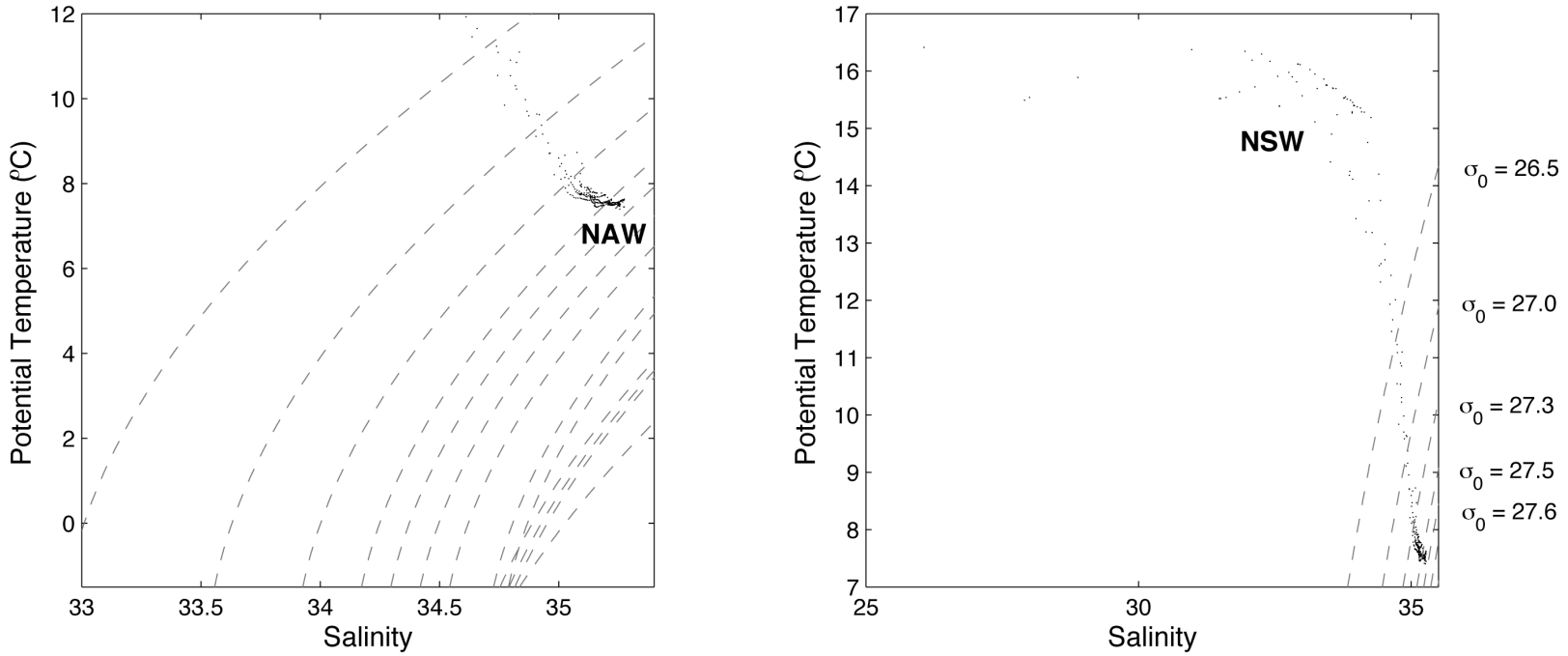

Figure 5.4c: □□S diagram (potential temperature / salinity plot) for the section across the Skagerrak (the opening to the Baltic Seas). The isopycnals used to define layers for the flux and inverse calculations are also illustrated. The scale for the panel on the left is the same for all sections to allow inter-comparison, the scale for the panel on the right is chosen to best illustrate the water masses present on this section. Some of the major water masses are marked; **NAW** Norwegian Atlantic Water, **NSW** Norwegian Shelf Water.

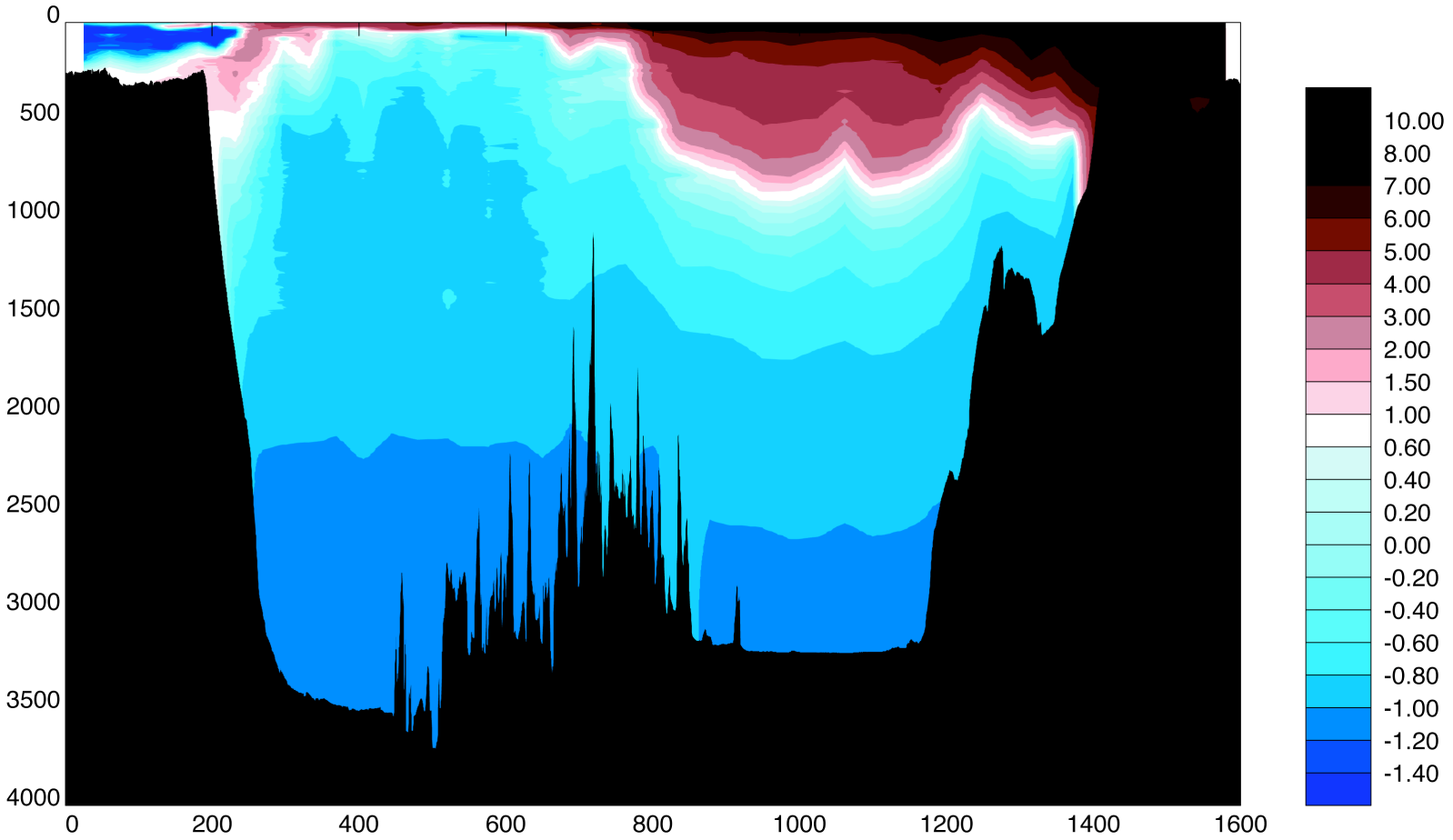

Figure 5.5a: Contoured potential temperature (°C) section for the Greenland to Norway section, from Greenland on the left, eastwards to Norway on the right. The x and y axes represent distance from the start of the section (km) and pressure (db) respectively. The sharp vertical contours in the temperature field are artefacts of the contouring.

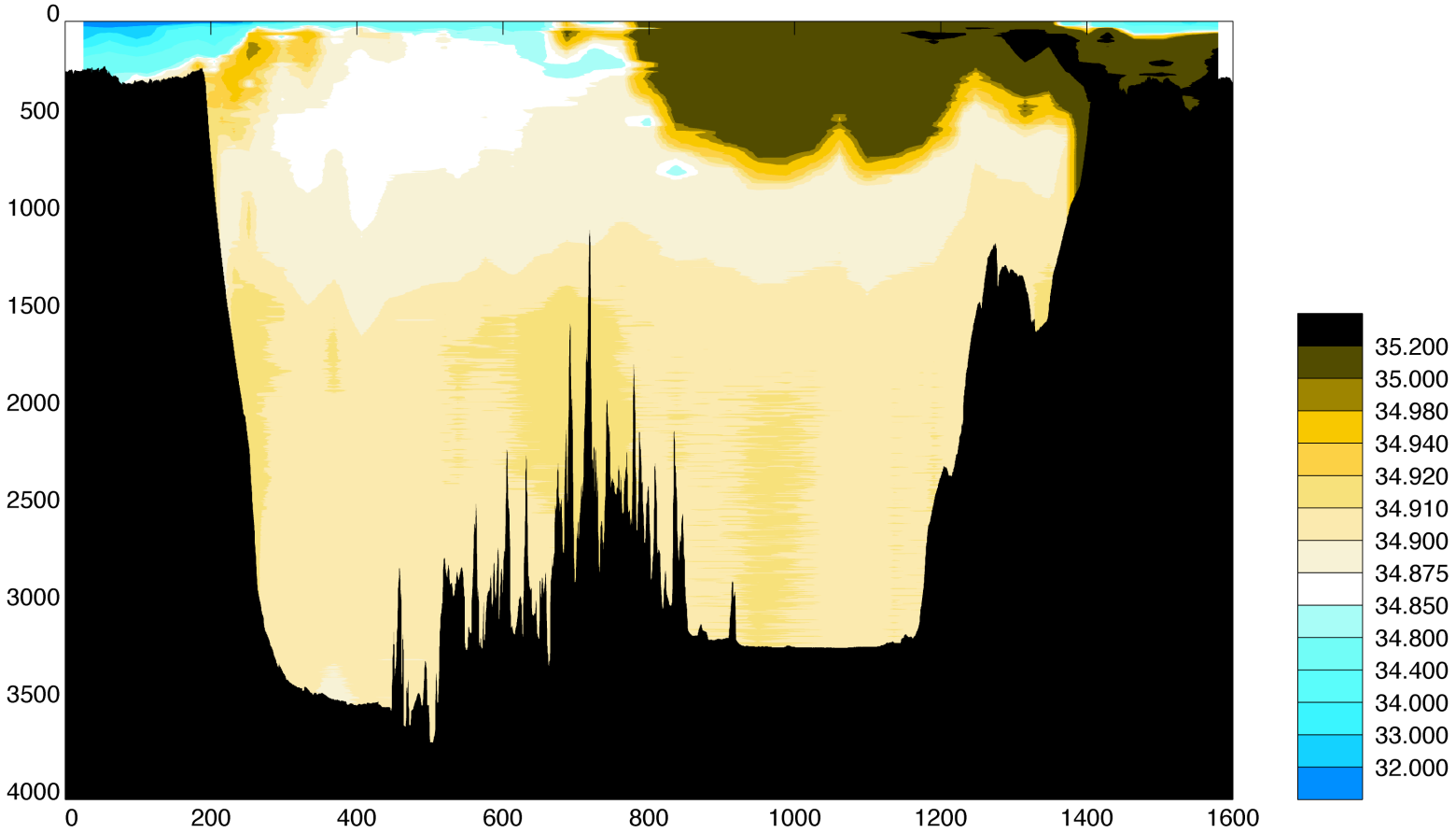

Figure 5.5b: Contoured salinity section for the Greenland to Norway section, from Greenland on the left, eastwards to Norway on the right. The x and y axes represent distance from the start of the section (km) and pressure (db) respectively. The sharp vertical contours in the salinity field are artefacts of the contouring.

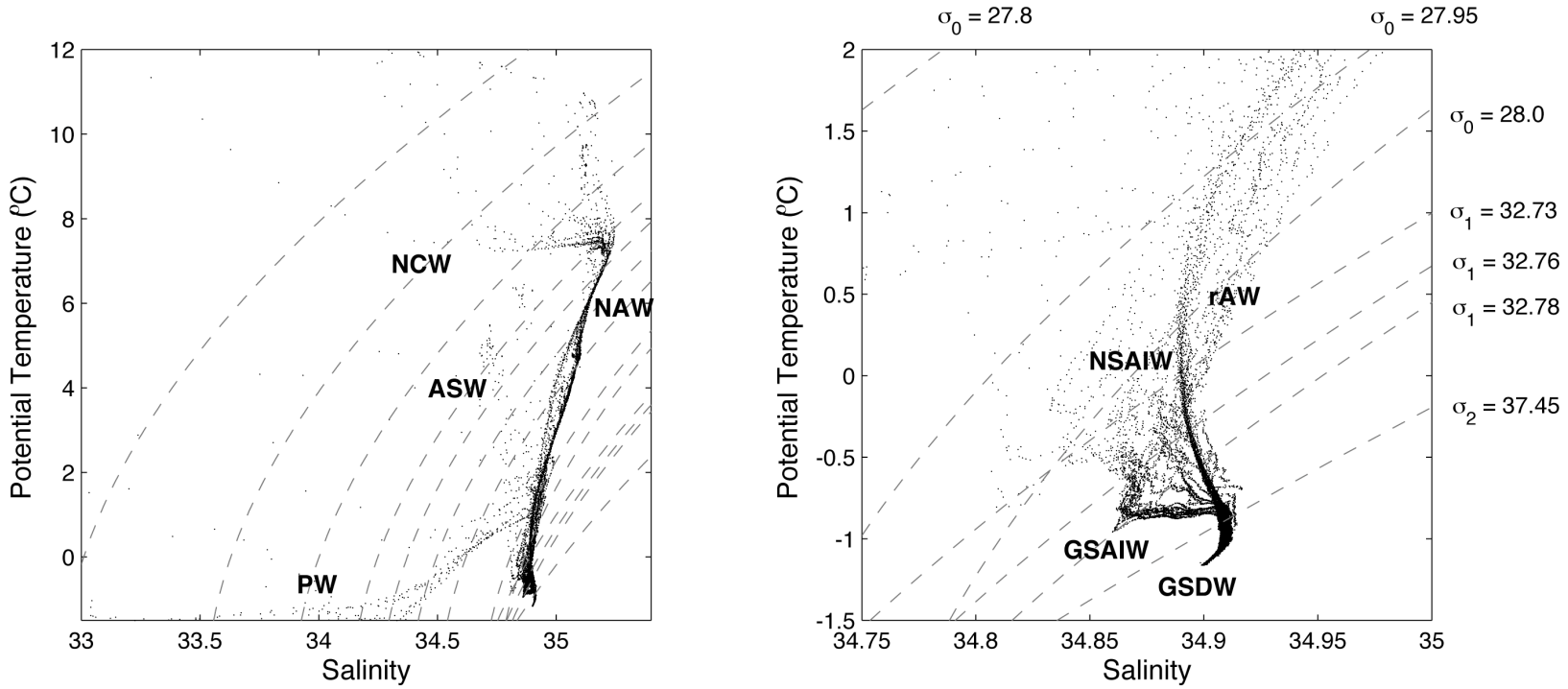

Figure 5.5c: TS diagram (potential temperature / salinity plot) for the section from Greenland to Norway. The isopycnals used to define layers for the flux and inverse calculations are also illustrated. The scale for the panel on the left is the same for all sections to allow inter-comparison, the scale for the panel on the right is chosen to best illustrate the water masses present on this section. Some of the major water masses are marked; **PW** Polar Water, **NAW** Norwegian Atlantic Water, **rAW** return Atlantic Water, **NCW** Norwegian Coastal Water, **ASW** Arctic Surface Water, **GSAIW** Greenland Sea Arctic Intermediate Water, **NSAIW** Norwegian Sea Arctic Intermediate Water.

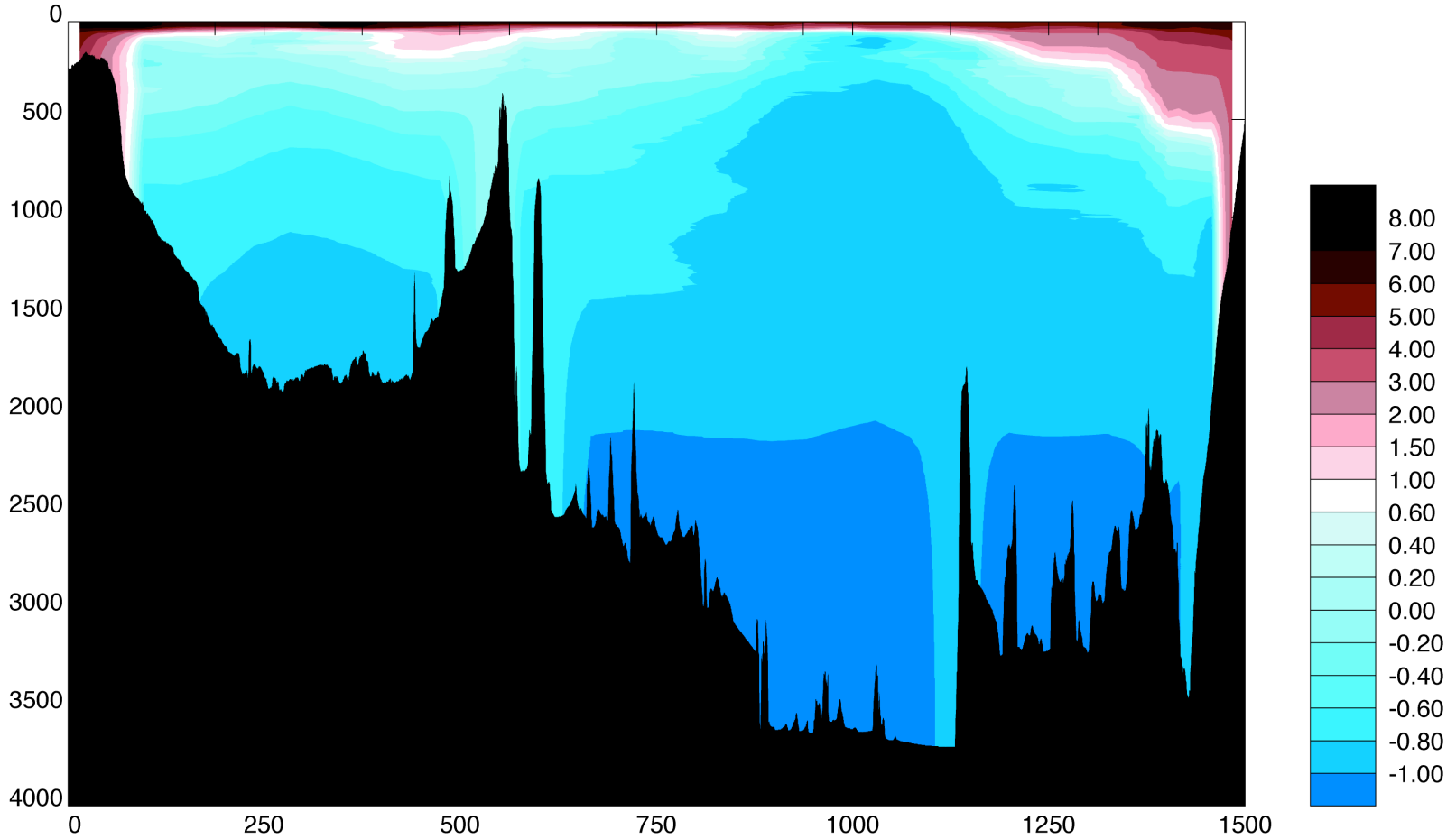

Figure 5.6a: Contoured potential temperature (°C) section for the Iceland to Svalbard section, from Iceland on the left, eastwards to Svalbard on the right. The x and y axes represent distance from the start of the section (km) and pressure (db) respectively. The sharp vertical contours in the temperature field are artefacts of the contouring.

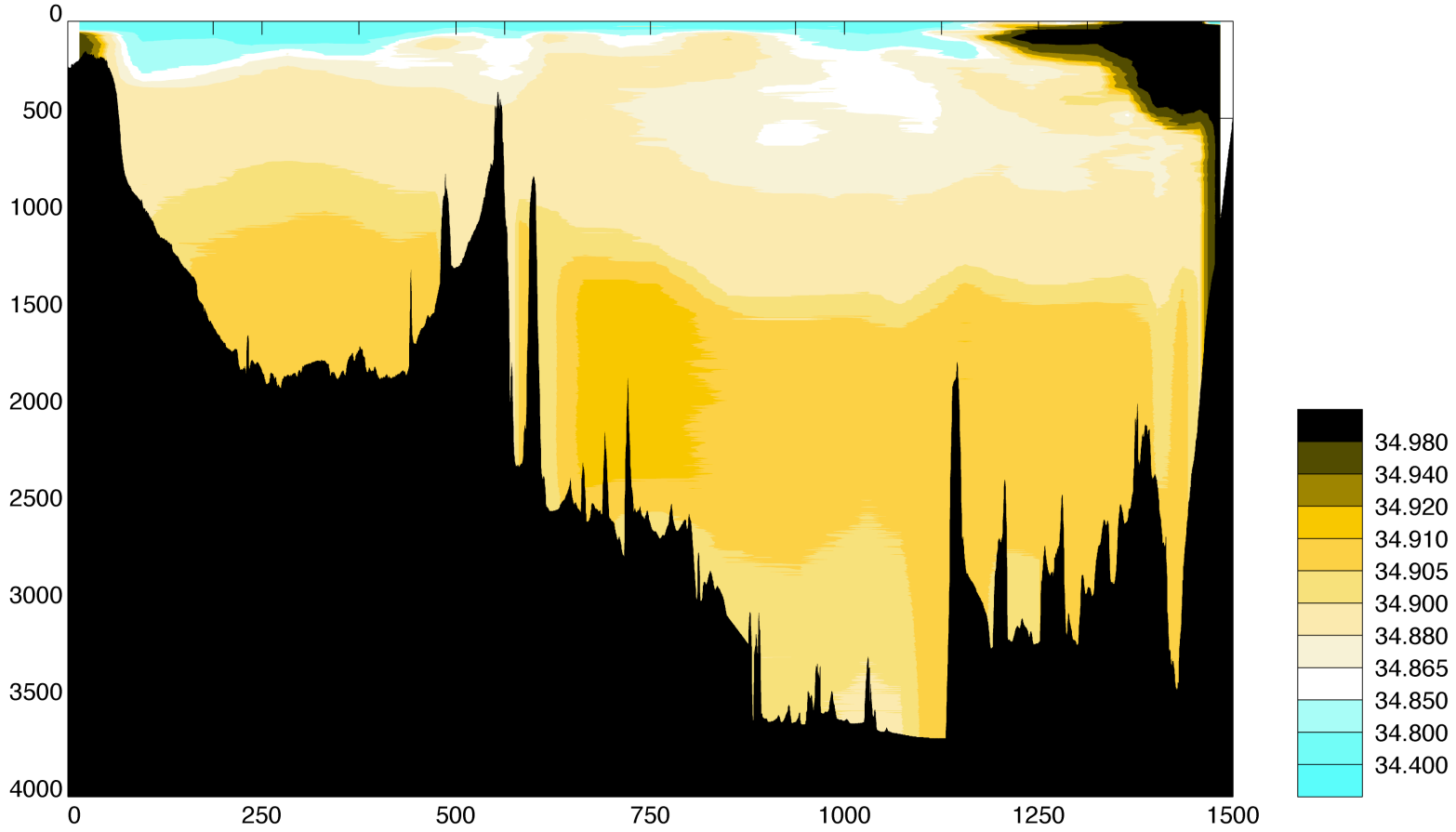

Figure 5.6b: Contoured salinity section for the Iceland to Svalbard section, from Iceland on the left, eastwards to Svalbard on the right. The x and y axes represent distance from the start of the section (km) and pressure (db) respectively. The sharp vertical contours in the salinity field are artefacts of the contouring.

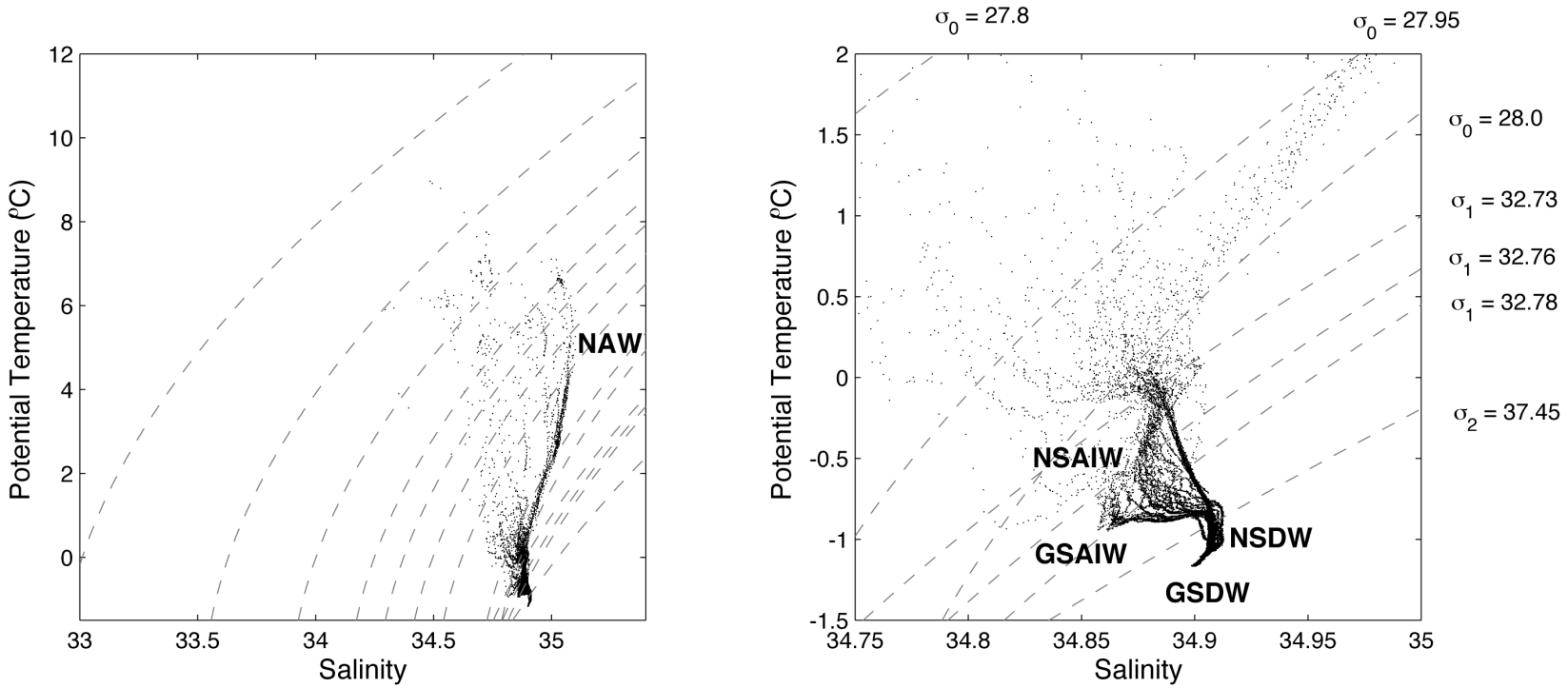

Figure 5.6c: □⊡S diagram (potential temperature / salinity plot) for the Iceland to Svalbard section. The isopycnals used to define layers for the flux and inverse calculations are also illustrated. The scale for the panel on the left is the same for all sections to allow inter-comparison, the scale for the panel on the right is chosen to best illustrate the water masses present on this section. Some of the major water masses are marked; **NAW** Norwegian Atlantic Water, **NSDW** Norwegian Sea Deep Water, **GSDW** Greenland Sea Deep Water, **NSAIW** Norwegian Sea Arctic Intermediate Water, **GSAIW** Greenland Sea Arctic Intermediate Water.

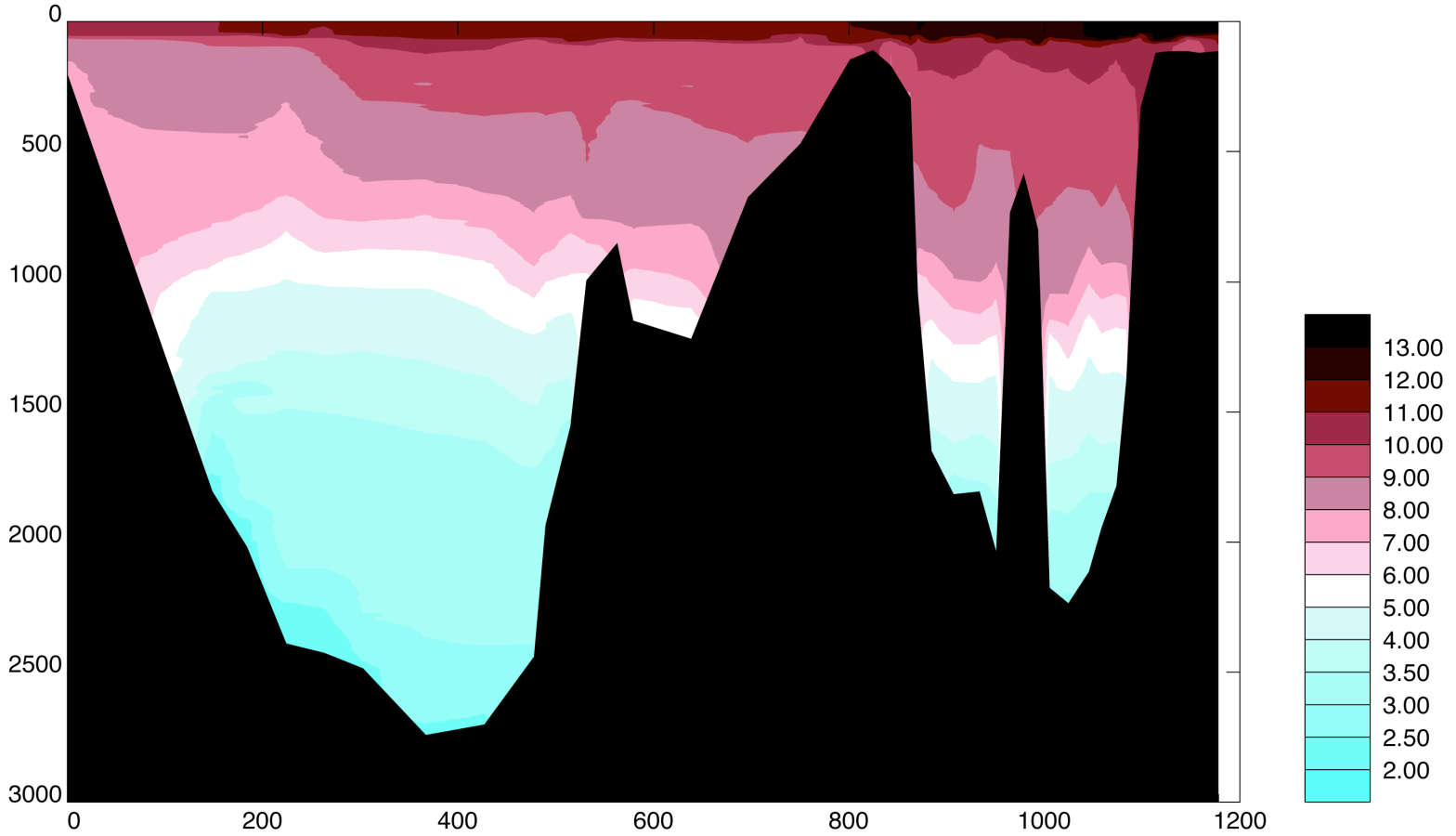

Figure 5.7a: Contoured potential temperature (°C) section for the Iceland to Scotland section, from Iceland on the left, eastwards to Scotland on the right. The x and y axes represent distance from the start of the section (km) and pressure (db) respectively. The sharp vertical contours in the temperature field are artefacts of the contouring.

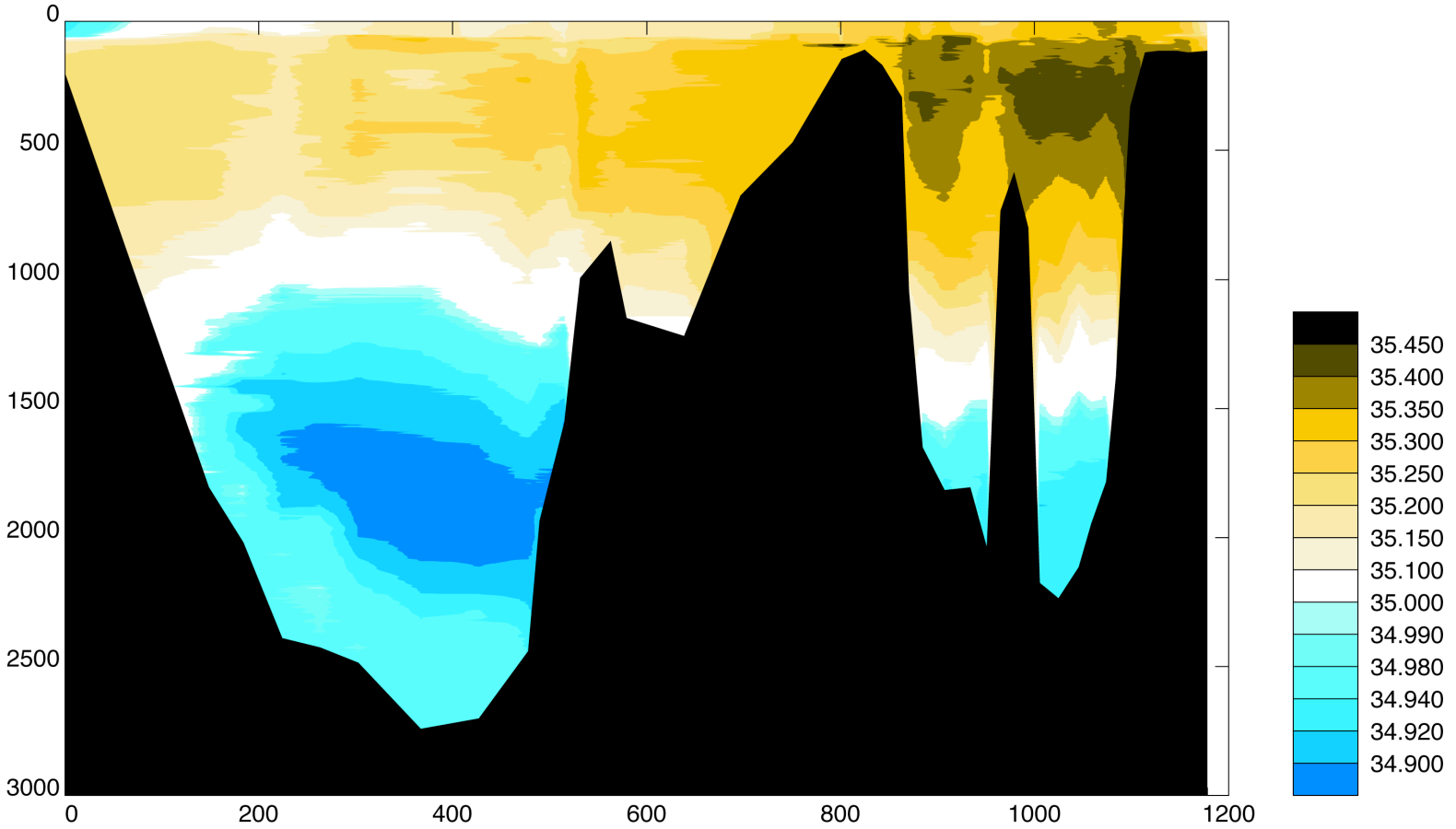

Figure 5.7b: Contoured salinity section for the Iceland to Scotland section, from Iceland on the left, eastwards to Scotland on the right. The x and y axes represent distance from the start of the section (km) and pressure (db) respectively. The sharp vertical contours in the salinity field are artefacts of the contouring.

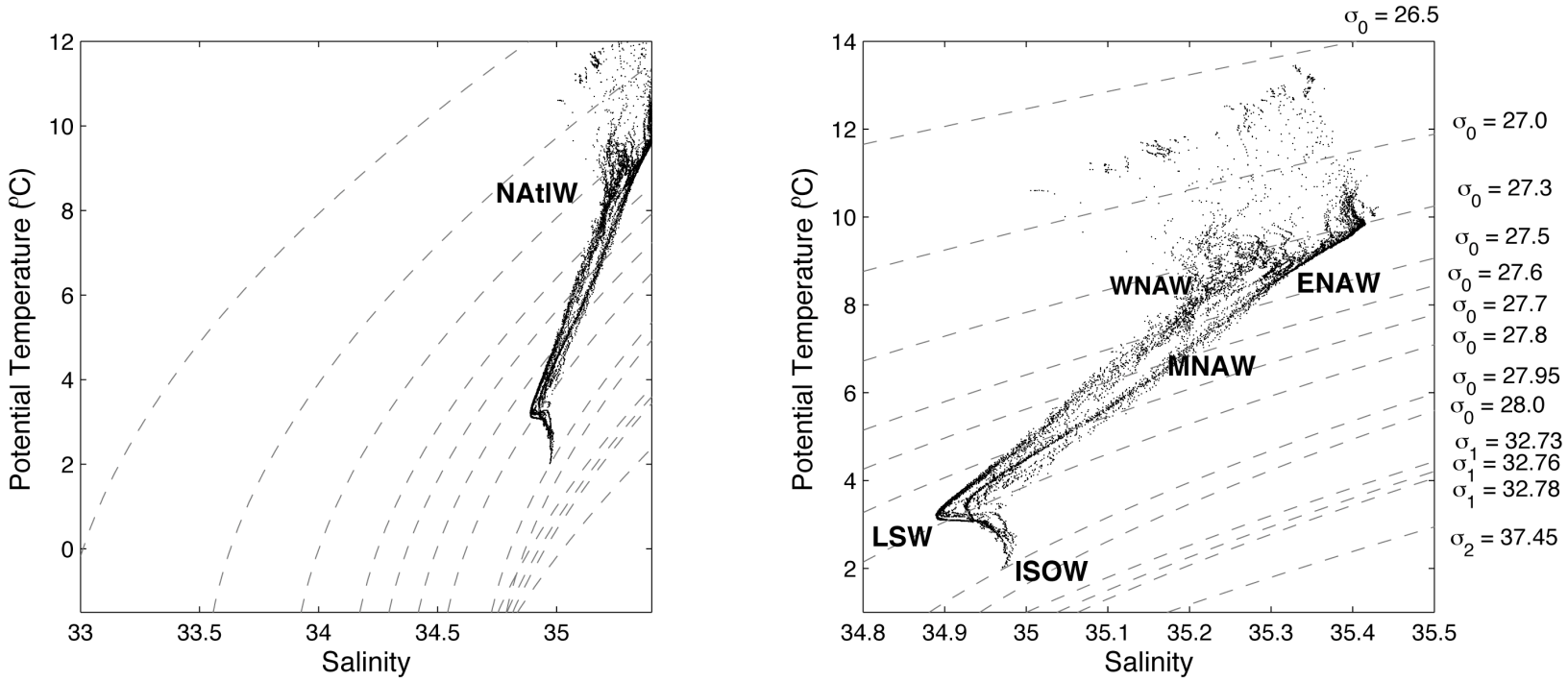

Figure 5.7c: TS diagram (potential temperature / salinity plot) for the Iceland to Scotland section. The isopycnals used to define layers for the flux and inverse calculations are also illustrated. The scale for the panel on the left is the same for all sections to allow inter-comparison, the scale for the panel on the right is chosen to best illustrate the water masses present on this section. Some of the major water masses are marked; **NAtlW** North Atlantic Water, **LSW** Labrador Sea Water, **ISOW** Iceland-Scotland Overflow Water, **ENAW** Eastern North Atlantic Water, **WNAW** Western North Atlantic Water, **MNAW** Modified North Atlantic Water.

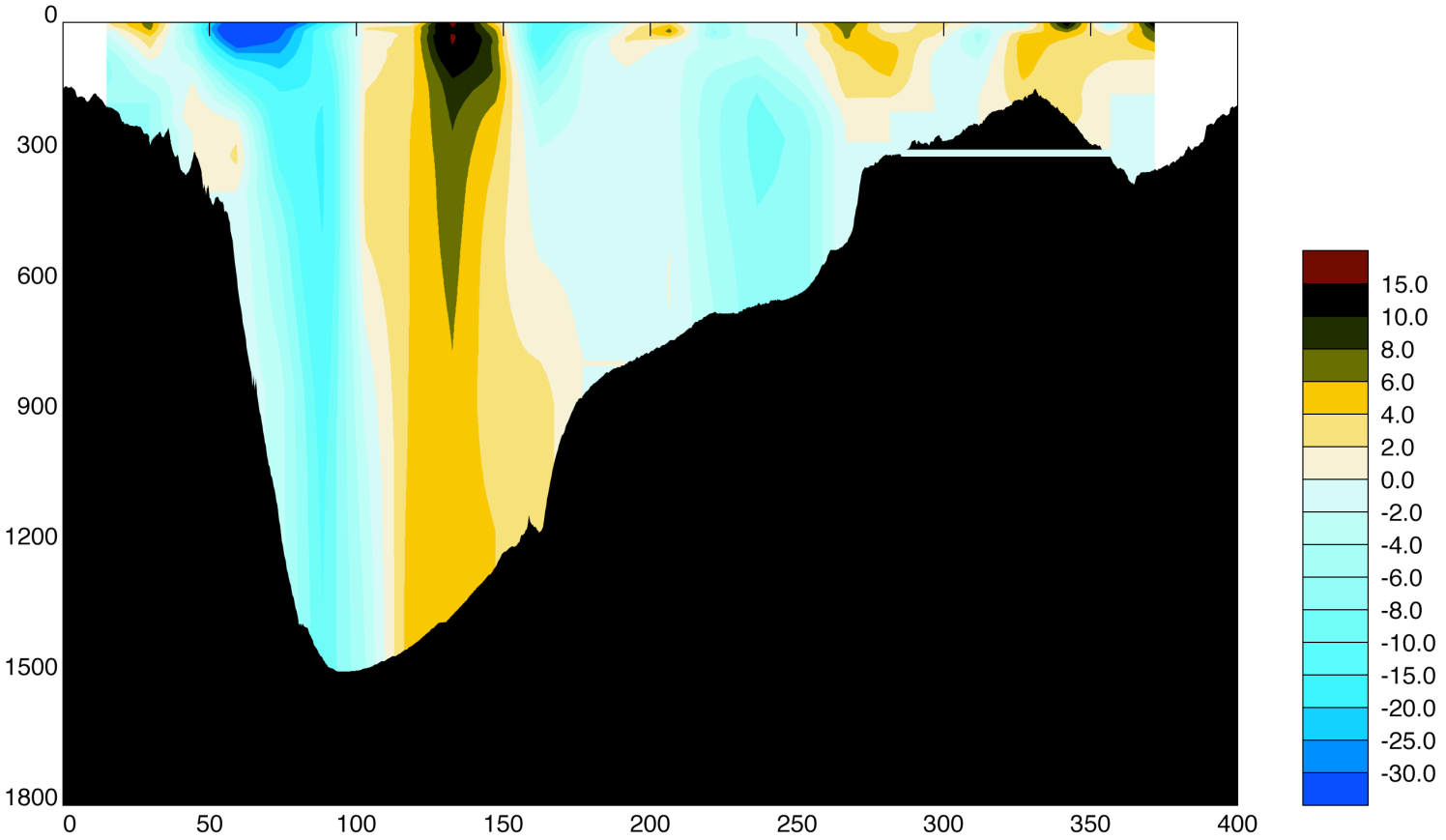

Figure 5.8: Contoured section of the initial velocity field (cm□[1]; LADCP referenced geostrophy) for Denmark Strait, from Greenland on the left, eastwards to Iceland on the right. The x and y axes represent distance from the start of the section (km) and pressure (db) respectively. Positive velocities are directed northwards into the Nordic Seas.

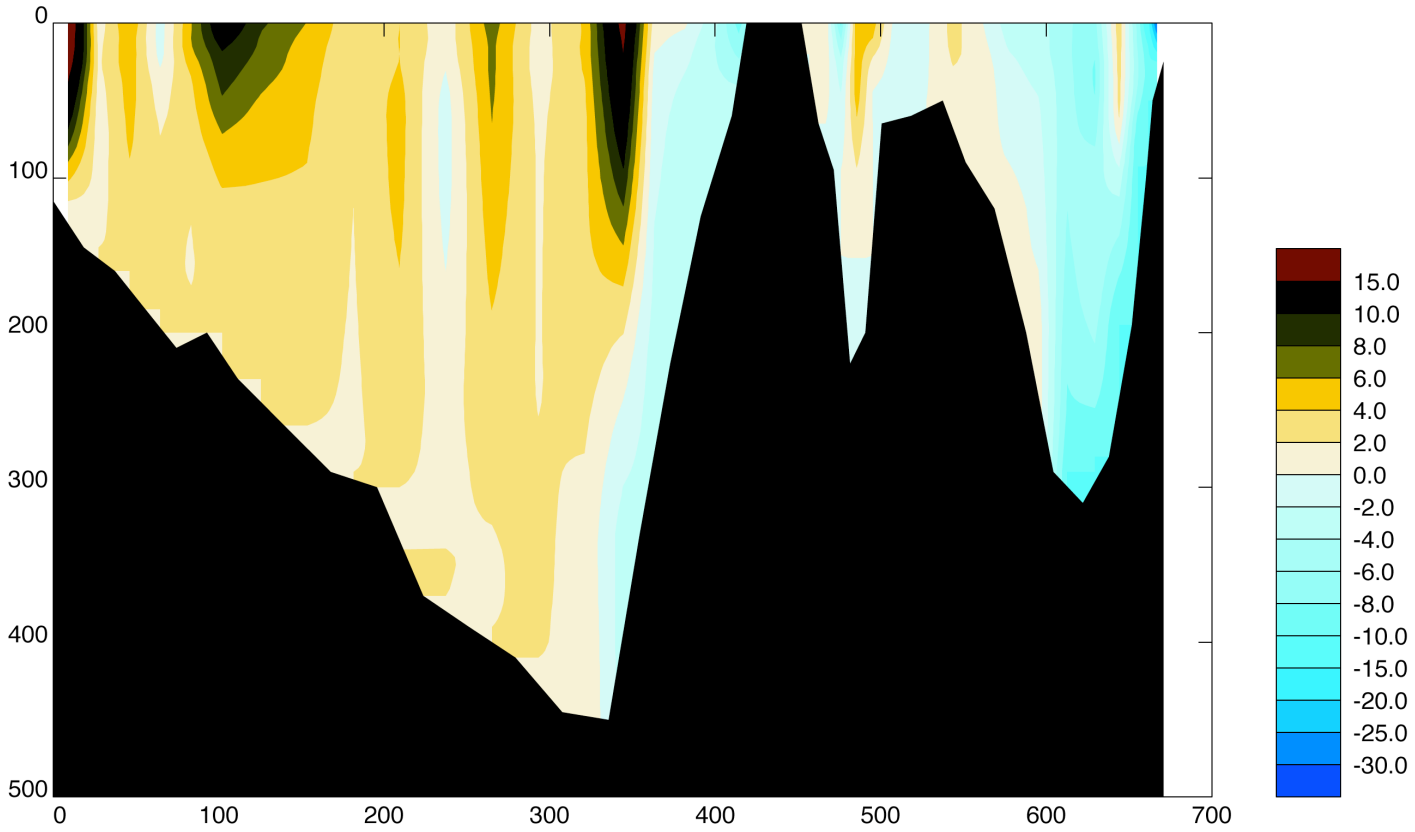

Figure 5.9: Contoured section of the initial velocity field (cm□$^{-1}$; referenced geostrophy) across the Barents Sea Opening, from Norway on the left, northwards to Svalbard on the right. The x and y axes represent distance from the start of the section (km) and pressure (db) respectively. Positive velocities are directed eastwards across the section into the Barents Sea.

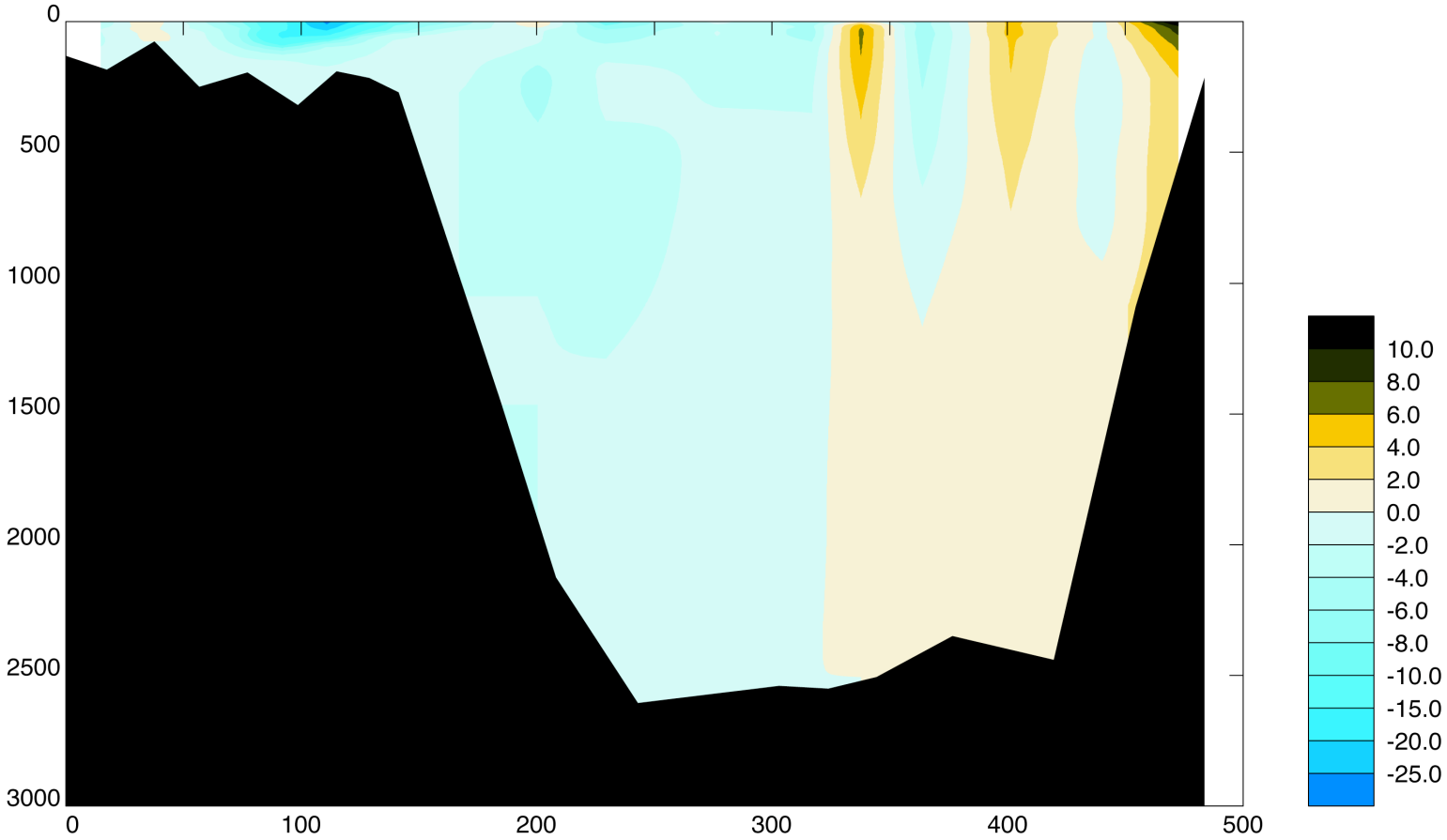

Figure 5.10: Contoured section of the initial velocity field (cm^{-1}; LADCP referenced geostrophy) across Fram Strait, from Greenland on the left, eastwards to Svalbard on the right. The x and y axes represent distance from the start of the section (km) and pressure (db) respectively. Positive velocities are directed northwards into the Arctic Ocean.

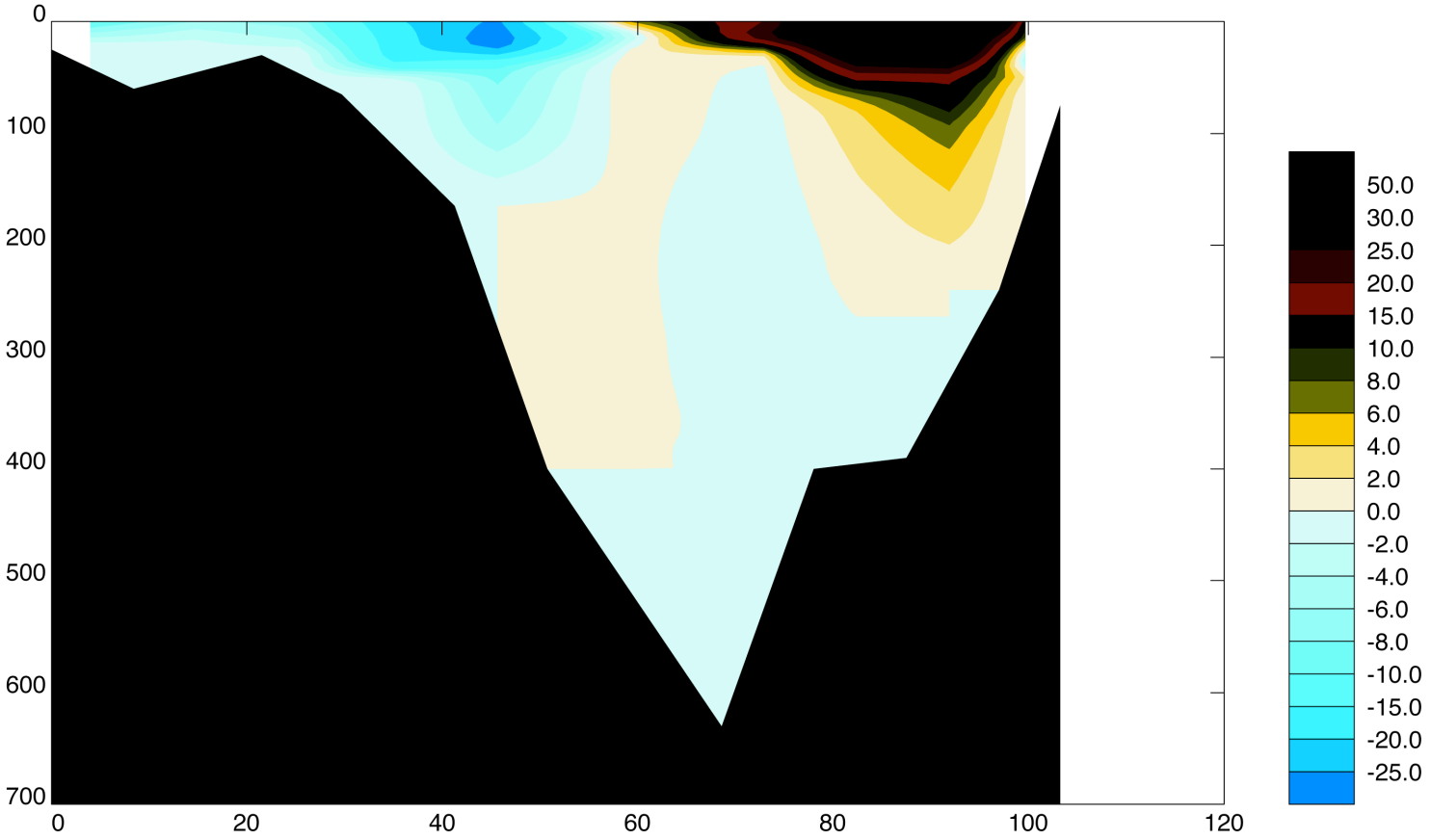

Figure 5.11: Contoured section of the initial velocity field (cm^{-1}; referenced geostrophy) across the Skagerrak (the opening to the Baltic Seas), from Denmark on the left, northwards to Norway on the right. The x and y axes represent distance from the start of the section (km) and pressure (db) respectively. Positive velocities are directed westwards across the section into the Nordic Seas.

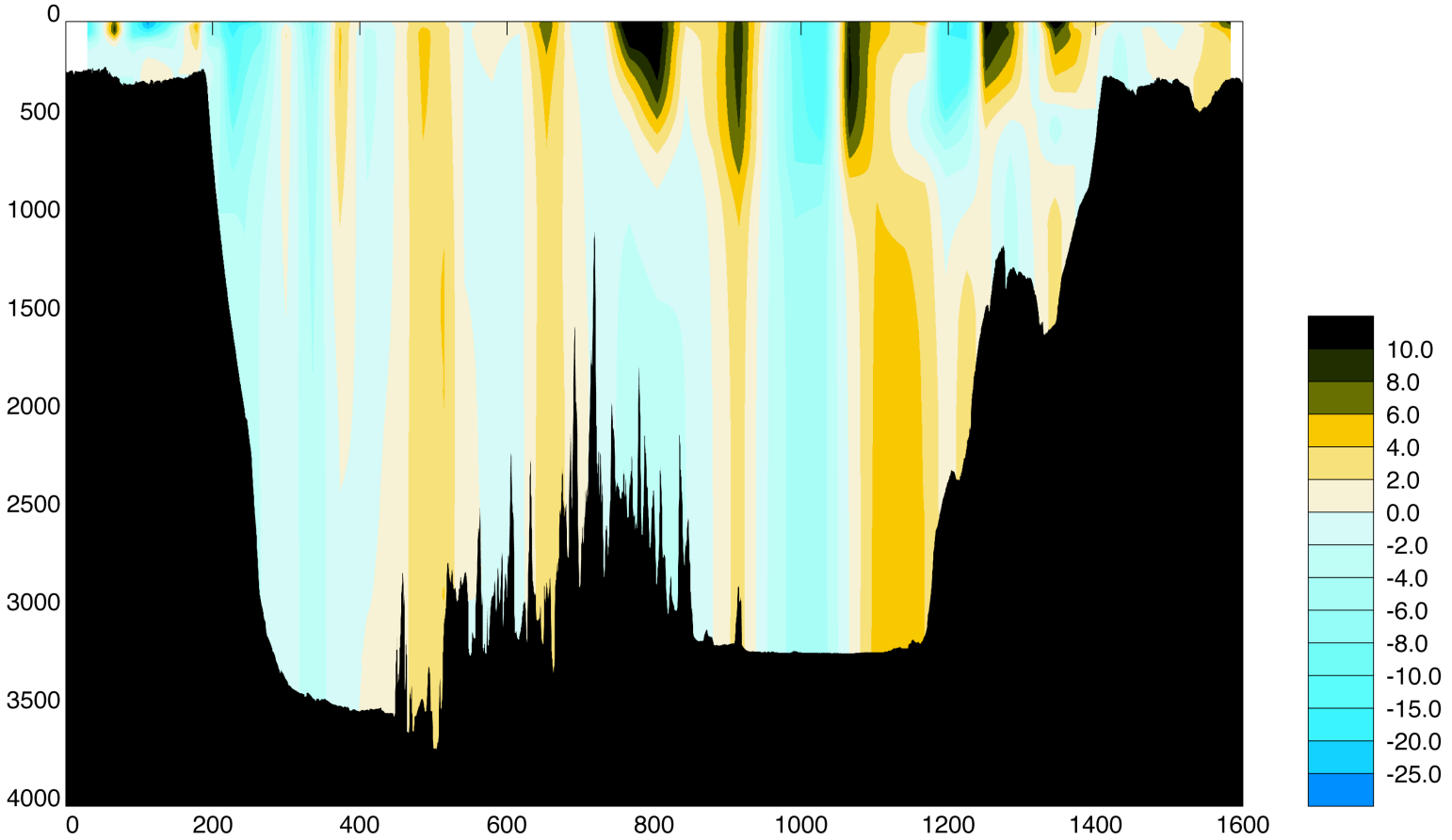

Figure 5.12: Contoured section of the initial velocity field (cm□$^{-1}$; LADCP referenced geostrophy) for the Greenland to Norway section, from Greenland on the left, eastwards to Norway on the right. The x and y axes represent distance from the start of the section (km) and pressure (db) respectively. Positive velocities are directed northeast across the section towards the Arctic.

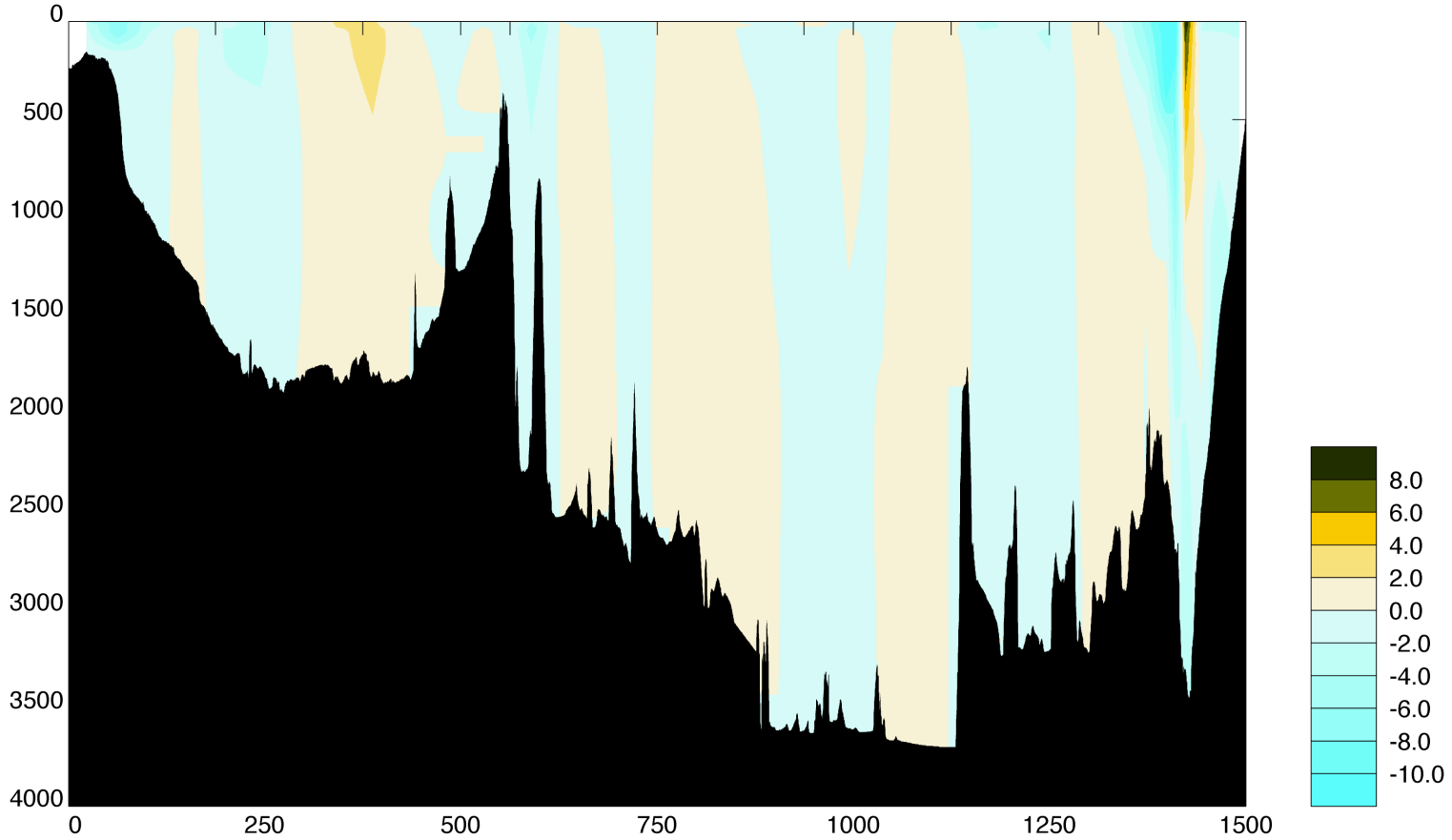

Figure 5.13: Contoured section of the initial velocity field (cm□$^{-1}$; LADCP referenced geostrophy) for the Iceland to Svalbard section, from Iceland on the left, eastwards to Svalbard on the right. The x and y axes represent distance from the start of the section (km) and pressure (db) respectively. Positive velocities are directed northwest across the section.

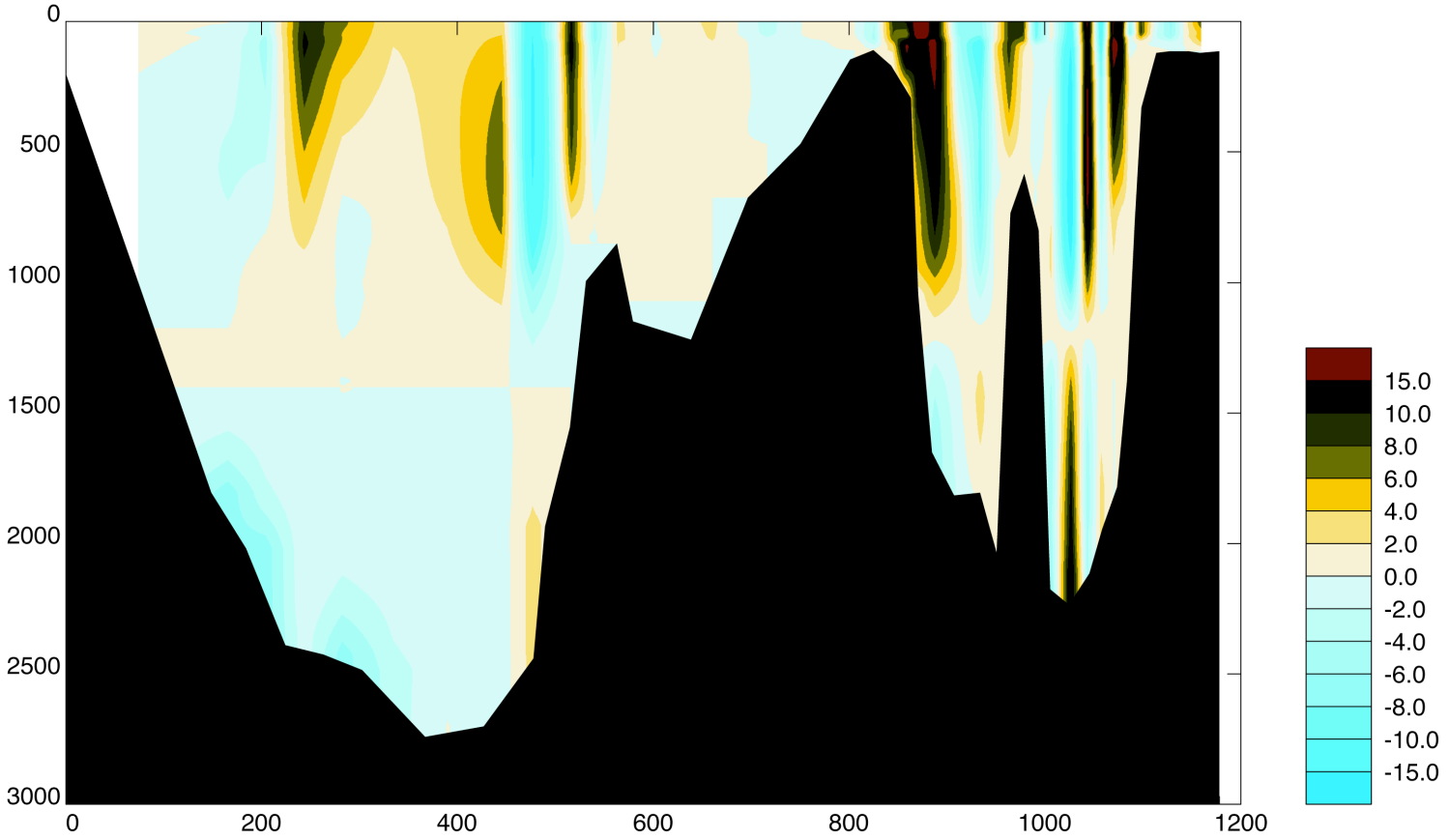

Figure 5.14: Contoured section of the initial velocity field (cm□$^{-1}$; referenced geostrophy) for the Iceland to Scotland section, from Iceland on the left, eastwards to Scotland on the right. The x and y axes represent distance from the start of the section (km) and pressure (db) respectively. Positive velocities are directed east and northeast across the section towards the Nordic Seas,

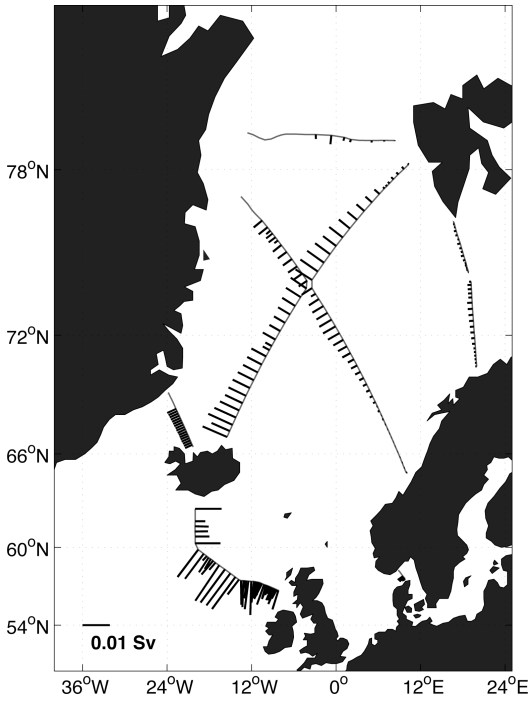

Figure 5.15: Ekman volume transports (Sv) on station pair positions, calculated using the Southampton Oceangraphy Centre (SOC) Ocean-Atmosphere Heat, Momentum and Freshwater Flux Atlas (Josey et al., 1998). The inverse boxes are marked in grey.

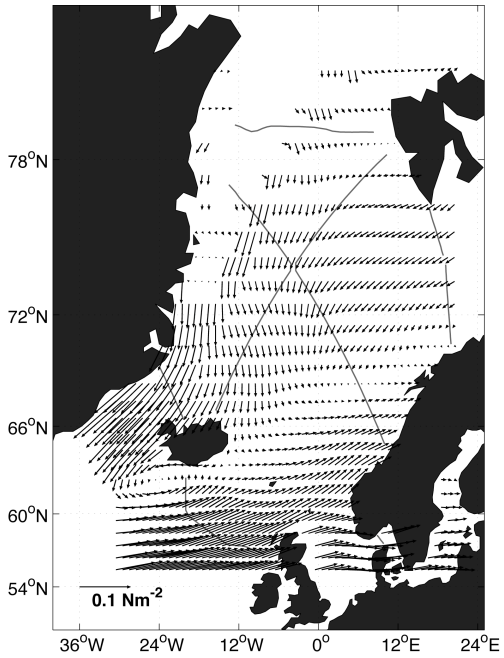

Figure 5.16: Summer mean windstress field (Nm^{-2}) from the Southampton Oceangraphy Centre (SOC) Ocean-Atmosphere Heat, Momentum and Freshwater Flux Atlas (Josey et al., 1998). The inverse boxes are marked in grey.

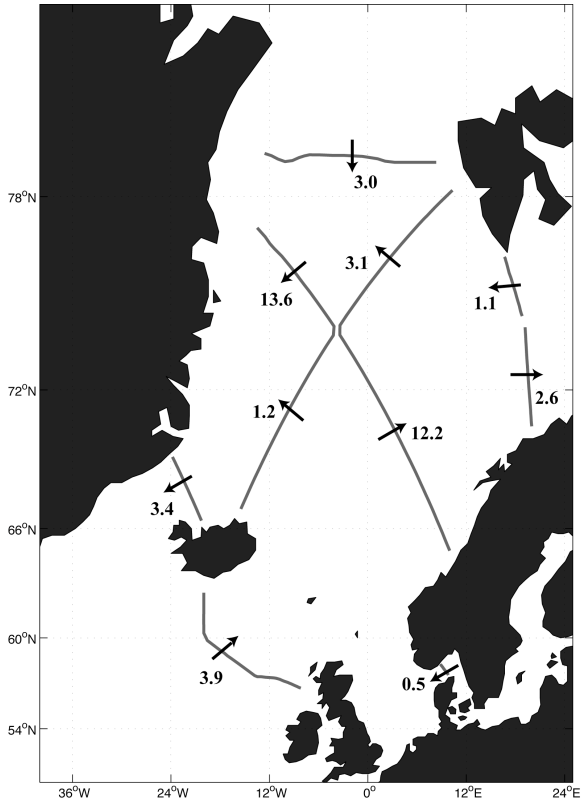

Figure 5.17: Full depth transports (Sv) across each section used to form the inverse boxes calculated from the initial velocity field.

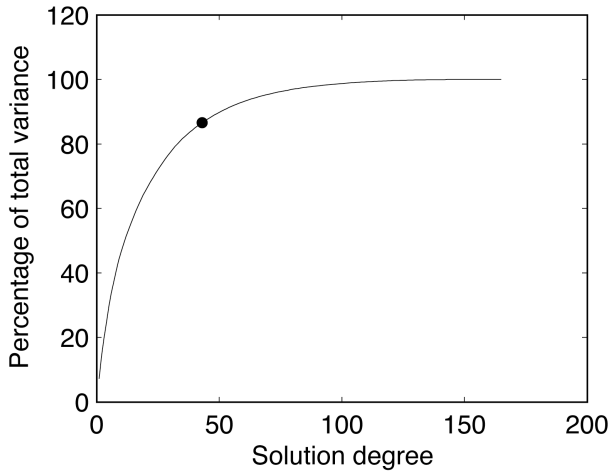

Figure 5.18: Cumulative sum of the percentage of total variance for each solution degree of the standard model. Rank 43 is marked by the black circle.

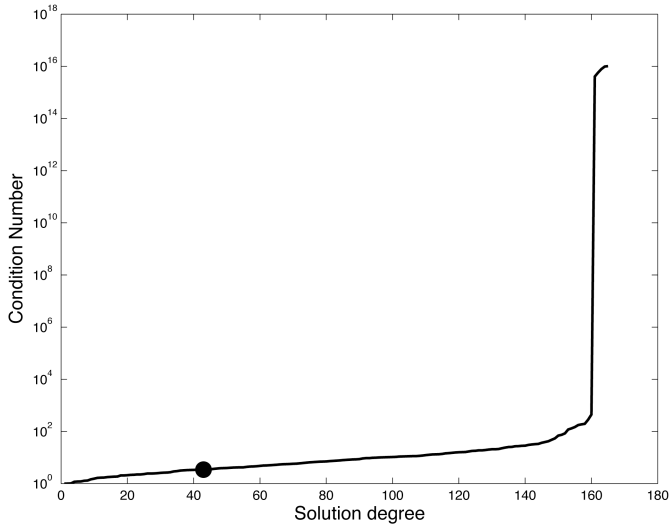

Figure 5.19: Condition number for each solution degree of the standard model. Rank 43 is marked by the black circle.

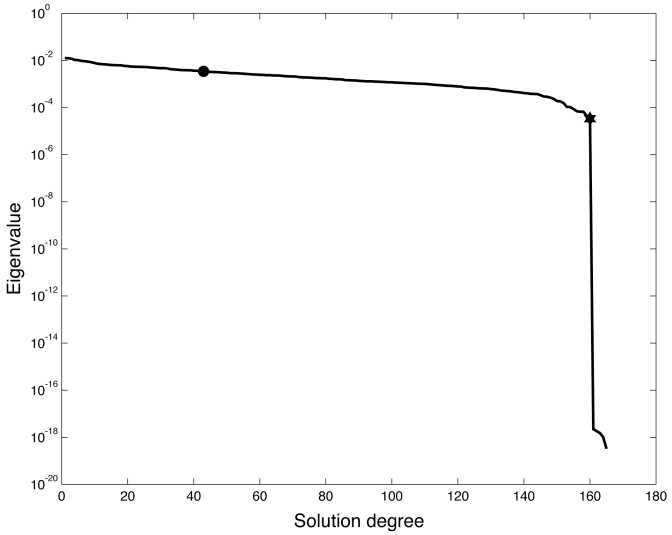

Figure 5.20: Eigenvalues for each solution degree of the standard model. The eigenvalue for the standard solution, rank 43, is marked by a black circle. The eigenvalue just prior to a sudden decrease in size, rank 160, is marked by a black star.

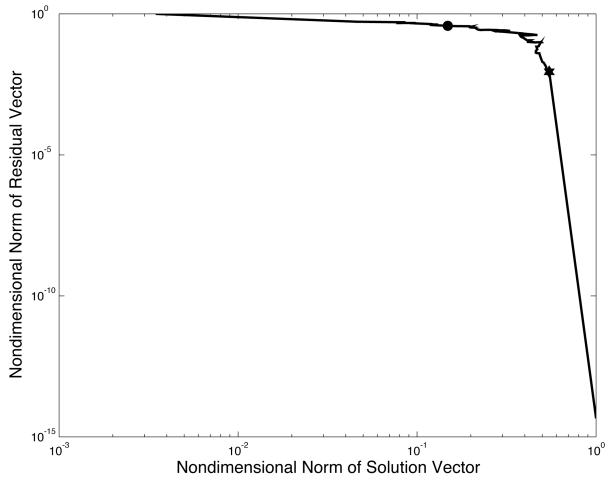

Figure 5.21: Nondimensional norm of residual versus nondimensional norm of solution. The standard solution, rank 43, is marked by a black circle. The point just prior to where solution magnitude increases rapidly with little or no reduction in residual magnitude, rank 159, is marked by a black star.

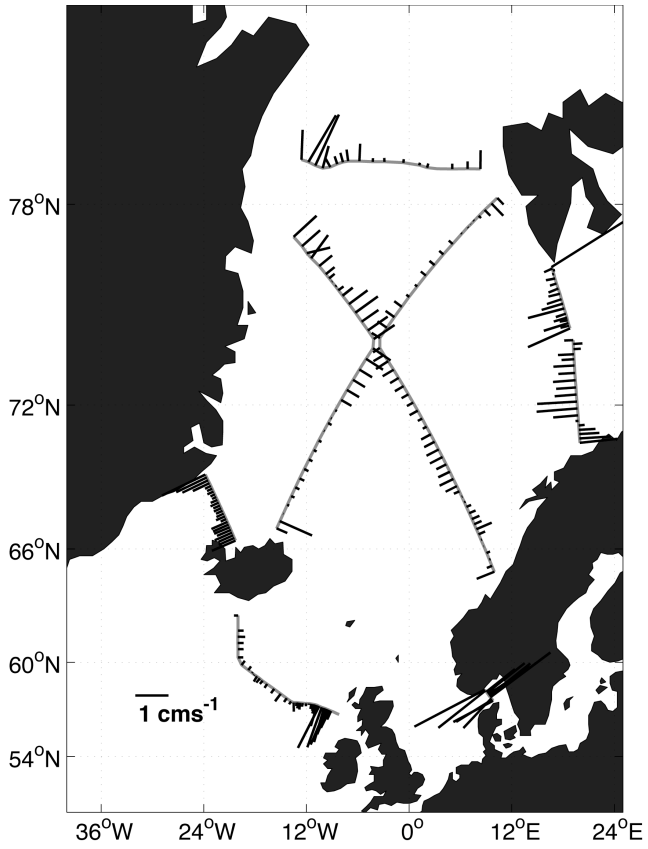

Figure 5.22: Reference velocities (cms^{-1}) from the standard solution (rank 43 of the standard model) for each station pair. The inverse boxes are marked in grey.

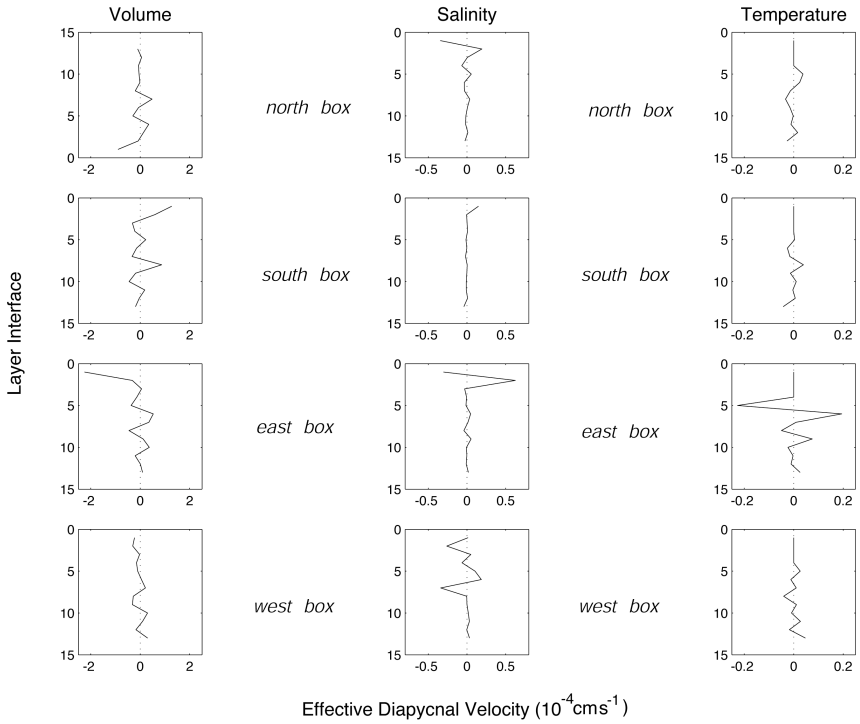

Figure 5.23: Effective diapycnal velocities (x10^{-4}cms^{-1}) from the standard solution (rank 43 of the standard model) for volume and salinity (layer interfaces 1 to 13) and temperature (layer interfaces 6 to 13), for the *north*, *south*, *east* and *west* boxes. Note the different horizontal scales for velocity in each column, i.e. for volume, salinity and temperature. Positive velocities represent an upward flux, towards the surface.

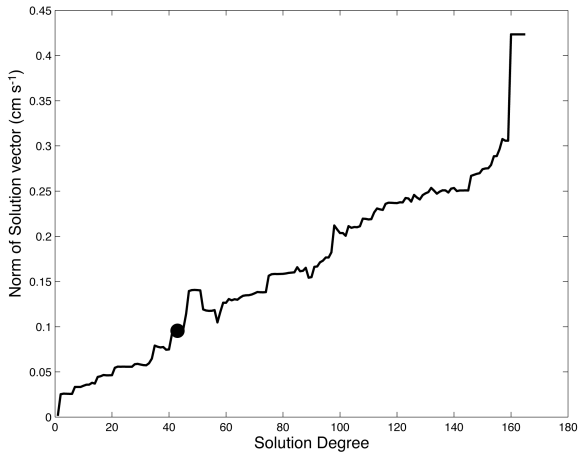

Figure 5.24: Norm of solution vector (cms^{-1}) for each solution degree of the standard model. Rank 43 is marked by the black circle.

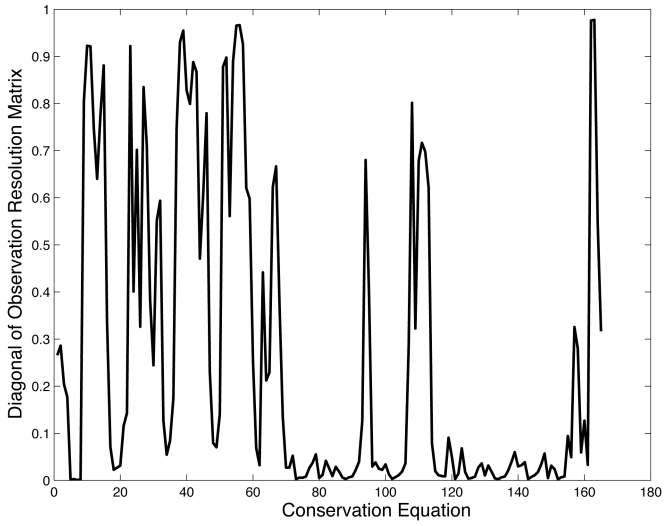

Figure 5.25: Diagonal of the observation resolution matrix for the standard solution (rank 43 of the standard model). The details of the conservation equations are described fully in Table 5.8.

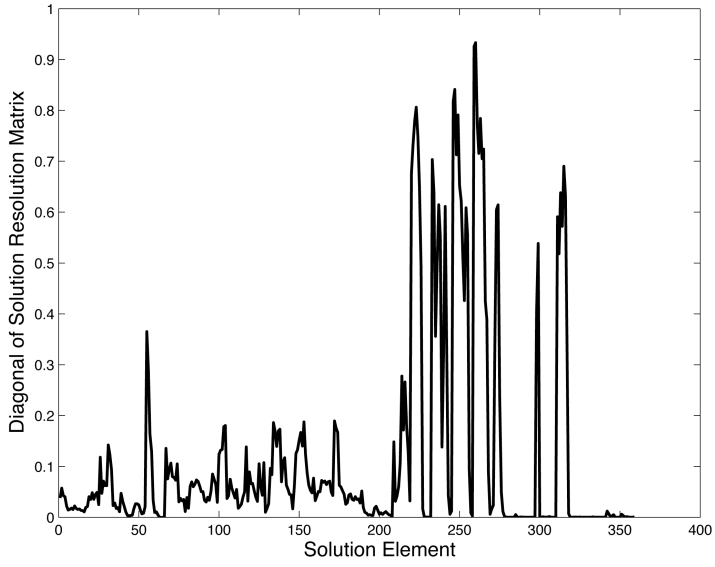

Figure 5.26: Diagonal of the solution resolution matrix for the standard solution (rank 43 of the standard model). Solution elements between 1 and 224 refer to the reference velocities and the locations are described in Table 3.1. Solution elements between 225 and 364 refer to the diapycnal velocities (225:237, 238:250, 251:263 and 264:276 represent volume fluxes for layer interfaces 1:13 in the north, south, east and west boxes respectively; 277:289, 290:302, 303:315 and 316:328 represent salinity fluxes for layer interfaces 1:13 in the north, south, east and west boxes respectively; 329:337, 338:346, 347:355 and 356:364 represent temperature fluxes for layer interfaces 6:13 in the north, south, east and west boxes respectively).

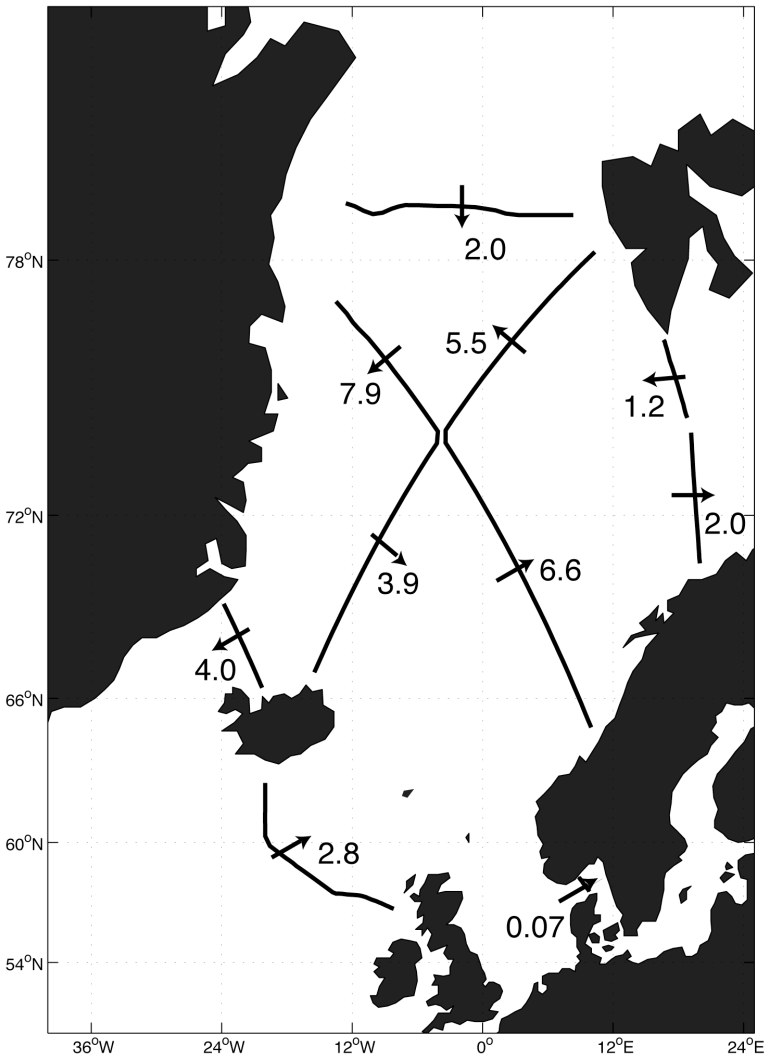

Figure 5.27: Full depth volume transports (Sv) across each section, calculated from the standard solution and further adjusted for zero net volume flux in each box.

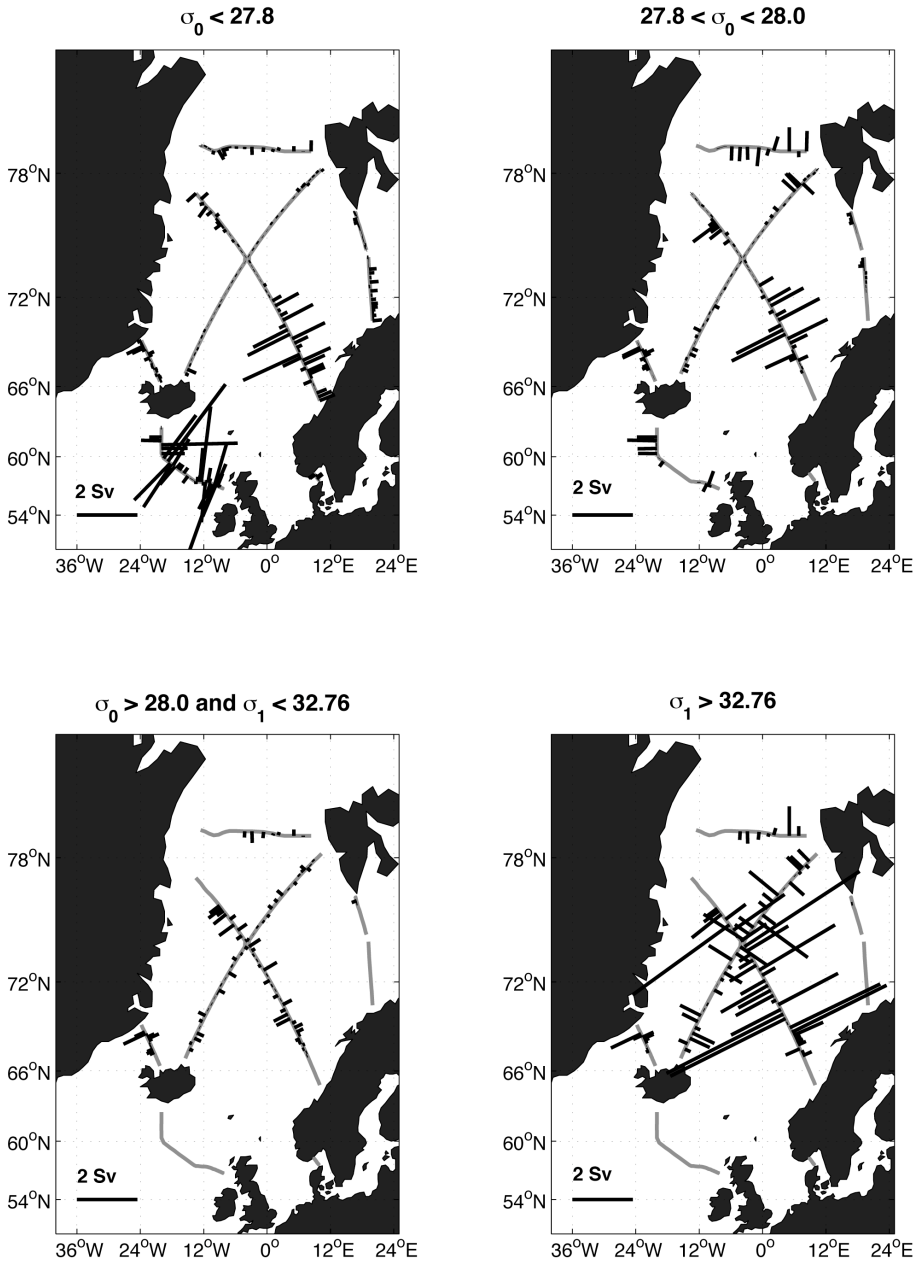

Figure 5.28: Volume transports (Sv) for each station pair, calculated from the standard solution and further adjusted for zero net volume flux in each box. The upper left panel presents transports for $\sigma_0 < 27.8$ (layers 1–7), the upper right hand panel presents transports for $27.8 < \sigma_0 < 28.0$ (layers 8-9), the lower left hand panel presents transports for $\sigma_0 > 28.0$ and $\sigma_1 < 32.76$ (layers 10-11) and the lower right hand panel presents transports for $\sigma_1 > 32.76$ (layers 12-14).

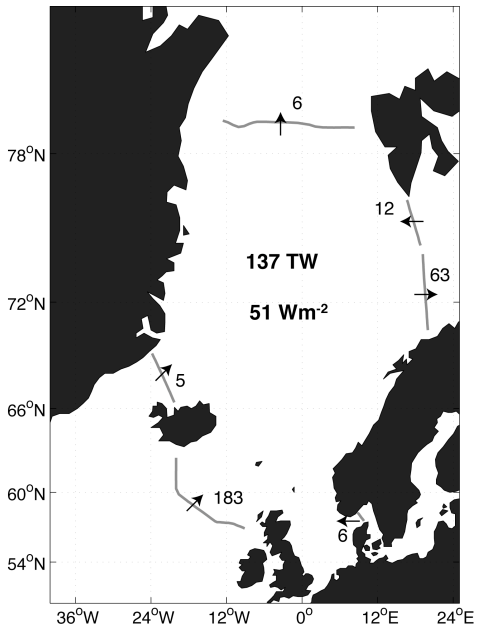

Figure 5.29: Total heat fluxes across the northern and southern boundaries of the Nordic Seas, and total heat flux convergence (TW; 1 TW = 10^{12} J s^{-1}) over the region. The average heat flux per unit area (Wm^{-2}) is also given, based on a total surface area of 2.7 x 10^{12} m^2 for the Nordic Seas.

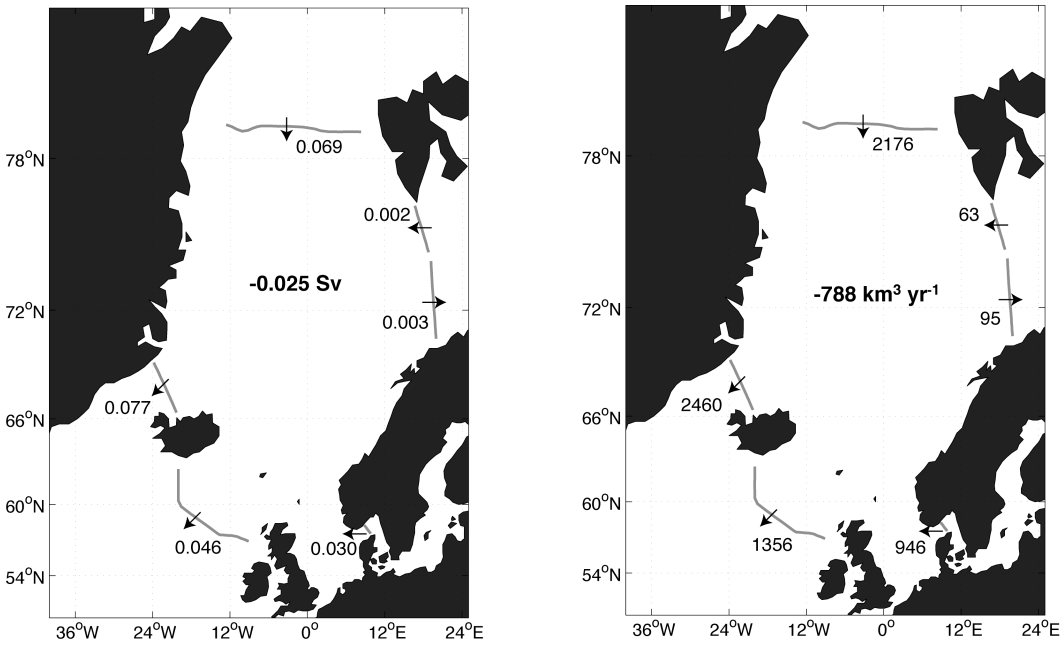

Figure 5.30: Total freshwater fluxes across the northern and southern boundaries of the Nordic Seas, and total freshwater divergence over the region. Fluxes are quoted in Sv and km^3 yr^{-1} in the left hand and right hand panels respectively.

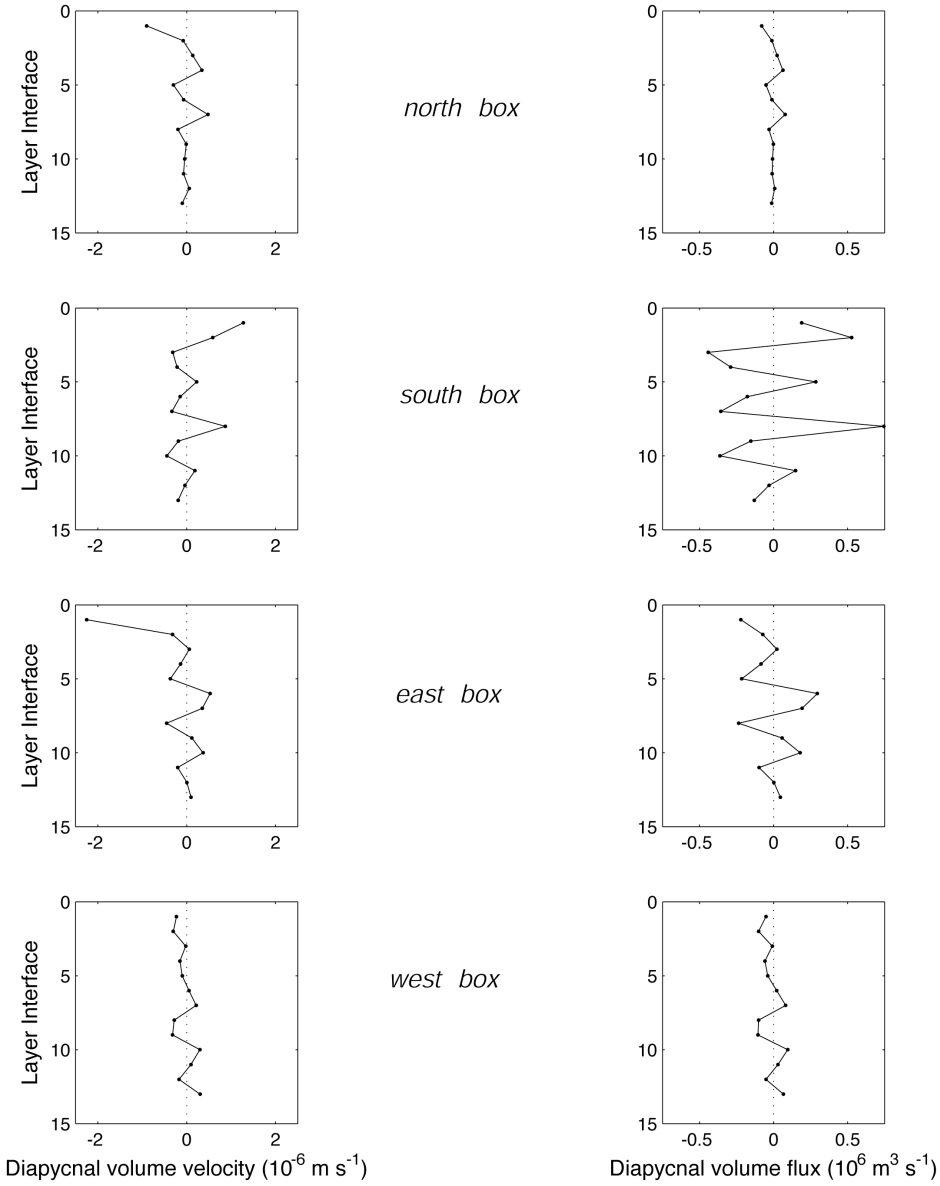

Figure 5.31: Interior diapycnal velocities (10^{6} m s^{-1}; left panel) and associated diapycnal volume transports (10^{6} m^{3} s^{-1}; right panel) for each box. Positive velocities and transports are directed towards the surface.

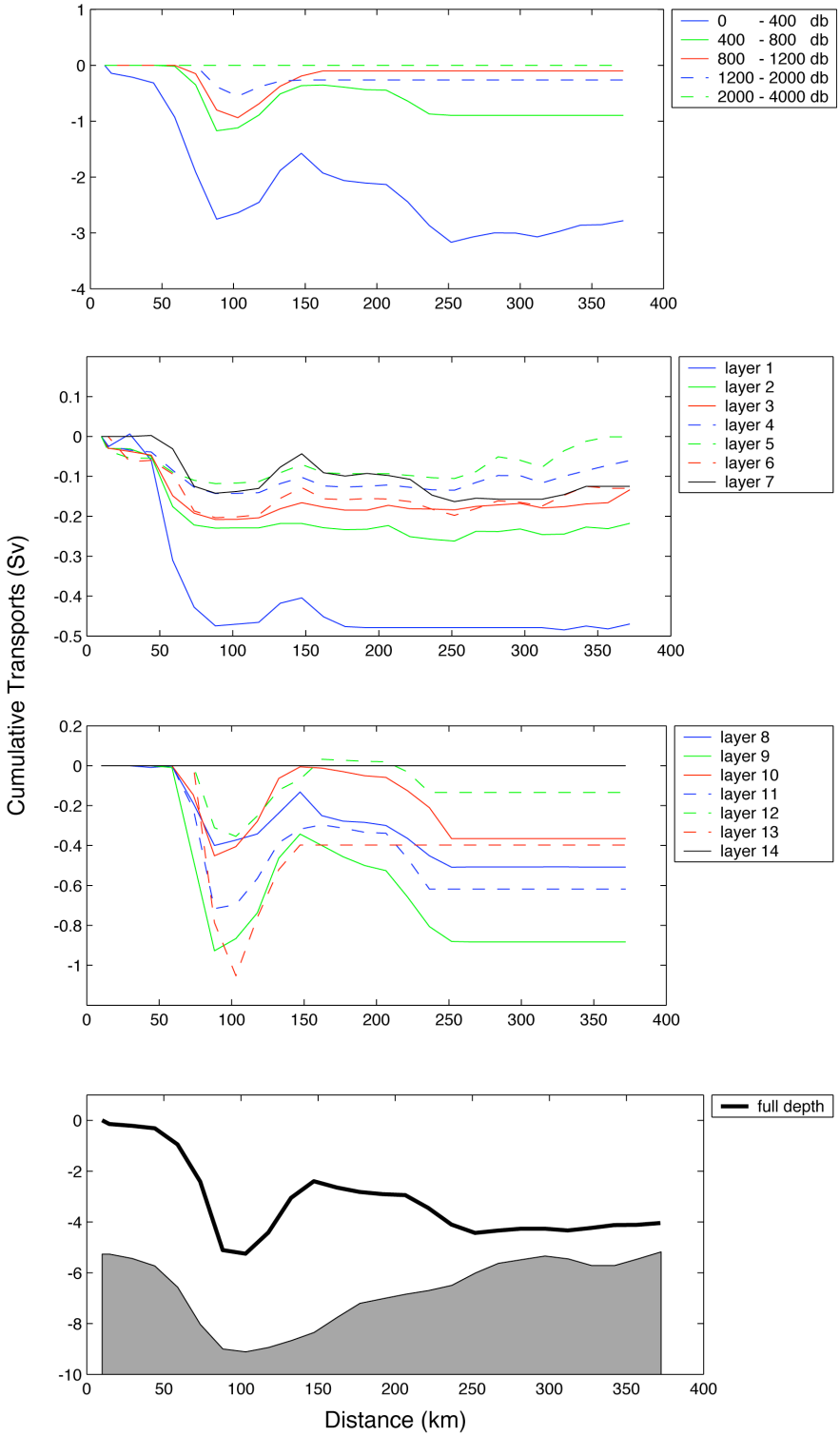

Figure 5.32: Cumulative volume transports (Sv) for the Denmark Strait section, from Greenland on the left, eastwards to Iceland on the right. Transports are accumulated from zero at Greenland. Positive transports are directed north across the section, towards the Arctic. The upper panel gives transports in layers defined by pressure, and the middle panels give transports in layers defined by isopycnals. These were identical to those used in the inverse model (see Table 5.2). The lower panel gives the full depth volume transport, with the coarse topography of the section represented by the grey shading as a visual aid to interpretation.

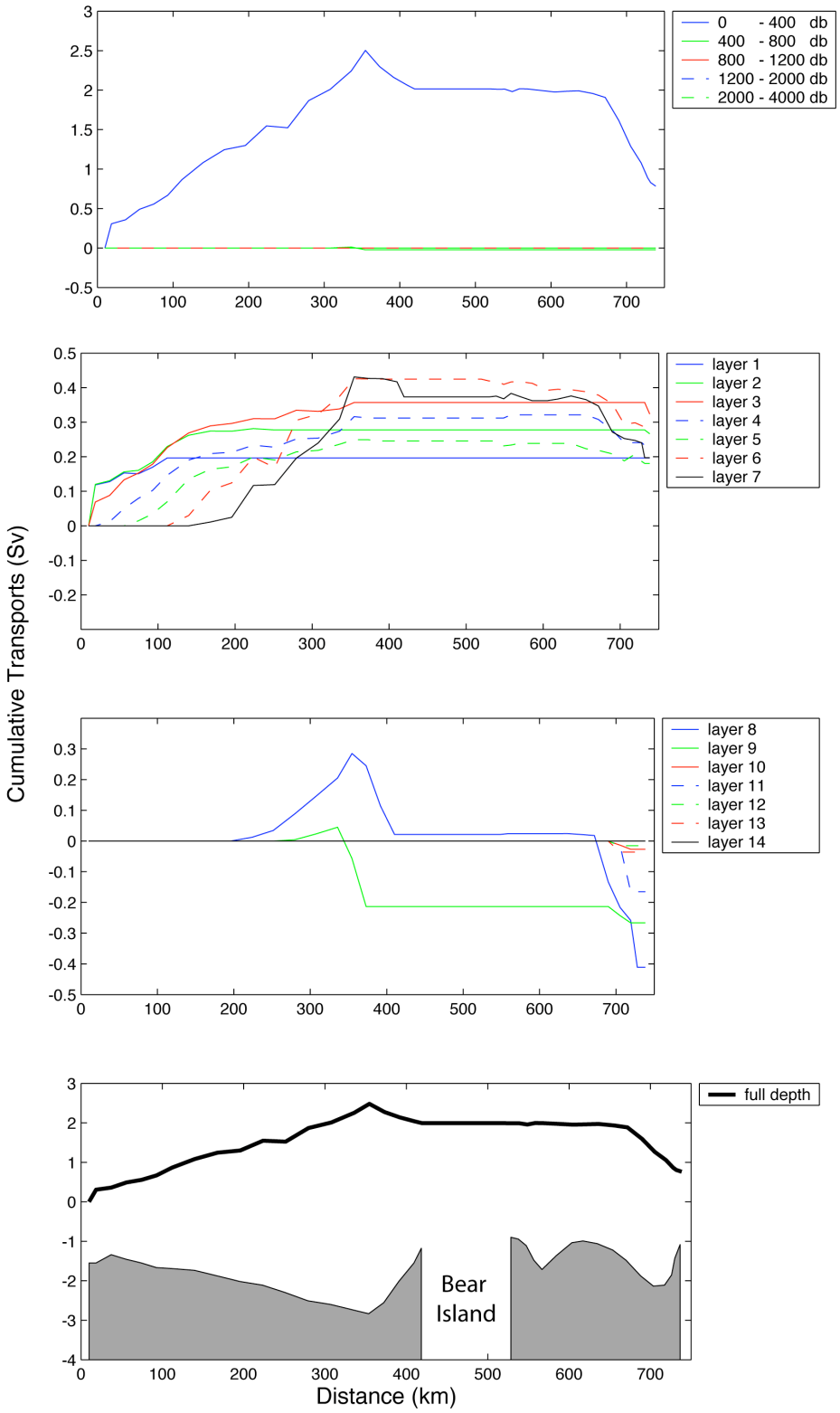

Figure 5.33: Cumulative volume transports (Sv) across the Barents Sea Opening, from Norway on the left, northwards to Svalbard on the right. Transports are accumulated from zero at Norway. Positive transports are directed east across the section, into the Barents Sea. The upper panel gives transports in layers defined by pressure, and the middle panels give transports in layers defined by isopycnals. These were identical to those used in the inverse model (see Table 5.2). The lower panel gives the full depth volume transport, with the coarse topography of the section represented by the grey shading as a visual aid to interpretation.

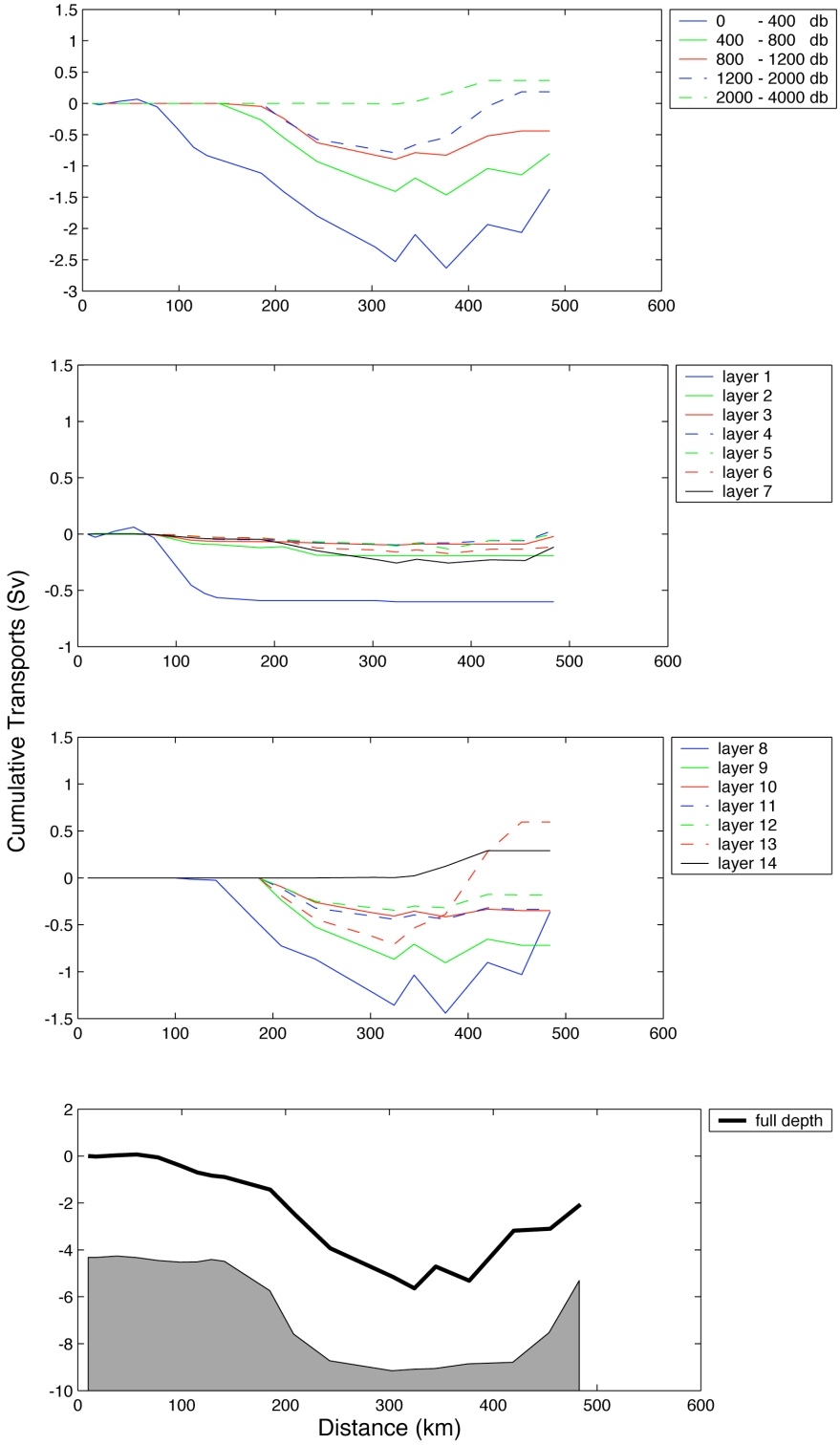

Figure 5.34: Cumulative volume transports (Sv) for the Fram Strait section, from Greenland on the left, eastwards to Svalbard on the right. Transports are accumulated from zero at Greenland. Positive transports are directed north across the section, towards the Arctic. The upper panel gives transports in layers defined by pressure, and the middle panels give transports in layers defined by isopycnals. These were identical to those used in the inverse model (see Table 5.2). The lower panel gives the full depth volume transport, with the coarse topography of the section represented by the grey shading as a visual aid to interpretation.

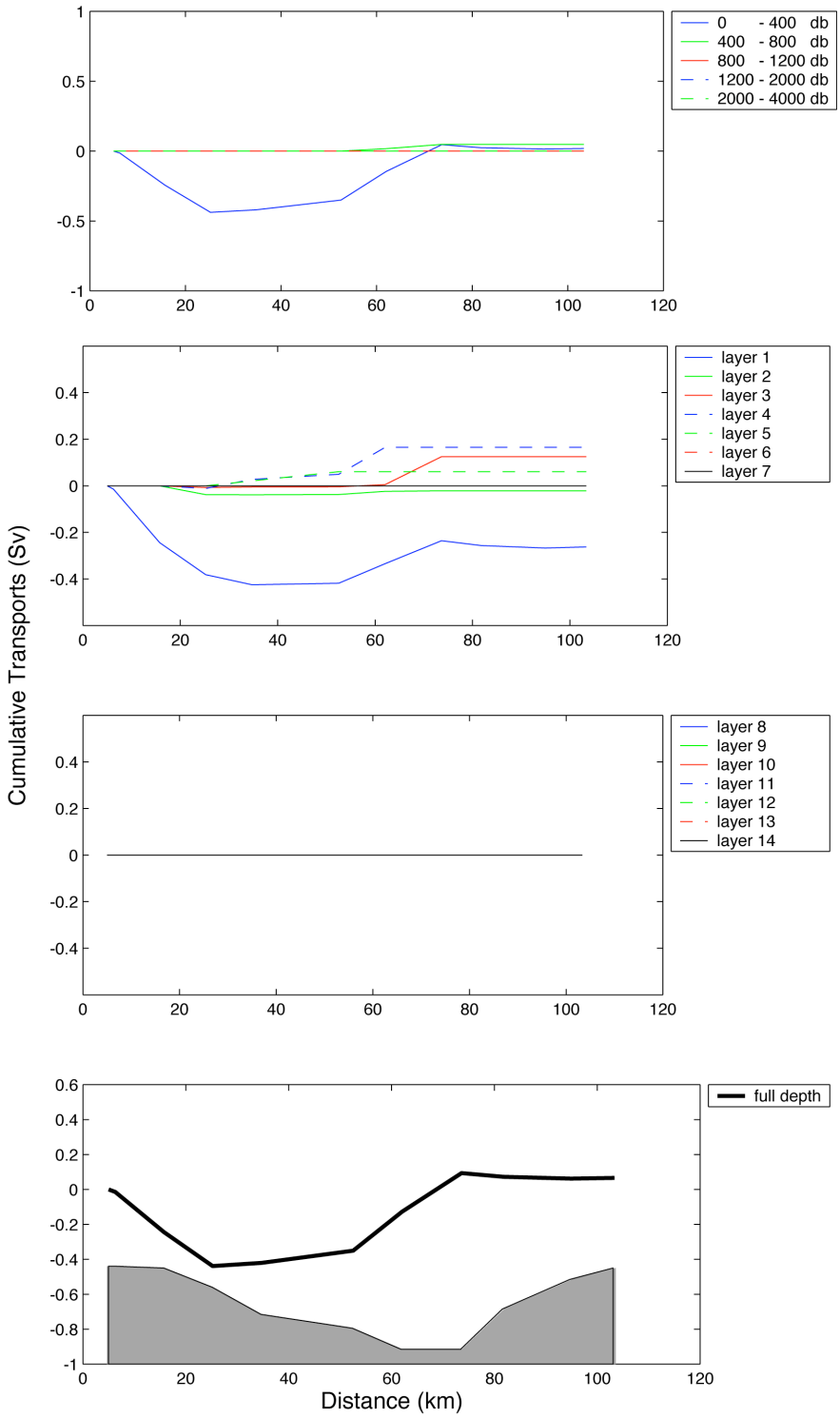

Figure 5.35: Cumulative volume transports (Sv) across the Skagerrak (the opening to the Baltic Seas), from Denmark on the left, northwards to Norway on the right. Transports are accumulated from zero at Denmark. Positive transports are directed east across the section, into the Baltic Seas. The upper panel gives transports in layers defined by pressure, and the middle panels give transports in layers defined by isopycnals. These were identical to those used in the inverse model (see Table 5.2). The lower panel gives the full depth volume transport, with the coarse topography of the section represented by the grey shading as a visual aid to interpretation.

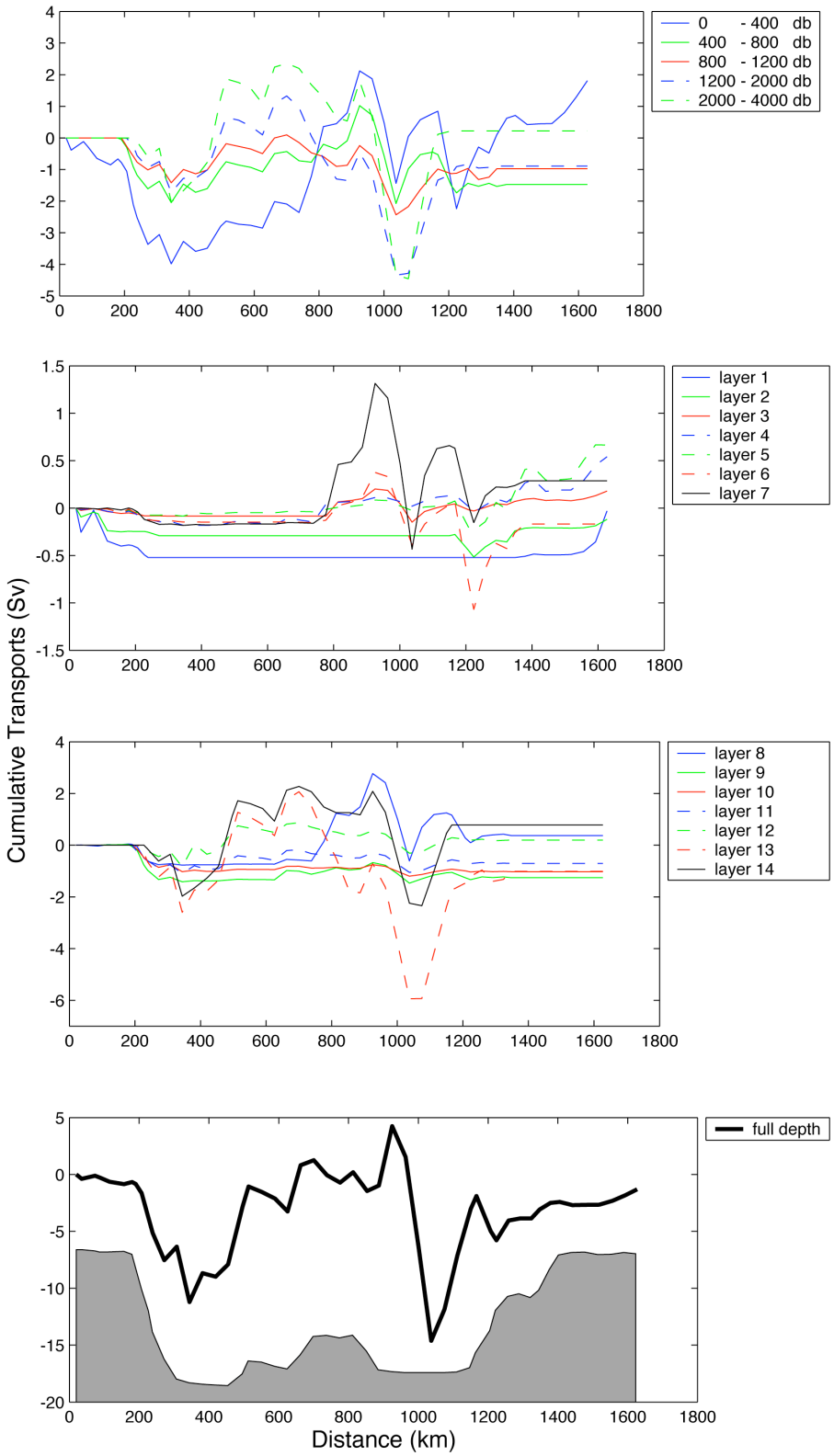

Figure 5.36: Cumulative volume transports (Sv) for the Greenland to Norway section, from Greenland on the left, eastwards to Norway on the right. Transports are accumulated from zero at Greenland. Positive transports are directed northeast across the section, towards the Arctic. The upper panel gives transports in layers defined by pressure, and the middle panels give transports in layers defined by isopycnals. These were identical to those used in the inverse model (see Table 5.2). The lower panel gives the full depth volume transport, with the coarse topography of the section represented by the grey shading as a visual aid to interpretation.

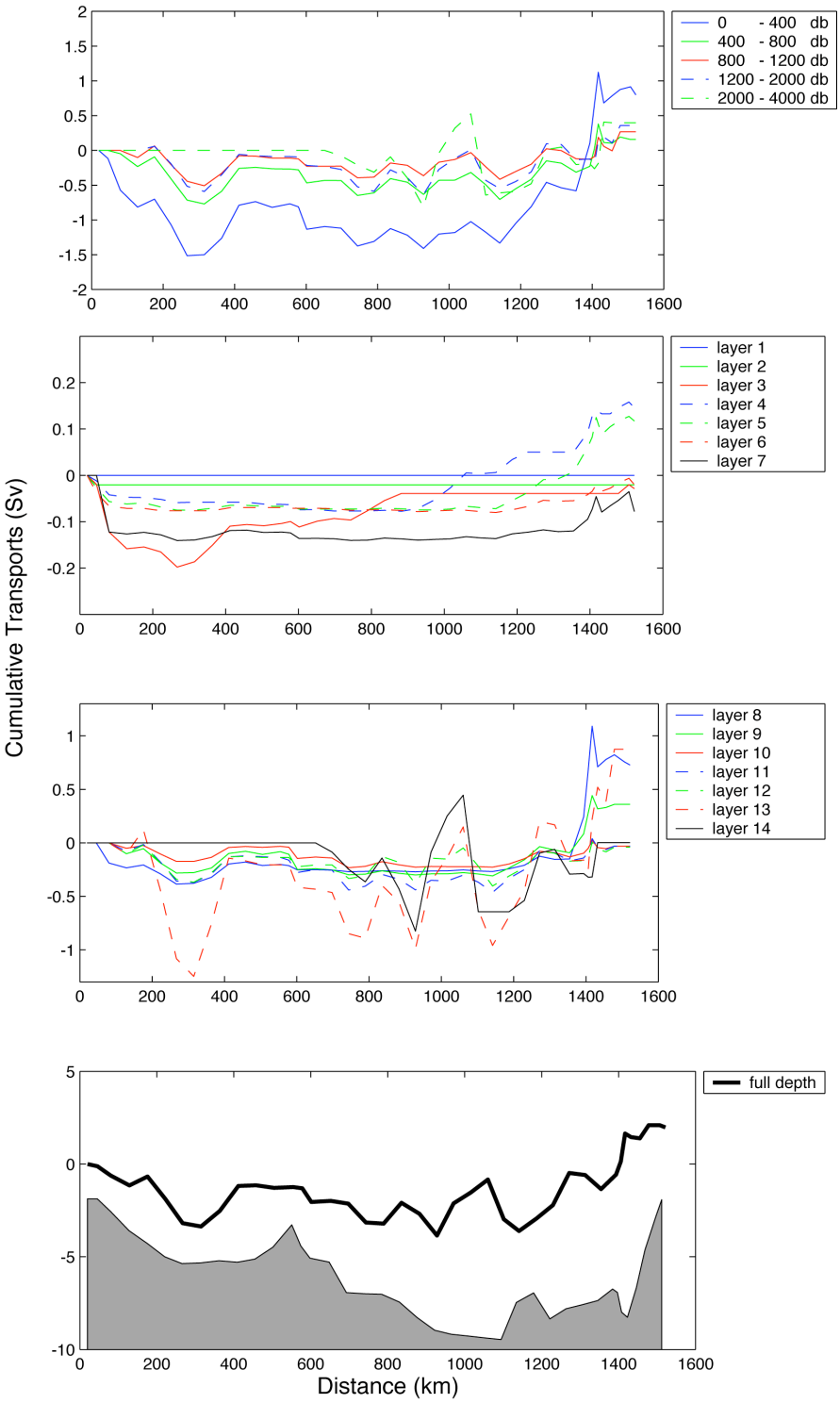

Figure 5.37: Cumulative volume transports (Sv) for the Iceland to Svalbard section, from Iceland on the left, northwards to Svalbard on the right. Transports are accumulated from zero at Iceland. Positive transports are directed northwest across the section, towards the Arctic. The upper panel gives transports in layers defined by pressure, and the middle panels give transports in layers defined by isopycnals. These were identical to those used in the inverse model (see Table 5.2). The lower panel gives the full depth volume transport, with the coarse topography of the section represented by the grey shading as a visual aid to interpretation.

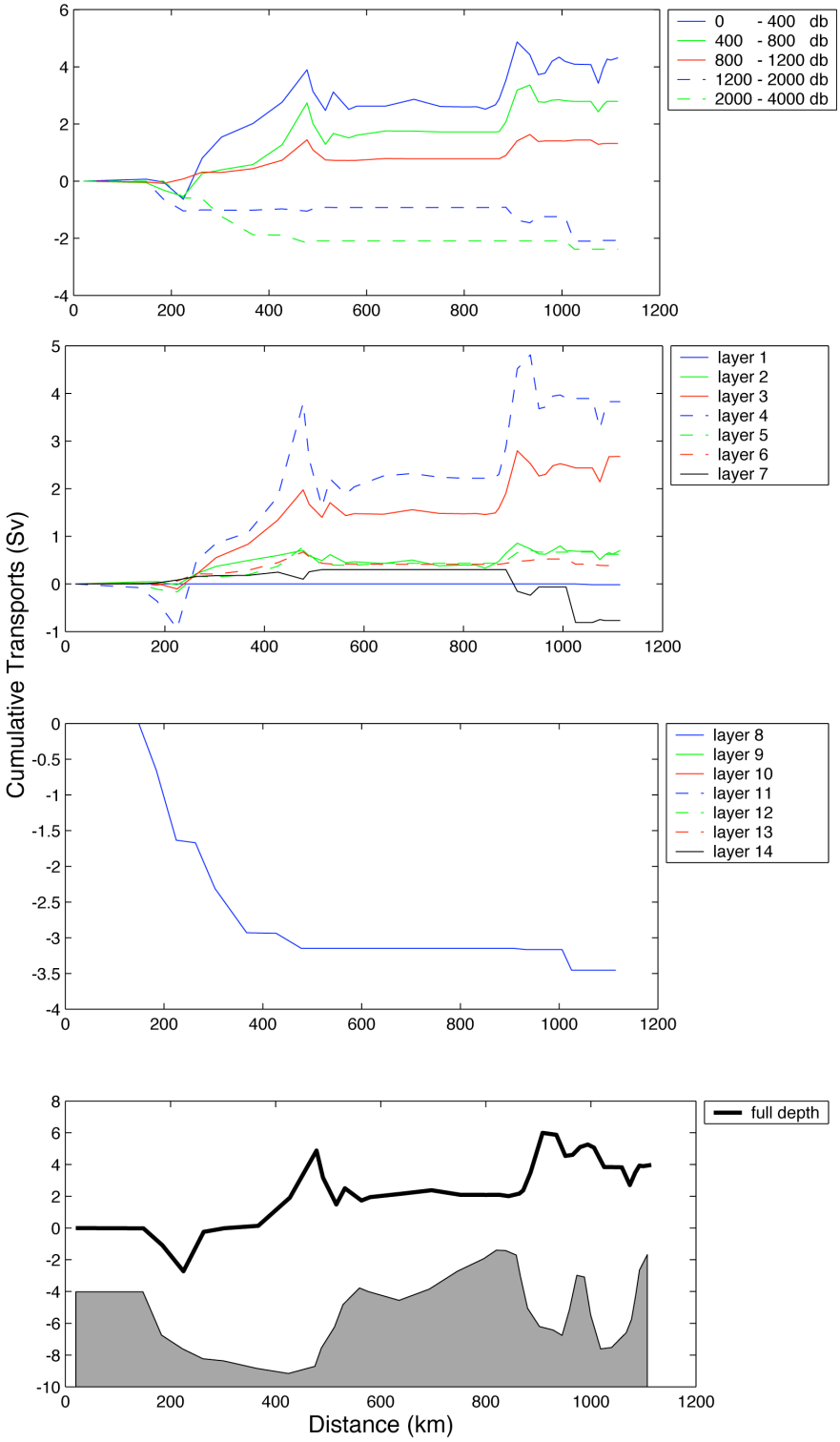

Figure 5.38: Cumulative volume transports (Sv) for the Iceland to Scotland section, from Iceland on the left, eastwards to Scotland on the right. Transports are accumulated from zero at Iceland. Positive transports are directed north across the section, into the Nordic Seas. The upper panel gives transports in layers defined by pressure, and the middle panels give transports in layers defined by isopycnals. These were identical to those used in the inverse model (see Table 5.2). The lower panel gives the full depth volume transport, with the coarse topography of the section represented by the grey shading as a visual aid to interpretation.

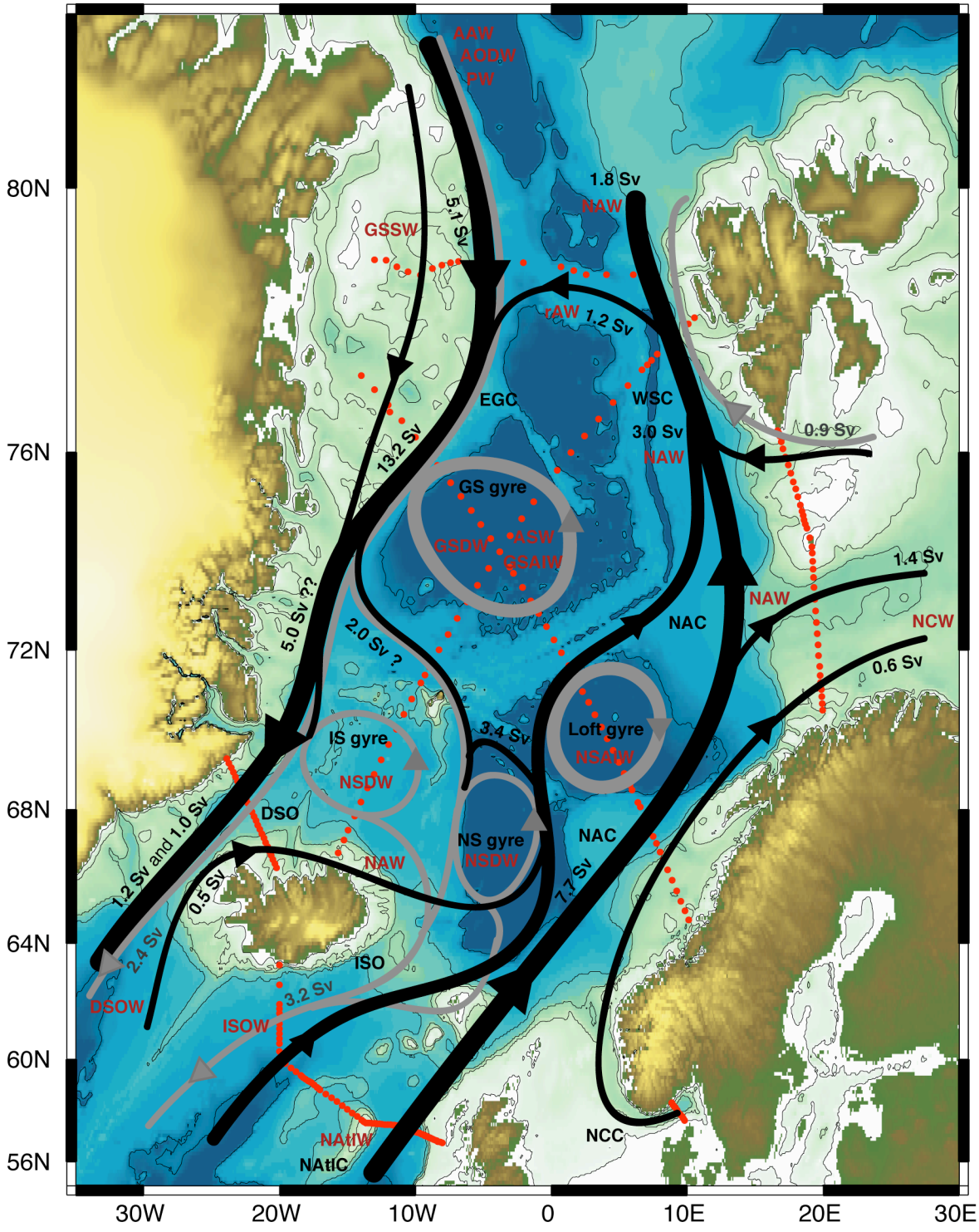

Figure 5.39: Circulation scheme for the Nordic Seas (surface in black and mid-depth in grey) based on results from the standard inverse model. The major currents, water masses (see Table 5.1) and fluxes (see discussion in sections 5.7, 5.8 and 5.9) are marked. The deep circulation is discussed in section 5.8.3.

The following abbreviations are used:
(i) Surface Currents: **EGC** for the East Greenland Current; **NAC** for the Norwegian Atlantic Current; **NAtlC** for the North Atlantic Current; **NCC** for the Norwegian Coastal Current; **WSC** for the West Spitsbergen Current
(ii) Mid-depth Currents: **DSO** for the Denmark Strait Overflow; **ISO** for the Iceland-Scotland Overflow
(iii) Gyres: **GS gyre** for the Greenland Sea Gyre; **IS Gyre** for the Iceland Sea Gyre; **Loft Gyre** for the Lofoten Basin Gyre; **NS gyre** for the Norwegian Basin Gyre
(iv) Water Masses: **AAW** for Arctic Atlantic Water; **AODW** for Arctic Ocean Deep Water; **ASW** for Arctic Surface Water; **DSOW** for Denmark Strait Overflow Water; **GSAIW** for Greenland Sea Arctic Intermediate Water; **GSDW** for Greenland Sea Deep Water; **GSSW** for Greenland Sea Shelf Water; **ISOW** for Iceland-Scotland Overflow Water; **NAtlW** for North Atlantic Water; **NAW** for Norwegian Atlantic Water; **NCW** for Norwegian Coastal Water; **NSAIW** for Norwegian Sea Arctic Intermediate Water; **NSDW** for Norwegian Sea Deep Water; **rAW** for return Atlantic Water; **PW** for Polar Water.

Chapter Six

Sensitivity of the Summer Circulation and Fluxes

6.1 Introduction

The net fluxes of volume, heat and freshwater across the region of the Nordic Seas are presented in Chapter 5, and a circulation scheme for the Nordic Seas is described. This chapter discusses the estimation of errors for the net fluxes and the sensitivity of the inverse.

Two approaches to obtaining a quantification of the errors can be taken. The first is to calculate the formal error estimates using statistical formulations related to the inverse method itself. The second more subjective approach explores the sensitivity of the net fluxes both due both errors in the specifications and formulation of the inverse, and to errors introduced by other factors such as the asynopticity of data and oceanographic variability.

6.2 Errors in Flux Calculations

Following Naveira Garabato et al. (2002) the *a priori* uncertainties in the volume transport calculations are estimated by applying random barotropic perturbations to individual velocity profiles, and calculating the root-mean-square deviation of 50 realizations of the resulting transport. The perturbations followed a normal distribution with a standard deviation of 3□m□s^{-1}, the characteristic accuracy of the barotropic component of the LADCP flow (section 4.2.3). This assumes that the dominant source of error is in the barotropic component of the LADCP flow, and that errors are horizontally uncorrelated. These transport error estimates do not include the sampling error due to poor resolution within regions of steep topography where there are large differences in the depths of the stations making up a station pair (see section 6.5.2).

The uncertainties in the property equations were estimated to be the product of the *a priori* errors in volume conservation and 2□ the standard deviation of property variations within the relevant layer. This *ad hoc* best guess was proposed by Ganachaud et al. (2000) where the factor of 2 accounts for possible correlations between the section-averaged and mesoscale components in the property conservation equations.

These uncertainties provided an estimate of the *a priori* equation error covariance matrix which was used in the weighting scheme for the inverse (see section 4.6.3). They are summarised in Table 6.1, which includes the *a priori* errors in the volume conservation equations (standard deviation of the layer volume transports for 50 realisations), and the layer mean and standard deviations of potential temperature and salinity for each box.

The greatest uncertainties in the volume transports are in the lower layers, but these are a function of the thickness of each particular layer within each box. Over the full water column the uncertainties within each box are of the order 3□Sv.

Layer	Error (Sv)				Mean ± std θ (°C)				Mean ± std salinity			
	north	*south*	*east*	*west*	*north*	*south*	*East*	*west*	*north*	*south*	*east*	*west*
1	0.2	0.2	0.1	0.6	-1.234 ± 1.527	12.896 ± 2.369	11.356 ± 1.480	0.601 ± 1.452	31.965 ± 2.987	33.881 ± 1.266	34.101 ± 1.127	31.963 ± 3.121
2	0.1	0.4	0.2	0.2	-0.752 ± 1.477	11.522 ± 11.327	9.667 ± 9.880	2.595 ± 4.432	33.323 ± 1.625	35.161 ± 0.240	34.801 ± 0.326	33.673 ± 1.425
3	0.1	0.6	0.2	0.2	0.606 ± 2.682	9.307 ± 9.580	8.412 ± 8.548	5.183 ± 6.430	33.912 ± 1.061	35.201 ± 0.344	34.955 ± 0.188	34.487 ± 0.427
4	0.2	1.5	0.4	0.2	2.639 ± 4.278	8.467 ± 8.387	7.076 ± 7.393	3.295 ± 4.793	34.488 ± 0.543	35.248 ± 0.308	35.036 ± 0.186	34.523 ± 0.518
5	0.2	0.6	0.4	0.2	3.230 ± 4.745	6.971 ± 6.991	6.858 ± 7.188	3.170 ± 4.918	34.684 ± 0.351	35.160 ± 0.235	35.140 ± 0.265	34.687 ± 0.351
6	0.2	0.6	0.3	0.2	1.313 ± 2.341	5.692 ± 5.609	5.863 ± 6.050	2.470 ± 4.458	34.606 ± 0.463	35.082 ± 0.146	35.111 ± 0.208	34.711 ± 0.253
7	0.2	1.0	0.5	0.2	2.042 ± 2.581	4.962 ± 3.727	4.739 ± 4.876	1.429 ± 2.128	34.772 ± 0.252	34.962 ± 0.039	35.065 ± 0.156	34.704 ± 0.270
8	0.7	1.0	0.6	0.4	2.458 ± 2.535	2.734 ± 2.977	3.056 ± 3.225	0.992 ± 1.572	34.957 ± 0.059	34.957 ± 0.057	35.003 ± 0.087	34.819 ± 0.103
9	0.5	0.5	0.5	0.5	0.983 ± 1.091	0.378 ± 0.480	0.743 ± 0.860	0.386 ± 0.541	34.917 ± 0.024	34.872 ± 0.065	34.901 ± 0.050	34.873 ± 0.067
10	0.4	0.5	0.4	0.5	0.152 ± 0.214	-0.003 ± 0.087	0.028 ± 0.136	0.035 ± 0.135	34.893 ± 0.037	34.881 ± 0.049	34.883 ± 0.047	34.884 ± 0.047
11	0.6	0.8	0.8	0.7	-0.328 ± 0.371	-0.294 ± 0.306	-0.364 ± 0.415	-0.263 ± 0.262	34.882 ± 0.051	34.883 ± 0.049	34.878 ± 0.056	34.885 ± 0.046
12	0.7	0.8	0.8	0.7	-0.717 ± 0.773	-0.596 ± 0.657	-0.675 ± 0.746	-0.636 ± 0.700	34.876 ± 0.060	34.886 ± 0.050	34.879 ± 0.057	34.883 ± 0.054
13	1.8	1.7	1.8	0.7	-0.863 ± 0.875	-0.824 ± 0.829	-0.864 ± 0.872	-0.815 ± 0.828	34.901 ± 0.030	34.905 ± 0.026	34.902 ± 0.029	34.902 ± 0.028
14	1.4	1.2	1.5	1.0	-1.073 ± 1.088	-1.035 ± 1.045	-1.051 ± 1.067	-1.071 ± 1.078	34.900 ± 0.026	34.908 ± 0.022	34.907 ± 0.024	34.906 ± 0.024
Full Depth	**3.1**	**3.4**	**3.1**	**2.5**	**-0.417 ± 1.017**	**2.042 ± 3.951**	**0.241 ± 1.223**	**-0.399 ± 0.913**	**34.868 ± 0.067**	**34.976 ± 0.137**	**34.922 ± 0.039**	**34.859 ± 0.058**

Table 6.1: *a priori* errors in the volume conservation equations (standard deviation of the layer volume transports for 50 realisations), and layer mean and standard deviations of potential temperature and salinity for each box used in the inverse calculation.

The layer mean and standard deviations of potential temperature and salinity for the inverse boxes clearly show the dichotomy in the hydrography of the Nordic Seas with the east-west contrast in hydrographic characteristics. The average temperature over the full water column in the south box (2.0°C) is far greater than for any of the other boxes. This is due to the influence of both the warm North Atlantic waters present on the Iceland-Scotland section, and the warm inflowing Atlantic Waters that cross the Greenland-Scotland Ridge to enter the Norwegian Sea. The west and north boxes both have an average temperature of -0.4°C over the full water column, due to the presence of cold Polar Waters. The average salinities over the full water column in the southeast (south and east boxes) sector are also far greater than in the northwest (north and west boxes) sector (S = 34.949 compared to S = 34.864). Within individual layers the standard deviations in temperature are greater in the southeast sector than the northwest, whereas whereas the standard deviations in salinity are generally lower.

6.3 Formal Error Estimates

The statistical formulation of the inverse problem can directly provide a formal estimate of the errors in the solution (McIntosh and Rintoul, 1997). These are the errors associated with determining the barotropic velocities and diapycnal fluxes. As such, the formal errors do not take into account errors due to the asynopticity of the data, the sensitivity of the solution to the initial velocity field, or the oceanic variability.

The solution standard deviation is given by the square root of the diagonal elements of the posterior covariance matrix, $\mathbf{P}_{xx}$ (see section 4.6.3 and Appendix I for details of the calculation). $\mathbf{P}_{xx}$ is an updated version of the prior covariance matrix. The latter contains the statistical information which is known or estimated before the inversion and $\mathbf{P}_{xx}$ then takes into account the introduction of new information represented by the vector of reference velocities, **b**. This formal estimate gives a mean error of 2.2 cm s^{-1} for the reference level velocities (with standard deviation of 0.1 cm s^{-1}), and 0.017 cm s^{-1} (with standard deviation of 5.6×10^{-4} cm s^{-1}) for the effective diapycnal velocities. These error estimates were used to calculate individual errors for each station pair (both full depth and in individual layers). The magnitude of the errors in volume transport for each station pair are illustrated in Figure 6.1. The station pair errors are a function of the depth, hence the greatest errors are over the central part of Fram Strait, the Iceland Basin of the Iceland-Scotland section, and over the central parts of the Greenland, Norwegian and Iceland Basins.

The estimated error in volume transport, S, for an entire section is given by

$$S = \sqrt{\sum_n N_{er}^2} \qquad 6.1$$

where N_{er} is the error for a station pair, and n represents the station pairs included in the section. The corresponding temperature and salinity flux errors are estimated from the product of the volume flux error and the standard deviation of property variations within the relevant section. These formal errors are summarised in Table 6.4.

6.4 Inverse Sensitivity

The sensitivity to variations in the inverse model can be investigated by running a number of different models, each varying from the reference state by one factor. The reference state was defined as the standard model and the preferred solution from this reference state was defined as the standard solution (section 5.6). The sensitivity of this reference state was examined by allowing each of its components to vary within a prescribed range. A number of models were used to illustrate the importance of various characteristics, and the effects of these variations on the net fluxes were inspected. Some models were deliberately ‘unreasonable’, producing a set of flux

estimates significantly different to those obtained from the preferred solution from the standard model, so illustrating the importance of that particular model component. Other more 'reasonable' models were selected so as to provide a range of realistic solutions. The standard deviation of the solutions given by these latter models provided an estimate of the sensitivity of the inverse.

The model states and their 'plausibility' are categorised in Table 6.2 and the results are given in Table 6.3. If row and column weighting are not included (States 1 to 3), the model is implausible, since without the former, the property transport equations are affected by the magnitude of the property being transported, and without the latter, the solution is scaled by the cross-sectional area of its station pair. If the model includes layer-specific conservation equations, then diapycnal exchange must also be included else the model will be physically inconsistent (State 8). An unreasonable initial circulation (State 16) will produce an implausible solution since the inverse can only be expected to be close to correct if the first guess is realistic. A reasonable model will yield implausible solutions if too high or too low a rank is chosen (States 4,6,7). The choice of very low ranks will give solutions very close to the initial state, while choice of high ranks will yield solutions incorporating a high level of noise.

Model	**Specifications**	**Plausibility**	
		Model	*Solution*
State 1	standard model with no weighting	☐	☐
State 2	standard model with column weighting only	☐	☐
State 3	standard model with row weighting only	☐	☐
State 4	standard model but rank 10		☐
State 5	standard model but rank 30		
State 6	standard model but rank 100		☐
State 7	standard model but rank 140		☐
State 8	standard model but no diapycnal velocities	☐	☐
State 9	only full depth volume fluxes for each box, full rank		
State 10	layer specific volume fluxes		
State 11	layer specific salt fluxes	☐	☐
State 12	layer specific salt and volume fluxes		
State 13	standard model but with bottom referenced geostrophy for initial velocity field	☐	☐
State 14	standard model but with ekman fluxes at upper limit		
State 15	standard model but with ekman fluxes at lower limit		
State 16	standard model but no ekman fluxes	☐	☐
State 17	standard model but with bottom triangles calculated by extrapolation of shear		
State 18	standard model but coarse realisation of denmark strait section		
State 19	standard model with subsampled fine resolution denmark strait section		
State 20	standard model with alternative crossover station		
State 21	standard model with alternative EGC		

Table 6.2: Specifications of alternative models to test inverse and oceanographic sensitivity. The 'reasonable' and 'unreasonable' model states and solutions are noted by a or a ☐, respectively.

6.4.1 Weighting scheme

If the system is solved at full rank then row weighting makes no difference to the solution. The standard solution, however, is not the full rank solution, but rather the solution for rank 43. Since residuals are allowed in the equations, the weighting of these residuals becomes important.

Without column weighting the solutions for States 1 and 3 at rank 43 (Table 6.2) give similar results to the transport estimates from the initial velocity field (pre-inverse). The condition of requiring residuals to be zero within 3 standard deviations is only satisfied at ranks 148 and 145 respectively. With only column weighting (State 2) the same condition is satisfied at a rank of 13. Without the row weighting, however, the property transport equations are affected by the magnitude of the property being transported. In particular, the inflow of the NAW across the Greenland-Scotland Ridge is very low, which in turn reduces the total heat convergence within the Nordic Seas. This might be attributed to the anomalously high salinity on the Iceland-Scotland section (average salinity of >35.25 in the upper waters) compared to all other sections: without row weighting the inverse reduces the northward transport across the section in order to satisfy the salinity constraints.

6.4.2 Choice of rank

The rank of the standard solution was chosen to be such that the residuals are required to be zero to within three standard deviations of the error estimate. To illustrate the effect the choice of rank has on the final result, the results are compared for arbitrary ranks of 10, 30, 100 and 140.

The higher rank solutions of 100 and 140 (States 6 and 7) have smaller residuals, but a less 'reasonable' circulation with reduced fluxes across the individual sections. In particular, the magnitudes of the Atlantic inflow across the Greenland-Scotland Ridge are reduced to 2.4 and 2.7 Sv. Also, the magnitudes of the East Greenland Current are roughly halved, as are the magnitudes of the dense overflows into the North Atlantic. The resultant heat fluxes across the Greenland-Scotland Ridge are reduced by almost a factor of 3, such that the total heat convergence in the Nordic Seas is reduced to an average of 5 TW (compared to the 123 TW of the standard solution).

The lower rank solution of 10 (State 4) gives generally higher fluxes across individual sections and greater heat fluxes. The lower rank solutions are close to the fluxes given by the initial velocity field (see section 5.5 and Tables 5.5 and 5.6), since the adjustments made by the inverse are small. The mid rank solution (30) is included as a plausible alternative to the standard solution.

6.4.3 Inclusion of diapycnal velocities

The solution given by State 8 illustrates the importance of the inclusion of diapycnal velocities when the inverse model is formulated to include layer-specific conservation. If, however, only top-to-bottom constraints are applied (see section 6.4.4 below), then the inclusion of diapycnal velocities is obviously irrelevant and has no effect on the solution. When fluxes between layers are not allowed although the total fluxes within the inverse boxes are constrained to be zero within the expected errors, the fluxes across individual sections are unrealistically low. Also, the solution for rank 43 without diapycnal velocities gives very large reference velocities with a standard deviation of

3.4 cm s^{-1} and peak value of 25.8 cm s^{-1}, compared to a standard deviation of 0.5 cm s^{-1} and peak value of 1.8 cm s^{-1} for the standard solution.

6.4.4 Choice of constraints

A number of models are run with different constraints applied. For State 9 full depth volume conservation is required in each inverse box. Since there is only one constraint for each box, State 9 was solved to full rank. For States 10 - 12 layer-specific volume, layer-specific salinity and layer-specific volume and salinity constraints, respectively, are applied. These states are required to satisfy the same conditions as for the standard solution i.e. residuals are required to be zero within three standard deviations of the error estimate, and the solution is required to be within one standard deviation of the *a priori* error estimate.

These models do go part way to providing a 'reasonable' representation of the circulation although since temperature flux conservation is not required, an accurate description of the heat fluxes, in particular, is lacking. State 11, where only layer-specific salinity conservation is required, does not satisfactorily reduce the flux residuals within each box since the salinity residuals are within the error estimate at very low ranks. This suggests that there is insufficient information in salinity alone to satisfactorily constrain the inverse solution.

6.4.5 Choice of initial velocity field

To illustrate the poor representation of the circulation that is obtained by using a level of no motion throughout the Nordic Seas, State 13 was required to be identical to the standard model with the exception that no direct velocities were applied. This allowed the impact of the direct velocity measurements in the solution to be evaluated. Since an initial level of no motion is prescribed at the deepest common level between stations, the initial velocity field is effectively set to bottom-referenced geostrophy. The solution for rank 43 is selected to allow a direct comparison to the standard solution (size of the residuals etc.). The solution is of poorer quality than that of the standard solution: there are larger residuals at the same rank, overflows and inflows are reduced to values inconsistent with literature and the bulk fluxes of the standard solution are not reproduced. In particular, the total inflow of AW across the Greenland-Scotland Ridge is reduced to 4.4 Sv (compared to 6.1 Sv in the standard solution). Although the 0.8 Sv inflow of Atlantic waters to the Barents Sea remains reasonable (1.0 Sv in the standard solution), this is at the expense of reducing the northward transport in the WSC through Fram Strait to zero. The net southward flow in the EGC is also reduced by about half, both in Fram Strait and futher south in the Greenland Sea (~75°N). Although the overflows across the Iceland-Scotland Ridge are unchanged, the magnitude of the Denmark Strait Overflow is reduced by almost half to 1.7 Sv.

This behaviour emphasises the importance of direct velocity observations (or transport estimates based on observations) in inverse box models to compensate for only being able to use a crude,

diagonal representation of the a priori errors. Numerous recent inverse studies have found that incorporating direct velocity measurements makes a significant impact on the solution (Bacon, 1997; Bingham and Talley, 1991; Naveira Garabato et al., 2003; Joyce et al., 1986; Vanicek and Siedler, 2002). In particular, it is found here that the prevailing circulation of the Nordic Seas cannot be reasonably approximated with a level of no motion.

6.5 Oceanographic Sensitivity

A number of models were studied to investigate the relative contributions of the Ekman fluxes and bottom triangle calculations to the errors of the net fluxes. As for the inverse sensitivity tests, the models and their 'plausibility' are categorised in Table 6.2 and the results are given in Table 6.3.

6.5.1 Ekman flux

The summer average wind stress field from the adjusted SOC climatology was used to estimate the cross-track Ekman fluxes of volume, temperature and salt (Table 5.3). These fluxes were used as the Ekman flux elements of the reference state. The average values of potential temperature and salinity over the surface 50□m (see section 4.2.5) were chosen for the determination of the Ekman contribution to property fluxes. The Ekman volume fluxes were allowed to vary by ± 20%. This was approximately the range between the summer and annual average fluxes calculated from both the SOC and HR climatologies (see sections 3.4.1 and 4.2.5).

Model States 14 and 15 were formulated to include Ekman fluxes at the lower and upper limits, respectively (± 20%), while State 16 did not include any Ekman fluxes. The solutions for the first two states do give a reasonable circulation and are minimally different to the standard solution. Although State 16 gives reasonable fluxes across the sections individually, the complete omission of ekman fluxes does influence the surface circulation. In particular, the circulation of the upper waters on the Iceland-Scotland section is altered such that the inflow of Atlantic waters across the Iceland-Scotland Ridge is reduced to 3.3□Sv (from the 5.6□Sv in the standard solution).

6.5.2 Bottom triangles

Numerous methods have been used to estimate the property transports in the bottom triangles below the deepest common depth of adjacent stations (Wunsch, 1996). In this thesis the deepest common velocity is held constant and extrapolated to the mean pair depth (see section 4.2.2). The associated property transport is then included in the deepest layer at each station pair. State 17 uses an alternative method where the velocity shear at the deepest common depth was extrapolated through the bottom triangle area of each station pair, and thus gives some indication of how the method chosen to deal with the problem of these bottom triangles influences the net fluxes.

Although this alternative method of bottom triangle calculation does not significantly alter the net fluxes, it does illustrate that the full depth transport is most sensitive to choice of bottom triangle formulation in regions where there are high near-bottom velocities and large bottom triangles due to steep topography, for example the continental shelf slope off Greenland, and near the coasts of Svalbard, Bear Island and Iceland. The maximum difference in volume flux for a station pair given by the two methods is 0.5 Sv (in Fram Strait over steep topography off Svalbard), but for most station pairs the differences are <0.01 Sv.

6.6 Asynopticity

A measure of the sensitivity of the inverse solution to oceanic variability can be obtained by using alternative realisations of the available data. The scientific design of the ARCICE JR44 cruise was such that a repeat Denmark Strait section was occupied. The immediate repeat of the Denmark Strait section occupied a reduced subset of the station positions such that the station spacing was effectively doubled. Model State 18 was formulated exactly as for the standard model but using this coarse resolution Denmark Strait section. To allow a direct comparison State 19 used stations from the original Denmark Strait section but only those which were occupied during the coarse resolution repeat.

The 'crossover' station at 74.1°N 3.8°W was occupied twice, once on the Norway to Greenland section, and once on the Svalbard to Iceland section. Model State 20 was set up as for the standard model but instead included the alternative station occupied at the section crossover location.

Also, as described in section 3.7, one station on the Norway to Greenland section was conducted out of sequence. To treat the stations consistently with respect to time, station 042 is excluded from the setup in the standard model (i.e. a station order of 040–041–043–044). Model State 21 presents the alternative scenario, which instead excludes station 043 (i.e. a station order of 040–041–042–044).

The flux differences between results from these states and the standard solution are minimal. The main conclusion is that in the alternative Denmark Strait sections (i.e. the coarse resolution, and the sub-sampled fine resolution sections) the strength of the overflow is reduced by ~0.5 Sv. This indicates that the wider station spacing may not fully resolve the circulation. While using different realizations of a single section or station clearly does not provide a complete assessment of the impact of oceanic variability on circulation estimates, the results show that robust estimates of the large-scale circulation and fluxes can be made from models such as the one used here.

6.7 Conclusions

The alternative model states are listed in Table 6.2 and a detailed description of the results is given in Table 6.3. The final sensitivities are calculated from the standard deviation of fluxes from the alternative states. The estimate of the inverse sensitivity is based on the standard solution and solutions from model States 5, 9, 10 and 12. The estimate of the oceanographic sensitivity was based on the standard solution and solutions from model States 14, 15, 17, 18, 19, 20 and 21 (including ekman fluxes, bottom triangles, asynopticity).

A final estimation of the net volume flux errors, E_{net}, is calculated following

$$E_{net} = \sqrt{\frac{\sum_{i}^{N} w_i E_i^2}{\sum_{i}^{N} w_i}} \qquad 6.2$$

where E_i is the estimated error from the inverse sensitivity tests, oceanographic sensitivity tests or the formal error for section i, w_i is the area of section i, and N is the number of sections. These errors are summarised in Table 6.4 (the section across the Skagerrak is excluded since the volume flux <0.1 Sv).

Section	Section Area (km^2)	Inverse Sensitivity $E_{inverse}$	Oceanographic Sensitivity E_{ocean}	Formal Error E_{formal}
Denmark Strait	243	8 %	8 %	8 %
BSO	148	72 %	33 %	75 %
Fram Strait	713	50 %	38 %	30 %
Greenland-Norway	3404	33 %	26 %	64 %
Iceland-Svalbard	3397	21 %	31 %	65 %
Iceland-Scotland	1653	38 %	34 %	36 %
NET ERROR, E_{net}		**33%**	**30 %**	**58 %**

Table 6.4: Summary of errors in volume flux from sensitivity tests.

The standard inverse model was formulated in such that it was physically consistent and included all available sources of information. The semi-subjective choice of solution rank gave a standard solution that was reasonably robust in the flux estimates that it provided. The formal (*a posteriori*) error estimates are most probably an overestimate; since they are cumulative for fluxes across a section (see section 6.3), it may not be quite appropriate to use the random LADCP errors as the *a priori* error. A final error estimate of 32% is therefore obtained from the average net error of the inverse and oceanographic sensitivity tests to provide an upper and lower bound to the fluxes and circulation presented in Chapter 5 (illustrated in Figure 6.2).

Empirically, these errors are likely to be overestimates. In the standard model of the inverse the net Nordic Seas throughflow is unconstrained, with constraints being applied only to individual boxes, but even so the computed net fluxes are ~1□Sv southwards. Net flux calculations for the Arctic Ocean (Aagaard and Carmack, 1989; Bacon, 1997, Bacon, 2001) infer the true Nordic Seas throughflow to be probably 1□±□□Sv southwards, with much of the error depending on the Canadian Archipelago throughflow. This suggests that the net fluxes estimated in this thesis are accurate to ±□□Sv; as Naveira Garabato et al. (2003) noted, although individual reference velocities may be poorly resolved, inverse models may accuarately determine lateral fluxes on larger scales.

VOLUME FLUXES (Sv)	Stadard Solution	State 1	State 2	State 3	State 4	State 5	State 6	State 7	State 8	State 9	State 10	State 11	State 12	State 13	State 14	State 15	State 16	State 17	State 18	State 19	State 20	State 21
north box	-0.4	-7.5	0.2	-7.5	0.9	0.3	-0.4	0.1	0.1	0.0	-0.6	-7.5	-1.5	-0.6	-0.7	-0.7	-0.4	-0.3	-1.6	-1.7	-0.7	-0.1
south box	0.0	-9.2	-0.2	-9.2	0.2	-1.1	0.1	-0.1	-0.1	0.0	-0.3	-9.2	-1.8	0.5	0.4	0.4	-1.8	-0.4	1.5	1.8	0.5	0.2
east box	-0.3	7.3	0.3	7.3	0.0	-1.1	0.0	-0.0	0.2	-0.0	-1.2	7.3	-2.0	-2.0	-0.6	-0.6	1.2	-0.4	-0.4	-0.1	-0.5	-1.1
west box	0.0	11.3	-0.2	11.3	0.7	0.9	-0.0	0.0	-0.1	0.0	1.0	11.3	0.1	-0.1	0.0	0.0	1.2	0.1	-1.0	-0.5	0.3	0.3
Nordic Seas	**-0.1**	**1.9**	**0.1**	**1.9**	**1.9**	**-0.9**	**-0.3**	**0.0**	**0.1**	**0.0**	**-1.2**	**1.9**	**-5.2**	**-0.8**	**-0.8**	**-0.8**	**0.1**	**-1.0**	**-1.5**	**-0.5**	**-0.4**	**-0.7**
Denmark Strait	4.0	3.4	3.6	3.4	3.9	3.6	1.5	1.2	-0.1	4.4	3.8	3.4	4.5	2.3	4.2	4.1	3.3	3.8	4.0	3.4	4.2	4.0
Barents Sea Opening	0.8	1.9	1.4	1.9	0.0	2.2	1.0	0.6	-0.4	2.3	1.8	1.9	2.0	1.1	1.3	1.2	2.0	1.7	1.2	1.0	1.2	1.0
Fram Strait	-2.0	-3.1	2.5	-3.1	-4.0	-3.7	-1.0	-1.0	0.0	-3.2	-2.9	-3.1	-1.2	-2.0	-2.0	-2.1	-3.1	-2.1	-1.3	-2.0	-1.5	-2.0
Skagerrak	-0.07	0.3	0.4	0.3	-0.0	0.0	0.0	0.0	-0.0	0.3	0.4	0.3	0.3	-0.0	-0.0	-0.0	-0.0	-0.0	-0.0	-0.0	-0.1	-0.1
Greenland-Norway	-1.3	-1.4	-0.7	-1.3	-0.8	-2.2	-0.4	-0.4	-0.1	-1.0	-3.0	-1.3	-2.5	-1.1	-1.9	-2.2	-0.3	-1.2	-2.1	2.8	-1.5	-2.1
Iceland-Svalbard	1.6	4.1	1.2	4.1	1.6	1.2	0.1	0.3	0.0	1.2	1.3	4.1	1.8	0.4	1.7	1.2	0.9	1.4	0.1	-0.8	2.2	2.2
Iceland-Scotland	-2.8	-3.9	-2.3	-3.9	-4.0	-1.2	-1.2	-0.8	0.4	-3.1	-1.0	-3.9	0.1	-1.6	-2.8	-2.4	-2.4	-2.3	-2.4	-2.0	-3.5	-2.4
Total AW inflow across GS Ridge	6.1	6.5	2.6	6.5	6.5	5.0	1.6	-1.7	-0.9	5.9	4.6	6.5	2.3	4.4	5.1	5.1	2.9	4.3	4.2	4.4	5.3	5.3
AW inflow through eastern DS	0.5	0.6	0.6	0.6	0.6	0.6	0.6	0.4	-0.9	0.5	0.5	0.6	0.5	0.7	0.5	0.5	0.6	0.5	0.7	0.4	0.5	0.5
AW inflow across IS Ridge	5.6	6.8	2.9	6.8	6.9	5.3	1.9	2.1	1.1	6.3	5.1	6.8	2.8	4.6	5.6	5.6	3.3	4.7	5.0	5.1	5.7	5.7
net northward flow of NAW above 600-800m	1.8	1.6	1.8	1.6	1.6	1.0	1.0	0.4	0.3	1.5	1.6	1.6	1.4	1.2	1.6	1.6	1.3	1.5	1.6	1.6	1.7	1.5
net northward flow of NCW (GN section)	0.6	0.6	0.7	0.6	0.6	0.6	0.6	0.5	0.3	0.6	0.6	0.6	0.6	0.5	0.6	0.6	0.5	0.6	0.6	0.6	0.6	0.6
net outflow of AW into Barents Sea	1.0	1.1	1.0	1.1	1.1	1.1	1.0	1.0	0.7	1.1	1.1	1.1	1.2	0.8	1.0	1.0	1.8	1.0	1.0	1.0	1.1	0.9
net northward flow in WSC through FS	2.6	2.2	2.8	2.2	2.0	2.0	3.2	1.5	3.3	2.2	2.2	2.2	2.9	0.0	2.7	2.6	2.4	1.9	2.9	2.6	2.8	2.6
net AO outflow through FS: total	6.8	7.4	7.4	7.4	7.9	7.8	6.2	6.1	6.2	7.5	7.3	7.4	6.2	5.3	6.8	6.8	7.5	6.0	6.3	6.7	6.4	6.7
deep waters	3.2	3.4	3.6	3.4	3.7	3.7	2.8	2.7	2.7	3.5	3.5	3.4	2.8	2.4	3.1	3.2	3.9	2.8	2.9	3.1	2.9	3.1
surface/IW	3.6	4.0	3.8	4.0	4.2	4.1	3.4	3.4	3.5	4.1	3.9	4.0	3.3	2.9	3.6	3.7	3.6	3.2	3.4	3.6	3.6	3.7
PW inflow through western FS	1.0	1.2	1.2	1.2	1.2	1.2	1.1	1.1	0.8	1.2	1.0	1.2	1.0	0.8	1.0	1.0	1.0	1.1	1.0	1.0	1.1	1.0
net southward flow in EGC in FS	5.0	5.7	5.8	5.7	6.1	6.0	4.8	2.4	3.0	5.8	5.5	5.7	4.6	2.6	5.0	5.2	5.6	4.5	4.7	5.1	4.9	5.1
EGC at ~75°N: to 3080m offshore	8.1	9.0	6.6	9.0	8.0	8.2	4.0	3.1	3.4	7.9	8.2	9.0	8.2	4.2	8.1	8.2	8.0	7.5	8.0	8.3	8.3	6.8
to 3440m offshore	13.0	14.9	11.7	15.0	13.4	13.5	9.2	8.0	8.3	13.3	13.7	14.9	13.7	5.0	13.2	13.3	12.6	12.6	13.2	13.5	13.3	12.1
Total IW/DW overflow over GS Ridge	6.0	5.8	5.0	5.8	6.2	6.3	2.7	2.4	1.1	6.7	6.3	5.8	6.4	4.7	6.1	6.1	4.6	4.9	5.4	5.1	6.0	6.1
IW/DW overflow through DS	2.9	2.6	2.7	2.6	2.9	2.7	0.6	0.3	-0.8	3.3	2.8	2.6	3.2	1.7	3.0	2.9	2.2	2.7	2.4	2.0	3.1	2.9
IW/DW overflow across IS Ridge	3.1	3.3	2.3	3.3	3.3	3.5	2.1	2.0	1.8	3.4	3.5	3.3	3.1	3.1	3.1	3.2	2.4	2.1	3.0	3.1	2.9	3.2

HEAT FLUXES (TW)	Standard Solution	State 1	State 2	State 3	State 4	State 5	State 6	State 7	State 8	State 9	State 10	State 11	State 12	State 13	State 14	State 15	State 16	State 17	State 18	State 19	State 20	State 21
Oceanic poleward heat flux across GS Ridge	187	241	117	241	243	167	68	63	10	216	155	241	81	151	186	182	138	159	167	162	202	186
Heat flux through FS into AO	9	7	13	7	6	6	11	15	13	7	8	7	12	-1	9	8	12	6	11	9	9	8
Total heat flux into AO (via FS and BSO)	64	76	71	76	78	80	65	57	32	82	72	76	84	49	64	62	93	64	70	64	68	64
Total heat transport convergence in NS	123	165	46	165	165	86	3	6	-22	135	83	165	-3	102	121	120	44	94	97	98	134	123

Table 6.3: Volume Transport estimates (Sv) and Heat Fluxes (TW) for the Nordic Seas for the standard solution and the alternative model runs (see specifications in Table 6.2).

GS Ridge Greenland-Scotland Ridge; **IS Ridge** Iceland-Scotland Ridge; **GN section** Greenland to Norway section; **FS** Fram Strait; **DS** Demark Strait; **AO** Arctic Ocean; **BSO** Barents Sea Opening; **AW** Atlantic Water; **PW** Polar Water; **IW** Intermediate Water; **DW** Deep Water; **NCW** Norwegian Coastal Water; **WSC** West Spitsbergen Current; **EGC** East Greenland Current.

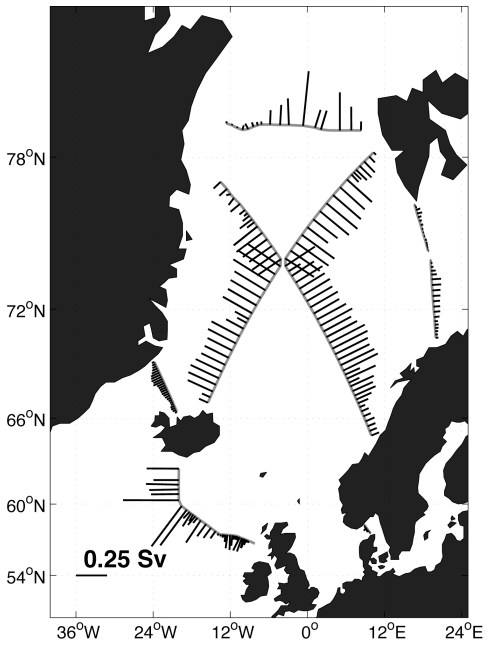

Figure 6.1: The magnitude of the formal errors in volume transport (Sv) for each station pair.

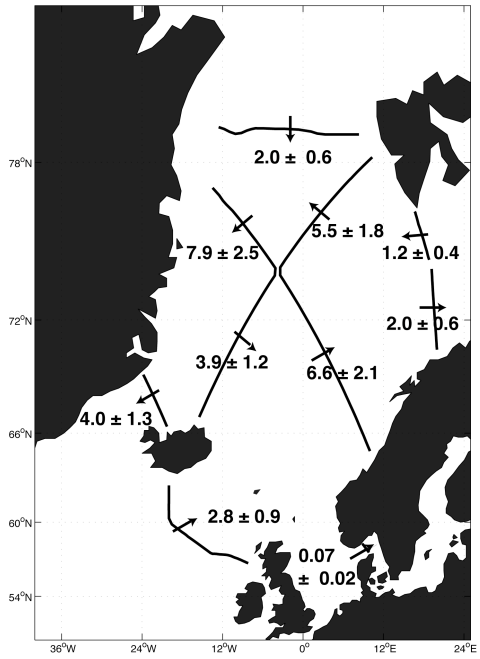

Figure 6.2: Full depth volume transports (Sv) with errors, for each section, calculated from the standard solution and further adjusted for zero net volume flux in each box.

Chapter Seven

Variability in the Circulation

7.1 Introduction

The variability of the circulation and fluxes of the Nordic Seas is the subject of this chapter. Winter hydrographic data, over a reduced region of the Greenland Sea, is used to consider seasonality in the hydrography, particularly within the central Greenland Sea. Elements of the winter circulation are then inferred using a combination of this data and the summer mean general circulation (Chapter 5). Aspects of ocean climate are also discussed to give an indication of how typical the oceanic and atmospheric conditions were during the summer of 1999.

7.2 Seasonal variability in hydrography

A secondary winter cruise, JM3, was conducted under the auspices of the ARCICE programme over a reduced region of the Nordic Seas during winter 2000 (described in Chapter 3). This cruise provided winter hydrographic data mainly within the Greenland Sea. In particular, a number of the summer JR44 stations were reoccupied providing winter repeats for direct comparison. The positions of these stations are shown in Figure 7.1.

The seasonal changes in the properties of the upper water column are revealed by direct comparisons between the summer and winter hydrography. The winter data can be divided into different regions by location and water mass characteristics; *(i)* central Greenland Sea, *(ii)* eastern edge of the Greenland Sea gyre and over Mohns Ridge, *(iii)* western edge of the Greenland Sea gyre and onto the continental slope off the coast of east Greenland, *(iv)* to the south of the Greenland Sea gyre, and *(v)* within the Norwegian Basin. Figure 7.2 illustrates the hydrographic characteristics of stations occupied in both summer and winter in each of these regions. The locations of these five stations are marked in red on Figure 7.1.

Within the central and eastern parts of the gyre of the Greenland Basin (Figure 7.2 (i)) the main differences in the temperature and salinity characteristics are the absence of ASW on the winter stations. This is a surface water mass present during the summer, formed by a combination of summer heating and mixing with the cool, fresh PW. On the winter stations the summer thermocline is eroded and the winter mixed layer extends to depths of about 700–900 m. A similar pattern is observed within stations towards the east of the gyre (Figure 7.2 (ii)).

To the west of the Greenland Sea gyre, within the eastwards extension of the EGC, the summer and winter profiles differ down to depths of ~1000 m or deeper. On the station illustrated in Figure 7.2 (iii) the signal of rAW above ~400 m is absent on the winter station. This suggests that during summer the flow of rAW extends further east into the Greenland Basin than in the winter months. To the south of the Greenland Sea gyre (Figure 7.2 (iv)), near to the Jan Mayen Fracture Zone, the

hydrographic properties converge at depths of ~500 to 600□m in the summer and winter stations. The summer thermocline and halocine are eroded to leave deep mixed layers in the winter profiles.

Within the Norwegian Basin (Figure 7.2 (v)), the salinities show the deep winter mixed layer to extend to about 400□m. In general, the summer profile is fresher than the winter, with a shallow mixed layer of ~150□m below the fresh surface waters. In winter there are lower temperatures down to depths of about 800□m.

7.3 Observations in the central Greenland Sea

The JM3 cruise occupied a number of stations within the central Greenland Sea, providing winter hydrographic data within the cyclonic gyre centred over the Greenland Basin. The region of this gyre is of particular interest with respect to the occurrence or absence of deep convection and the data provide an opportunity to study how the hydrography within the Greenland Sea gyre changes from summer to winter.

During past decades the occurrence of deep convection within the Greenland Sea (see section 2.3.1) has varied considerably. The water temperature at 2000□m is generally regarded to be an indicator of the intensity of deep water renewal driven by winter cooling over the Greenland Sea (Aagaard, 1968). Based on oceanographic cruises to the central Greenland Sea between 1991 and 2000, using temperature and salinity data, Budeus et al. (1998) conclude that winter convection was extremely weak after 1993, not even ventilating the intermediate waters, despite increasing salinities in the upper layers. Tracer inventories from the same cruises, however, do show that some ventilation of the deeper waters did occur, with the strongest ventilation between 1994 to 1995 and 1999 to 2000 (Bonisch et al., 1997; Karstensen et al. 2002). The correlations of temperature with transient tracers confirm a close relation between low temperatures in the deep waters and high rates of deep water formation, and conversely, high temperatures in the deep waters and low formation rates of deep water (Bonisch et al., 1997).

Oceanographic data from 1950 to 1998 has been used to determine the interannual variations in convection and water mass structure in the Greenland Sea (Alekseev et al., 2001). Periods of increased deep water formation occurred in the early 1950s and from the late 1960s to the early 1970s. During the cold winters of 1965 to 1970 there was an intensification of the vertical exchanges within the Greenland and Norwegian Seas, with a high production of cold, fresh GSDW in the central Greenland Sea, and a deepening of the warm and salty waters in the Norwegian Sea. Contrasted with this is the period of reduced deep water formation from the early 1980s to the present (Dickson et al., 1996).

Figure 7.3 to 7.6 illustrate the potential temperature and salinity characteristics of the winter stations in the central Greenland Sea. Figure 7.3 is a classical □/S plot which shows the characteristics of

the water masses observed, particularly evident is the signature of GSDW. Individual station profiles are shown in Figure 7.4, with station 073 indicated in red. On this station convection appeared to occur to a depth of about 900□m, this was the deepest direct observation of convection made on the JM3 cruise. Within the Greenland Sea the summer stations have warm, fresh surface waters from summer heating and ice-melt. In contrast, the winter stations show evidence of a deep winter mixed layer to depths between 700 and 900□m.

Figures 7.5 and 7.6 represent the mean profiles over the region in both the summer and winter data. The mean winter profile shows a mixed water column in which the summer thermocline and halocline have been eroded. In summer, the surface waters are warm and fresh from summer heating and ice-melt. Temperature profiles are almost the same below a depth of about 1000□m in both summer and winter.

Considering the deepest waters (below 2000□m) for stations within the gyre, potential temperatures range between -0.884°C and –1.147°C and salinities range between 34.877 and 34.910. The temperatures of these deep waters have a mean of -1.052°C. This is warmer than many of the classic descriptions of Greenland Sea Deep Water (GSDW), which has been defined to as having temperatures in the region of -1.28°C (Smethie et al., 1986) to -1.242°C (Swift and Koltermann, 1988). This data is further confirmation of warming trends within the deep waters of the Greenland Sea.

Observations have revealed a continuous rise in Greenland Sea bottom temperatures under the absence of deep winter convection (Bonisch et al., 1997). Initial warming has been attributed to mixing with the warmer Arctic Ocean Deep Waters (Canadian Basin Deep Water (CBDW) and Eurasian Basin Deep Water (EBDW) and the lack of the cooling effect of winter convection (Aagaard et al., 1991). Continued warming has since been observed, for example Budeus et al. (1998) noted a steady increase in the temperatures of the deeper waters of the Greenland Gyre of about 0.03°C between 1993 and 1995. Significant warming of the sub-surface waters (200□-□400□m) was also observed during the 1980s progressing to a rapid temperature increase throughout the entire water column during the 1990s (Alekseev et al., 2001). This warming in the upper layers of the interior Greenland Sea gyre has been suggested to originate from an increase in the advection of return Atlantic Water into the region.

7.4 Winter Atmosphere - Ocean Exchanges

The winter atmosphere□-□ocean heat flux exchanges were investigated using the adjusted SOC (Grist and Josey, 2003; Josey et al., 1999) climatology, and the same procedure as for the summer heat flux exchanges (section 5.4).

A summary of the annual and winter fluxes is presented in Table 7.1. Negative values indicate a net heat loss from the ocean to the atmosphere. The annual average values are discussed in section 5.4 and can be compared to those found by Mauritzen (1996b) and Isachsen (2003).

	nordic seas		***north box***		***south box***		***east box***		***west box***	
	Wm^{-2}	TW	Wm^{-2}	TW	Wm^{-2}	TW	Wm^{-2}	TW	Wm^{-2}	TW
Annual	-76	-207	-82	-15	-68	-102	-114	-74	-40	-16
Winter	-139	-381	-118	-22	-137	-207	-202	-131	-88	-23
November	-167	-460	-201	-38	-152	-229	-217	-141	-134	-54
December	-197	-542	-184	-35	-190	-286	-260	-169	-136	-55
January	-195	-535	-157	-29	-197	-297	-270	-175	-88	-36
February	-162	-445	-119	-22	-166	-250	-228	-148	-63	-26
March	-134	-368	-112	-21	-133	-201	-194	-126	-52	-21
April	-65	-177	-84	-16	-52	-79	-115	-75	-20	-8
Surface Area (m^2)	2.7×10^{12}		1.9×10^{11}		1.5×10^{12}		6.5×10^{11}		4.1×10^{11}	

Table 7.1: Atmosphere-Ocean Heat fluxes per unit area (Wm^{-2}), and total (TW; 1 TW = 10^{12} Js^{-1}), over both the Nordic Seas region and the individual inverse boxes. The annual, winter (November to April), November, December, January, February, March and April averages are given for comparison. The surface areas for each region (used in the per unit area calculations) are also quoted. Negative values indicate a net heat loss from the ocean to the atmosphere.

The annual cycle is shown in Figures 7.7 and 7.8. The main conclusions to draw are that the average winter atmosphere - ocean exchanges are considerably larger than the average summer fluxes. This demonstrates how the Nordic Seas contribute to the global climate system by substantial heat loss to the atmosphere during the winter months. The fluxes are largest over the east and south boxes, since it is from the warmer inflowing Atlantic Waters that most heat is lost. As these Atlantic Waters continue on their path through the Nordic Seas (and Arctic Ocean) they are effectively cooled and their density increases (see Chapter 2 for discussion).

7.5 Winter fluxes across the Greenland to Norway Section

Since a complete winter occupation of the Greenland to Norway section is lacking, it was decided to 'manufacture' an estimate of such a section, in order to give some indication of the differences between the winter and summer circulations. This was achieved by 'winterising' the summer section; firstly, the potential temperature and salinity characteristics in the upper part of the water column were adjusted with reference to the winter stations occupied during the JM3/2000 cruise and on the Svinøy section, secondly, the strength of the boundary currents (NAC and EGC) were adjusted with reference to data from the PIMMs drifters and long term current meter measurements, and thirdly, flux balance was required across the section (to 1 Sv).

Using the JM3 winter hydrographic data and data available from Norwegian repeat sections in the Norwegian Sea, the changes in the hydrography of the upper layers of the Greenland to Norway

section are estimated. From the volume, heat and freshwater fluxes across the section, a feasible winter circulation was then be inferred. The locations and depths of the Greenland–Scotland section station pairs are given in Table 7.2.

Section Stn Pair #	Station Pair (JR44)	Lat °N	Lon °E	Depth of shallow station of pair (m)	Mean depth of station pair (m)	Depth of 'bottom triangle' area (m)
1 (1/2)	054 053	77.18	-13.49	245	250	5
2 (2/3)	053 052	76.94	-12.50	245	280	35
3 (3/4)	052 051	76.75	-11.94	305	310	5
4 (4/5)	051 050	76.62	-11.44	305	305	0
5 (5/6)	050 049	76.40	-10.50	270	290	20
6 (6/7)	049 048	76.18	-9.73	270	365	95
7 (7/8)	048 047	76.06	-9.33	460	700	240
8 (8/9)	047 046	75.96	-9.01	940	1215	275
9 (9/10)	046 045	75.83	-8.60	1490	1560	270
10 (10/11)	045 044	75.72	-8.26	2030	2275	245
11 (11/12)	044 043	75.56	-7.76	2515	2940	425
12 (12/13)	043 041	75.32	-7.02	3365	3435	70
13 (13/14)	041 040	75.06	-6.27	3505	3525	20
14 (14/15)	040 039	74.79	-5.53	3545	3560	15
15 (15/16)	039 038	74.51	-4.81	3570	3580	10
16 (16/17)	038 037	74.24	-4.11	3590	3595	5
17 (17/18)	037 036	73.95	-3.42	3025	3310	285
18 (18/19)	036 035	73.73	-2.91	2955	2990	35
19 (19/20)	035 034	73.52	-2.44	2955	3015	60
20 (20/21)	034 033	73.24	-1.81	3070	3120	50
21 (21/22)	033 032	72.95	-1.22	3170	3185	15
22 (22/23)	032 031	72.67	-0.64	2490	2845	355
23 (23/24)	031 030	72.38	-0.08	2275	2385	110
24 (24/25)	030 029	72.09	0.47	2275	2360	85
25 (25/26)	029 028	71.80	1.01	2400	2420	20
26 (26/27)	028 027	71.50	1.53	2305	2355	50
27 (27/28)	027 026	71.20	2.05	2305	2745	440
28 (28/29)	026 025	70.91	2.53	3185	3205	20
29 (29/30)	025 024	70.62	2.98	3220	3250	30
30 (30/31)	024 023	70.32	3.46	3275	3275	0
31 (31/32)	023 022	70.02	3.91	3275	3275	0
32 (32/33)	022 021	69.72	4.34	3275	3275	0
33 (33/34)	021 020	69.42	4.76	3270	3275	5
34 (34/35)	020 019	69.12	5.18	3250	3260	10
35 (35/36)	019 018	68.82	5.59	3055	3155	100
36 (36/37)	018 017	68.60	5.88	2515	2785	270
37 (37/38)	017 016	68.37	6.17	1975	2245	270
38 (38/39)	016 015	68.13	6.46	1515	1745	230
39 (39/40)	015 014	67.93	6.72	1280	1400	120
40 (40/41)	014 013	67.65	7.05	1280	1335	55
41 (41/42)	013 012	67.38	7.36	1385	1430	45
42 (42/43)	012 011	67.15	7.63	1025	1250	225
43 (43/44)	011 010	66.93	7.88	445	735	290
44 (44/45)	010 009	66.69	8.14	310	380	70
45 (45/46)	009 008	66.43	8.42	310	320	10
46 (46/47)	008 007	66.13	8.74	295	310	15
47 (47/48)	007 006	65.81	9.07	295	370	75
48 (48/49)	006 005	65.49	9.39	285	365	80
49 (49/50)	005 004	65.18	9.69	285	320	35
50 (50/71)	004 003	64.89	9.98	340	350	10

Table 7.2: Station Pairs on the Greenland to Norway 'winter' section. Depths refer to the deepest property measurement (on the shallowest station of the pair) interpolated onto a 5db grid.

7.5.1 Hydrography

Firstly, summer and winter data on the repeat stations within the Greenland Sea were examined. This gave an indication of the seasonal changes in the structure of the upper water column in that region. A similar procedure was undertaken with summer and winter data from the Svinøy section in the Norwegian Sea (see section 3.3.7). This section runs parallel to and south of the Greenland to Norway section and extends to a latitude of ~65°N in the Norwegian Sea (Figure 7.1). Since contemporary data from summer 1999 and winter 2000 were made available, the seasonal changes in properties on the Svinøy section were used to determine the seasonal variability in the upper water column of stations at similar longitudes on the Greenland–Norway section. The summer

stations of the Greenland–Norway section were grouped into regions with different oceanic regimes, subject to their location and water mass characteristics.

From the information gleaned from the summer-winter changes between the repeat ARCICE stations and the Svinøy stations, a scheme was constructed whereby the properties in the upper water column of stations on the Greenland to Norway section were adjusted to create a section representative of a winter circulation. The general principle was to find the 'local' winter mixed layer depth and to set the winter mixed layer properties to the summer value at that depth. Figure 7.9 illustrates a station profile within each region for the Greenland to Scotland section, with red and blue representing the summer and winter properties, respectively.

(i) For each of the shallow stations on the Greenland shelf (e.g. Figure 7.9a) the hydrographic properties (temperatures and salinities) above 150 m were set to the respective values at 150 m, and then adjusted to continue the gradient in properties between depths of 200 m and 150 m to the surface.

(ii) For stations within the EGC over the shelf break and shelf slope (e.g. Figure 7.9b) the properties above 500 m were set to the value at 500 m and adjusted to the average gradient in characteristics of the JM3 stations that were similarly sited on the shelf slope (to the south of the Greenland–Scotland section).

(iii) For stations in the central Greenland Basin and towards the east over Mohns Ridge (Figure 7.9c) the JM3 stations provided winter repeats, so that for these locations the properties of the upper water column were adjusted to match the winter stations directly.

(iv) Two of the JM3 stations were located south of Mohns Ridge to the west of the Norwegian Basin, and the summer repeats of these stations were typical of stations within the western part of the Basin. Hence the properties in the upper 500 m at the stations within the western part of the Norwegian Basin (e.g. Figure 7.9d) were set to the respective values at 500 m and adjusted to the gradient in properties of the upper 500 m of the southernmost winter JM3 station.

(v) Further to the east within the basin and over the Norwegian continental slope station profiles were similar to the northern stations on the Svinøy section. The properties of the upper water column were therefore set to the value at ~400 m and adjusted to the average property gradient of the relevant Svinøy stations (e.g. Figure 7.9e).

(vi) Similarly, for the shallow station pairs on the Norwegian continental shelf the hydrographic properties (temperatures and salinities) above 120 m were set to the value at 120 m and then adjusted to the average gradient in characteristics typical of similar coastal stations on the Svinøy section (e.g. Figure 7.9f).

7.5.2 Velocity Field

There is no simple solution when it comes to calculating the winter geostrophic velocity field. As has already been discussed (section 4.5.1), it is not appropriate to select a level of no motion at the sea-bed over the region of the Nordic Seas. The measurements of the summer direct velocity field show the boundary currents (EGC and NAC) to be primarily barotropic, but also that bottom velocities over the deep basins are non-zero, and of the order 5–10 cms^{-1} in places, in contrast to the classic picture of weak (around zero) geostrophic flow in the deep basins.

Jakobsen et al. (2003) investigated the surface circulation of the Nordic Seas using current data obtained from satellite-tracked drifters. They found a seasonal intensification of the circulation during winter over most of the Nordic Seas. The strongest intensification was found in the boundary currents and jets associated with topographic features. The winter increase of the flow was suggested to be of the order 5 cms^{-1}, although stronger (an increase of up to 15 cms^{-1}) in some regions, for example over the Norwegian continental slope. Long term measurements with moored instruments have also provided evidence of such seasonal variability. In the NAC, near 63°N, Orvik et al. (2001) found an annual cycle in which the winter transports (~6 Sv and 4 Sv in the eastern and western branches, respectively) were approximately double the summer transports (~3 Sv and 2 Sv in the eastern and western branches, respectively). Similarly, in the EGC near 75°N, Woodgate et al. (1999) found a large seasonal variation, with 11±5 Sv in summer and 37±5 Sv in winter. Strong seasonality is also evident in the wind stress curl (Jonsson, 1991). It is positive over most of the Nordic Seas with two maxima in the Greenland Sea (over the southern part of the Greenland Basin, and over the Boreas Basin). In January, the wind stress curl over much of the Greenland Sea is greater than 0.4 Pa per 1000 km, with a maximum exceeding 0.8 Pa per 1000 km. However, during the summer (May to August) there is near zero wind stress curl for the entire region.

During the JM3 cruise, deployments of Pancake Ice Motion Monitors (PIMMs floats) were made in addition to the hydrographic stations (see section 3.3.6 and Figure 7.1). PIMMs floats are an innovative type of freely drifting expendable surface float capable of deployment within open ocean ice fields. They give a novel approach to tracking ice motion and the data obtained from floats deployed on ice floes in the EGC allow estimates of its speed to be made between latitudes of 75°N to 60°N. The mean velocities of the floats deployed in ice show how the speed of the EGC varies with latitude (Figure 7.10). These estimates were based on data from 5 floats and an average of 350 values over each degree of latitude. The current is faster further north where it forms part of the Greenland Sea Gyre and has an average speed of the order 60 cms^{-1} in the region of the Greenland–Norway section. This is consistent with the results, mentioned above, from the study by Woodgate et al. (1999) using current meters at 75°N. These showed the flow to be to the southwest with individual surface readings of up to 80 cms^{-1}.

Since it is the hydrography of the upper water column (generally above 500□m) that has been adjusted here, initially the summer estimates of the bottom velocity are used for each station pair. A number of alternatives were then considered when referencing the geostrophic velocity field produced from the constructed 'winter' section. These alternative initial fields were based on *(i)* bottom referenced geostrophy, *(ii)* boundary currents (the NAC and EGC) referenced to direct velocities (bottom referenced geostrophy elsewhere), *(iii)* boundary currents referenced to direct velocities and increased to be consistent with observations of the winter intensification reported in the literature, and *(iv)* boundary currents referenced to direct velocities and increased as in *(iii)* and a small increase made to the bottom velocities over the remainder of the section. The scenarios in *(i)* to *(iii)* produced unreasonable circulations in which the cyclonic gyres were not reproduced. It was therefore finally decided to use the scenario in *(iv)* to represent the winter intensification of the circulation; with an increase to the boundary currents (NAC and EGC) by a barotropic adjustment of 5□cms^{-1} and an increase to the bottom velocities over the remainder of the section by a factor of 2 (i.e. a small barotropic adjustment of the order 1 to 2□cms^{-1} for most stations pairs). Empirically this latter adjustment was found to be reasonable.

This is a conservative estimate of the winter increase in flow, but provides a reasonable circulation consistent with the limited data available within the Nordic Seas during winter (see section 7.5.7). The speculative aspects of this winter circulation could be reinforced using satellite altimetry to investigate sea surface height variability, for example.

The full depth summer volume transports calculated from the standard solution and further adjusted for zero net volume flux in each box (Chapter 5; section 5.7) result in a southwards flux of 1.3□Sv across the Greenland□–□Norway section. To constrain the imbalance in the full depth volume fluxes across the winter section to also be ~1□Sv southwards, a small northwards barotropic adjustment (0.1□cms^{-1}) was made. Additionally, topographic constraints were applied over the deep basins of the Greenland and Norwegian Seas below depths of 2800m (the deep circulation in these basins is closed below the depths of Fram Strait and the gaps within Mohns Ridge separating the Greenland and Norwegian Seas). To constrain these deep circulations to zero, further small northwards barotropic adjustments of 0.3□cms^{-1} and 0.9□cms^{-1} were made to stations in the Greenland and Norwegian Seas, respectively. The final net flux over the 'winterised' Greenland to Norway section is 1.1□Sv southwards.

7.5.3 Ekman transport

The winter Ekman transports across the section were calculated using climatological wind stress fields. The transports were calculated from the winter average wind stress field from the SOC climatology (Josey et al., 1998) as described in Chapter 4 (for the summer fluxes). The salinity and temperature transports were calculated relative to a salinity of 34.93 and a temperature of 0°C

respectively. The winter wind stress field over the Nordic Seas is greatly intensified during the winter months, although the ocean beneath the ice covered regions is insulated from this forcing.

The fluxes across the section are calculated to be 0.1□Sv for volume transport, 1.0□Sv□°C for temperature transport, and -0.04□Sv□psu for salinity transport. The fluxes are given as positive northeast towards the Arctic. The error associated with the summer Ekman fluxes was taken to be 20% (see section 5.3), however the associated error for the winter fluxes is likely to be far greater. The SOC climatology uses an ice mask over a large part of the western domain of the Nordic Seas (Alexander and Mobley, 1976), however there is considerable interannual variability in the actual ice cover (Toudal, 1999). In addition to this, the SOC climatology is based on very sparse data, particularly over the Greenland Sea during winter months.

7.5.4 Volume fluxes

The volume transports across each of the sections are summarised in Table 7.3. The transports are given for each layer, for surface waters (e.g. NAW and PW; σ_0□< 27.8), and for the denser intermediate and deep waters (σ_0□> 27.8). The isopycnal σ_0□=□27.8 was selected since, within the domain of the Nordic Seas, it generally implies the separation of the North Atlantic Water (NAW) and the lighter Polar Waters from the denser Intermediate and Deep Waters.

The net transport across the section is ~1.2□Sv to the south in both summer and winter, with net southwards transport below σ_0□= 27.8, and net northwards transport of the lighter waters (1.4□Sv in summer and 8.4□Sv in winter). The depth of the 27.8 isopycnal rises from 200□m on the Greenland Shelf to about 50□m over the Greenland Basin, and then deepens to ~400□m within the Norwegian Sea to the east of Mohns Ridge. The changing depth of the isopycnal across the section accounts for the apparent large northwards flow above, and southwards flow below, without contradicting the conservation of the deeper waters required within the separate basins below sill depth.

Layer	Layer Boundaries	GN summer	GN winter
1	$\sigma_0 < 26.5$	-0.03	-0.18
2	$26.5 < \sigma_0 < 27.0$	-0.12	-0.71
3	$27.0 < \sigma_0 < 27.3$	0.18	1.22
4	$27.3 < \sigma_0 < 27.5$	0.54	2.14
5	$27.5 < \sigma_0 < 27.6$	0.67	2.29
6	$27.6 < \sigma_0 < 27.7$	-0.17	1.08
7	$27.7 < \sigma_0 < 27.8$	0.29	2.52
8	$27.8 < \sigma_0 < 27.95$	0.37	-0.61
9	$27.95 < \sigma_0 < 28.0$	-1.26	-2.34
10	$\sigma_0 > 28.0$, $\sigma_1 < 32.73$	-1.03	-2.04
11	$32.73 < \sigma_1 < 32.76$	-0.71	-1.35
12	$32.76 < \sigma_1 < 32.78$	0.20	-3.18
13	$\sigma_1 > 32.78$, $\sigma_2 < 37.45$	-1.01	-0.46
14	$37.45 < \sigma_2$	0.78	0.50
1-7	$\sigma_0 < 27.8$	1.36	8.37
8-14	$\sigma_0 > 27.8$	-2.66	-9.49
1-14	**Full Depth**	**-1.30**	**-1.12**

Table 7.3: Volume transports (Sv) across the Greenland to Norway (GN) section, for summer and winter, and for each layer, for surface waters (e.g. NAW and PW; $\sigma_0 \leq 27.8$), for the denser intermediate and deep waters ($\sigma_0 > 27.8$) and full depth. Positive transports are directed northwards towards the Arctic.

To ascertain the magnitude and pathways of the winter circulation, the cumulative transports along the section were derived for the layers defined by isopycnals (σ_0, σ_1 and σ_2) and pressure. These are illustrated in Figures 7.11 and 7.12. For comparison the summer circulation across the section is illustrated in Figure 5.36. The following discussion of the winter circulation along the Greenland-Norway section begins to the west of the section on the Greenland continental shelf, and considers the flow of particular water masses defined by temperature and salinity properties (Table 5.1).

To the far west of the section, there is a southwards flow of surface waters on the shallow continental shelf off Greenland. Here, the 3.7 Sv flow is divided equally between GSSW ($\theta \leq$ 1.5°C), PW (–1.5 $\leq \theta \leq$ 0°C) and an underlying layer of rAW (0 $\leq \theta \leq$ 2°C). This compares to a total southwards flow of 0.9 Sv in summer.

Beyond the shelf, over the continental slope and into the Greenland Basin, there is a broadly southwards flow in the EGC. If the EGC is taken to include the southwards transport on the shelf, then it is ~33.7 Sv in winter, compared to 11.3 Sv in summer. Beyond the shelf break there is southwards transport of a further 0.6 Sv PW (both summer and winter) below which there is a layer of waters characteristic of rAW (0 $\leq \theta \leq$ 2°C). This has a magnitude of ~4.3 Sv in both summer and winter. Below 2000 m there is a southwards flow of 7.7 Sv (c.f. a summer transport of 1.7 Sv). This is a mixture of GSDW and AODW. Above this depth, the EGC carries ~20.7 Sv intermediate waters characteristic of the Greenland Sea, defined as GSAIW (-1 $\leq \theta \leq$ 0°C and 34.8 $\leq S \leq$ 34.9). This compares to a transport of 4.1 Sv of GSAIW in summer. There is, as expected, no winter signal of ASW. This is present in summer as a thin surface layer over the deeper part of the basin, formed by summer heating and mixing with the fresh PW.

The northward limb of the Greenland Sea gyre is sandwiched between the southward flowing EGC and the Arctic Front west of Mohns Ridge. In winter, the northwards flow has a magnitude of 24.8□Sv over the full water column (approximately double the summer transport). Below 2000□m there is a northwards transport of 7.4□Sv, this is a mixture of the deep GSDW (6.7 Sv if defined as □□□□°C) and denser forms of GSAIW. This closes the deep part of the gyre such that there is no net transport out of the Greenland Sea below the topographic constraints of the basin. There is no signal of rAW in this northwards limb of the gyre, in either summer or winter, indicating that rAW crosses the Greenland□Norway section in the EGC and continues south with little interaction with the intermediate waters within the Greenland Sea gyre itself. The northwards transport of ~18.0□Sv of GSAIW compares to a summer transport of 8□Sv. There is no signal of AODW (S□□□4.90) in this northwards limb of the gyre, suggesting that is carried south in the deeper parts of the EGC rather than forming part of the deep waters of the Greenland Sea Gyre.

East of the Arctic front and Mohns Ridge, the southwards limb of the cyclonic circulation of the Lofoten Basin is evident, although there is complicated flow in the surface waters due to the individual branches of the northward Atlantic water inflow, which are separated by southward recirculations. In winter, over this part of the section, the 3.0□Sv flow in the upper 500□m of the water column is southwards. If NSDW is defined as □□□0.5°C then during winter there is a 25.4□Sv southward flow, compared to the summer flow of 13.3□Sv to the south. If, alternatively, NSDW is defined as the waters below ~1500□m then the transport would be 20.0□Sv in winter (c.f. 10.4□Sv in summer). Defining NSAIW to be –0.5□□□□□□°C, there is a southwards flow of 6.0□Sv in winter (c.f. 1.2□Sv in summer).

The northward limb of the cyclonic circulation in the Lofoten Basin dominates the circulation in the southern part of the Lofoten Basin. Within this region there is a northwards transport of 12.0□Sv of NAW in winter. The total winter northwards transport of NAW in the Norwegian Sea as it crosses the Greenland-Norway section is therefore ~9□Sv (compared to a summer NAW inflow of 3.4□Sv). This is comparable to the summer□□winter variations of ~□□Sv to 10□Sv quoted by Orvik et al. (2001). In winter, the majority of the transport is concentrated on the Norwegian Slope. East of the NAW inflow, on the continental shelf off Norway there is a 1.8□Sv flow of NCC (c.f. 0.7 in summer). This buoyant coastal current is confined to the shelf region near in to the coast. It is created mostly by the freshwater supply to the Nordic Seas from the Baltic Sea which has a pronounced maximum in spring (Gustafsson, 1997), and hence winter minimum would be expected. For the purposes of this study, however, no further adjustment was made to correct this. Turning to the deeper waters there is northwards flow of NSDW of 21.6□Sv in winter (c.f. 8.2□Sv in summer). If defined as waters below 1500□m, this transport of NSDW is reduced to 14.4□Sv (c.f. 6.9□Sv in summer). This suggests that there is southwards transport of the deep waters into the Norwegian Basin, of the order 4□□□Sv, in both summer and winter. Above the deep waters, the intermediate

waters are defined as NSAIW. If we assume waters below 1500 m to be NSDW, then the northwards transport of NSAIW in winter is 12.6 Sv (c.f. 1.0 Sv in summer).

7.5.5 Heat fluxes

The winter heat flux across the section Greenland – Norway section is 298 ± 100 TW (see section 7.5.7 for error analysis). This is three times greater than the summer heat flux (90 TW). For both summer and winter most of the heat flux across the section is confined to the NAC carrying the warm Atlantic inflow.

Some studies of the Atlantic inflow do suggest a summer minimum in heat transport. Orvik et al. (2001) observed a 2:1 ratio in the heat transport between winter and summer in the eastern branch of the NAC in the Svinøy section. A similar seasonal signal was also seen by Pistek and Johnson (1992) and Skagseth and Orvik (1999). However, these studies were restricted to the depth-dependent geostrophic component.

Figure 7.12 shows that the net heat loss over the Greenland Sea is the same during both summer and winter, i.e.there is no net effect on the heat fluxe within the Greenland Sea during winter. The seasonal difference, and most of the heat transport, occurs within the NAC over the Norwegian continental slope.

7.5.6 Freshwater fluxes

Ignoring net throughflow in the Nordic Seas, and thus assuming zero net mass flux, then

$$F + V = 0 \qquad 7.1$$

and so,

$$\bar{S}\,F + \bar{S}\,V = 0 \qquad 7.2$$

with terms defined as for section 4.2.4. Assuming steady state (i.e. the ocean is neither losing nor gaining salt), the net salinity flux across the Greenland-Scotland section is given by

$$\int\left(S\,v\right) dx\,dz = \bar{S}\,V + \int\left(S'\,v'\right) dx\,dz = 0 \qquad 7.3$$

so equating equation 7.2 and 7.3,

$$\bar{S}\,F = \int\left(S'\,v'\right) dx\,dz \qquad 7.4$$

and hence the freshwater flux, F, for the section can be derived following

$$F = \frac{1}{\bar{S}} \int\left(S'\,v'\right) dx\,dz \qquad 7.5$$

The derived winter freshwater flux is equal to a southwards freshwater flux of 0.130 ± 0.042 Sv ($\bar{S}$ = 34.841). The equivalent summer freshwater flux is 0.059 ± 0.019 Sv ($\bar{S}$ = 34.802).

7.5.7 Error analysis

The scenario presented above is likely to be the closest representation of the winter circulation that can be recreated with the data available (see section 7.5.2). This is, however, a partly subjective estimate of the circulation, but at least gives an indication of the seasonal variability within both the boundary currents (NAC and EGC) and the interior of the Nordic Seas.

Further sensitivity tests were conducted changing the depth of the winter mixed layer by ±100m, and changing the barotropic adjustment by ±50%. These provide a check on the reasonableness of the assumptions made in the construction of the 'winter' section. They also give an estimate of the errors in the net fluxes (Table 7.4). With regards to the heat fluxes, the sensitivity tests suggest that all the variability occurs over the Norwegian Slope (within ~300km of the Norwegian coast) leading to an error of 34%. Although the 'winterised' section cannot be expected to describe the details of the winter circulation with any degree of certainty, it is encouraging that major sensitivity tests provide error estimates of ~30%. The implication is that even if not accurate in its details, the winter circulation does nevertheless give a reasonably robust indication of the net winter fluxes.

Sensitivity test	ΔV (Sv)	ΔQ (TW)
changing depth of mixed layer by +100m	-1.8	+91
changing depth of mixed layer by -100m	+1.7	-124
changing barotropic adjustment by +50%	+0.9	-70
changing barotropic adjustment by -50%	-0.9	+37
Net error	**±1.6Sv**	**±100TW**

Table 7.4: Net errors derived from the net volume fluxes (Sv) and heat fluxes (TW) across the Greenland to Norway section from sensitivity tests. ΔV is the change in volume flux (V = -1.1Sv), and ΔQ is the change in heat flux (Q = 298TW).

7.6 Ocean Climate

The Nordic Seas are strongly influenced by both the atmospheric and oceanic climate variability, and ocean climate is therefore an important issue for any study of the circulation. It will, for example, be affected by the dynamics of the atmospheric regime and large scale oceanic anomalies such as pulses of freshwater and ice emitted from the Arctic (Curry and Mauritzen, 2005).

7.6.1 Long-term climate of the Nordic Seas

Climate variability is strongly influenced by recurrent modes of atmospheric behaviour. Although controversy over the North Atlantic Oscillation (NAO) and the Arctic Oscillation (AO) is unresolved (see Chapter 2), the NAO paradigm does describe the dominant recurrent mode of

atmospheric behaviour in the Atlantic sector, extending from the eastern seaboard of the United States to Siberia and from the Arctic to the subtropical Atlantic. It is therefore relevant to note that the hydrographic observations underpinning this thesis were made at the end of an unusual period in the climatic history of the North Atlantic, in which the NAO had increased, within three to four decades, to its most extreme positive state in a 135-year instrumental record (Hurrell and Dickson, 2004; Wohlert, 2002).

The NAO is not the only source of variability in the climate of the North Atlantic, however it does account for about one-third of the variance in Atlantic sea level pressure during December to March. Jung and Hilmer (2001) showed the centre for maximum variability in sea level pressure associated with the NAO to be located further to the east since the late 1970s when the NAO has been predominantly positive.

The significance of the recent long-term shift in the NAO lies within its influence on a wide range of variables, which in turn have the potential to cause change in the marine environment. These include variation in wind speed, atmosphere - ocean heat and freshwater fluxes, distribution and intensity of Atlantic storms, sea surface temperature and intensity of deep convection (e.g. Cayan, 1992; Dickson et al., 1996; Hurrell, 1995; Rogers, 1990).

7.6.2 Climate of the Nordic Seas in the 1990s

One of the major changes in the hydrographic character of the Nordic Seas is the interdecadal change in the depth and intensity of convection, which is part of a large-scale change in the pattern of Atlantic convective activity driven by the changing NAO (Dickson et al., 1996). The intensity of deep convection in the Greenland Sea was progressively suppressed as the NAO amplified to extreme positive values in the early-to-mid 1990s. There is also evidence of a collapse of the domed density structure in the Greenland Sea through the deepening of intermediate and deep isopycnals from the early 1980s (Bonisch et al., 1997). It has also been suggested that a reduced windstress curl (Jonsson, 1991) supported a less intense cyclonic circulation within the Greenland Sea (Rudels and Quadfasel, 1991).

The second major change within the Nordic Seas is in the temperatures of the upper water column. During winters of positive NAO index there has been an extension of the Atlantic winter storm activity towards the northeast resulting in a broadscale cooling over much of the Nordic Seas (Wohlert, 2002), with concurrent warm, moist southerly flow of air along the eastern boundary of the North Atlantic producing increased sea-surface temperatures west of Norway in the domain of the Norwegian Atlantic Current to the Barents Sea.

The third major recent change within the Nordic Seas is the large-scale freshening of the upper ocean within the past three to four decades. This has been partly attributed to the amplified NAO, but also to export of sea ice from the Arctic Ocean (Vinje, 2001), decrease in the local late-winter

production of sea-ice throughout the marginal ice zone of the Nordic Seas in the last 40 years (Deser et al., 2000), and the extension of storm activity to the Nordic Seas under extreme NAO-positive conditions increasing precipitation in the region of the Norwegian Atlantic Current (Dickson et al., 2000). Blindheim et al. (2000) also describe an increased freshwater supply from the East Icelandic Current and a narrowing of the saline Norwegian Atlantic Current.

7.6.3 The Nordic Seas during 1999 / 2000

Regional studies have considered how the ocean climate of the Nordic Seas during 1999 and 2000, in particular, compares to the long-term scenario. Aure et al. (2000) found 1999 to be characterised by a warm summer and autumn, during which there was an increased inflow of Atlantic Water. The warmth of the summer led to abnormally high temperatures in the upper layers of the coastal waters and the eastern and central parts of the Norwegian Sea, the Barents Sea and the North Sea. Interannual variability in the temperature and salinity of the northeast Atlantic (Rockall Trough region) has also been reported by Holliday (2003) who found 'highs' during the late 1990s. She related these changes to the propagation of anomalies developed upstream of the basin, the effect of local air-sea interaction, and the result of changes of regional circulation bringing different water masses into the region. This variability implies a warmer than usual inflow of Atlantic Water to the Nordic Seas during the late 1990s (including the summer of 1999).

There is some evidence that the Atlantic inflow (specifically the summer geostrophic transport referenced to 1000□m) is positively correlated with the February-April NAO index (see Chapter 2 for discussion; Mork and Blindheim, 2000). The appropriate February-April 1999 index is 0.5, a midphase value[1]. Hence, although Aure et al. (2000) found an increased inflow of Atlantic Water, with an average temperature of 0.4□°C above normal, this is unlikely to be towards the extreme state. They also found the central and western parts of the Norwegian Sea to be dominated by a relatively large inflow of fresh, cold, Arctic water.

This thesis focuses on hydrographic observations from summer 1999 so interpretation of results should consider; *(i)* that waters in the Atlantic domain of the Nordic Seas may have been of above average temperatures, and *(ii)* there may have been an increased inflow of colder, fresher Arctic waters than is usual. The implication of these factors is a reduced likelihood of the occurrence of deep convection within the Nordic Seas during the winter of 2000. Warmer inflowing waters will increase heat loss to the atmosphere through surface cooling, and this decreases the likelihood of winter erosion of the stratification of the upper waters of the Greenland Sea (through formation of the Odden ice tongue, for example). An increase of freshwater serves to increase stratification, which in turn reduces the likelihood of deep convection. A warmer Atlantic inflow also increases

[1] Jones, P.D., T. Jonsson, and D. Wheeler, Extension to the North Atlantic Oscillation using early instrumental pressure observations from Gibraltar and south-west Iceland., *International Journal of Climatology*, *17*, 1433-1450, 1997.; updated to the present by T.J.Osborne, Climatic Research Unit, University of East Anglia; http://www.cru.uea.ac.uk/~timo/projpages/nao_update.htm.

the melting and retreat of the sea ice cover in the Barents Sea, and increases the spread of Atlantic type waters from the Eurasian Basin into the Marakov Basin within the Arctic Ocean, accompanied by retreat of the cold halocline layer.

Sea level pressure maps show anomalous circulation of the subpolar gyre in the summer of 1999 (see section 4.5.2). The range of this anomaly in sea level pressure is actually greater than the range of the climatological mean for the entire region (Figure 4.12). The anomalous wind field had the effect of forcing the surface currents eastward such that the inflow of Atlantic Water in the NAtlC was confined to the Rockall Trough to the east of the Hatton-Plateau. Caution must therefore be taken if extrapolating from the summer 1999 mean circulation in the southern domain of the eastern Nordic Seas.

Ocean climate in the Nordic Seas during last two decades has been influenced by the increased impact of PW. This has resulted in a reduction in deep convection, leading to a redirection of the low salinity water pathway and widespread freshening of waters within the Nordic Seas. The coordinated increases in GSDW temperature and winter NAO index reflect the correlation between the atmosphere and thermohaline circulation. This is manifested through the stability of upper layers of the water column, which are governed by salinity.

7.7 Analysis of Summer 1999 Circulation

The ARCICE project, of which this thesis forms a part, seeks to determine the oceanic fluxes connecting the Nordic Seas with the Arctic Ocean and North Atlantic. The work of this thesis is novel, in that it is based on a onetime near-synoptic hydrographic survey during the summer of 1999, both closing the major passageways and crossing the interior of the Nordic Seas, and the flux calculations are, for the most part, based on measurements of the direct velocity field as well as geostrophy.

It is necessary to set the 'snapshot' presented by the results of this thesis into the context of decadal change. This will illustrate how representative this circulation is, and how the processes and mechanisms observed should be considered within the context of climate variability.

7.7.1 Comparison to previous work

The fluxes derived from the standard model can be compared to similar studies within the Nordic Seas. In particular, the studies of Mauritzen (1996a and 1996b), Isachsen (2003) and Oliver and Heywood (2003) are relevant to the work of this thesis.

Oliver and Heywood (2003) study the fluxes through the Nordic Seas using the same CTD and LADCP data from the Greenland–Norway section as for this thesis. Comparison of the results shows how the use of additional sections to constrain the fluxes and exchanges modifies the

circulation obtained from their simple inverse model. The major difference between the two studies is the magnitude of the cyclonic circulation of the Greenland Basin. They define the transport of cyclonic circulation in the Greenland Sea Gyre to be 19 Sv, whereas the results here imply a cyclonic circulation of ~10 Sv. The stronger circulation of the Oliver and Heywood (2003) study is closer to the winter strength of the gyre (see section 7.5.4) of 24 Sv. The apparent bias identified in the initial currents is 'fixed' by the box inverse of this thesis to give a more typical summer Greenland Sea gyre (see section 5.5). Oliver and Heywood also suggest the Atlantic inflow to divide into four branches south of the section, following Østerhus et al. (1996): one of which (i) recirculates before the Greenland–Norway section, and the remaining three branches being (ii) 5.3 Sv above the Norwegian continental slope, (iii) 4.3 Sv in the Lofoten Basin, and (iv) 5.0 Sv above the Mohn Ridge slope. These branches are separated by jets of recirculating water with transports of 3.0 and 4.7 Sv, respectively. The net transport of AW towards the Arctic Ocean across the section is thus given as 6.9 Sv. In this thesis, the structure of the Atlantic inflow is interpreted differently, with two major branches identified (east of Mohns Ridge and over the Norwegian Slope) giving an Atlantic inflow of 4.3 Sv.

The Isachsen (2003) study examines the oceanic mass and heat transport through the lateral openings to the Nordic Seas and Arctic Ocean using modern hydrographic data and inverse methods. In the following discussion of the major fluxes, the results from this thesis are given in brackets for comparison. The flow field suggests that the total northward transport of NAW across the Greenland–Scotland Ridge is 9.9 Sv, or 7.9 Sv (7.7 Sv) if local recirculation features in Denmark Strait and Faroe–Shetland Channel are ignored. The net full-depth transport through Denmark Strait is 4.5 Sv (4.0 Sv) southwards into the North Atlantic, while across the Iceland–Scotland Ridge, the net full-depth transport is 4.5 Sv (2.8 Sv) into the Nordic Seas. Similarly, the net full-depth transport through Fram Strait is 0.7 Sv (2.0 Sv) southwards into the Nordic Seas, and 1.1 Sv (0.8 Sv) across the Barents Sea Opening into the Barents Sea.

A study by Mauritzen (1996a and 1996b) uses non-synoptic hydrographic data in a kinematic inverse model to quantitatively evaluate her proposed circulation scheme. An Atlantic inflow to the Nordic Seas of 6.8 Sv (7.2 Sv) over the Iceland-Scotland Ridge was defined, with an additional 0.9 Sv (0.5 Sv) inflow through Denmark Strait north of Iceland. The majority of this continues through the Nordic Seas to the Arctic Ocean, with 1.6 Sv (1.4 Sv) following a path via the Barents Sea and 3.4 Sv (1.8 Sv) flowing north in the WSC through Fram Strait. Mauritzen suggests 1.1 Sv (1.2 Sv) of the Atlantic inflow recirculates in Fram Strait to join the 1.5 Sv (2.0 Sv) inflow of Arctic Atlantic Water (Atlantic Water modified during its passage through the Arctic Ocean) in the EGC. The dense overflow in Denmark Strait is 2.8 Sv (2.5 Sv) composed of 1.9 Sv AAW and 0.8 Sv rAW (1.2 Sv rAW). The total overflow of dense water across the Iceland-Scotland ridge is 2.6 Sv (3.2 Sv), composed of 0.7 Sv North Icelandic Winter Water, 0.6 Sv Intermediate water from the gyres and 1.3 Sv Deep waters.

The major difference between the Mauritzen (1996b) scenario and the circulation presented here is the implication in the former that within the Nordic Seas the Atlantic Water interacts mainly with the atmosphere rather than the surrounding water masses; whereas here almost half the Atlantic inflow is modified or mixes with intermediate waters south of the Greenland - Norway section, resulting in a smaller flow of AW in the WSC into the Arctic Ocean. The Mauritzen (1996b) work is based on data from 11 cruises between 1980 and 1989, whereas this thesis is based on near-synoptic data collected during a survey across the entire Nordic Seas during the summer of 1999. The difference, therefore, can be attributed to the use of near synoptic data from a more recent time period (during which the Nordic Seas were subject to different atmospheric and oceanic influences). However, this study supports the main contention of the circulation constructed from the Mauritzen (1996b) flux model. Most of the transformation of the Atlantic inflow occurs within southeastern part of the Nordic Seas, due to heat loss to the atmosphere during winter cooling. Further water mass modifications occur through isopycnal mixing as the inflow follows pathways through the Nordic Seas and Arctic Ocean.

7.7.2 Main questions and issues

There are a number of important questions that can be asked pertaining to the circulation and water mass transformations in the Nordic Seas. There have been significant changes in recent years within the Nordic Seas. The region has been under the influence of a dynamically different atmosphere as indicated by the NAO index, with significant low frequency variations and a general rise towards an extreme positive phase. In addition to this, the Nordic Seas have become significantly fresher since the 1970's, and deep convection in the Greenland Sea has been much reduced.

An important issue is, therefore, whether or not the circulation was significantly different in 1999 compared to the earlier period, during which it was subject to both a different atmospheric forcing, and more saline conditions. Whether or not the circulation was significantly different, it is important to understand why it was the way it was.

One interesting feature of the circulation derived from the inverse model is that although at the time of the survey, the AW inflow to the Nordic Seas was confined mainly to the Rockall Trough, the preferred solution divides the inflow equally between the Rockall Trough and Iceland Basin pathways. Recent observations of the AW inflow also give an equipartitioned inflow when averaged over the years from 1999 to 2001 (Osterhus et al., 2005). This supports the hypothesis that the circulation derived from the inverse can be extrapolated to give a picture of the conditions during the late 1990's rather than it being confined to the 'snapshot' of summer 1999. The magnitude of the inflow is 8.2±2.6Sv. This is consistent with the recent estimate (derived from observational data from moorings and regular CTD data from the late 1990's) of 8.5Sv (Osterhus et al., 2005) and is close to the classical value published by Worthington (1970). The strength of the

overflows, 2.5±0.8Sv through Denmark Strait and 3.2±1.0Sv over the Iceland-Scotland Ridge, was also not significantly different in 1999 compared to earlier periods.

The major changes appear to be within the interior circulation of the Nordic Seas. In particular, there is no evidence of deep convection occurring within either the Greenland or Iceland Sea gyres, and the export of intermediate waters out of the Greenland Sea gyre occurs below the sensitivity levels of the inverse model.

The second important issue concerns the formation of the overflows which give rise to >50% of the dense water transport of the Meridional Overturning Circulation (MOC) of the North Atlantic. Is formation mainly "pathway convection" due to cooling along the northward path of the inflowing Atlantic Water, is it due to deep convection in the gyres of the Greenland and Iceland Seas, or is it a consequence of brine rejection as ice freezes? Each of these processes is likely to play some role, but what was the relative importance of each during the summer of 1999, and has it changed since earlier times? Perhaps it is not possible to assign a relative importance from the data used in this thesis, but if not then why?

Results from this study suggest that the main sources of the dense northern overflows during the summer of 1999 and winter of 2000 were a combination of water mass transformations within the inflowing Atlantic Water through heat loss in the southern parts of the Nordic Seas, and deep winter mixing. There was no evidence within the gyres of the Greenland and Iceland Seas of what is conventionally known as 'deep convection', although deep winter mixing did extend to depths of ~900m in places. The southern region of the Nordic Seas (i.e. the south box) was more important than the Greenland Sea for water mass transformations, implying a greater importance of pathway convection during 1999. Observations of the spreading of anthropogenic tracers in the Greenland Sea (Visbeck and Rhein, 2000) have, in fact, indicated that some form of turbulent mixing may contribute to the ventilation of the intermediate and deep layers of the Nordic Seas, and the associated diapycnal closure of the MOC. Within the central region of the gyre, results from a tracer-release experiment suggest that, under present conditions vertical mixing may be dominated by rapid year-round turbulent mixing, rather than convection (Watson et al., 1999). Naveira Garabato et al. (2004) also diagnosed intense turbulent mixing across the deep Nordic Seas and much of the Greenland Sea. Dense water formation due to brine rejection through the freezing of ice was likely to have had a relatively minor contribution. Some fraction of the brine enriched shelf water that is formed in the western Barents Sea was topographically diverted so that it drained into the Norwegian Sea (c.f. Schauer, 1995). However, since a saline plume from the Storfjord was traced down to 2000m along the slope in Fram Strait. these dense waters were too deep to directly contribute to the overflows which are of intermediate depth.

To summarise, the main results of this thesis are that water mass transformations suggest ~4Sv of the inflowing Atlantic waters (about half) undergo sufficient densification within the southern part

of the Nordic Seas to provide a source for the overflow waters; ~50% of the overflows are derived from Atlantic Waters (both those components which have been directly recirculated in Fram Strait, and those which have been further modified during the longer passage through the Arctic Ocean); and that since there is no evidence of a net transport of intermediate waters out of the Greenland Sea gyre, the remainder of the overflows must be derived from intermediate water masses originating in the Arctic Ocean and Iceland Sea.

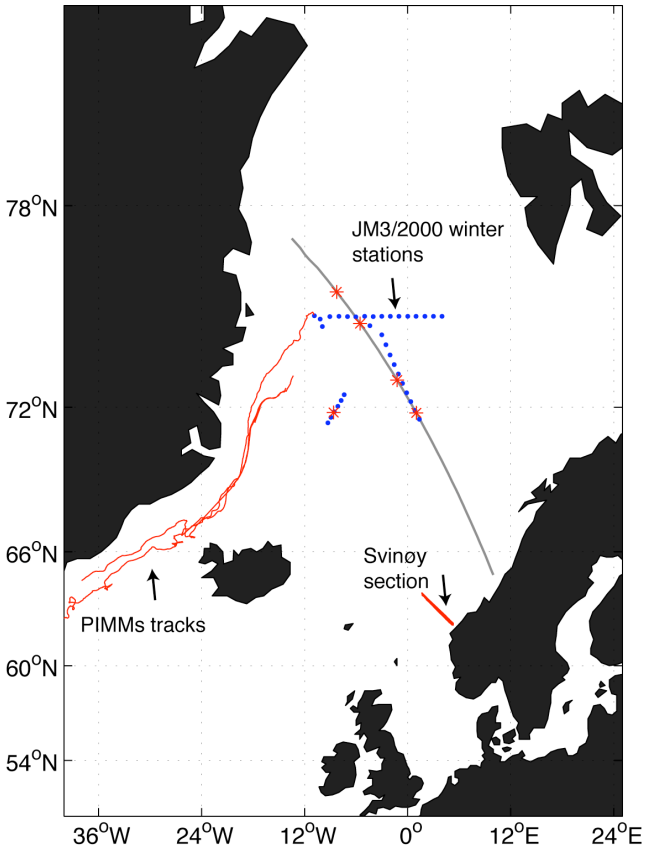

Figure 7.1: Map of the Nordic Seas showing the position of the winter reoccupations of the summer JR44 stations (blue dots) and the five stations described in section 7.2 and illustrated in Figure 7.2 (red asterisks). The tracks of the PIMMs floats are shown in red. For reference, the positions of the Svinøy and Greenland-Norway sections ares also marked in red and grey, respectively.

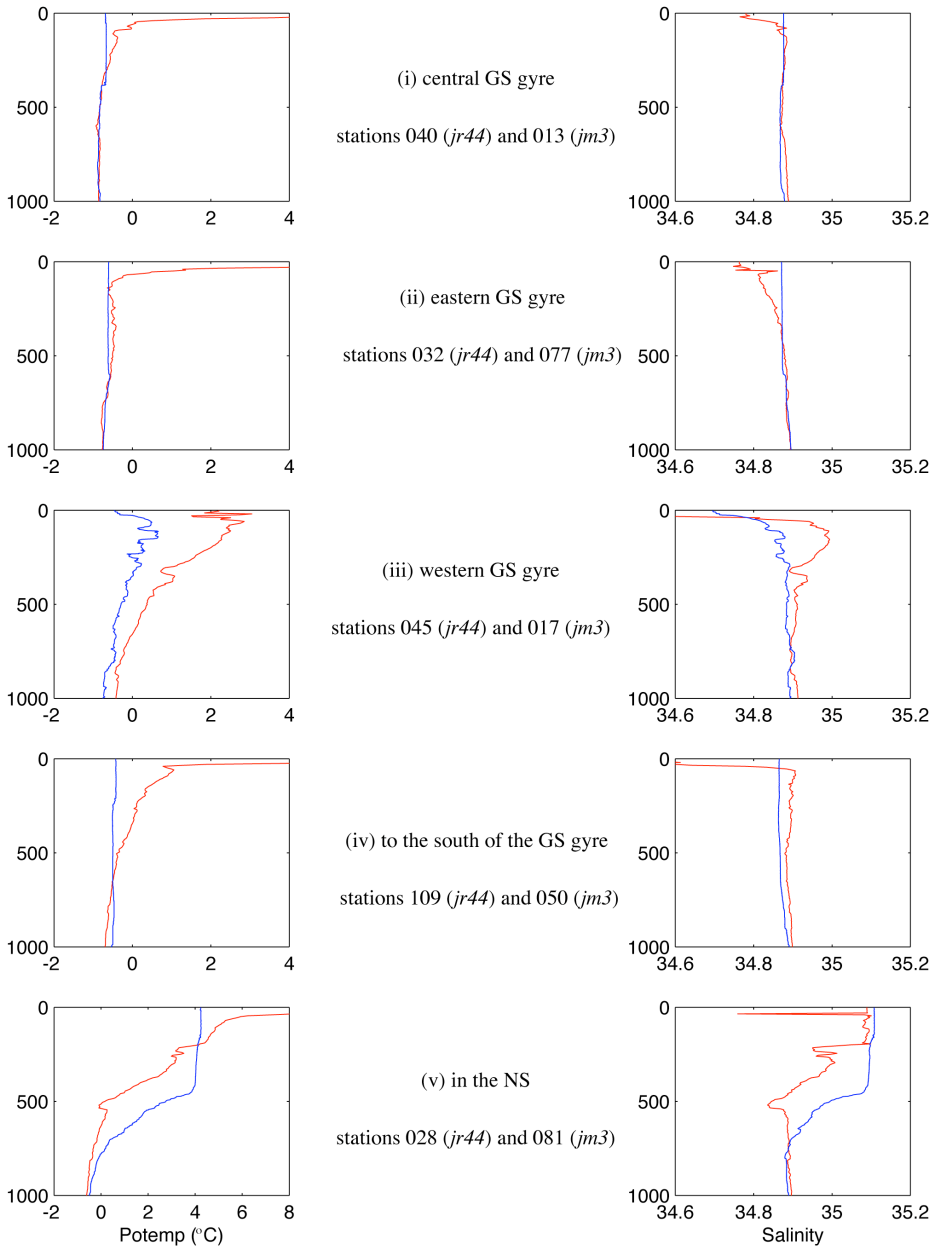

Figure 7.2: Potential temperature and salinity profiles for stations occupied in both summer and winter (i) in the central Greenland Sea, (ii) on the eastern edge of the Greenland Sea gyre and over Mohns Ridge, (iii) on the western edge of the Greenland Sea gyre and onto the continental slope off the coast of east Greenland, (iv) to the south of the Greenland Sea gyre, and (v) within the Norwegian Sea (note increased scale for potential temperature). The JM3 winter profiles are shown in blue, while the equivalent summer JR44 profiles are shown in red. Potential temperatures for the summer stations (left hand panel) are <0°C in the Greenland Sea and <3.5°C in the Norwegian Sea within the upper 500m (off scale in the se diagrams). Pressure (db) is plotted on the y-axis. **GS** and **NS** represent the Greenland and Norwegian Seas, respectively.

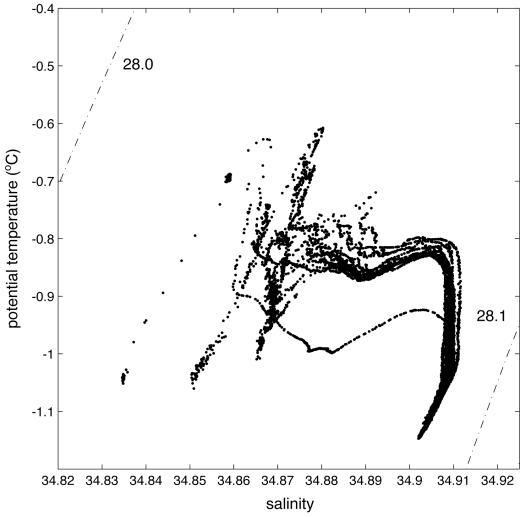

Figure 7.3: Plot of potential temperature and salinity, with contoured isopycnals, for winter stations in the central Greenland Sea.

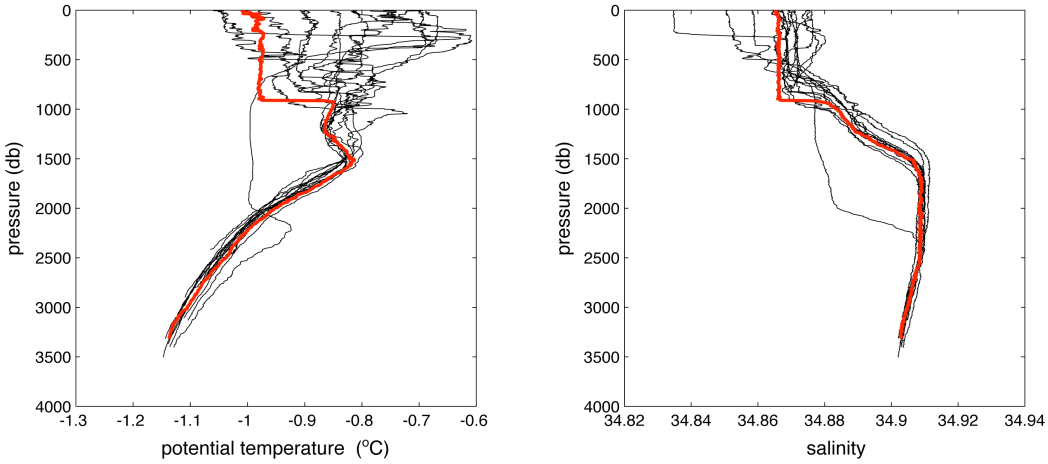

Figure 7.4: Potential temperature and salinity profiles from stations occupied in the central Greenland Sea during winter 2000. The profile from station 073 is given in red indicating the greatest depth to which convection was observed on these stations.

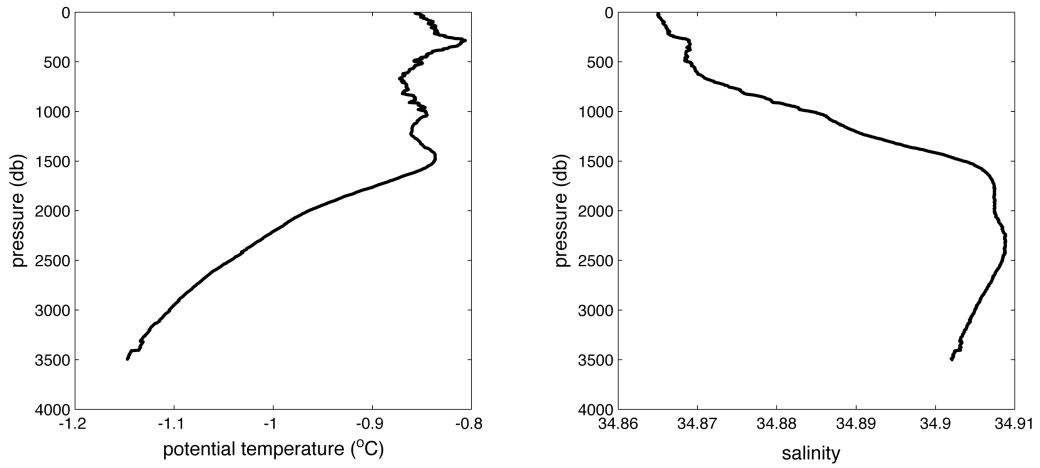

Figure 7.5: The mean profiles of temperature and salinity observed on stations occupied in the central Greenland Sea during winter 2000.

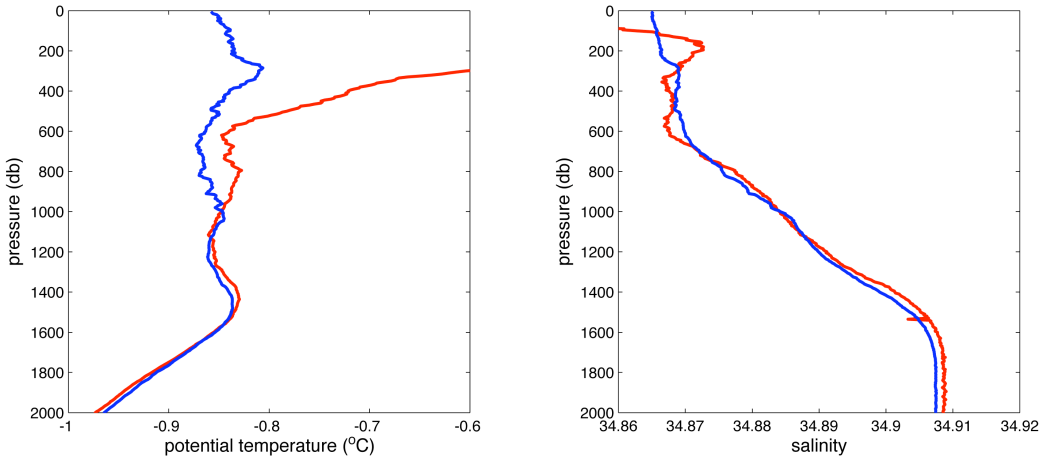

Figure 7.6: Comparison of the mean profiles of temperature and salinity on stations occupied in the central Greenland Sea. Data from winter 2000 and summer 1999 are represented by the blue and red profiles, respectively.

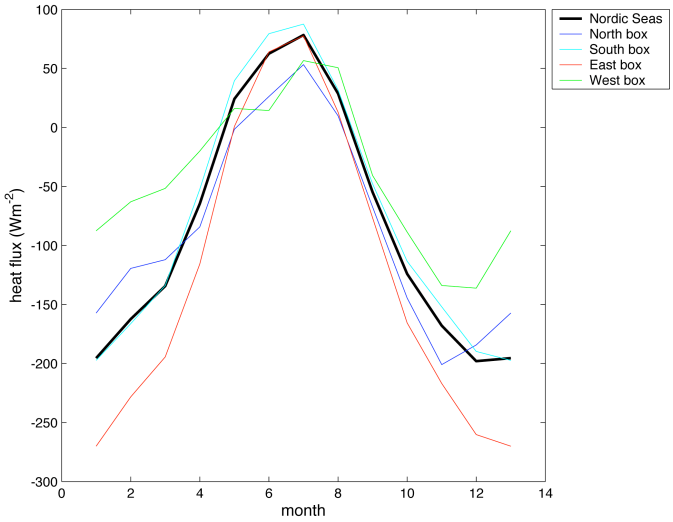

Figure 7.7: Annual cycle in Atmosphere-Ocean Heat fluxes per unit area (Wm^{-2}) over both the Nordic Seas region and the individual inverse boxes, derived from the adjusted SOC climatology. Negative values indicate a net heat loss from the ocean to the atmosphere.

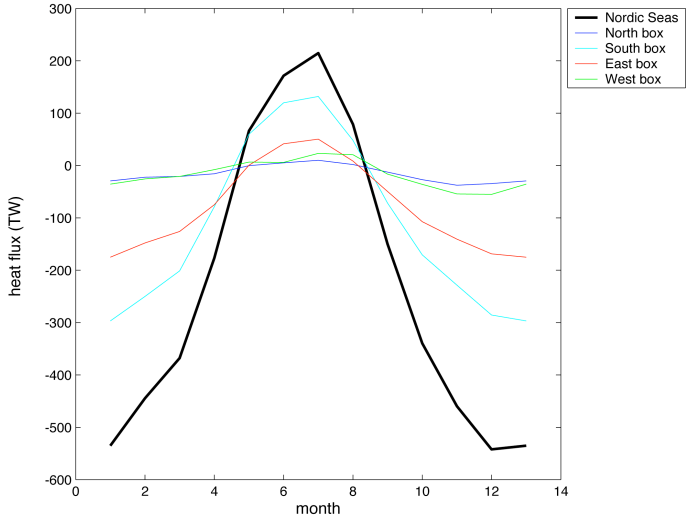

Figure 7.8: Annual cycle in total Atmosphere-Ocean Heat fluxes (TW) over both the Nordic Seas region and the individual inverse boxes, derived from the adjusted SOC climatology. Negative values indicate a net heat loss from the ocean to the atmosphere.

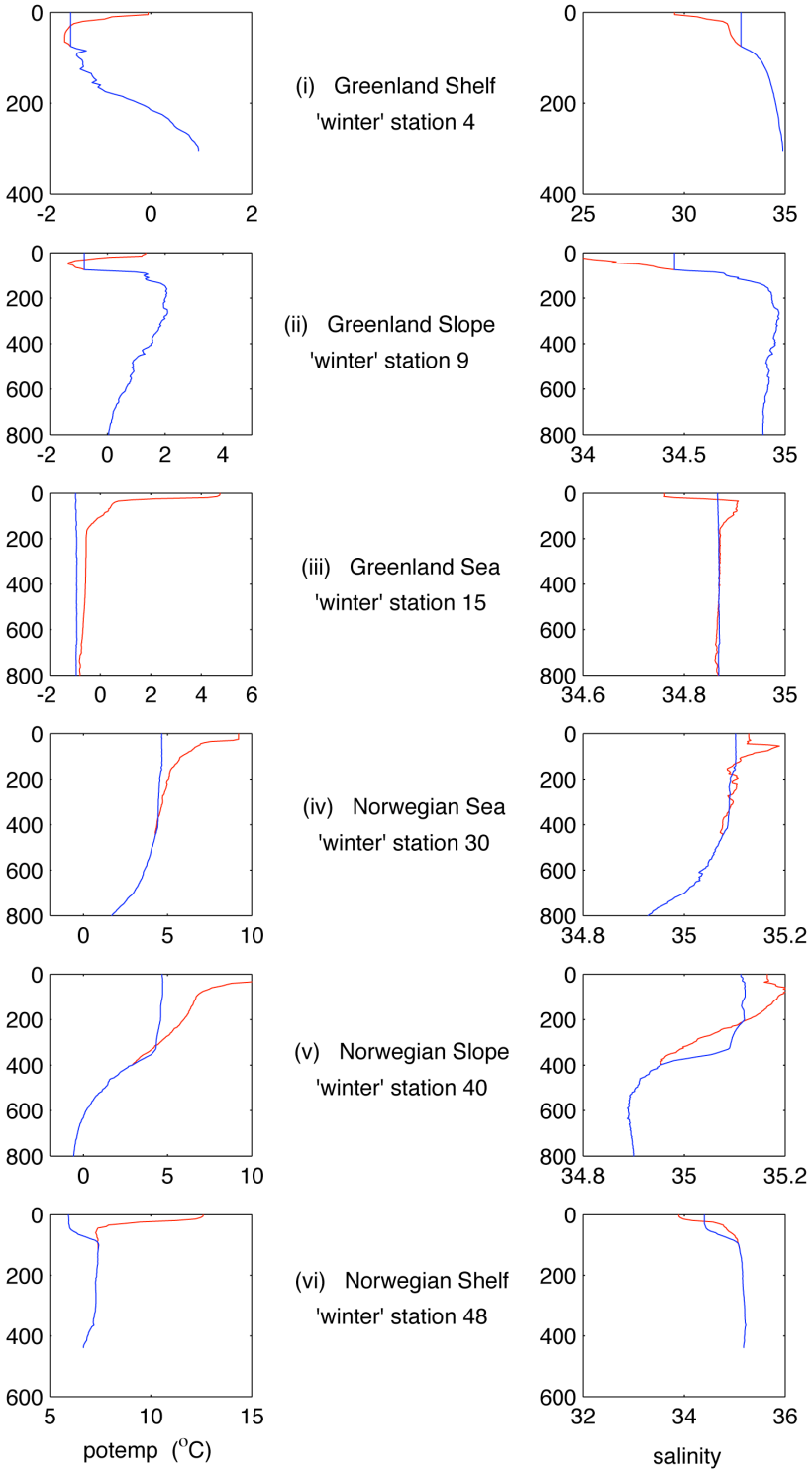

Figure 7.9: Potential temperature and salinity profiles for stations on the 'winter' Greenland to Norway section (see Table 7.2). The adjusted winter stations are shown in blue, while the equivalent summer JR44 profiles are shown in red. Pressure (db) is plotted on the y-axis.

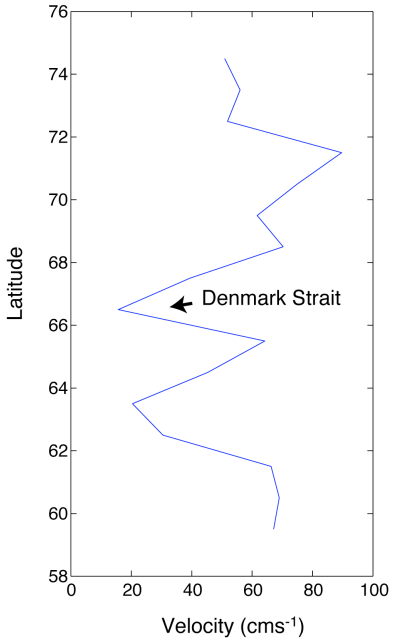

Figure 7.10: Mean velocities (cms^{-1}) of the PIMMs floats deployed in ice against latitude. The upper part of the diagram refers to the velocities between north of Denmark Strait (75°N to 67°N).

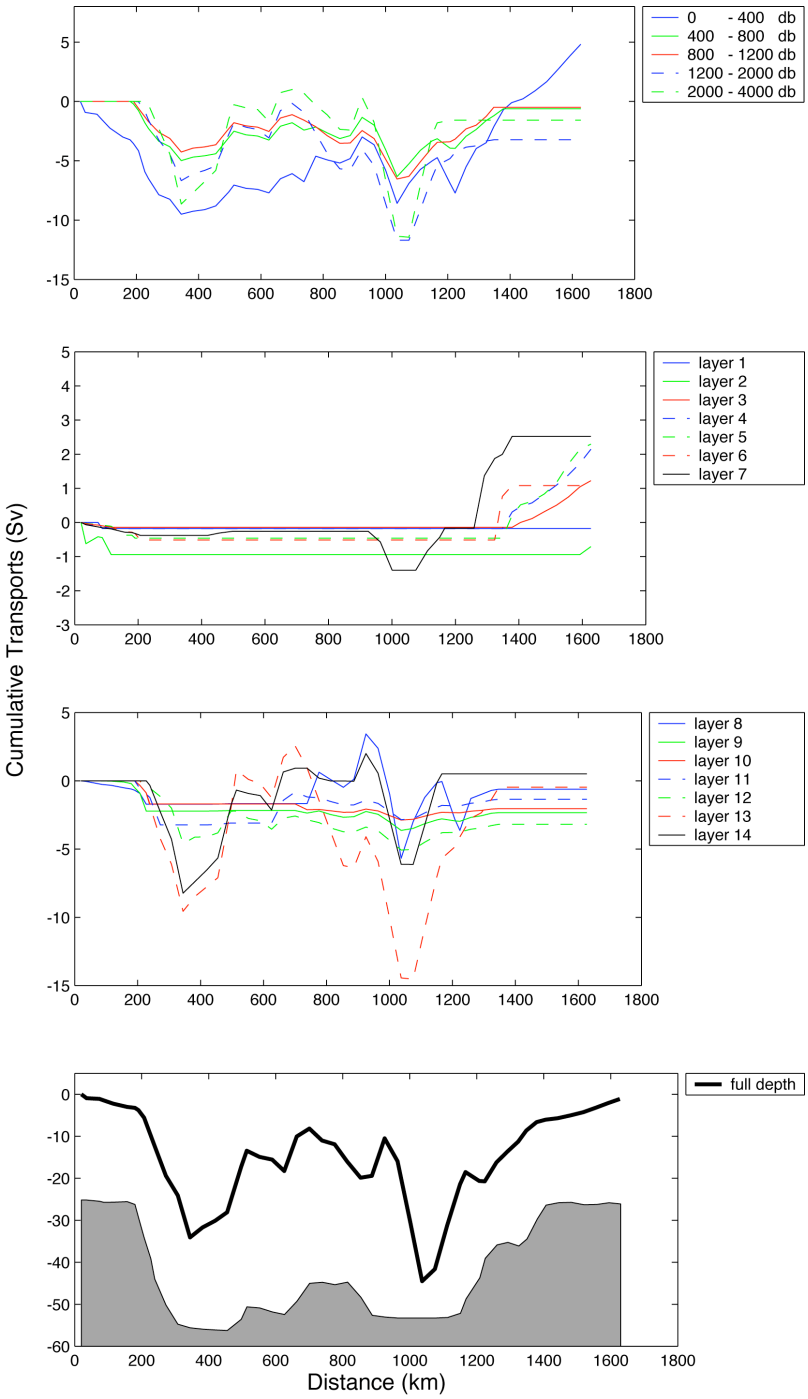

Figure 7.11: Winter cumulative volume transports (Sv) for the Greenland to Norway section, from Greenland on the left, eastwards to Norway on the right. Transports are accumulated from zero at Greenland. Positive transports are directed northeast across the section, towards the Arctic. The upper panel gives transports in layers defined by pressure, and the middle panels give transports in layers defined by isopycnals. These were identical to those used in the inverse model (see Table 5.2). The lower panel gives the full depth volume transport, with the coarse topography of the section represented by the grey shading as a visual aid to interpretation.

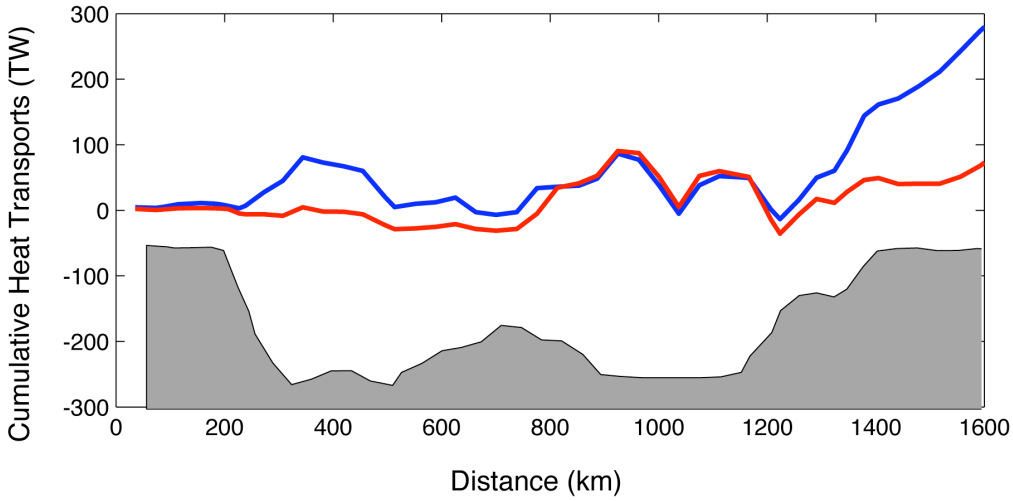

Figure 7.12: Cumulative heat transports (TW) for the Greenland to Norway section, from Greenland on the left, eastwards to Norway on the right. Summer and Winter transports are represented by the solid red and blue lines respectively. All transports are accumulated from zero at Greenland. Positive transports are directed northeast across the section, towards the Arctic.

Chapter Eight

Summary

8.1 Overview

In this chapter the main conclusions of this thesis are summarised, and some thought is given to the future of hydrography within the Nordic Seas. The major contribution of this thesis is the incorporation of simultaneous direct velocity measurements to provide an estimate of the summer circulation within the Nordic Seas and the net fluxes across its boundaries.

In Chapter 1 an introduction to the subject and motivation of this thesis was given. Chapter 2 presented an overview of the Nordic Seas, their topography, climate and circulation, and of high latitude climate change, concluding with the aims of this thesis. Chapter 3 gave a detailed description of the data used in this thesis, and Chapter 4 described the methods used. The summer circulation and fluxes of the Nordic Seas were presented in Chapter 5, and a discussion of errors given in Chapter 6. The variability of the circulation, with reference to winter data and the general ocean climate, was discussed in Chapter 7.

Hydrographic data provided the framework for this PhD, and the majority were collected as part of the NERC ARCICE programme. The concepts of ocean circulation dynamics were applied to these and supplementary data to provide initial flux estimates. Direct velocity measurements and inverse techniques were then applied to improve estimates of the large-scale mean circulation. The full Nordic Sea flux field (volume, heat and freshwater) was estimated, thus determining the exchanges between the Nordic Seas and the Arctic Ocean to the north, the Barents Sea to the east, and North Atlantic to the south, via the North Atlantic Current inflow and the Denmark Strait and Iceland-Scotland overflows. This was the first study to be able to make use of synoptic hydrographic data across the entire region with concurrent direct velocity measurements on most sections; and therefore provides a new estimate of the long-term mean summer fluxes and exchanges. The winter data also allowed a winter circulation to be constructed suggesting how the circulation within the interior of the Nordic Seas changes from summer to winter.

Inverse models inevitably leave a legacy of future work and unfinished business. A balance must be attained between including all prior information and introducing unnecessary noise into the system. Care must be taken to create an initial circulation that is reasonable since the inverse can only improve this estimate, and cannot be expected to find a solution that is close to correct if the first guess is highly divergent. Although, to some extent, inverse methods can enhance the information content of insufficient data, as Bacon (1996) pointed out, their main worth lies in forcing consistency on asynoptic data.

The model presented here is of medium complexity (see section 4.6.1). Full depth and layer-specific (all layers) conservation of volume and salinity (for salt) was required for each of the four boxes (*north*, *south*, *east*, *west*). The conservation of potential temperature (for heat) was also required in all layers that did not outcrop at the surface. To allow for some form of interlayer

exchange, diapycnal fluxes (volume, heat, salinity) were explicitly included for the relevant layer interfaces such that layer-specific conservation was physically consistent. One feature, included in some recent inverse models (Sloyan and Rintoul, 2001), is a heat flux at the ocean surface to represent the ocean-atmosphere exchanges. However, over the region of the Nordic Seas there is a high degree of uncertainty in the available climatologies, so a surface heat flux constraint would not be useful. Should a more accurate climatology be developed in the future, this would be a useful addition to the model.

8.2 Summer Circulation and Fluxes

The circulation scheme described and discussed in Chapter 5, and illustrated in Figure 5.39, is summarised here.

The initial velocity field for the inverse model was derived from a combination of the geostrophic velocity field and direct current measurements, where available (see section 5.5). The estimated fluxes associated with this field were reasonable and consistent with previous studies, although imbalances over individual boxes suggest the net fluxes were described more adequately than the internal circulation of the Nordic Seas. Sensitivity studies (see Chapter 6) indicate that the prevailing circulation of the Nordic Seas cannot be reasonably approximated with any level of no motion. When direct velocity measurements were not incorporated into the initial field for the inverse model, the solution was of poorer quality than that of the standard solution; there were larger residuals at the same rank, overflows and inflows were reduced to values inconsistent with literature and the net fluxes of the standard solution were not reproduced. The transport estimates described here were achieved using an initial velocity field based on direct current observations. It might, therefore, be expected that larger fluxes would be obtained than for estimates based on balance calculations using hydrographic measurements alone, as noted in Fram Strait by Fahrbach et al. (2001).

8.2.1 Net fluxes

Total volume transports from the standard solution suggest an input of 1.3±0.4Sv into the Nordic Seas from the Arctic Ocean (Fram Strait and the Barents Sea Opening), and a net export of 1.2±0.4Sv across the Greenland-Scotland Ridge into the North Atlantic from the Nordic Seas. These net fluxes can be given a crude separation to give an idea of the various exchanges.

The total inflow of AW is 8.2±2.6Sv, with a small 0.5±0.2Sv inflow through Denmark Strait, and the remainder over the Iceland-Scotland Ridge. Over a third of this inflow (3.1±1.0Sv) flows directly to the Arctic via Fram Strait and the Barents Sea (becoming denser through ocean-atmosphere exchanges). An inflow of 1.0±0.3Sv PW through Fram Strait, together with modified

AW (some of which have circuited the Arctic Ocean, and some of which have recirculated in Fram Strait), contribute to a southward flow of 5.1±1.6 Sv in the EGC. The addition of intermediate waters from the Greenland Sea gyre increase the strength of the EGC to 13.2±4.2 Sv at ~75°N. The net inflow of 2.0±0.6 Sv to the Nordic Seas through Fram Strait is divided almost equally between the surface and intermediate and the deep waters. There is a total outflow of 4.1±1.3 Sv through Denmark Strait, with an inferred overflow of 2.5±0.8 Sv (intermediate waters) and a surface outflow of 1.2±0.4 Sv PW. The total overflow of dense waters across the Iceland-Scotland Ridge is 3.2±1.0 Sv.

A total heat convergence within the Nordic Seas of 137 TW was found, giving an average flux of 51 Wm^{-2}. The corresponding poleward heat flux between the North Atlantic and the Nordic Seas is 188 TW, and between the Nordic Seas and the Arctic Ocean is 57 TW. Over the individual inverse boxes, the greatest average heat flux is 70 Wm^{-2} over the south box, implying the NAC interacts most strongly with the atmosphere over the southern part of the Nordic Seas.

The net input of freshwater to the Nordic Seas was found to be 0.053 Sv, with a southward freshwater flux of 0.068 Sv between the Arctic Ocean and the Nordic Seas, and a southward freshwater flux of 0.121 Sv between the Nordic Seas and the North Atlantic. The net freshwater flux into the North Atlantic is thus derived from contributions from the Arctic Ocean (0.068 Sv), the Baltic Seas (0.030 Sv), and runoff and P−E (0.023 Sv).

The effective diapycnal volume velocities representing the advective velocities were typically found to be less than 0.5×10^{-6} ms^{-1} over the interior of the Nordic Seas. The interlayer fluxes implied by these solution vertical velocities were of the order 0.5±0.2 Sv, which were no greater than the individual layer residuals.

8.2.2 Circulation

The circulation of the Nordic Seas is summarised in Figure 5.39. If σ_0=27.8 is taken to define the density of waters overflowing the Greenland–Scotland Ridge into the North Atlantic (Dickson and Brown, 1994; Hansen and Østerhus, 2000) then the net transport of waters above this level are towards the Arctic. Between the Greenland–Scotland Ridge and the openings to the Arctic Ocean, 4.0±1.3 Sv of the warm, saline inflow are converted to more dense waters. The majority of this transformation occurs between the Greenland–Scotland Ridge and the Greenland–Norway section.

The standard solution divides the AW inflow to the Nordic Seas between a pathway through the Rockall Trough and a pathway through the Iceland Basin, although at the time of the survey, it was confined to the Rockall Trough pathway. The structure of the Atlantic inflow consists of two major branches as it crosses the Greenland-Norway section. The eastern (barotropic) branch is concentrated over the continental slope, and the western branch is associated with the Polar Front and has significant baroclinicity. The strong cyclonic slope current (NAC) was also noted by Nøst

and Isachsen (2003). To the east there is a buoyant coastal current created by the freshwater supply to the Nordic Seas (from the Baltic and river-runoff along the Norwegian coast), which doesn't seem to significantly interact with the warm Atlantic waters in the NAC. The AW inflow to the Barents Sea occurs in narrow barotropic cores, with return flow in between. The magnitude of the net inflow is 1.4±0.5Sv. There is a small westward flow from the Barents Sea into the Nordic Seas of cold Arctic type water and dense winter waters. Further north, the branches of the AW inflow rejoin as they cross the Iceland-Svalbard section.

Within Fram Strait, large recirculation components both to the north and south make interpretation of the net northward and southward fluxes (in the WSC and EGC) difficult. The magnitude of the WSC is 4.8±1.5Sv, including 1.4±0.5Sv of AW. The southward flow of the EGC through Fram Strait is 5.1±1.6Sv. Included within the transport of the EGC at the latitude of Fram Strait is 1.5±0.5Sv of PW and 3.5±1.1Sv of rAW. The magnitude of the EGC increases to 13.2±4.2Sv at ~75°N due to the addition of intermediate waters from the Greenland Sea gyre, with a contribution of 3.3±1.1Sv from rAW and 1.9±0.6Sv of PW.

The strength of the Denmark Strait overflow is 2.5±0.8Sv at the latitude of the section (upstream of the sill itself). Since there is no evidence of a net transport of GSAIW out of the Greenland Sea, the source of the overflow waters must be derived from ~50% from rAW and ~50% from other intermediate water masses originating in the Arctic Ocean and Iceland Sea. The magnitude of the Iceland-Scotland overflow is 3.2±1.0Sv.

The data presented here provide observational evidence that the northward flowing Atlantic water does appear to be guided into the central basin (due to topographic features in the deep parts of the Nordic Seas). This aspect of the circulation was described as far back as Helland-Hansen and Nansen (1909), and there has been both recent theoretical analysis (Nøst and Isachsen, 2003), and dynamical evidence from numerical simulations (Walin et al., 2004). The data also give evidence of the cyclonic circulations associated with the major basins (Greenland, Lofoten and Iceland Basins) that were inferred from bathymetric features by Helland-Hansen and Nansen (1909).

There is significant circulation within the deep waters, contrary to the suggestion by Walin et al. (2004). The observed behaviour from studies using surface drifters (Jakobsen et al., 2003; Orvik and Niiler, 2002) suggests that bottom currents in the Nordic Seas must be nonzero for the lower layer to communicate the shape of the ocean basin to the upper layers. Other direct observations also show currents near the bottom that are as large as anywhere else in the water column (Fahrbach et al., 2001; Orvik et al., 2001; Woodgate et al., 1999).

8.3 Seasonal Variability

With hydrographic flux calculations, it is assumed that the ocean is in steady state and that synoptic surveys can allow an estimate of the circulation. However, in reality, the ocean is in a time-evolving state, and its variability must be characterised in terms of both its temporal and spatial structure. The sources of the variability and its relationship to forcing (in response to changing atmospheric conditions, for example) must also be understood. A key issue when looking at ocean circulation and fluxes is, therefore, to consider oceanic variability at time scales relevant for climate (Talley et al., 2001).

In this thesis, the variability in the circulation and fluxes of the Nordic Seas was investigated by direct consideration of seasonality within the Greenland Sea, inferred seasonal changes along the Greenland to Norway section, and then by looking at aspects of ocean climate to indicate, in view of the prevailing oceanic and atmospheric conditions during summer 1999, how this 'snapshot' might relate to the longer term mean circulation.

Seasonality in the hydrography within the central Greenland Sea was considered by direct comparison between the repeat summer / winter hydrographic stations which formed part of the ARCICE project. Within the Greenland Sea, during the winter months, the summer thermocline is eroded and the winter mixed layer extends to depths of 700–900m. Winter stations are characterised by the absence of ASW, a surface water mass formed by a combination of summer heating and mixing with the cool, fresh PW. Station profiles suggest some seasonality in the flow of rAW, with the flow extending further east into the Greenland Basin during summer.

Confirmation of warming trends within the deep waters of the Greenland Sea was found, with an average temperature of -1.052°C below 2000m. This compares to classical descriptions of GSDW with temperatures of –1.28°C to –1.242°C.

A combination of the repeat Greenland Sea stations, summer and winter data on the Svinøy section, and the summer mean circulation were used to construct a winter version of the Greenland to Norway section. Elements of the winter circulation within the Nordic Seas were inferred from this, in particular; the magnitudes of the gyre circulations, the strength of the EGC as it crosses the northern part of section, and the structure and magnitudes of the branches of the Atlantic inflow as they cross the southern part of the section. The more speculative aspects of the winter circulation could be reinforced with further work using satellite altimetry to investigate sea surface height variability, for example.

If the EGC is taken to include the southwards transport on the shelf, then it is 37Sv in winter, compared to 11Sv in summer. This compares well to the maximum winter transport found by Woodgate et al. (1999). The strength of the gyres within the Greenland and Lofoten Basins was found to increase significantly (approximately doubling) during winter (e.g. Isachsen et al., 2003;

Jakobsen et al., 2003; Orvik and Niiler, 2002). The total winter northwards transport of Atlantic Water within the NAC is ~9 Sv (approximately double the summer transport). The structure of the inflow does vary, with a weaker western branch and stronger recirculation within the Lofoten Basin gyre, so that the majority of the transport is concentrated on the Norwegian Slope.

A winter heat flux across the Greenland-Norway section of 298 ± 108 TW was estimated, compared to a summer heat flux of 90 TW. This flux is mostly confined to the NAC carrying the warm Atlantic inflow. The seasonal difference, and most of the heat transport, occurs within the NAC over the Norwegian continental slope. The acceleration of the Greenland Sea gyre in winter is not observed here to significantly alther the net horizontal heat fluxes. Were deep convection to occur within the Greenland Sea, under conditions of strong atmospheric forcing etc., it could be expected that this would no longer be the case.

This winter circulation is a partly subjective estimate, but does give a suggestion of the seasonal variability within the interior of the Nordic Seas, and the major currents of the NAC and EGC. Although the net fluxes from this winter reconstruction may not be as robust as for the summer circulation presented in Chapter 5, its value lies in emphasising that the circulation within the Nordic Seas has significant seasonal variability. An estimate of the annual mean fluxes and circulation based on summer data alone cannot, therefore, be justified.

The data upon which this thesis is based were from a period during which the NAO was at the end of an extreme positive phase, although during summer 1999 the NAO had only a midphase value of 0.5 (see section 7.6). This may prove to be a reason for increased sea-surface temperatures in the domain of the NAC west of Norway, and an increased inflow of Atlantic Water. Additionally, there is a suggestion that there was an increased inflow of cold, fresh Arctic waters (Aure et al., 2000). The combined effect would be to reduce the likelihood of winter erosion of the stratification of the upper waters of the Greenland Sea, and hence the occurrence of deep convection.

8.4 Future directions

The future of oceanography in the Nordic Seas is likely to be a combination of synoptic ship based surveys, remote sensing and, as new technology develops, new methods of remote monitoring. It is probable that technological developments for remote monitoring will improve instruments such as profiling floats, profiling CTD systems capable of sub-ice hydrography and sea gliders. Continued development in remote sensing techniques will allow the monitoring of ice thickness as well as extent, and the monitoring of snow cover properties over the entire Arctic. Even if there is a shift in bias away from ship based hydrographic work, there will still be a need for ground truthing of both remote sensing information and remote monitoring data.

A number of current projects have ensured the short to medium term future of hydrography within the Nordic Seas. In particular there are projects initiated under the auspices of the Norwegian Ocean Climate Project (NOClim), the UK NERC Rapid Climate Change thematic programme, and the Arctic / sub-Arctic Ocean Fluxes (ASOF) Programme put forward by the Arctic Ocean Science Board (AOSB)[1]. These projects have complimentary objectives and it is hoped that the outcome will be to improve the long term monitoring of the Nordic Seas.

The principal objectives of NOClim are to 'improve and enhance our understanding of rapid changes in the thermohaline circulation in the Northern seas, improve and enhance our understanding of ocean and ice processes related to climate, and mechanisms causing significant variability in the hydrography, circulation and ice cover in the Northern seas, maintaining time series for detecting climate change in the Northern seas. The second phase of NOClim (2003□ □2006) aims to 'significantly improve our understanding of processes which govern oceanic heat transport towards the Nordic Seas, and which provide the basis for atmospheric heat transport from the Atlantic sector towards northern Europe.'

The aim of ASOF is: 'To measure and model the variability of fluxes between the Arctic Ocean and the Atlantic Ocean with a view to implementing a longer term system of critical measurements needed to understand the high-latitude ocean's steering role in decadal climate variability.' The purpose is to create an Arctic Observing System and, with this in mind, ASOF has defined six regional tasks to measure the key ocean exchanges between the Arctic Ocean and Sub-arctic Seas, and their impact on the overturning circulation of the Northern North Atlantic. These include the warm water inflow to the Nordic Seas, exchanges with the Arctic Ocean, ice and fresh water outflow, Greenland-Scotland Ridge exchanges, overflows to the deep western boundary current and the Canadian Archipelago throughflow. A seventh modelling task will provide the link between the regional observational tasks. ASOF is a sub program of the International Study of Environmental Arctic Change (SEARCH) and an endorsed project of both CLIVAR (Climate Variability and Predictability Study) and CliC (Climate and Cryosphere).

The scope of the RAPID programme is wider, its objective being 'to improve our ability to quantify the probability and magnitude of future rapid change in climate'. The programme aims to investigate and understand the causes of rapid climate change, with a main focus on the role of the Atlantic Ocean's THC. Its specific objective pertaining to the Nordic Seas is 'to support long-term direct observations of water, heat, salt and ice transports at critical locations in the northern North Atlantic, to quantify the atmospheric and other (e.g. river run-off, ice sheet discharge) forcing of these transports, and to perform process studies of ocean mixing at northern high latitudes.'

---

[1] Norwegian Ocean Climate Project (NOClim) http://www.noclim.org
UK NERC Rapid Programme http://www.soc.soton.ac.uk/rapid/rapid.php
Arctic / sub-Arctic Ocean Fluxes (ASOF) http://www.asof.npolar.no

8.5 Final remarks

Despite historical knowledge of the Nordic Seas extending back to the voyages of the sealers and whalers, and a tradition of oceanographic observations for over a century (Knudsen, 1899; Nansen, 1902), the Nordic Seas remain an exciting and rewarding region to study. As Mauritzen (1994) pointed out a decade ago, we can still question our understanding of the oceanic regime of Nordic Seas on even a basic level. The complexity of the processes involved in the ventilation, pathways and overflows and their key role within the global oceanic circulation provide continued incentive for research.

Difficulties arise from the complexity of describing the components of the circulation of the Nordic Seas as a coherent whole. Water mass definitions vary between locations within the Nordic Seas and to a certain extent seasonally and on longer time-scales. The work presented here is as consistent as possible, but its value will be realised when set in context with future studies of similar kind. In particular, a coordinated effort of further measurements is needed so that this short term 'snapshot' can be set into the context of decadal change.

There remain a number of outstanding questions. Not least is the question of how climate signals propagate through the circulation and exchanges of the northern seas. The dense northern overflows are key elements of the THC since the overflow and descent of cold dense water across the Greenland Scotland Ridge is the principle means by which the deep ocean is ventilated. Many projections of climate change anticipate a weakening of the THC in the North Atlantic in response to increased freshening and warming in the sub-polar seas (Rahmstorf and Ganopolski, 1999). Although these dense northern overflows are likely to be one means by which this climate signal is communicated to the deep ocean, the precise mechanisms remain as yet unknown. In order to address these questions, there is a need for simultaneous transport measurements in the important gateways of the Nordic Seas, and development of regional high-resolution ice-ocean models to address regional aspects of climate variability. To further understanding of the processes within the Nordic Seas there is also a need for year round data (winter in particular).

Appendix I.

The posterior covariance matrix can be calculated in the framework of the Gauss-Markov formulation of the inverse problem (Wunsch, 1996). It gives an estimate of the accuracy of the model reference and effective diapycnal velocities.

As described in section 4.6.1 the inverse problem is formulated as a matrix equation:

$$\mathbf{A}\,\mathbf{x} + \mathbf{n} = \mathbf{b} \qquad A1.1$$

The (M x N) matrix, **A**, contains information about the geometry of the system; station pair layer areas multiplied by property concentrations, and layer interface areas multiplied by average interfacial property concentrations. The (1 x N) vector, **x**, contains the unknown reference velocities and the unknown interfacial 'fluxes' for mass, heat, and salt anomaly (w_m, w_h and w_s respectively) such that $\mathbf{x} = \left[\mathbf{v}\ \mathbf{w}_m\ \mathbf{w}_h\ \mathbf{w}_s\right]^T$. The (M x 1) vector, **b**, contains information about the divergence due to the horizontal baroclinic property flux and the Ekman flux (i.e. the values to which the system is to be constrained). The vector, **n**, represents the noise.

The model posterior covariance $\mathbf{P}_{xx}$ is given by

$$\mathbf{P}_{xx} = \left\langle \left(\tilde{\mathbf{x}} - \mathbf{x}\right)\left(\tilde{\mathbf{x}} - \mathbf{x}\right)^T \right\rangle \qquad A1.2$$

where $\tilde{\mathbf{x}}$ is an estimate and $\mathbf{x}$ is the unknown true value. An estimate of $\mathbf{x}$, $\tilde{\mathbf{x}}$, can be generated with a linear combination of the data **b**:

$$\tilde{x}_i = \sum_j^M K_{ij} b_j \qquad or \qquad \tilde{\mathbf{x}} = \mathbf{K}\,\mathbf{b} \qquad A1.3$$

Substituting into the expression for $\mathbf{P}_{xx}$ and expanding

$$\mathbf{P}_{xx} = \mathbf{K}\left\langle \mathbf{b}\,\mathbf{b}^T \right\rangle \mathbf{K}^T - \left\langle \mathbf{x}\,\mathbf{b}^T \right\rangle \mathbf{K}^T - \mathbf{K}\left\langle \mathbf{b}\,\mathbf{x}^T \right\rangle + \left\langle \mathbf{x}\,\mathbf{x}^T \right\rangle \qquad A1.4$$

Using the notation **C** for a covariance matrix, the symmetry $\mathbf{C}_{xb} = \mathbf{C}_{bx}^T$ and subscripts to identify the covarying vectors:

$$\mathbf{P}_{xx} = \mathbf{K}\mathbf{C}_{bb}\,\mathbf{K}^T - \mathbf{C}_{xb}\,\mathbf{K}^T - \mathbf{K}\mathbf{C}_{bx}^T + \mathbf{C}_{xx} \qquad A1.5$$

Using the matrix identity (eg. Wunsch 1996, equation 3.1.26), where '**A**, **B**, **C**' refer to arbitrary matrices, rather than the previously defined matrices:

$$\mathbf{A}\mathbf{C}\mathbf{A}^T - \mathbf{B}\mathbf{A}^T - \mathbf{A}\mathbf{B}^T = \left(\mathbf{A} - \mathbf{B}\mathbf{C}^{-1}\right)\mathbf{C}\left(\mathbf{A} - \mathbf{B}\mathbf{C}^{-1}\right)^T - \mathbf{B}\mathbf{C}^{-1}\mathbf{B}^T \qquad A1.6$$

then since the LHS of equation A1.7 is of the same form as the first three terms of the RHS of equation A1.6:

$$\mathbf{P}_{xx} = \left(\mathbf{K} - \mathbf{C}_{xb}\,\mathbf{C}_{bb}^{-1}\right)\mathbf{C}_{bb}\left(\mathbf{K} - \mathbf{C}_{xb}\,\mathbf{C}_{bb}^{-1}\right)^T - \mathbf{C}_{xb}\,\mathbf{C}_{bb}^{-1}\,\mathbf{C}_{xb}^T + \mathbf{C}_{xx} \qquad A1.7$$

The variance in $\mathbf{P}_{xx}$ is a minimum when the first term on the RHS of equation A1.8 is zero, ie when:

$$\mathbf{K} = \mathbf{C}_{xb}\,\mathbf{C}_{bb}^{-1} \qquad A1.8$$

so the minimum variance estimate of $\tilde{\mathbf{x}}$, $\tilde{\mathbf{x}}$, is:

$$\tilde{\mathbf{x}} = \mathbf{C}_{xb}\,\mathbf{C}_{bb}^{-1}\,\mathbf{b} \qquad A1.9$$

Now substituting equation A1.9 into equation A1.6:

$$\mathbf{P}_{xx} = \mathbf{C}_{xb}\,\mathbf{C}_{bb}^{-1}\,\mathbf{C}_{bb}\left(\mathbf{C}_{xb}\,\mathbf{C}_{bb}^{-1}\right)^{T} - \mathbf{C}_{xb}\left(\mathbf{C}_{xb}\,\mathbf{C}_{bb}^{-1}\right)^{T} - \left(\mathbf{C}_{xb}\,\mathbf{C}_{bb}^{-1}\right)\mathbf{C}_{xb}^{T} + \mathbf{C}_{xx} \qquad A1.10$$

leading to the optimal (minimum variance) definition of $\mathbf{P}_{xx}$:

$$\mathbf{P}_{xx} = \mathbf{C}_{xx} - \mathbf{C}_{xb}\left(\mathbf{C}_{xb}\,\mathbf{C}_{bb}^{-1}\right)^{T} \qquad A1.11$$

Returning to the original system of linear equations with the noise vector, **n**, included explicitly:

$$\mathbf{A}\,\mathbf{x} + \mathbf{n} = \mathbf{b} \qquad A1.12$$

and calculating the covariance matrices $\mathbf{C}_{bb}$ and $\mathbf{C}_{xb}$ explicitly:

$$\begin{aligned}
\mathbf{C}_{bb} &= \left\langle \mathbf{b}\,\mathbf{b}^{T} \right\rangle \\
&= \left\langle \left(\mathbf{A}\,\mathbf{x} + \mathbf{n}\right)\left(\mathbf{A}\,\mathbf{x} + \mathbf{n}\right)^{T} \right\rangle \\
&= \left\langle \mathbf{A}\,\mathbf{x}\left(\mathbf{A}\,\mathbf{x}\right)^{T} + \mathbf{n}\,\mathbf{n}^{T} + \mathbf{n}\left(\mathbf{A}\,\mathbf{x}\right)^{T} + \mathbf{A}\,\mathbf{x}\,\mathbf{n}^{T} \right\rangle \\
&= \mathbf{A}\left\langle \mathbf{x}\,\mathbf{x}^{T} \right\rangle \mathbf{A}^{T} + \left\langle \mathbf{n}\,\mathbf{n}^{T} \right\rangle \\
&= \mathbf{A}\,\mathbf{C}_{xx}\,\mathbf{A}^{T} + \mathbf{C}_{nn}
\end{aligned} \qquad A1.13$$

$$\begin{aligned}
\mathbf{C}_{xb} &= \left\langle \mathbf{x}\,\mathbf{b}^{T} \right\rangle \\
&= \left\langle \mathbf{x}\left(\mathbf{A}\,\mathbf{x} + \mathbf{n}\right)^{T} \right\rangle \\
&= \left\langle \mathbf{x}\left(\mathbf{A}\,\mathbf{x}\right)^{T} + \mathbf{x}\,\mathbf{n}^{T} \right\rangle \\
&= \left\langle \mathbf{x}\,\mathbf{x}^{T} \right\rangle \mathbf{A}^{T} \\
&= \mathbf{C}_{xx}\,\mathbf{A}^{T}
\end{aligned} \qquad A1.14$$

then equation A1.12 becomes

$$\begin{aligned}
\mathbf{P}_{xx} &= \mathbf{C}_{xx} - \mathbf{C}_{xb}\left(\mathbf{C}_{xb}\,\mathbf{C}_{bb}^{-1}\right)^{T} \\
&= \mathbf{C}_{xx} - \mathbf{C}_{xx}\,\mathbf{A}^{T}\left(\mathbf{A}\,\mathbf{C}_{xx}\,\mathbf{A}^{T} + \mathbf{C}_{nn}\right)^{-1}\mathbf{A}\,\mathbf{C}_{xx}
\end{aligned} \qquad A1.15$$

The posterior noise covariance matrix, $\mathbf{P}_{nn}$, can be defined by

$$\mathbf{P}_{nn} = \left\langle \left(\tilde{\mathbf{n}} - \mathbf{n}\right)\left(\tilde{\mathbf{n}} - \mathbf{n}\right)^{T} \right\rangle \qquad A1.16$$

The original system of equations is expressed as **b = Ax+n**, so in estimated terms,

$$\mathbf{b} = \mathbf{A}\,\tilde{\mathbf{x}} + \tilde{\mathbf{n}} \qquad A1.17$$

Since $\mathbf{A}$ and $\mathbf{b}$ are the 'geometry' and the data respectively, and are unchanged by the inverse, the process of estimating $\mathbf{x}$ and producing $\tilde{\mathbf{x}}$ is intimately linked to the resulting noise estimator $\tilde{\mathbf{n}}$.

$$\begin{aligned}\tilde{\mathbf{n}} - \mathbf{n} &= \left(\mathbf{y} - \mathbf{A}\,\tilde{\mathbf{x}}\right) - \left(\mathbf{y} - \mathbf{A}\,\mathbf{x}\right) \\ &= \mathbf{A}\left(\mathbf{x} - \tilde{\mathbf{x}}\right)\end{aligned} \qquad A1.18$$

such that

$$\begin{aligned}\mathbf{P}_{nn} &= \left\langle \mathbf{A}\left(\tilde{\mathbf{x}} - \mathbf{x}\right)\left(\tilde{\mathbf{x}} - \mathbf{x}\right)^{T}\mathbf{A}^{T} \right\rangle \\ &= \mathbf{A}\,\mathbf{P}_{xx}\,\mathbf{A}^{T}\end{aligned} \qquad A1.19$$

References

Aagaard, K., Temperature variations in the Greenland Sea deep-water, *Deep Sea Research*, *15*, 281-296, 1968.

Aagaard, K., and E.C. Carmack, The Role of Sea Ice and Other Fresh Water in the Arctic Circulation, *Journal of Geophysical Research*, *94* (C10), 14485 - 14498, 1989.

Aagaard, K., and L.K. Coachman, The East Greenland Current north of Denmark Strait. Part I., *ARCTIC*, *21*, 181-200, 1968.

Aagaard, K., E. Fahrbach, J. Meincke, and J.H. Swift, Saline Outflow from the Arctic Ocean: Its Contribution to the Deep Waters of the Greenland, Norwegian, and Iceland Seas, *Journal of Geophysical Research*, *96* (C11), 20433-20441, 1991.

Aagaard, K., and S.A. Malmberg, Low frequency characteristics of the Denmark Strait Overflow, in *ICES CM 1978/C:47*, 1978.

Aagaard, K., J.H. Swift, and E.C. Carmack, Thermohaline circulation in the Arctic Mediterranean Seas, *Journal of Geophysical Research*, *90* (C3), 4833-4846, 1985.

Aksenov, Y., and A.C. Coward, The Arctic Ocean Circulation as Simulated in a Very High Resolution Global Ocean Model (OCCAM), *Annals of Glaciology*, *33*, 567-576, 2001.

Alekseev, G.V., O.M. Johannessen, and A.A. Korablev, Interannual variability in water masses in the Greenland Sea and adjacent areas, *Polar Research*, *20* (2), 201 - 208, 2001.

Alexander, R., and R. Mobley, Monthly average sea-surface temperature and ice pack limits on a 1 degree global grid., *Monthly Weather Review*, *104*, 143-148, 1976.

Ambaum, M.H.P., B.J. Hoskins, and D.B. Stephenson, Arctic Oscillation or North Atlantic Oscillation? *Journal of Climate*, *14*, 3495-3507, 2001.

Anderson, L.G., E.P. Jones, K.P. Kolterman, P. Schlosser, J.H. Swift, and D.W.R. Wallace, The first oceanographic section across the Nansen Basin in the Arctic Ocean, *Deep Sea Research*, *36* (3), 475 - 482, 1989.

Aure, J., et. al, Havets Miljo 2000, *Fisken Hav*, *2*, 2000.

Bacon, S., Circulation and Fluxes in the Sub-Polar North Atlantic, University of Southampton, Southampton, 1996.

Bacon, S., Circulation and Fluxes in the North Atlantic between Greenland and Ireland, *Journal of Physical Oceanography*, *27*, 1420-1435, 1997.

Bacon, S., The Dense Overflows from the Nordic Seas into the deep North Atlantic, *ICES Journal of Marine Science*, 2000.

Bacon, S., G. Reverdin, I. Rigor, and H. Snaith, A Freshwater Jet on the East Greenland Shelf, *Journal of Geophysical Research*, *107* (C7), 2001.

Bacon, S., H.M. Snaith, and M.J. Yelland, An Evaluation of Some Recent Batches of IAPSO Standard Seawater, *Journal of Atmospheric and Oceanic Technology*, *17*, 854-861, 2000.

Bacon, S., and M. Yelland, RRS James Clark Ross Cruise 44 23 July - 31 August 1999. Circulation And Thermohaline Structure - Mixing, Ice And Ocean Weather CATS-MIAOW., pp. 140 pp, Southampton Oceanography Centre Cruise Report No. 33, 2000.

Barth, N., and C. Wunsch, Oceanographic Experiment Design by Simulated Annealing, *Journal of Physical Oceanography*, *20*, 1249-1263, 1990.

Bauch, D., P. Schlosser, and R.G. Fairbanks, Freshwater balance and the sources of deep and bottom waters in the Arctic Ocean inferred from the distribution of $H_2{}^{18}O$, *Progress in Oceanography*, *35*, 53-80, 1995.

Beal, L.M., Observations of the Velocity Structure of the Agulhas Current, University of Southampton, Southampton, 1997.

Beal, L.M., and H.L. Bryden, The velocity and vorticity structure of the Agulhas Current at 32 S, *Journal of Geophysical Research*, *104*, 5151 - 5176, 1999.

Bengtsson, L., V. Semenov, and O.M. Johannessen, The early 20th century warming in the Arctic - a possible mechanism, *Journal of Climate*, *in press*, 2004.

Bigg, G.R., An Estimate of the Flux of Iceberg Calving from Greenland, *Arctic, Antarctic, and Alpine Research*, *31* (2), 174-178, 1999.

Bingham, F.M., and L.D. Talley, Estimates of Kuroshio transport using an inverse technique, *Deep Sea Research*, *38* (Suppl. 1), S21 - S43, 1991.

Blindheim, J., V. Borovkov, B. Hansen, S.A. Malmberg, W.R. Turrell, and S. Østerhus, Upper layer cooling and freshening in the Norwegian Sea in relation to atmospheric forcing, *Deep Sea Research I*, *47*, 655 - 680, 2000.

Bonisch, G., J. Blindheim, J.L. Bullister, P. Schlosser, and C.W.R. Wallace, Long-term trends of temperature, salinity, density, and transient tracers in the central Greenland Sea, *Journal of Geophysical Research*, *102* (C8), 18553-18571, 1997.

Bourke, R.H., J.L. Newton, R.G. Paquette, and M.D. Tunnicliffe, Circulation and Water Masses of the East Greenland Shelf, *Journal of Geophysical Research*, *92* (C7), 6729-6740, 1987.

Bourke, R.H., R.G. Paquette, and R.F. Blythe, The Jan Mayen Current of the Greenland Sea, *Journal of Geophysical Research*, *97*, 7241-7250, 1992.

Brandon, M.A., and P. Wadhams, The near surface hydrography beneath the Odden ice tongue., *Deep-Sea Research II*, *46*, 1301-1318, 1999.

Brown, J., A. Colling, D. Park, J. Phillips, D. Rothery, and J. Wright, *Ocean Chemistry and Deep-Sea Sediments*, Pergamon Press and the Open University, Oxford, 1989.

Brummer, B., G. Muller, B. Affeld, R. Gerdes, M. Karcher, and F. Kauker, Cyclones over Fram Strait: impact on sea ice and variability, *Polar Research*, *20* (2), 147 - 152, 2001.

Bryden, H.L., and S. Imawaki, Ocean Heat Transport, in *Ocean Circulation and Climate*, edited by J. Gould, Academic Press, London, 2001.

Buch, E., S.-A. Malmberg, and S.S. Kristmannsson, Arctic Ocean deep water masses in the western Iceland Sea, *Journal of Geophysical Research*, *101* (C5), 11965-11973, 1996.

Budeus, G., W. Schneider, and G. Krause, Winter convective events and bottom water warming in the Greenland Sea, *Journal of Geophysical Research*, *108* (C9), 18513-18527, 1998.

Budyko, M.I., *Climate and Life*., Academic Press, New York, 1974.

Bunker, A.F., Computations of Surface Energy Flux and Annual Air-Sea Interaction Cycles of the North Atlantic Ocean., *Monthly Weather Report*, *104*, 1122-1140, 1976.

Carmack, E., and K. Aagaard, On the deep water of the Greenland Sea, *Deep Sea Research*, *20*, 687-715, 1973.

Cattle, H., Diverting Soviet rivers: Some possible repercussions for the Arctic Ocean, *Polar Record*, *22*, 485-498, 1985.

Cayan, D.R., Latent and sensible heat flux anomalies over the Northern Oceans: the connection to monthly atmospheric circulation, *Journal of Climate*, *5*, 354-369, 1992.

Cisewski, B., G. Budeus, and G. Krause, Absolute transport estimates of total and individual water masses in the northern Greenland Sea derived from hydrographic and acoustic Doppler current profiler measurements, *Journal of Geophysical Research*, *108* (C9), 3298, doi:10.1029/2002JC001530, 2003.

Coachman, L.K., and K. Aagaard, Physical oceanography of Arctic and Subarctic Seas., in *Marine Geology and Oceanography of the Arctic Seas*., edited by Y. Herman, pp. 1-72, Springer-Verlag, Berlin, 1974.

Comiso, J.C., P. Wadhams, L.T. Pedersen, and R.A. Gersten, Seasonal and interannual variability of the Odden ice tongue and a study of environmental effects, *Journal of Geophysical Research*, *106* (C5), 9093-9116, 2001.

Conkright, M.E., R.A. Locarnini, H.E. Garcia, T.D. O'Brien, T.P. Boyer, C. Stephens, and J.I. Antonov, World Ocean Atlas 2001: Objective Analyses, Data Statistics, and Figures, CD-ROM Documentation., pp. 17, National Oceanographic Data Center, Silver Spring, MD, 2002.

Cooper, L.H.N., Deep Water movements in the North Atlantic as a link between climatic changes around Iceland and biological productivity of the English Channel and Celtic Sea., *Journal of Marine Research*, *14*, 347-362, 1955.

Culkin, F., and P. Ridout, Salinity: Definitions, determinations, and standards., *Sea Technology*, *October 1989*, 47-49, 1989.

Cunningham, S.A., RRS Discovery Cruise 242 7 September - 6 October 1999. Atlantic - Norwegian Exchanges., pp. 128 pp, Southampton Oceanography Centre Cruise Report No. 28, 2000.

Cunningham, S.A., S.G. Alderson, B.A. King, and M.A. Brandon, Transport and Variability of the Antarctic Circumpolar Current in Drake Passage, *Journal of Geophysical Research*, *108* (C5), 8084: doi10.1092/2001JC001147, 2003.

Curry, R. and C. Mauritzen, Dilution of the Northern North Atlantic Ocean in Recent Decades, *Science*, *308*, 1772-1774, 2005.

Deser, C., J. Walsh, and M. Timlin, Arctic Sea Ice Variability in the Context of Recent Atmospheric Circulation Trends, *Journal of Climate*, *13*, 617-633, 2000.

Dickson, B., All change in the Arctic, *Nature*, *397* (6718), 389-391, 1999.

Dickson, R., and J. Brown, The production of North Atlantic Deep Water: Sources, rates, and pathways., *Journal of Geophysical Research*, *99* (C6), 12319-12341, 1994.

Dickson, R., E.M. Gmitrowiz, and A.J. Watson, Deep-water renewal in the northern North Atlantic, *Nature*, *344*, 848-850, 1990.

Dickson, R., J. Lazier, J. Meincke, P. Rhines, and J. Swift, Long-term coordinated changes in the convective activity of the North Atlantic, *Progress in Oceanography*, *38*, 241-295, 1996.

Dickson, R., J. Meincke, S.-A. Malmberg, and A.J. Lee, The "Great Salinity Anomaly" in the Northern North Atlantic 1968-1982, *Progress in Oceanography*, *20*, 103-151, 1988.

Dickson, R.R., T.J. Osborne, J.W. Hurrell, J. Meincke, J. Blindheim, B. Adlandsvik, T. Vinje, G. Alekseev, and W. Maslowski, The Arctic Ocean Response to the North Atlantic Oscillation, *Journal of Climate*, *13* (15), 2671-2696, 2000.

Dickson, B., I. Yashayaev, J. Meincke, B. Turrell, S. Dye, and J. Holfort, Rapid freshening of the deep North Atlantic Ocean over the past four decades, *Nature*, *416*, 832 - 837, 2002.

Donohue, K.A., E. Firing, and L. Beal, Comparison of three velocity sections of the Agulhas Current and Agulhas Undercurrent, *Journal of Geophysical Research*, *105* (C10), 28585 - 28593, 2000.

Egbert, G.D., A.F. Bennett, and M.G.G. Foreman, TOPEX/POSEIDON tides estimated using a global inverse model, *Journal of Geophysical Research*, *99* (C12), 24821-24852, 1994.

Egbert, G.D., and S.Y. Erofeeva, Efficient inverse modelling of barotropic ocean tides., College of Oceanic and Atmospheric Sciences, Oregan State University, Corvallis., 2000.

Ekman, V.W., On the influence of the earth's rotation on ocean currents., *Royal Swedish Academy of Science, Arkiv for matematik, astonomi och fysik*, *2* (11), 1-53, 1905.

Ekwurzel, B., P. Schlosser, R.A. Mortlock, R.G. Fairbanks, and J.H. Swift, River runoff, sea ice meltwater, and Pacific water distribution and mean residence times in the Arctic Ocean, *Journal of Geophysical Research*, *106* (C5), 9075-9092, 2001.

Fahrbach, E., J. Meincke, S. Østerhus, G. Rohardt, U. Schauer, V. Tverberg, and J. Verduin, Direct measurements of heat and mass transports through Fram Strait, *Polar Research*, *20* (2), 217-224, 2001.

Fiadero, M.E., and G. Veronis, Circulation and Heat Flux in the Bermuda Triangle, *Journal of Physical Oceanography*, *13* (7), 1158-1169, 1983.

Firing, E., and R.L. Gordon, Deep Ocean Acoustic Doppler Current Profiling, in *Proceedings of the IEEE Fourth Working Conference on Current Measurements, 3 - 5 April, 1990.*, edited by G.F. Appell, and T.B. Curtin, pp. 334, New York, IEEE., Maryland, 1990.

Fischer, J., and M. Visbeck, Deep velocity profiling with self contained ADCPs., *Journal of Atmospheric and Oceanic Technology*, *10*, 764-773, 1993.

Fogelqvist, E., J. Blindheim, T. Tanhua, S. Østerhus, E. Buch, and F. Rey, Greenland-Scotland overflow studied by hydro-chemical multivariate analysis, *Deep Sea Research I*, *50*, 73-102, 2003.

Fukumori, I., and C. Wunsch, Efficient representation of the North Atlantic hydrographic and chemical distributions, *Progress in Oceanography*, *27*, 111-195, 1991.

Ganachaud, A.S., Large Scale Oceanic Circulation and Fluxes of Freshwater, Heat, nutrients and Oxygen., Massachusetts Institute of Technology / Woods Hole Oceanographic Institute Joint Programme, Cambridge, 1999.

Ganachaud, A., and C. Wunsch, Improved estimates of global ocean circulation, heat transport and mixing from hydrographic data, *Nature*, *408*, 453-457, 2000.

Ganachaud, A., C. Wunsch, J. Marotzke, and J. Toole, Meridional overturning and large-scale circulation of the Indian Ocean, *Journal of Geophysical Research*, *105* (C11), 26117-26134, 2000.

Gascard, J.-C., A.J. Watson, M.-J. Messias, K.A. Olsson, T. Johannessen, and K. Simonsen, Long-lived vortices as a mode of deep ventilation in the Greenland Sea, *Nature*, *416*, 525 - 527, 2002.

Gill, A., *Atmosphere-Ocean Dynamics*, Academic Press, London, 1982.

Girton, J.B., Dynamics of Transport and Variability in the Denmark Strait Overflow, University of Washington, Seattle, 2001.

Girton, J., T. Sanford, and R. Kase, Synoptic sections of the Denmark Strait Overflow, *Geophysical Research Letters*, *28* (8), 1619-1622, 2001.

Gloersen, P., W.J. Campbell, D.J. Cavalieri, J.C. Comiso, C.L. Parkinson, and H.J. Zwally, Arctic and Antarctic Sea ice, 1978-1987: satellite passive-microwave observations and analysis., pp. 290, National Aeronautics and Space Administration, Report of NASA SP-511, 1992.

Gorshkov, S.E., *Arctic Ocean*, Pergamon Press, New York, 1983.

Griffies, S.M., and K. Bryan, Predictability of North Atlantic Multidecadal Climate Variability, *Science*, *275*, 181-184, 1997.

Grist, J.P., and S.A. Josey, Inverse analysis of the SOC air-sea flux climatology using ocean heat transport constraints, *Journal of Climate*, *16*, 3274-3295, 2003.

Gustafsson, B., Interaction between Baltic Sea and North Sea, *Deutsch Hydrographische Zeitschrift*, *49* (2/3), 165-183, 1997.

Hakkinen, S., An Arctic Source for the Great Salinity Anomaly: A Simulation of the Arctic Ice-Ocean System for 1955-1975, *Journal of Geophysical Research*, *98* (C9), 16397-16410, 1993.

Hall, M.M., and H.L. Bryden, Direct estimates and mechanisms of ocean heat transport, *Deep-Sea Research*, *29* (3A), 339-359, 1982.

Hansen, B., and S. Østerhus, North Atlantic - Nordic Seas exchanges, *Progress in Oceanography*, *45*, 109 - 208, 2000.

Hansen, B., S. Østerhus, H. Hatun, R. Kristiansen, and K.M.H. Larsen, The Iceland-Faroe inflow of Atlantic water to the Nordic Seas, in *ICES Annual Science Conference*, Tallinn, Estonia., 2003.

Hansen, B., W.R. Turrell, and S. Østerhus, Decreasing overflow from the Nordic seas into the Atlantic Ocean through the Faroe Bank channel since 1950, *Nature*, *411*, 927 - 930, 2001.

Hardy, R.J., J.L. Bamber, and S. Orford, The delineation of drainage basins on the Greenland ice sheet for mass-balance analyses using a combined modelling and geographical information system approach, *Hydrological Processes*, *14*, 1931-1941, 2000.

Helland-Hansen, B., and F. Nansen, The Norwegian Sea, its physical oceanography. Based on the Norwegian researches 1900-1904., pp. 390 pp, Mallingske, Christiania., 1909.

Hellerman, S., and M. Rosenstein, Normal monthly wind stress over the world ocean with error estimates., *Journal of Physical Oceanography*, *13*, 1093-1104, 1983.

Holliday, N.P., Air-sea interaction and circulation changes in the northeast Atlantic, *Journal of Geophysical Research*, *108* (C8), 3259, 2003.

Holliday, N.P., R.T. Leach, J.F. read, and H. Leach, Water mass properties and fluxes in the Rockall Trough, 1975-1998, *Deep Sea Research*, *47*, 1303-1332, 2000.

Hopkins, T.S., The GIN Sea - A synthesis of its physical oceanography and literature review 1972-1985, *Earth-Science Reviews*, *30*, 175-318, 1991.

Hurdle, B.G., *The Nordic Seas*, 777 pp., Springer-Verlag, New York, NY., 1986.

Hurrell, J., Decadal Trends in the North Atlantic Oscillation Regional Temperatures and Precipitation, *Science*, *269*, 676-679, 1995.

Hurrell, J.W., and R.R. Dickson, in *Marine ecosystems and climate variation: the North Atlantic. A comparative perspective*., edited by N.C. Stenseth, G. Ottersen, J.W. Hurrell, and A. Belgrano, Oxford University Press, Oxford, 2004.

Ingvaldsen, R.B., L. Asplin, and H. Loeng, The seasonal cycle in the Atlantic transport to the Barents Sea during the years 1997-2001., *Continental Shelf Research*, *24*, 1015-1032, 2004a.

Ingvaldsen, R.B., L. Asplin, and H. Loeng, Velocity field of the western entrance to the Barents Sea, *Journal of Geophysical Research*, *109* (C03021), doi:10.1029/2003JC001811, 2004b.

(IPCC), I.P.C.C., Climate Change 2000 - Third Assessment Report., Cambridge University Press., 2001.

Isachsen, P.E., On the ocean circulation of the Arctic Mediterranean: internal large-scale currents and exchanges with the global oceans, University of Bergen, Bergen, Norway and Tromso, Norway, 2003.

Isachsen, P.E., J.H. LaCasce, C. Mauritzen, and S. Hakkinen, Wind-driven variability of the large-scale recirculating flow in the Nordic Seas and Arctic Ocean, *Journal of Physical Oceanography*, *33*, 2534-2550, 2003.

Jakobsen, P.K., M.H. Nielsen, D. Quadfasel, and T. Schmith, Variability of the surface circulation of the Nordic Seas during the 1990s, *ICES Marine Science Symposia*, *219*, 367-370, 2003.

Jakobsen, P.K., M.H. Ribergaard, D. Quadfasel, T. Schmith, and C.W. Hughes, Near-surface circulation in the northern North Atlantic as inferred from Lagrangian drifters: Variability from the mesoscale to interannual, *Journal of Geophysical Research*, *108* (C8), 3251, 2003.

Jakobsson, M., Hypsometry and volume of the Arctic Ocean and its consituent seas., *Geochemistry, Geophysics, Geosystems*, *3* (5), 1-18, 2002.

Jakobsson, M., N.Z. Cherkis, J. Woodward, R. Macnab, and B. Coakley, New grid of Arctic bathymetry aids scientists and mapmakers, *Eos*, *81* (9), 89,93,96, 2000.

Jayne, S.R., and J. Marotzke, The Dynamics of Ocean Heat Transport Variability, *Reviews of Geophysics*, *39*, 385-411, 2001.

Johannessen, O.M., L. Bengtsson, M.W. Miles, S.I. Kuzmina, V.A. Semenov, G.V. Alekseev, A.P. Nagurnyi, V.F. Zakharov, L. Bobylev, L.H. Pettersson, K. Hasselmann, and H.P. Cattle, Arctic Climate Change - observed and modeled temperature and sea ice variability, *Tellus*, *56A*, 328-341, 2004.

Jones, P.D., T. Jonsson, and D. Wheeler, Extension to the North Atlantic Oscillation using early instrumental pressure observations from Gibraltar and south-west Iceland., *International Journal of Climatology*, *17*, 1433-1450, 1997.

Jonsson, S., Seasonal and Interannual Variability of Wind Stress Curl over the Nordic Seas, *Journal of Geophysical Research*, *96* (C2), 2649-2659, 1991.

Jonsson, S., The circulation in the northern part of Denmark Strait and its variability., Marine Research Institute and University of Akureyri., 1999.

Josey, S.A., E.C. Kent, and P.K. Taylor, The Southampton Oceanography Centre (SOC) Ocean - Atmosphere Heat, Momentum and Freshwater Atlas., pp. 30 pp & figs, Southampton Oceanography Centre, Southampton, UK., 1998.

Josey, S., E. Kent, and P. Taylor, New insights into the ocean heat budget closure problem from analysis of the SOC air-sea flux climatology., *Journal of Climate*, *12* (9), 2856-2880, 1999.

Josey, S., E. Kent, and P. Taylor, On the Wind Stress Forcing of the Ocean in the SOC and Hellerman and Rosenstein Climatologies, *Journal of Physical Oceanography*, *submitted*, 2000.

Joyce, T.M., World Ocean Circulation Experiment; WOCE Operations Manual; Volume 3: The Observational Programme; Section 3.1: WOCE Hydrographic Programme; Part 3.1.3: WHP Operations and Methods, Woods Hole Oceanographic Institution, Massachusetts, U.S.A., 1991.

Joyce, T.M., A. Hernandez-Guerra, and W.M. Smethie, Zonal Circulation in the NW Atlantic and Caribbean from a meridional World Ocean Circulation Experiment hydrographic section at 66 W, *Journal of Geophysical Research*, *106* (C10), 22095 - 22113, 2001.

Joyce, T.M., C. Wunsch, and S.D. Pierce, Synoptic Gulf Stream Velocity Profiles Through Simultaneous Inversion of Hydrographic and Acoustic Doppler Data, *Journal of Geophysical Research*, *91* (C6), 7573 - 7585, 1986.

Jung, T., and M. Hilmer, The link between the North Atlantic oscillation and Arctic Sea ice export through Fram Strait., *Journal of Climate*, *14* (19), 3932-3943, 2001.

Kaleschke, L., G. Heygster, C. Lupkes, A. Bochert, J. Hartmann, J. Haarpaintner, and T. Vihma, SSM/I Sea Ice Remote Sensing for Mesoscale Ocean-Atmosphere Interaction Analysis, *Canadian Journal of Remote Sensing*, *27* (5), 526-537, 2001.

Karstensen, J., P. Schlosser, J. Bullister, and D. Wallace, Hydrographic and Transient Tracer Response to Atmospheric Changes over the Nordic Seas, *CLIVAR Exchanges*, *7* (3/4), 62-64, 2002.

Kent, E.C., P.K. Taylor, and J.S. Hopkins, The accuracy of voluntary observing ships meteorological observations - Results of the VSOP-NA., *Journal of Atmospheric and Oceanic Technology*, *10*, 591-608, 1993.

Kent, E.C., R.J. Tiddy, and P.K. Taylor, Correction of marine air temperature observations for solar radiation effects, *Journal of Atmospheric and Oceanic Technology*, *10*, 900-906, 1993.

Knudsen, M., Hydrography, in *The Danish Ingolf Expedition 1 (2)*, pp. 23-161, Bianco Luno, Copenhagen, 1899.

Koch, The east Greenland ice, *Medd. Groen.*, *130* (3), 1945.

Kowalik, Z., and A.Y. Proshutinsky, Diurnal Tides in the Arctic Ocean, *Journal of Geophysical Research*, *98* (C9), 16449-16468, 1993.

Krabill, W., W. Abdalati, E. Frederick, S. Manizade, C. Martin, J. Sonntag, R. Swift, R. Thomas, W. Wright, and J. Yungel, Greenland Ice Sheet: High-Elevation Balance and Peripheral Thinning, *Science*, *289* (428-430), 2000.

Kristmannsson, S.S., Flow of Atlantic Water into the northern Icelandic shelf area, 1985-1989, pp. 124-135, Marine Research Institute, Reykajvik, Iceland, 1998.

Kwok, R., H.J. Awally, and D. Yi, ICESat observations of Arctic sea ice: A first look, *Geophysical Research Letters*, *31* (L16401), doi:10.1029/2004GL020309, 2004.

Lanczos, C., *Linear differential operators*, 564pp pp., Van Nostrand, 1961.

Lawson, C.L., and R.J. Hanson, *Solving Least Square Problems*, 340 pp., Prentice-Hall, Englewood Cliffs, N. J., 1974.

Laxon, S., N. Peacock, and D. Smith, High interannual variability of sea ice thickness in the Arctic region, *Nature*, *425*, 947-950, 2003.

Lazier, J., R. Hendry, A. Clarke, I. Yashayaev, and P. Rhines, Convection and restratification in the Labrador Sea, 1990-2000, *Deep Sea Research*, *49*, 1819-1835, 2002.

Loeng, H., J. Blindheim, B. Adlandsvik, and G. Ottersen, Climatic variability in the Norwegian and Barents Sea., *ICES Marine Science Symposia*, *195*, 52-61, 1992.

Malmberg, S.A., H.G. Gade, and H.E. Sweers, Current velocities and volume transports in the East Greenland Current off Cape Nordenskjold in August-September 1965, in *Sea Ice*, pp. 130-139, National Research Council, Reykjavik, 1972.

Manabe, S., R.G. Stouffer, M.J. Spellman, and K. Bryan, Transient response of a coupled ocean-atmosphere model to gradual changes of atmospheric CO2. I. Annual mean response., *Journal of Climate*, *4*, 785-818, 1991.

Mann, C.R., Temperature and salinity characteristics of the Denmark Strait overflow, *Deep-Sea Research*, *Supplement to Vol 16*, 125-137, 1969.

Marshall, J., and F. Schott, Open-ocean Convection: Observations, Theory and Models, *Reviews of Geophysics*, *37* (1), 1-64, 1999.

Mauritzen, C., A Study of the Large Scale Circulation and Water Mass Transformation in the Nordic Seas and Arctic Ocean, Massachusetts Institute of Technology, Woods Hole, 1994.

Mauritzen, C., Production of dense overflow waters feeding the North Atlantic across the Greenland-Scotland Ridge. Part I: Evidence for a revised circulation scheme., *Deep Sea Research*, *43* (6), 769-806, 1996a.

Mauritzen, C., Production of dense overflow waters feeding the North Atlantic across the Greenland-Scotland Ridge. Part 2: An inverse model., *Deep Sea Research*, *43* (6), 807-835, 1996b.

McCartney, M.S., Recirculating components to the Deep Boundary Current of the Northern North-Atlantic, *Progress in Oceanography*, *29* (4), 283-383, 1992.

McCartney, M.S., and C. Mauritzen, On the origin of the warm inflow to the Nordic Seas, *Progress in Oceanography*, *51*, 125-214, 2001.

McDonagh, E.L., and B.A. King, Oceanic Fluxes in the South Atlantic, *Journal of Physical Oceanography*, *submitted*, 2002.

McDougall, T.J., Parameterising mixing in inverse models., in *Aha Hulio'a Winter Workshop*, edited by P. Muller, and D. Henderson, pp. 355-386, University of Hawaii, 1991.

McIntosh, P.C., and S.R. Rintoul, Do Box Inverse models work?, *Journal of Physical Oceanography*, *27*, 291-308, 1997.

Meincke, J., The Modern Current Regime Across the Greenland-Scotland Ridge, in *Structure and Development of the Greenland-Scotland Ridge, New Methods and Concepts*, edited by M.H. Bott, S. Saxov, M. Talawi, and J. Theide, pp. 637-650, Plenum Press, New York, 1983.

Meredith, M., K. Heywood, P. Dennis, L. Goldson, R. White, E. Fahrbach, U. Schauer, and S. Østerhus, Freshwater fluxes through the western Fram Strait, *Geophysical Research Letters*, *28* (8), 1615-1618, 2001.

Metcalf, W.G., A note on water movement in the Greenland-Norwegian Sea, *Deep-Sea Research*, *7*, 190-200, 1960.

Morison, J., M. Steele, and R. Anderson, Hydrography of the upper Arctic Ocean measured from the nuclear submarine U.S.S. *Pargo*, *Deep Sea Research I*, *45*, 15-38, 1998.

Mork, K.A., and J. Blindheim, Variations in the Atlantic inflow to the Nordic Seas, 1955-1996, *Deep Sea Research*, *47*, 1035 - 1057, 2000.

Nansen, F., The oceanography of the North Polar Basin, in *Norwegian North Polar Expedition, 1893-1896, Scientific ResultsV (IX)*, pp. 427, 1902.

Nansen, F., Das Bodenwasser und die Abkuhlung des Meeres., *Internationale Revue der gesamten Hydrobiologie und Hydrographie*, *5* (1), 1-42, 1912.

Naveira Garabato, A.C., E.L. McDonagh, D.P. Stevens, K.J. Heywood, and R.J. Saunders, On the export of Antarctic Bottom Water from the Weddell Sea, *Deep Sea Research II*, *49*, 4715-4742, 2002.

Naveira Garabato, A.C., K.I.C. Oliver, A.J. Watson, and M.-J. Messias, Turbulent diapycnal mixing in the Nordic Seas, *Journal of Geophysical Research*, *109* (C12010), doi:10.1029/2004JC002411, 2004.

Naveira Garabato, A.C., D.P. Stevens, and K.J. Heywood, Water mass conversion, fluxes and mixing in the Scotia Sea diagnosed by an inverse model, *Journal of Physical Oceanography*, *33*, 2565-2587, 2003.

New, A.L., S. Barnard, P. Herrmann, and J.M. Molines, On the origin and pathway of the saline inflow to the Nordic Seas: insights from models, *Progress in Oceanography*, *48*, 255-287, 2001.

Niiler, P., The World Ocean Surface Circulation, in *Ocean Circulation and Climate*, edited by G. Siedler, J. Church, and J. Gould, Academic Press, London, 2001.

Nøst, O.A., and P.E. Isachsen, The large-scale time-mean ocean circulation in the Nordic Seas and the Arctic Ocean estimated from simplified dynamics., *Journal of Marine Research*, *61*, 175-210, 2003.

O'Dwyer, J., Y. Kasajima, and O.A. Nost, North Atlantic Water in the Barents Sea Opening 1997 to 1999, *Polar Research*, *20* (2), 209 - 216, 2001.

Oliver, K.I.C., and K.J. Heywood, Heat and Freshwater Fluxes through the Nordic Seas, *Journal of Physical Oceanography*, 33, 1009-1026, 2003.

Orvik, K.A., and P. Niiler, Major pathways of Atlantic water in the northern North Atlantic and Nordic Seas toward Arctic, *Journal of Geophysical Research Letters*, *29* (19), 1-4, 2002.

Orvik, K.A., O. Skagseth, and M. Mork, Atlantic inflow to the Nordic Seas: current structure and volume fluxes from moored current meters, VM-ADCP and SeaSoar CTD observations, 1995 - 1999, *Deep Sea Research I*, *48*, 937 - 957, 2001.

Østerhus, S., and T. Gammelsrod, The Abyss of the Nordic Seas is Warming, *Journal of Climate*, *12*, 3297-3304, 1999.

Østerhus, S., T. Gammelsrod, and R. Hogstad, Ocean Weather Ship Station M (66N, 2E): The Longest Homogeneous Time Series from the Deep Ocean, *International WOCE Newsletter*, *24*, 31-33, 1996.

Østerhus, S., B. Hansen, R. Kristiansen, and P. Lundberg, The Overflow through the Faroe Bank Channel, *International WOCE Newsletter*, *35*, 35-37, 1999.

Østerhus, S., W. R. Turrell, S. Jonsson and B. Hansen, Measured volume, heat, and salt fluxes from the Atlantic to the Arctic Mediterranean, *Geophysical Research Letters*, *32*, L07603, doi:10.1029/2004GL022188, 2005.

Pickart, R.S., and S.S. Lindstrom, A comparison of techniques for referencing geostrophic velocities., *Journal of Atmospheric and Oceanic Technology*, *11*, 814-824, 1993.

Pistek, D., and D.R. Johnson, Transport of the Norwegian Atlantic Current as determined from satellite altimetry., *Geophysical Research Letters*, *19*, 1379-1382, 1992.

Pollard, R.T., J.F. Read, N.P. Holliday, and H. Leach, Water masses and circulation pathways through the Iceland Basin during Vivaldi 1996, *Journal of Atmospheric and Oceanic Technology*, *109* (C04004), doi:10.1029/2003JC002067, 2004.

Polyakov, I.V., G.V. Alekseev, R.V. Bekryaev, U. Bhatt, R.L. Colony, M.A. Johnson, V.P. Karklin, A.P. Makshtas, D. Walsh, and A.V. Yulin, Observationally based assessment of polar amplification of global warming, *Geophysical Research Letters*, *29* (18), 1878, 2002.

Polyakov, I.V., A.Y. Proshutinsky, and M.A. Johnson, Seasonal cycles in two regimes of Arctic climate, *Journal of Geophysical Research*, *104* (C11), 25761-25788, 1999.

Pond, S., and G.L. Pickard, *Introductory Dynamical Oceanography*, Butterworth-Heinemann, Oxford, 1983.
Proshutinsky, A.Y., and M.A. Johnson, Two circulation regimes of the wind-driven Arctic Ocean, *Journal of Geophysical Research*, *102* (C6), 12493-12514, 1997.
Quadfasel, D., B. Rudels, and K. Kurz, Outflow of dense water from a Svalbard fjord into Fram Strait, *Deep Sea Research*, *35* (7), 1143-1150, 1988.
Rahmstorf, S., Bifurcations of the Atlantic thermohaline circulation in response to changes in the hydrological cycle, *Nature*, *378*, 145-149, 1995.
Rahmstorf, S., On the freshwater forcing and transport of the Atlantic thermohaline circulation, *Climate Dynamics*, *12*, 799-811, 1996.
Rahmstorf, S., Shifting Seas in the greenhouse?, *Nature*, *399*, 523-534, 1999.
Rahmstorf, S., and A. Ganopolski, Long-term global warming scenarios computed with an efficient coupled climate model., *Climatic Change*, *43* (2), 353-367, 1999.
RDInstruments, Direct reading and self contained broadband acoustic Doppler current profiler, RD Instruments, 1995.
Read, J.F., CONVEX-91: water masses and circulation of the Northeast Atlantic subpolar gyre, *Progress in Oceanography*, *48* (461-510), 2001.
Reid, J.L., On the contribution of the Mediterranean Sea outflow to the Norwegian-Greenland Sea., *Deep Sea Research*, *26A*, 1199-1223, 1979.
Rhein, M., Ventilation rates of the Greenland and Norwegian Seas derived from distributions of the chlorofluoromethanes F11 and F12, *Deep Sea Research*, *38* (4), 485 - 503, 1991.
Robitaille, D.Y., L.A. Mysak, and M.S. Darby, A box model study of the Greenland Sea, Norwegian Sea, and Arctic Ocean, *Climate Dynamics*, *11*, 51-70, 1995.
Rodhe, J., and P. Winsor, On the influence of the freshwater supply on the Baltic Sea mean salinity, *Tellus*, *55A*, 455-456, 2003.
Rogers, J.C., Patterns of Low-Frequency Monthly Sea Level Pressure Variability (1899-1986) and Associated Wave Cyclone Frequencies, *Journal of Climate*, *3*, 1364-1379, 1990.
Ross, C.K., Temperature - salinity characteristics of the "overflow" water in Denmark Strait during "OVERFLOW '73", *Rapp. p.-v Reun. Consl int. Explor. Mer.*, *185*, 111-119, 1984.
Rothrock, D.A., J. Zhang, and Y. Yu, The arctic ice thickness anomaly of the 1990s: A consistent view from observations and models, *Journal of Geophysical Research*, *108* (C3), 3083, 2003.
Rudels, B., Greenland Sea Convection in the Winter of 1987-1988, *Journal of Geophysical Research*, *94* (C3), 3223-3227, 1989.
Rudels, B., The thermohaline circulation of the Arctic Ocean and the Greenland Sea, *Phil. Trans. R. Soc. London A*, *352*, 287-299, 1995.
Rudels, B., P. Eriksson, H. Gronvall, R. Hietala, and J. Launiainen, Hydrographic Observations in Denmark Strait In Fall 1997, and their Implications for the Entrainment of the Overflow Plume, *Geophysical Research Letters*, *26* (9), 1325-1328, 1999.
Rudels, B., E. Fahrbach, and J. Meincke, The East Greenland Current from Fram Strait to beyond Denmark Strait in 1998: Observations from RV Polarstern and RV Valdivia, *ICES*, 1999.
Rudels, B., E. Fahrbach, J. Meincke, G. Budeus, and P. Eriksson, The East Greenland Current and its contribution to the Denmark Strait overflow, *ICES Journal of Marine Science*, *59*, 1133-1154, 2002.
Rudels, B., H.J. Friedrich, and D. Quadfasel, The Arctic Circumpolar Boundary Current, *Deep-Sea Research II*, *46*, 1023-1062, 1999.
Rudels, B., and D. Quadfasel, Convection and deep water formation in the Arctic Ocean - Greenland Sea System, *Journal of Marine Systems*, *2*, 435-450, 1991.
Saloranta, T.M., and H. Svendsen, Across the Arctic front west of Spitsbergen: high-resolution CTD sections from 1998 - 2000, *Polar Research*, *20* (2), 177 - 184, 2001.
Saunders, P.M., Practical Conversion of Pressure to Depth, *Journal of Physical Oceanography*, *11* (4), 255-574, 1981.
Saunders, P.M., Cold Outflow from the Faroe Bank Channel, *Journal of Physical Oceanography*, *20*, 29-43, 1990a.
Saunders, P.M., The International Temperature Scale of 1990, ITS-90., *International WOCE Newsletter*, *10*, 10, 1990b.
Saunders, P.M., The Flux of Dense Cold Overflow Water Southeast of Iceland, *Journal of Physical Oceanography*, *26*, 85-95, 1996.
Saunders, P.M., The Dense Northern Overflows, in *Ocean Circulation & Climate*, edited by G. Siedler, J. Church, and J. Gould, Academic Press, London, 2001.
Schauer, U., The release of brine-enriched shelf water from Storfjord into the Norwegian Sea., *Journal of Geophysical Research*, *100* (C8), 16,015-16,028, 1995.
Schauer, U., The expedition ARKTIS XV/3 of the Research Vessel "Polarstern" in 1999., *Berichte zur Polarforschung, Reports on Polar Research*, *350*, 2000.
Schauer, U., H. Loeng, B. Rudels, V.K. Ozhigin, and W. Dieck, Atlantic Water flow through the Barents and Kara Seas, *Deep Sea Research I*, *49*, 2281-2298, 2002.
Schlichtholz, P., and M.-N. Houssais, An inverse modeling study in Fram Strait. Part II: water mass distribution and transports, *Deep Sea Research II*, *46*, 1137-1168, 1999.
Schlosser, P., G. Bonisch, M. Rhein, and R. Bayer, Reduction of Deepwater Formation in the Greenland Sea During the 1980s: Evidence from Tracer Data, *Science*, *251*, 1054-1056, 1991.
Schmitz, W.J., and M.S. McCartney, On the North Atlantic Circulation, *Reviews of Geophysics*, *31* (1), 29-49, 1993.
Serreze, M.C., J.A. Maslanik, T.A. Scambos, F. Fetterer, J. Stroeve, K. Knowles, C. Fowler, S. Drobot, R.G. Barry, and T.M. Haran, A record minimum arctic sea ice exent and area in 2002, *Geophysical Research Letters*, *30*, doi:10.1029/2002GL016406, 2003.

Serreze, M.C., J.E. Walsh, F.S. Chaplin, T. Osterkamp, M. Dyurgerov, V. Romanovsky, W.C. Oechel, J. Morison, T. Zhang, and R.G. Barry, Observational evidence of recent changes in the northern high-latitude environment., *Climatic Change*, *46*, 159-207, 2000.

Silva, A.M.d., C. Young, and S. Levitus, *Atlas of Surface Marine Data 1994; Volume 1: Algorithms and Procedures*., US Department of Commerce, NOAA, NESDIS., Washington DC, 1994.

Simonsen, K., and P.M. Haugan, Heat budgets of the Arctic Mediterranean and sea surface heat flux parameterizations for the Nordic Seas, *Journal of Geophysical Research*, *101* (C3), 6553-6576, 1996.

Sjøtun, K., Havets miljø 2004. Fisken og havet, saernr. 2-2004., pp. 120, Havforskningsinstituttet, Institute of Marine Research., Bergen, 2004.

Skagseth, O., and K.A. Orvik, On the heat flux associated with the Norwegian Atlantic Slope Current., in *ICES Annual Science Conference*, ICES, Stockholm, Sweden, 1999.

Slater, D.R., The Transport of Mediterranean Water in the North Atlantic Ocean, University of Southampton, Southampton, 2003.

Sloyan, B.M., and S.R. Rintoul, Estimates of area-averaged diapycnal fluxes from basin-scale fluxes., *Journal of Physical Oceanography*, *30*, 2320-2341, 2000.

Sloyan, B.M., and S.R. Rintoul, Circulation, Renewal, and Modification of Antarctic Mode and Intermediate Water, *Journal of Physical Oceanography*, *31*, 1005-1030, 2001a.

Sloyan, B.M., and S.R. Rintoul, The Southern Ocean Limb of the Global Deep Overturning Circulation, *Journal of Physical Oceanography*, *31*, 143-173, 2001b.

Smethie, W.M., H.G. Ostlund, and H. Loosli, Ventilation of the deep Greenland and Norwegian Seas: Evidence from krypton-8, tritium, carbon-14 and argon-39., *Deep Sea Research Part A*, *33*, 675-703, 1986.

Smethie, W.M., and J.H. Swift, The tritium:krypton-85 age of the Denmark Strait overflow water and Gibbs Fracture zone water just south of Denmark Strait, *Journal of Geophysical Research*, *94*, 8265-8275, 1989.

Soelen, O.H., On the exchange of bottom water between the Greenland and Norwegian Seas, in *Nordic perspectives on oceanography*, pp. 133-144, Kugl. Vetensdaps-och Vitterhets-Samhallet, Gothenburg, 1986.

Steele, M., and T. Boyd, Retreat of the cold halocline layer in the Arctic Ocean., *Journal of Geophysical Research*, *103* (5), 10419-10435, 1998.

Stefansson, U., North Icelandic Waters, *Rit Fiskideildar*, *3*, 1-269, 1962.

Strass, V., E. Fahrbach, U. Schauer, and L. Sellmann, Formation of Denmark Strait Overflow Water by Mixing in the East Greenland Current, *Journal of Geophysical Research*, *98* (C4), 6907-6919, 1993.

Sverdrup, H.U., M.S. Johnson, and R.H. Flemming, *The Oceans*., 1087 pp., Prentice-Hall, New York, 1942.

Swift, J.H., The Arctic Waters, in *The Nordic Seas*, edited by B.G. Hurdle, pp. 129-153, Springer-Verlag, New York, 1986.

Swift, J.H., Dissolved Oxygen in the Arctic Ocean and Nordic Seas, *Proc. ACSYS Conf.*, *2*, 259-261, 1997.

Swift, J.H., and K. Aagaard, Seasonal transitions and water mass formation in the Iceland and Greenland Seas, *Deep-Sea Research*, *28A*, 1107-1129, 1981.

Swift, J.H., K. Aagaard, and S.-A. Malmberg, The Contribution of the Denmark Strait overflow to the deep North Atlantic, *Deep-Sea Research*, *27A*, 29-42, 1980.

Swift, J.H., E.P. Jones, E.C. Carmack, M. Hingston, R.W. MacDonald, F.A. McLaughlin, and R.G. Perkins, Waters of the Makarov and Canada basins, *Deep Sea Research II*, *44* (8), 1503-1529, 1997.

Swift, J.H., and K.P. Koltermann, The Origin of Norwegian Sea Deep Water, *Journal of Geophysical Research*, *93* (C4), 3563-3569, 1988.

Talley, L.D., D. Stammer, and I. Fukumori, Towards a WOCE Synthesis, in *Ocean Circulation and Climate*, edited by G. Siedler, J. Church, and J. Gould, Academic Press, London, 2001.

Thompson, D., and J. Wallace, The Arctic Oscillation signature in the wintertime geopotential height and temperature fields, *Geophysical Research Letters*, *25* (9), 1297-1300, 1998.

Toudal, L., Ice extent in the Greenland Sea 1978 - 1995, *Deep Sea Research II*, *46*, 1237 - 1254, 1999.

Trenberth, K., J. Olson, and W. Large, A Global Ocean Wind Stress Climatology based on ECMWF Analyses, National Center for Atmospheric Research, Boulder, Colorado., 1989.

Treshnikov, A.F., *Arctic Atlas*, 204 pp., Arkt. Antarkt. Nauchno-Issled. Inst., Moscow, 1985.

Tsimplis, M.N., S. Bacon, and H.L. Bryden, The circulation of the subtropical South Pacific derived from hydrographic data, *Journal of Geophysical Research*, *103* (C10), 21443 - 21468, 1998.

Turrell, W., G. Slesser, R. Adams, R. Payne, and P. Gillibrand, Decadal variability in the composition of Faroe Shetland Channel bottom water, *Deep-Sea Research I*, *46*, 1-25, 1999.

Vanicek, M., and G. Siedler, Zonal Fluxes in the Deep Water Layers of the Western South Atlantic Ocean, *Journal of Physical Oceanography*, *32*, 2205-2235, 2002.

Vinje, T., Fram Strait Ice Fluxes and Atmospheric Circulation: 1950 - 2000, *Journal of Climate*, *14*, 3508 - 3517, 2001.

Vinje, T., N. Nordlund, and A. Kvambekk, Monitoring ice thickness in Fram Strait, *Journal of Geophysical Research*, *103* (C5), 10437-10449, 1998.

Vinnikov, K., A. Robock, R. Stouffer, J. Walsh, C. Parkinson, D. Cavalieri, J. Mitchell, D. Garrett, and V. Zakharov, Global Warming and Northern Hemisphere Sea Ice Extent, *Science*, *286*, 1934-1937, 1999.

Visbeck, M., J. Fischer, and F. Schott, Preconditioning the Greenland Sea for deep convection: Ice formation and ice drift, *Journal of Geophysical Research*, *100* (C9), 18489-18502, 1995.

Visbeck, M., and M. Rhein, Is Bottom Boundary Layer Mixing Slowly Ventilating Greenland Sea Deep Water?, *Journal of Physical Oceanography*, *30*, 215-224, 2000.

Wadhams, P., The ice cover in the Greenland and Norwegian Seas., *Rev. Geophys. Space Phys.*, *19* (3), 345-393, 1981.

Wadhams, P., Sea ice thickness distribution in the Greenland Sea and Eurasian Basin, May 1987, *Journal of Geophysical Research*, *97* (5331-5348), 1992.

Wadhams, P., J. Backhaus, and E.N. Hegseth, RV *Jan Mayen* 3/2000 Cruise Report. 16 February to March 10, 2000. SCORESBY. Ocean-ice physics cruise to the central Greenland Sea., pp. 57, 2000.

Wadhams, P., G. Budeus, J.P. Wilkinson, T. Loyning, and V. Pavlov, The multi-year development of long-lived convective chimneys in the Greenland Sea, *Geophysical Research Letters*, *31* (L06306), doi:10.1029/2003GL019017, 2004.

Walin, G., G. Brostrom, J. Nilsson, and O. Dahl, Baroclinic boundary current with downstream decreasing buoyancy: A study of an idealized Nordic Seas system, *Journal of Marine Research*, *62* (517-543), 2004.

Walsh, J.E., W.L. Chapman, and T.L. Shy, Recent Decrease of Sea Level Pressure in the Central Arctic, *Journal of Climate*, *9*, 480-486, 1996.

Warren, B.A., and C. Wunsch, *Evolution of Physical Oceanography: Scientific Surveys in honour of Henry Stommel*., 623 pp., MIT Press, Cambridge, MA, 1981.

Watson, A.J., M.J. Messias, K.A.V. Scoy, T. Johannessen, K.I.C. Oliver, D.P. Stevens, F. Rey, T. tanhua, K.A. Olsson, F. Carse, K. Simonsen, J.R. Ledwell, E. Jansen, D.J. Cooper, J.A. Kruepke, and E. Guilyardi, Mixing and Convection in the Greenland Sea from a tracer-release experiment, *Nature*, *401*, 902-904, 1999.

White, M.A., and K.J. Heywood, Seasonal and interannual changes in the North Atlantic subpolar gyre from Geosat and TOPEX/Poseidon altimetry, *Journal of Geophysical Research*, *100*, 24931-24941, 1995.

Wiffels, S.E., Ocean Transport of Fresh Water, in *Ocean Circulation and Climate Observing and Modelling the Global Ocean*, edited by G. Siedler, J. Church, and J. Gould, Academic Press, London, 2001.

Winsor, P., J. Rodhe, and A. Omstedt, Baltic Sea ocean climate: an analysis of 100 yr of hydrographic data with focus on the freshwater budget, *Climate Research*, *18*, 5-15, 2001.

Wohlert, H., Context, Results and Remaining Issues, 2002.

Wood, R., A. Keen, J. Mitchell, and J. Gregory, Changing spatial structure of the thermohaline circulation in response to atmospheric CO_2 forcing in a climate model, *Nature*, *399*, 572-575, 1999.

Woodgate, R.A., E. Fahrbach, and G. Rohardt, Structure and transports of the East Greenland Current at 75N from moored current meters, *Journal of Geophysical Research*, *104* (C8), 18059-18072, 1999.

Woodruff, S.D., S.J. Lubker, K. Wolter, S.J. Worley, and J.D. Elms, Comprehensive Ocean-Atmosphere DAta Set (COADS) release 1a: 1980-92, *Earth System Monitoring*, *4*, 4-8, 1993.

Worthington, L.V., An attempt to measure the volume transport of Norwegian Sea overflow water through Denmark Strait, *Deep-Sea Research*, *16*, 421-432, 1969.

Worthington, L.V., The Norwegian Sea as a Mediterranean basin, *Deep-Sea Research*, *17*, 77-84, 1970.

Wunsch, C., The North Atlantic General Circulation West of 50W Determined by Inverse Methods, *Reviews of Geophysics and Space Physics*, *16* (4), 583-620, 1978.

Wunsch, C., *The Ocean Circulation Inverse Problem*, 442 pp., Cambridge University Press, Cambridge, 1996.

Wunsch, C., and B. Grant, Towards the general circulation of the North Atlantic Ocean., *Progress in Oceanography*, *11*, 1-59, 1982.

Zhang, J., D.R. Thomas, D.A. Rothrock, R.W. Lindsay, Y. Yu, and R. Kwok, Assimilation of ice motion observations and comparisons with submarine ice thickness data, *Journal of Geophysical Research*, *108* (C6), 3170, doi:10.1029/2001JC001041, 2003.

Zwally, H.J., B. Schutz, W. Abdalati, J. Abshire, C. Bentley, A. Brenner, J. Bufton, J. Dezio, D. Hancock, D. Harding, T. Herring, B. Minster, K. Quinn, S. Palm, J. Spinhirne, and R. Thomas, ICESat's laser measurements of polar ice, atmosphere, ocean and land, *Journal of Geodynamics*, *34*, 405-445, 2002.

By the end, you can barely move your fingers.
So you have to learn how to work with your hands
when your hands get so tired they don't work any more.

APOLLO 16 COMMANDER John Young
Full Moon - The Furthest Place